Mechanical Properties of Tissue in Living Humans

Technical Report

February 2020

Caitlin Jackson, MS

Kevin Kerr, BS

Joshua Etu, MBA

AMERICAN SYSTEMS
Engineering, Strategy & Analysis Directorate

Matthew Panzer, PhD

Jason Foreman, PhD

Daniel Shedd, PhD

Kristen Reynier, BS

University of Virginia
Center for Applied Biomechanics

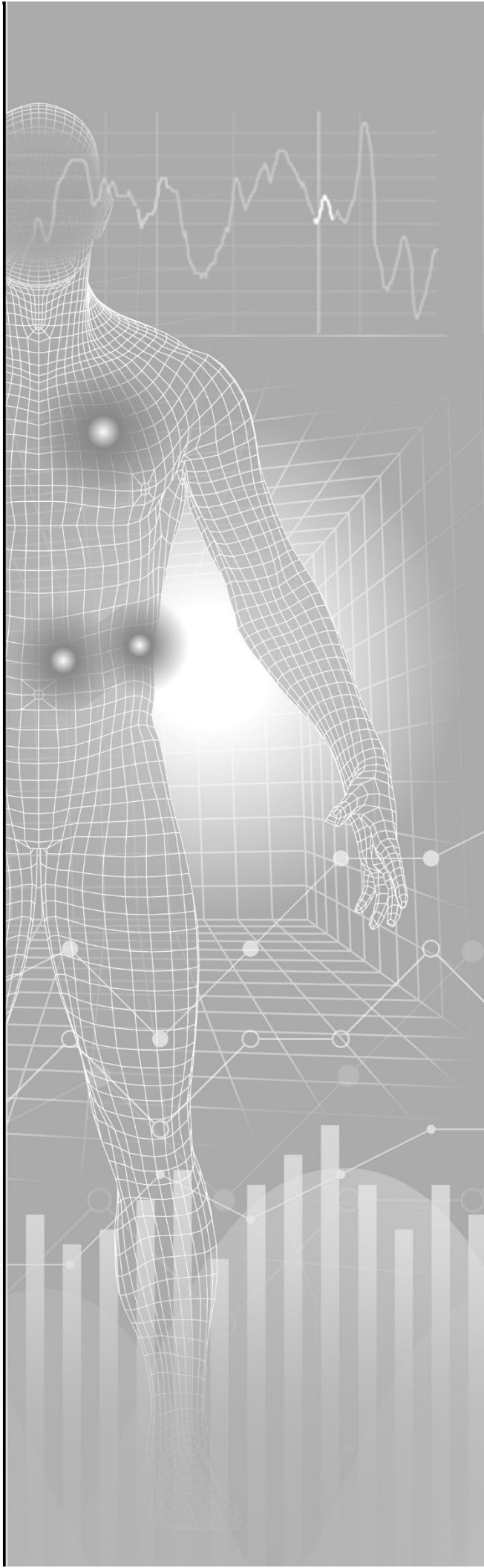

This work was conducted by AMERICAN SYSTEMS under # N000174-17-D-0031, Task Order #6 "Mechanical Properties of Tissue in Living Humans," for the Joint Non-Lethal Weapons Directorate. The views, opinions, and findings should not be construed as representing the official position of either the Department of Defense or the sponsoring organization.

Distribution Statement A: Unlimited Distribution (February 2020).

Table of Contents

Executive Summary **8**
Introduction 8
Aim 1 8
Aim 2 9
Aim 3 9
Aim 4 9
Conclusion 10
Introduction **11**
Background 11
Aims12
Aim 1: Shear Wave Elastography in Volunteers and Cadaveric Tissue **13**
Overview 13
Methods 13
Test Subjects 13
Volunteer Testing Procedure 13
PMHS Testing Procedure 16
Equipment 17
Data Analysis 19
Results 20
Anthropometry 20
Volunteer Results 21
Cadaver Results 25
Conclusions 28
Aim 2: Low-severity impacts in volunteers and cadaveric tissue, and higher-severity impacts in cadaveric tissue **29**
Overview 29
Methods 29
Test Subjects 29
Testing Procedure 29
Equipment 32
Data Analysis 33
Results 34
Volunteer Results 34
Cadaver Results 37
Tissue Thicknesses 40
Post-Test Survey 40
Conclusions 42
Aim 3: High-rate, high-deformation mechanical tests on *ex situ* in cadaveric tissue **43**
Overview 43
Methods 43
Test Subjects/Samples 43

Testing Procedure 44
Equipment 45
Drop Tower 45
Data Acquisition 45
Data Analysis 45
Results 46
Conclusions 48
Aim 4: Constitutive Model Development 49
Overview 49
Methods 49
QLV model fits for individual cadaveric test samples 49
Average QLV models per cadaveric muscle location 50
Average QLV models with muscle activation per muscle location 50
Comparison of muscle activation QLV fits with cadaver and volunteer impact data 50
Results 51
QLV model fits for individual cadaveric test samples 51
Average QLV models per cadaveric muscle location 52
Average QLV models with muscle activation per muscle location 53
Comparison of muscle activation QLV fits with cadaver and volunteer impact data 54
Conclusions 56
Discussion 58
Overall Conclusions 58
Limitations 58
References 60
Appendices 61
Appendix 1: Anthropometry Instructions 61
Appendix 2: Maximum weights per muscle and activity for each subject 66
Appendix 3: EMG sensor locations for each muscle 68
Appendix 4: SWE locations in relation to EMG sensors 70
Appendix 5: Average activation across all volunteers per muscle 72
Appendix 6: Combined average absolute shear wave velocity across all volunteers 75
Appendix 7: Individual relationships between muscle activation and absolute shear wave velocity 76
Appendix 8: Individual relationships between muscle activation and normalized shear wave velocity 81
Appendix 9: Log Fits for Muscle Activation and Normalized Shear Wave Velocities 86
Average normalized shear wave velocity and activation relationship (mean ± 1 SD) 86
Average normalized shear wave velocity and activation relationship (mean ± 2 SD) 89
Appendix 10: Log Fits for Muscle Activation and Absolute Shear Wave Velocities 92
Average absolute shear wave velocity and activation relationship (mean ± 1 SD) 92
Average absolute shear wave velocity and activation relationship (mean ± 2 SD) 95
Appendix 11: Volunteer Follow-Up Questionnaire 98

Appendix 12: Superficial temperature recordings for SWE and impactor tests for the PMHS. 100
Appendix 13: Volunteer/PMHS: Peak Impact Force & Indentation Depth 104
Appendix 14: The average tissue thickness for each muscle during each SWE muscle activation level 113
Appendix 15: Volunteer Force-Time and Force-Displacement Curves 116
Appendix 16: Volunteer Force-Time Corridors 136
Appendix 17: Volunteer Force-Displacement Average Curves 139
Appendix 18: PMHS Force-Time and Force-Displacement Curves 142
Appendix 19: PMHS Force-Time Corridors 150
Appendix 20: PMHS Force-Displacement Average Curves 153
Appendix 21: PMHS vs Volunteer Force-Time Corridors 156
Appendix 22: Superficial tissue temperatures during the mechanical testing on drop tower 159
Appendix 23: Displacement- and force-time histories for all cadaveric tissue from drop tower mechanical testing. 160
Appendix 24: Compressive strain - force relationship for each muscle. 164
Appendix 25: The parameters for individual QLV fits per muscle and PMHS. 167
Appendix 26: The average ideal strain input for each of the muscles 169
Appendix 27: The average QLV model fits for each muscle 170
Appendix 28: The ratios and scaled parameters for QLV instantaneous elastic function parameter 173
Appendix 29: The scaled QLV models for the volunteers at each muscle 175
Appendix 30: Validation curves for external oblique using scaled QLV models 178

List of Tables

Table I: Additional information about the PHMS used throughout the study 13
Table II: Muscle of interest and corresponding exercise to activate each muscle 14
Table III: The test matrix for the SWE and EMG measurements for the volunteer study 16
Table IV: The test matrix for the PMHS SWE study 17
Table V: Volunteer and PMHS anthropometry results 20
Table VI: Volunteer and PMHS body fat results 20
Table VII: The test matrix for volunteer impactor study 30
Table VIII: The test matrix for the PMHS impactor study 31
Table IX: The average (mean ± 1 SD) compressive strain and peak force per muscle between cadaver tissues 47
Table X: The average (mean ± 1 SD) maximum strain and time to peak across muscles 52

List of Figures

Figure 1: The six muscles of interest: 1. Pectoralis major, 2. Rectus abdominis, 3. External oblique, 4. Upper trapezius, 5. Lower trapezius, and 6. Latissimus dorsi 14

Figure 2: Shear wave elastography ultrasound machine (A) and probes – SuperLinear SL15-4 (B), SuperLinear SLH20-6 (C), and Single Crystal Curved XC6-1 (D) 18

Figure 3: Delsys Trigno EMG system (A) with the wireless sensor (B) 18

Figure 4: (Left) XMark Functional Trainer Cable Machine; (Right) SOLE F80 Treadmill 19

Figure 5: The average (mean ± 1 SD) muscle activation per activity for all muscles. (* = significantly different from passive. † = significant difference between 100% and 50%) 21

Figure 6: The average (mean ± 1 SD) EMG activation for each muscle during the dynamic activities 22

Figure 7: The average normalized shear wave velocity for all muscles and activities (* = significantly different from passive. † = significant difference between 100% and 50%) 23

Figure 8: The average shear wave velocity of liver and subcutaneous fat compared to the average passive muscle shear wave velocity 24

Figure 9: The average normalized shear wave velocity and muscle activation functions for pectoralis major and external oblique 25

Figure 10: The average shear wave velocity for right and left muscles during the seated, supine, and prone positions 26

Figure 11: The average shear wave velocities for the anterior muscles for both the volunteer and PMHS subjects. (*= significantly different from volunteer passive, † = significantly different from volunteer supine) 27

Figure 12: The average shear wave velocities for the posterior muscles for both the volunteer and PMHS subjects. (*= significantly different from volunteer passive) 27

Figure 13: The average shear wave velocity for volunteer and PMHS across all tissues 28

Figure 14: The custom-built impactor device used for all volunteer and PMHS impacts. This device was used for both low- and high-speed impacts by changing the spring 32

Figure 15: Validation of impactor data. (Left) Peak force measured by the accelerometer was validated against an external load cell. (Right) The velocity measured by the velocity gate was validated against high-speed video 33

Figure 16: Average (mean ± 1 SD) peak indentation depth and contact force for volunteer impacts at 5.5m/s (* = significantly different from passive for each muscle) 35

Figure 17: Example force-time and force-displacement curves for the upper trapezius of a single subject 36

Figure 18: Force-time corridors and average force-displacement curves for the upper trapezius (top) and rectus abdominis (bottom)..... 37

Figure 19: Average (mean ± 1 SD) peak indentation depth and contact force for PMHS impacts compared at 5.5m/s and 11m/s (* = significantly different from matched volunteer test, † = significantly different between seated and supine/prone) 39

Figure 20: PMHS force-displacement curves for seated, supine, and prone positions under 5.5 and 11m/s impact conditions..... 39

Figure 21: Comparison of 5.5m/s force-time corridors of seated PMHS, passive volunteers, and maximally contracted volunteers..... 40

Figure 22: The average tissue thickness (± 1 standard deviation) for the pectoralis major during each SWE muscle activation level 40

Figure 23: The survey results for the number of subjects with visible (top), sensitive (middle), and bruised (bottom) impact locations per muscle..... 41

Figure 24: The anterior and posterior tissue samples (black circles), y-shaped incision (white dashed line), and tissue slab edges (yellow dashed line) 43

Figure 25: Excised tissue samples in polycarbonate cylindrical dish..... 44

Figure 26: (Left) A tissue sample prior to a drop tower test and (Right) post-test with the indenter at a 50% compressive depth. 44

Figure 27: Drop tower assembly used for mechanical testing of excised cadaver tissue samples 45

Figure 28: The displacement time histories for all six muscles on a single cadaver, including full linear displacement-time history (top left), initial step in displacement until 0.5s (right), and full log displacement-time history (bottom left). 46

Figure 29: The force time histories for all six muscles on a single cadaver, including full linear force-time history (top left), initial relaxation until 0.5s (right), and full log force-time history (bottom left)..... 47

Figure 30: The force-compressive strain response of the lower trapezius during load for each PMHS 48

Figure 31: The stress-strain response and instantaneous elastic function for a single upper trapezius sample tissue 51

Figure 32: The stress log time-history (left) and linear time-history (right) with an individual QLV fit for the upper trapezius 52

Figure 33: The stress linear time-history (top left), stress log time-history (right), and stress-strain response for the upper trapezius of the four PMHS and the average QLV model..... 53

Figure 34: The scaled response for volunteer activities for the external oblique and the average PMHS response, including the linear stress-time history (top left), the log stress-time history (right), and the stress-strain response (bottom left) for passive, 100% MVC, 50% MVC, and supine volunteer conditions 54

Figure 35: The max force for the pectoralis major and external oblique impact model and experimental data 55

Figure 36: The max displacement for the pectoralis major and external oblique impact model and experimental data 55

Figure 37: The force time-history of the QLV model impact with the experimental data for the pectoralis major 56

Executive Summary

Introduction

To calculate the expected risk of significant injury (RSI) to individuals struck with blunt trauma munitions, the Joint Non-Lethal Weapons Program (JNLWP) has developed computational finite element models of the human to simulate the impact and predict the response of a living person. These models were developed and validated using biomechanical data collected during testing of post-mortem human surrogates (PMHS). The mechanical properties of PMHS tissue are known to differ from those of the live human, especially muscle and other soft tissues, limiting the biofidelity of existing models. Our research group, composed of AMERICAN SYSTEMS and the University of Virginia's Center for Applied Biomechanics (UVA-CAB), examined the difference in material properties between the soft tissue of PMHS and live humans in various states of muscle activation for the purpose of providing JNLWP with data intended to improve the biofidelity of their human body models. To achieve this, we completed the following four aims:

1. Perform shear wave elastography (SWE) experiments to quantify how a change in muscle activation can affect the *in vivo* and *in situ* soft tissue stiffness properties of the thorax.
2. Perform low-severity blunt impact tests to quantify how a change in muscle activation can affect the *in vivo* and *in situ* dynamic response of active and passive soft tissue.
3. Perform high-rate, high-deformation mechanical tests on *ex situ* cadaveric soft tissue to characterize non-linear, viscoelastic behavior of the passive tissue.
4. Translate the results from Aim 3, along with the relationships established in Aim 1, to develop a dynamic, high-deformation constitutive model for *in vivo* superficial soft tissue of a living human. This constitutive model can be validated in the future using results from dynamic blunt impact tests in Aim 2.

A summary of each Aim is provided below:

Aim 1

The stiffness of six thorax muscles was measured in various states of muscle activation using SWE in twenty healthy, male volunteers. A range of isometric muscle activation states was achieved in the volunteers, from fully relaxed (passive) to fully contracted (100% voluntary muscle contraction). Muscle activation was recorded in the six muscle groups using surface electromyography (EMG), and simultaneously, SWE data was collected at the same locations as the EMG data for various muscle activation states. Each test was repeated five times, and each volunteer was tested 153 times. In addition, a series of SWE tests was perform on four PMHS in conditions matching the passive muscle activation conditions tested in the volunteers. Each PMHS was tested 130 times.

Major results from this Aim showed that muscle stiffness in the volunteers increased with increased muscle activation, and the stiffness of 100% and 50% activation were both significantly different from the passive musculature. The stiffness of the average PMHS musculature was significantly greater than that of the volunteers for pectoralis major, rectus abdominis, and latissimus dorsi. The dataset collected in this aim can be used to develop more biofidelic tissue models to represent living tissue in the computational human body models.

Aim 2

The force-displacement response of six regions of the thorax was measured in various states of muscle activation in ten healthy, male volunteers using a custom-built, instrumented dynamic blunt indenter. The rigid cylindrical indenter had a mass of 40g and a diameter of 40mm and impacted the volunteers with a velocity of 5.5m/s. Using similar muscle activation states and locations as tested in Aim 1, each subject was impacted a total of 62 times. During each impact, acceleration was recorded, allowing the calculation of the force and displacement. In addition, a series of blunt indenter tests was performed on four PMHS in conditions matching the passive muscle activation conditions in the volunteers. An additional series of blunt indentations were performed on each PMHS at a higher-severity 11m/s impact. Each PMHS was tested 72 times.

Major results from this Aim showed that peak forces measured in the volunteers ranged from 112 to 480N, with peak indentation depths ranging from 3.4 to 18.4mm. Both the peak force and indentation depth differed significantly across the different postures and activation conditions. The peak forces were not significantly different between the PMHS and volunteers, but peak indentation depths were significantly different in the external oblique, rectus abdominis, and lower trapezius. Force and displacement corridors were generated for each location and condition for both volunteers and PMHS, and this dataset can be used to validate the computational human body models.

Aim 3

Cylindrical tissue samples were excised from the four PMHS at each of the thoracic locations previously tested in Aim 1 and 2. Tissue samples included all components of the flesh (skin, fat, and muscle) down to either bone or the organ wall, depending on location. Using a drop tower, dynamic step-hold tests were performed on the tissue using a cylindrical impactor, with a 15.25mm diameter and a 0.78kg mass. The initial velocity of the impactor was 4.5m/s, resulting in loading times ranging from 4 to 5ms. The impactor was held in place after 50% compression of the tissue to characterize viscoelastic relaxation. Tissue samples were kept in a water bath prior to testing to ensure equal temperature throughout testing. A total of 24 tissue samples were tested, and each sample was only tested once.

The major results from this Aim include the dynamic experimental data collected from each sample. Peak forces varied across locations and subjects, and variation of tissue response appeared to be a consequence of tissue composition (amount of skin, fat, muscle). The dataset collected in this aim can be used to develop more biofidelic tissue models for simulating blunt impacts with the computational human body models.

Aim 4

Data from each tissue sample in Aim 3 were fit using quasilinear viscoelasticity (QLV) theory, to capture the complex, nonlinear behavior of the soft tissue during both the rapid loading and relaxation of the tissue. The instantaneous elastic responses were modeled using Fung's exponential form. The resulting QLV fits were then combined at each muscle location by averaging the QLV parameters of the four PMHS. The resulting QLV models were compared against the PMHS impact response from Aim 2. Using the differences between volunteer and

PMHS shear wave velocity (Aim 1) and force-displacement relationships (Aim 2), scaled QLV models were created for living tissue at varying levels of activation.

Conclusion

Muscle activation may be a factor that affects the accuracy of models designed to predict the consequences and RSI from blunt trauma strikes to the human torso. We have demonstrated using SWE and EMG that muscle tissue stiffness increases with muscle activation, and we have quantified this relationship. We have also collected a unique dataset on low-rate dynamic blunt impact on human volunteers with varying levels of muscle activation. Furthermore, we performed matched tests on PMHS to quantify differences between live humans and the surrogates often used for injury research. When comparing between the volunteers and PMHS, volunteer tissue appears to be softer than what is measured in PMHS, and this may have consequences that affect the biofidelity of current human body models. Overall, we believe the differences between living and post-mortem tissue mechanics are likely greater at an individual tissue level (e.g., skin, fat, muscle) than the combined response (i.e., “flesh”). Although this was not a focus of the current study, anecdotally we also observed noticeable differences in soft tissue response, particularly the fat, with changes in temperature.

In summary, the data collected in this project will help improve the computational human body models that JNLWP has developed to simulate the impact and predict the response of a living person. This study is the first of its kind to examine the difference in material properties between the soft tissue of PMHS and live humans in various states of muscle activation for the purpose of improving the biofidelity of human body models.

Introduction

Background

The Joint Non-Lethal Weapons Program (JNLWP) has developed finite element models of the human body for predicting the Risk of Significant Injury (RSI) from non-lethal weapons (NLW) in development. These models were built, verified, and validated by testing human cadaveric tissue. However, there may be differences in the effect of an NLW on live humans compared to post-mortem human surrogates (PMHS) due to inherent differences in body composition, tissue properties, and muscle activation. This study examines the superficial soft tissue mechanics of human volunteers and human cadavers to categorize and correlate potential differences between *in vivo* and PMHS biomechanics. The results of this study can be used to evaluate and improve the biofidelity of human body finite element models, particularly those associated with blunt trauma, so that they can be scaled to better estimate outcomes on living targets.

One of the differences between living humans and PMHS is the stiffness of the musculature. Living physiology induces both passive and active muscle tone, altering the stiffness of the muscle even in relaxed states. In addition to the forces generated along the length of the muscle, moderate activation can dramatically change the transverse compressive stiffness of the muscle. The mechanical properties of tissue change post-mortem, and for muscle tissue specifically, PMHS cannot be used to investigate the effect of muscle activation on impact of a blunt trauma NLW. Skin and fat composition and stiffness may also differ between living humans and cadavers. All of these differences may affect the RSI of blunt trauma NLWs.

For example, it has been estimated that just a 6% activation, as measured by electromyography (EMG), can increase the transverse compressive stiffness of the biceps brachii muscle by 200% [1]. Through the combined effects of increased longitudinal stiffness (affecting the regional coupling and structural recruitment) and increased transverse stiffness, living passive muscle tone and muscle activation have the potential to affect the overall structural behavior and force transmission within the thorax, particularly in blunt impact. Previous experimental work at UVA with a porcine model has demonstrated that muscle activation can increase the overall compressive stiffness of the thorax under blunt impact loading up to two times, depending on the impact location and loading penetration [2], [3], [4]. By changing the overall compressive stiffness of the thorax, the musculature will have a direct effect on the forces transmitted—and strain induced—in the underlying organs and skeletal structures.

One of the challenges in quantifying and modeling changes in muscle stiffness is the wide range of possible values, depending on the degrees of activation. For example, the “resting” state of a particular muscle may be different for a person lying supine compared to standing at ease, depending on the role of the muscle in maintaining postural stability. In addition, the muscle activation baseline level may be influenced by the activity or laden state of an individual at any given time. For example, the minimum activation state of the thoracic musculature may be different for a person standing while carrying a pack, compared to a person standing unladen. Thus, to understand how the muscle model should be modified to represent the living physiological state, the change in muscle stiffness should be quantified under various personnel and activity scenarios spanning those anticipated to be represented by the model.

Aims

The goals of this study are to evaluate the differences between PMHS and live human tissue under blunt impact, and to investigate the role muscle activation plays in blunt trauma mechanics. The findings will be used to develop a transfer function to account for the effects of muscle activation state. This will be accomplished by estimating the mechanical properties of human tissue at extreme conditions by scaling from correlates between living human tissue and cadaveric tissue at mild conditions.

The specific aims of this research to achieve that goal are to:

1. Perform shear wave elastography (SWE) experiments to quantify how a change in muscle activation can affect the *in vivo* and *in situ* soft tissue stiffness properties of the thorax.
2. Perform low-severity blunt impact tests to quantify how a change in muscle activation can affect the *in vivo* and *in situ* dynamic response of active and passive soft tissue.
3. Perform high-rate, high-deformation mechanical tests on *ex situ* cadaveric soft tissue to characterize non-linear, viscoelastic behavior of the passive tissue.
4. Translate the results from Aim 3, along with the relationships established in Aim 1, to develop a dynamic, high-deformation constitutive model for *in vivo* superficial soft tissue of a living human. This constitutive model can be validated in the future using results from dynamic blunt impact tests in Aim 2.

Aim 1: Shear Wave Elastography in Volunteers and Cadaveric Tissue

Overview

Shear wave elastography is a minimally invasive technique that can be used to measure soft tissue stiffness. SWE was used to compare the stiffness in volunteers during different muscle activations with atonic, cadaveric tissue in different postures. Muscle activity is also measured in the volunteers to develop a relationship between the amount of activation and stiffness that can be used to predict tissue stiffness across different dynamic activities.

Methods

Test Subjects

The volunteer study was approved by both the University of Virginia Institutional Review Board for Health Sciences Research (IRB-HSR) and the Department of Navy Human Research Protection Official (HRPO), and all volunteers supplied written consent before beginning the study. Twenty, healthy male volunteers completed this study. Inclusion criteria included no history of thoracic injury or surgery, BMI of 20 to 30kg/m^2, aged 18 to 40 years, and capable of completing moderate amounts of exercise.

The cadaver study was approved by the UVA Center for Applied Biomechanics cadaver protocol committee and the University of Virginia IRB-HSU. The study included four male PMHS, with inclusion criteria of BMI of 20 to 30kg/m^2 and no previous thoracic injury or surgery (Table I: Additional information about the PHMS used throughout the study).

Table I: Additional information about the PHMS used throughout the study

Specimen	Age (yrs)	Height (in)	Weight (lb)	BMI (kg/m^2)	Notes
PMHS 1	70	70	159	22.8	
PMHS 2	58	71	177	24	
PMHS 3A	71	72	211	28.6	Ostomy bag on right side
PMHS 3B	56	69	214	31.6	Obese

Volunteer Testing Procedure

For the SWE volunteer study, all testing was completed in one appointment. Anthropometry measurements were taken of each subject and included measurements of overall stature and weight, as well as measurements of the shoulders, chest,-and waist. Body fat calipers measured fat thickness on the anterior right biceps brachii, the posterior right triceps brachii, inferior to the right scapula and superior to the right iliac crest (Appendix 1).

Muscle activity and stiffness were measured for the following six muscles: pectoralis major, rectus abdominis, external oblique, upper trapezius, lower trapezius, and latissimus dorsi (Figure 1). All measurements were taken on the right side.

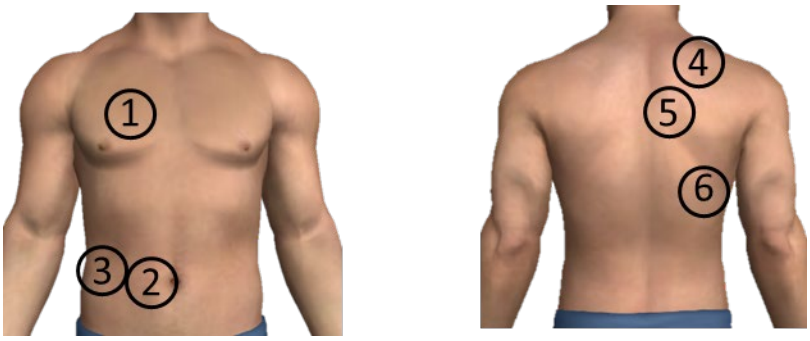

Figure 1: The six muscles of interest: 1. Pectoralis major, 2. Rectus abdominis, 3. External oblique, 4. Upper trapezius, 5. Lower trapezius, and 6. Latissimus dorsi

For each muscle of interest, a research team member demonstrated the proper technique to activate each muscle using a cable weight system (*Table II*). The subject determined their maximum weight per muscle; the maximum weight was defined as what the subject could comfortably hold for five seconds with shaking or straining. The maximum weight and 50% maximum was recorded for each subject and all muscles (Appendix 2).

Table II: Muscle of interest and corresponding exercise to activate each muscle

Muscle	Activity
Pectoralis Major	Pectoralis fly
Rectus Abdominis	Weighted crunch
External Oblique	Lateral bend
Upper Trapezius	Shoulder shrug
Lower Trapezius	Bent-over row
Latissimus Dorsi	Lat. pull down

EMG activity was recorded at each of the six muscle locations. The skin below the EMG sensor was abraded and cleaned with alcohol to ensure the best connection between the electrodes and the skin. EMG sensor locations were determined based on literature and applied to the same location for each subject (Appendix 3). The SWE measurement locations were 4cm off the center of the EMG sensor (Appendix 4). The three anterior markers—pectoralis major, rectus abdominis, and external oblique—were applied first to allow for the supine SWE measurements. With the subject supine and still, five sets of EMG and SWE recordings were taken at each of the three anterior muscles.

The remaining EMG sensors were applied to three posterior muscles: upper trapezius, lower trapezius, and latissimus dorsi. The next set of activation and stiffness measurements were taken with the subject passively standing with all of the muscles relaxed. Again, five EMG and SWE measurements were taken at each of the six muscle locations with the subject remaining passive and still.

The next set of measurements involved isometric muscle contractions using the cable weight system. For 100% activation (i.e., the previously determined maximum weight), the subject lifted and held the weight in the final position for approximately 5 seconds. The EMG sensor recorded

the muscle activation throughout the entire lift, and a SWE measurement was taken. The subject was then instructed to relax and lower the weight. This was repeated four additional times for 100% activation for a total of five measurements. For the same muscle, the weight was reduced to 50% of the maximum, and this process was repeated five times at 50% activation. Three repeated passive measurements were taken with the subject standing with relaxed muscles after the active measurements. This completed the isometric contractions for a single muscle, and these steps were repeated for four of the remaining muscles (rectus abdominis was completed at the very end). The muscles were measured in the following order for all subjects: pectoralis major, latissimus dorsi, lower trapezius, upper trapezius, external oblique, and rectus abdominis (after dynamic exercises).

After the isometric contractions, the subject completed the dynamic exercises : walking, running, and jumping. Muscle activity was measured at each of the six locations while the subject walked at 2.5 mph on the treadmill for 30 seconds using the EMG sensors. Muscle activity was again measured while the subject was running at 6.0 mph for 30 seconds. Subjects were instructed to walk and run naturally on the treadmill. The final dynamic activity was jumping; the subjects were instructed to jump as high as possible without a running start. To jump, the subject bent their legs, swung their arms, and extended their hands above their head to reach for the ceiling. The subjects completed three jumping trials. During each jump, muscle activity was recorded using the EMG sensors. No SWE recordings were taken during dynamic activities due to the motion of the subject and tissue.

To complete the sixth muscle (rectus abdominis) measurement, the subjects then returned to the isometric contractions. Before the weighted crunch, EMG and SWE measurements were taken of the rectus abdominis while the subject braced their core while standing. The subject was instructed to brace their core as if they were about to be impacted with a soccer ball. EMG and SWE measurements were taken for five bracing trials. The subject then completed the final isometric muscle activation—weighted crunch—for the rectus abdominis. Five EMG and SWE measurements were taken at 100% activation, five measurements at 50% activation, and finally, three repeated passive measurements. This completed the posterior muscle activation recordings, and the subject removed the posterior muscle sensors.

The last set of measurements were taken while the subject stood wearing a backpack loaded with 25 pounds of books. Five EMG and SWE measurements were recorded at the three anterior muscles while the subject stood passively wearing the backpack. This completed all of the muscle activation recordings, and the subject removed the remaining anterior sensors. Finally, with the subject supine, SWE measurements of the liver and subcutaneous fat at the rectus abdominis were recorded.

The test matrix for SWE measurements and EMG signals explains the data collected from each activity and muscle (Table III). The anterior muscle locations included the pectoralis major, rectus abdominis, and external oblique.

Table III: The test matrix for the SWE and EMG measurements for the volunteer study

Subjects	Activities	Muscle Locations	Repetitions	# SWE Measurements	# EMG Signals
20 Volunteers	Supine	3 Anterior muscles	5	15	15
	Passive	6 muscles	5	30	30
	100% MVC	6 muscles	5	30	30
	50% MVC	6 muscles	5	30	30
	Passive Repeat	6 muscles	3	18	18
	Backpack	3 Anterior muscles	5	15	15
	Bracing	Rectus Abdominis	5	5	5
	Additional SWE Measurements	Liver	5	5	-
		Subcut. Fat	5	5	-
Total Measurements				**3,060**	**2,860**

PMHS Testing Procedure

The PMHS testing protocol matched the volunteer protocol but with the absence of EMG recordings, because atonic muscle has no electrical activity. Additionally, all SWE measurements on the cadaver were done bilaterally. Each anterior SWE location was marked on the cadaver using the same body landmarks and measurements as the volunteers. The first set of SWE measurements were taken with the cadaver supine. Five SWE measurements were taken at each of the six anterior muscles (three muscles, both right and left sides). With the cadaver supine, the five liver and subcutaneous fat SWE measurements were taken. Before the position of the cadaver was altered, the impacts (more details to follow in Aim 2) were completed at each muscle location.

After all supine measurements were complete, the PMHS was then hoisted, with support from the head, into a seated position to mimic the passive standing position of the cadaver. With the cadaver in the seated position, the remaining posterior SWE locations were measured and marked on the cadaver; the anthropometry taken from the volunteers was completed on the cadavers in the seated position as well, but some measurements were excluded (Appendix 1). The SWE measurements were then taken at the twelve muscle locations, with five separate measurements per location. The impacts were then completed before the cadaver was flipped into a prone position.

With the prone cadaver, the final SWE measurements were recorded on the six posterior muscle locations. Final impacts were completed on the prone cadaver.

The total test matrix for SWE measurements explains the data collected from each position and muscle (Table IV). The anterior muscle locations included the pectoralis major, rectus abdominis,

and external oblique. The posterior muscle locations included the upper trapezius, lower trapezius, and latissimus dorsi.

Table IV: The test matrix for the PMHS SWE study

Subjects	Position	Muscle Locations	Repetitions	Bilateral Measurement (Y/N)	# SWE Measurements
4 PMHS	Supine	3 Anterior muscles	5	Y	30
	Passive/Seated	6 muscles	5	Y	60
	Prone	3 Posterior muscles	5	Y	30
	Additional SWE Measurements	Liver	5	N	5
		Subcut. Fat	5	N	5
Total Measurements					**520**

Equipment

Shear Wave Elastography System

All SWE measurements were recorded with an Aixplorer Multiwave ultrasound machine by Supersonic Imagine (Figure 2). Muscle SWE images were taken with the SuperLinear SLH15-4 probe with the musculoskeletal-muscle settings (SWE Opt: Penetration). Subcutaneous fat images were taken with the SuperLinear SL20-6 probe with general settings (SWE Opt: Standard). The liver images were taken with the Single Crystal Curved XC6-1 probe with general settings (SWE Opt: Standard).

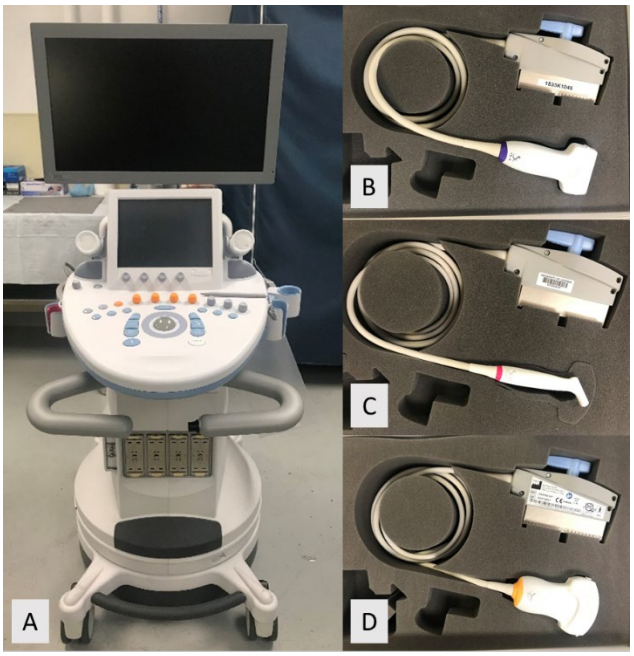

Figure 2: Shear wave elastography ultrasound machine (A) and probes – SuperLinear SL15-4 (B), SuperLinear SLH20-6 (C), and Single Crystal Curved XC6-1 (D)

Electromyography System

All muscle activity was recorded with a Delsys Trigno Avanti EMG system (Figure 3). The system included six wireless Trigno Avanti wireless EMG sensors that attached using an adhesive double-sided tape (sample rate = 2000 Hz).

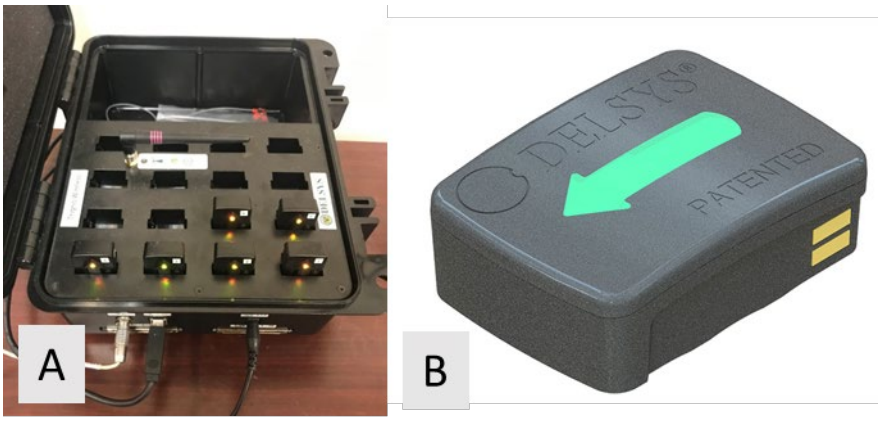

Figure 3: Delsys Trigno EMG system (A) with the wireless sensor (B)

Exercise Equipment

Weighted activities were performed using an XMark Functional Trainer Cable Machine (XM-76260) (Figure 4). Walking (2.5 mph) and running (6.0 mph) tasks were performed on a SOLE F80 treadmill (Figure 4).

Figure 4: (Left) XMark Functional Trainer Cable Machine; (Right) SOLE F80 Treadmill

Data Analysis

Shear Wave Elastography

Because shear stiffness and shear wave velocity are directly proportional, the output from the SWE machine was set to wave speed. The average shear wave velocity for each image was calculated using a custom Matlab script, which involved selecting the region of muscle within the entire B-mode image, calculating the shear wave velocity of each pixel in this region using the associated color bar values, and averaging the velocity at each pixel within the region of interest.

For statistical analysis of SWE between the volunteers, a two-sample paired t-test was used to compare statistically significant differences across all activities ($\alpha = 0.01$).

EMG Data

The EMG sensors measure the electrical activity of the muscle associated with activation in a voltage. Each signal was first filtered using a bandpass filter between 20 and 450Hz, and then the signal was full-wave rectified. To compare signals across different subjects, the signals were first normalized to a percentage of maximum activation. This normalizing factor is referred to as the maximum voluntary contraction (MVC). For this study, the MVC was defined as the average activation during the 100% maximum weight lift. For each of the five trials, MVC was calculated as the average voltage during the final three seconds of activation. The final three seconds were selected because the subject was instructed to release the weight after the SWE image was captured, and these three seconds corresponded to the activation associated with that SWE image. These five averages were then averaged again to determine the MVC associated with that muscle. Each filtered and rectified signal was then divided by the average MVC to convert into normalized signals with units of percent of MVC.

For the 100% and 50% isometric muscle contractions and rectus abdominis bracing, the average EMG activity was calculated using the average of the final three seconds of activation (as described above). For the passive, supine, passive repeat, backpack, walking, and running signals, the average EMG activation was the average over the entire signal. For jumping, the average EMG activation was the average during the region of activation.

For statistical analysis of EMG between the volunteers, a two-sample paired t-test was used to compare statistically significant differences between all activities and the passive response, as well as difference between 50% and 100% MVC ($\alpha = 0.01$).

Results

Anthropometry

The volunteer subjects and PMHS subjects had similar anthropometry for most measurements; however, the PMHS were on average older and heavier and had a larger chest and waist measurements than the volunteer subjects (Table V). The PMHS subjects also had larger body fat measurements at all four locations compared to the volunteer subjects (Table VI).

Table V: Volunteer and PMHS anthropometry results

	Volunteer (Mean ± 1 SD)	**PMHS (Mean** ± 1 SD)
Age (yr)	26.2 ± 5.3	63.8 ± 7.9
Height (in.)	70.6 ± 2.1	70.5 ± 1.3
Weight (lb.)	170.1 ± 22.9	190.3 ± 26.8
BMI (kg/m^2)	23.9 ± 2.5	26.9 ± 3.9
Shoulder height (cm)	148.1 ± 4.6	-
Shoulder length (cm)	19.2 ± 3.7	21.4 ± 4.1
Shoulder circumference (cm)	115.4 ± 7.2	113.3 ± 9.8
Shoulder breadth (cm)	42.6 ± 1.9	41.9 ± 2.4
Chest height (cm)	132.6 ± 4.2	-
Chest circumference (cm)	98.4 ± 6.5	104.9 ± 9.3
Chest breadth (cm)	32.1 ± 2.1	34.0 ± 2.7
Chest depth (cm)	21.9 ± 3.8	24.8 ± 1.2
Waist length (cm)	44.8 ± 7.8	49.4 ± 2.4
Waist circumference (cm)	85.4 ± 7.2	109.6 ± 13.8
Waist breadth (cm)	30.3 ± 2.6	37.2 ± 3.4
Waist depth (cm)	21.5 ± 2.4	29.4 ± 5.8

Table VI: Volunteer and PMHS body fat results

	Volunteer (Mean ± 1 SD)	**PMHS (Mean** ± 1 SD)
Back of arm (mm)	8.7 ± 3.1	18.0 ± 11.5
Front of arm (mm)	4.2 ± 1.4	10.8 ± 6.2
Scapula (mm)	11.1 ± 4.0	17.8 ± 6.9
Waist (mm)	13.4 ± 5.2	28.4 ± 13.1

Volunteer Results

EMG Results

The average passive, passive repeat, and supine muscle activity across all muscles and all subjects were very similar (7.8 ± 4.0, 7.8 ± 3.7, 7.8 ± 2.1 % MVC, respectively). The average 100% and 50% MVC for all muscles and all subjects were 91.2 ± 6.2 and 47.3 ± 7.6 % MVC, respectively.

The average backpack muscle activity was slightly larger than the passive and supine activities, with an average activation of 12.7 ± 9.0 % MVC. The average passive activation for all muscles was not significantly different than the passive repeat or supine positions; however, the average 100% and 50% activations for all muscles were both significantly different compared with the passive condition (Figure 5). Additionally, the average 100% activation and 50% activations were significantly different for all muscles. The average activation per activity for each individual muscle is included in Appendix 5.

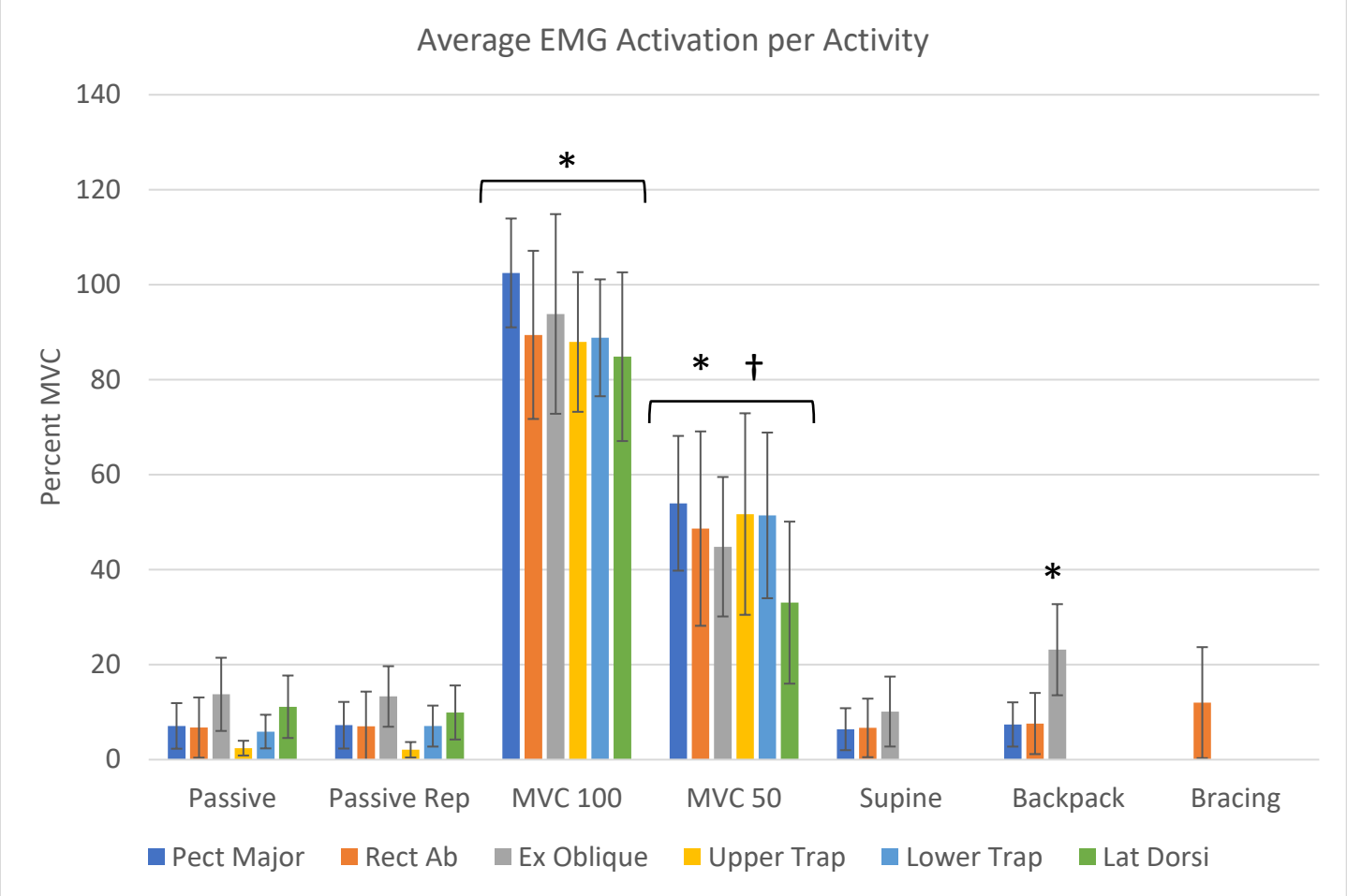

Figure 5: The average (mean ± 1 SD) muscle activation per activity for all muscles. (= significantly different from passive. † = significant difference between 100% and 50%)*

The average muscle activation was calculated for each of the muscles during the three dynamic activities: walking, running, and jumping (Figure 6). The average activation across all muscles during walking (11.5 ± 5.7 % MVC) was similar to the activation during the backpack activity, but

higher than passively standing. The average activation across all muscles while running (42.1 ± 20.8 % MVC) was similar to the 50% MVC activation. The average activation while jumping ranged from 67.6 % MVC in the latissimus dorsi to 230.7 % MVC in the external oblique, with an average across all muscles of 223.2 ± 75.7 % MVC. Due to the excessive noise during the dynamic movements, one signal out of the 120 was excluded from the running calculation, and 12 signals out of 120 were excluded for the jumping.

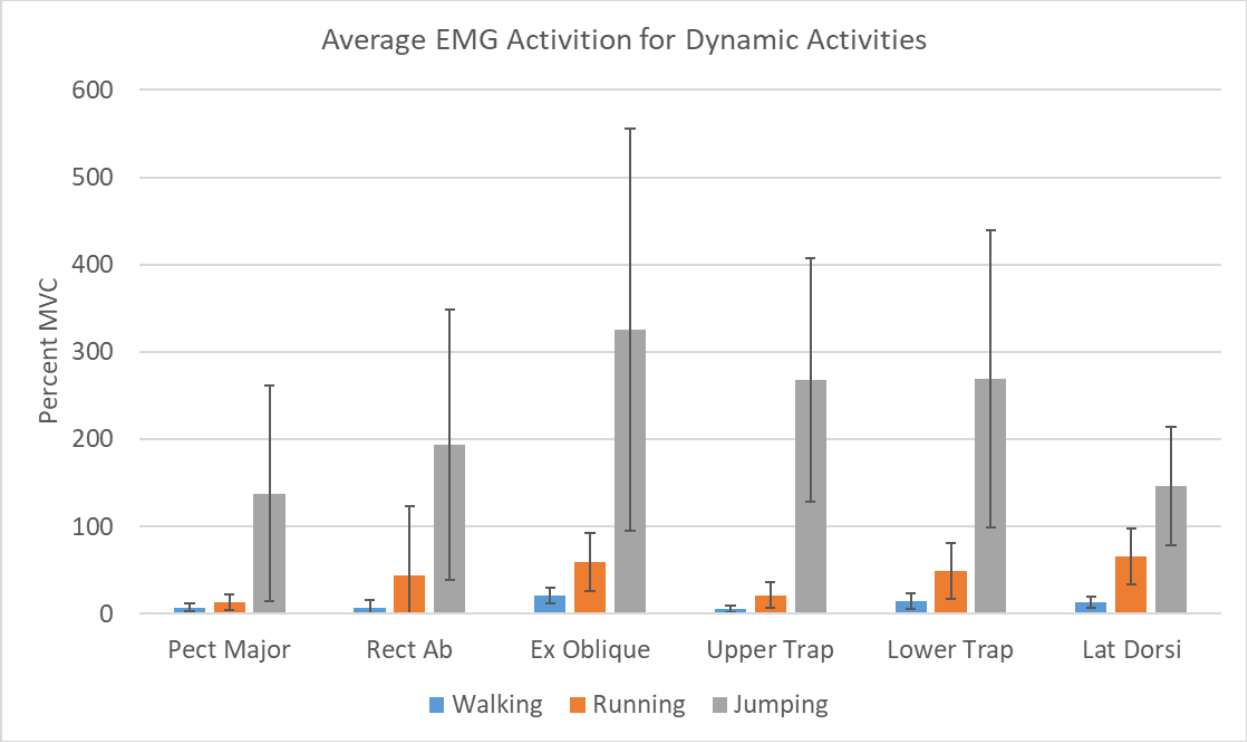

Figure 6: The average (mean ± 1 SD) EMG activation for each muscle during the dynamic activities

SWE Results

The average passive shear wave velocity was calculated for each muscle per subject; this average passive velocity was used to normalize the velocities in the other conditions. The averages are reported as the normalized velocity and the average of all isometric contractions (100% and 50% MVC) were greater than passive and supine measurements (Figure 7). The average absolute shear wave velocities is included in Appendix 6.

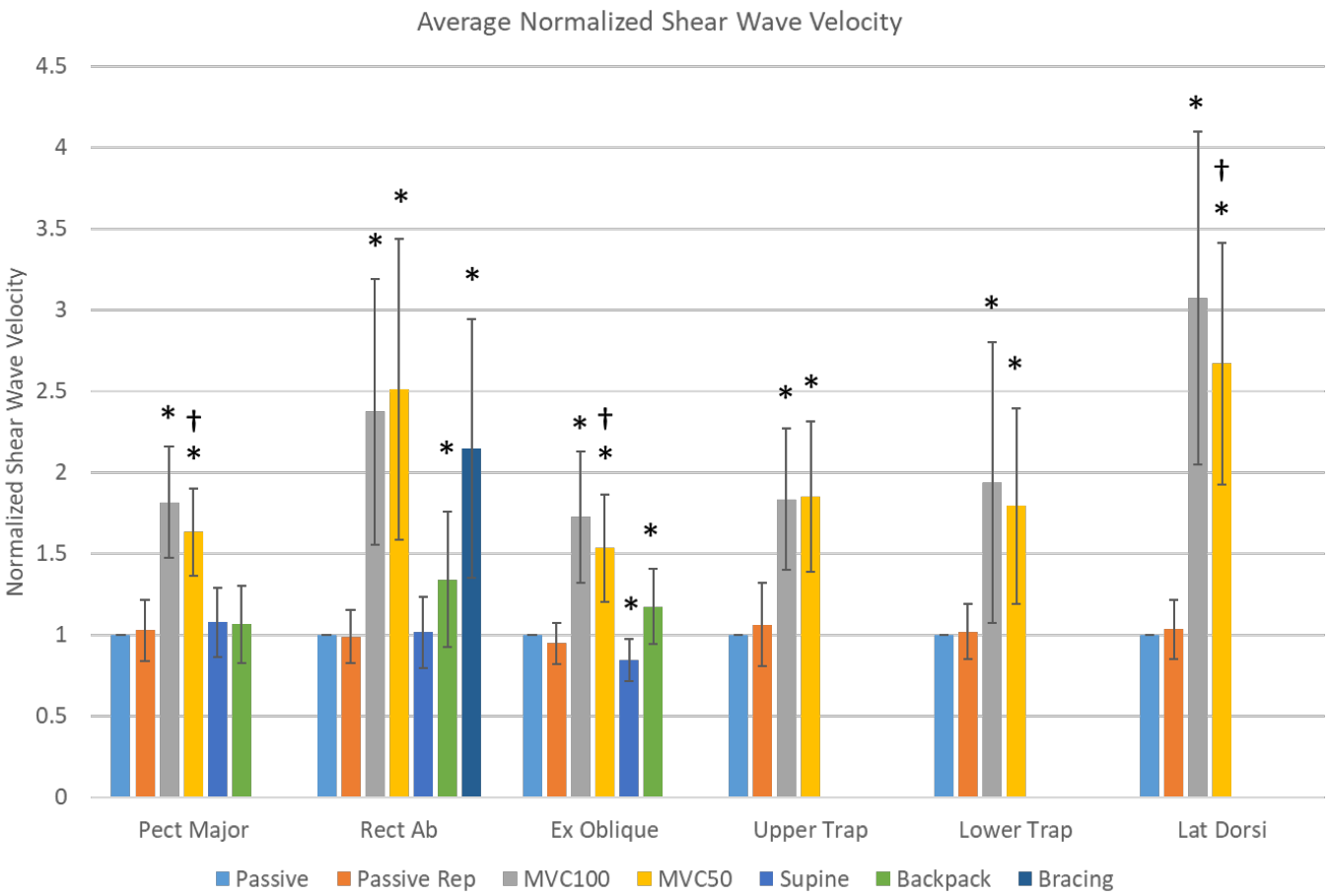

Figure 7: The average normalized shear wave velocity for all muscles and activities (= significantly different from passive. † = significant difference between 100% and 50%)*

The average shear wave velocity for both liver and subcutaneous fat at the rectus abdominis (2.1 ± 0.5m/s and 1.7 ± 0.4m/s, respectively) were both smaller than the shear wave velocity averaged over all subject's passive muscles (2.7 ± 0.7m/s) (Figure 8).

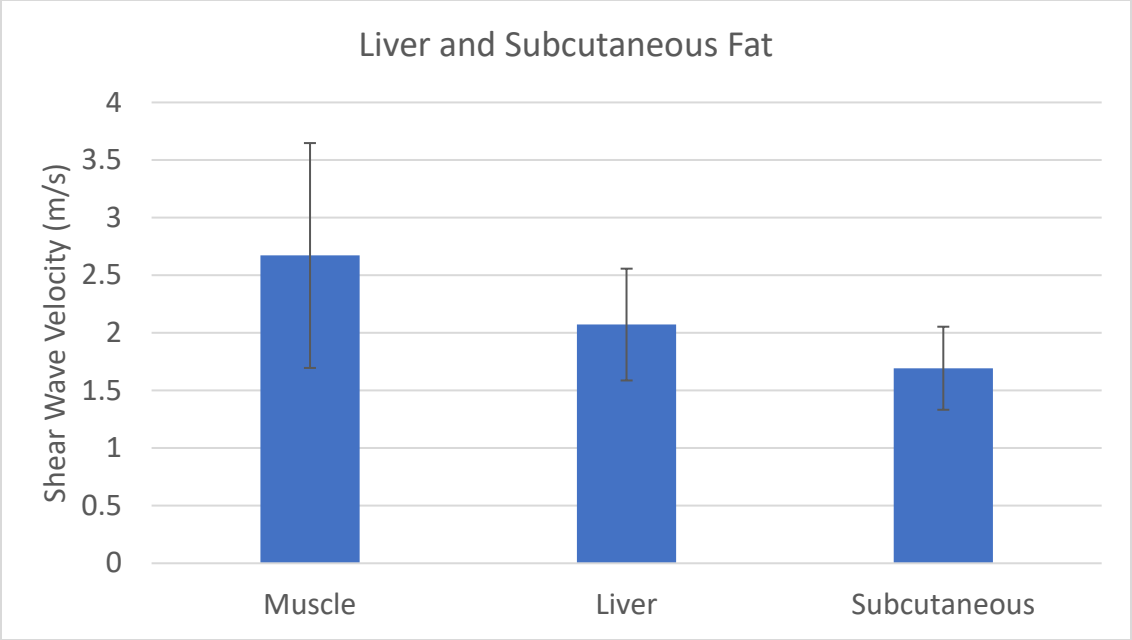

Figure 8: The average shear wave velocity of liver and subcutaneous fat compared to the average passive muscle shear wave velocity

To compare the muscle tissue stiffness across all activation levels, logarithmic functions were fit to individual subjects' muscles (i.e., one relationship for each muscle for each subject) and are included in Appendix 7 and Appendix 8. The average relationship between EMG activation and normalized muscle stiffness, or shear wave velocity, was calculated by averaging the individual fits for all subjects per muscle. The activation and normalized shear wave response for pectoralis major and external oblique are shown below (Figure 9), with the remaining relationships shown in Appendix 9. Relationships of the activation to absolute shear wave velocity are included in Appendix 10.

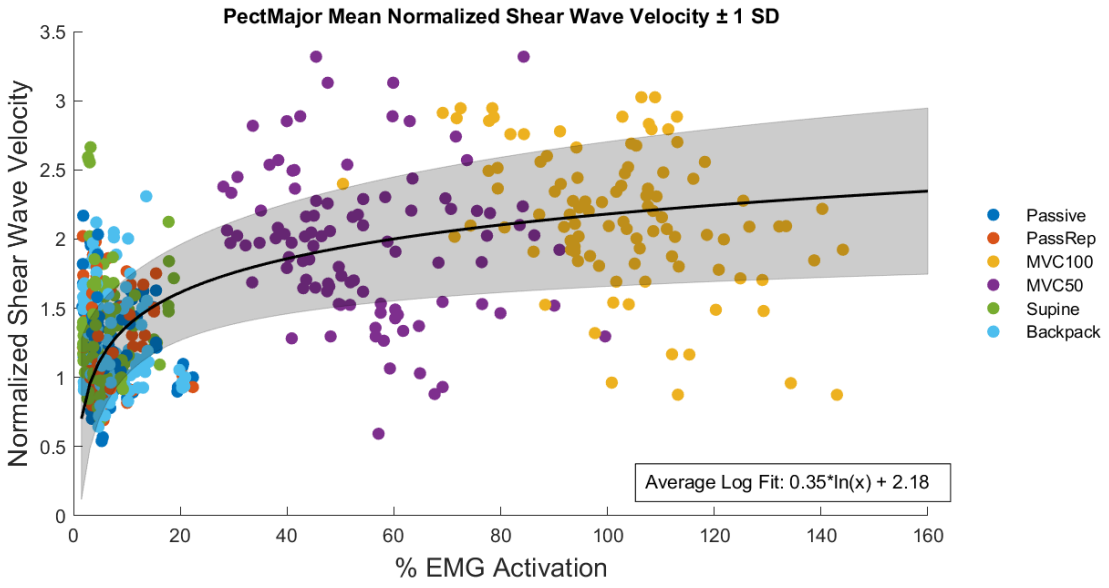

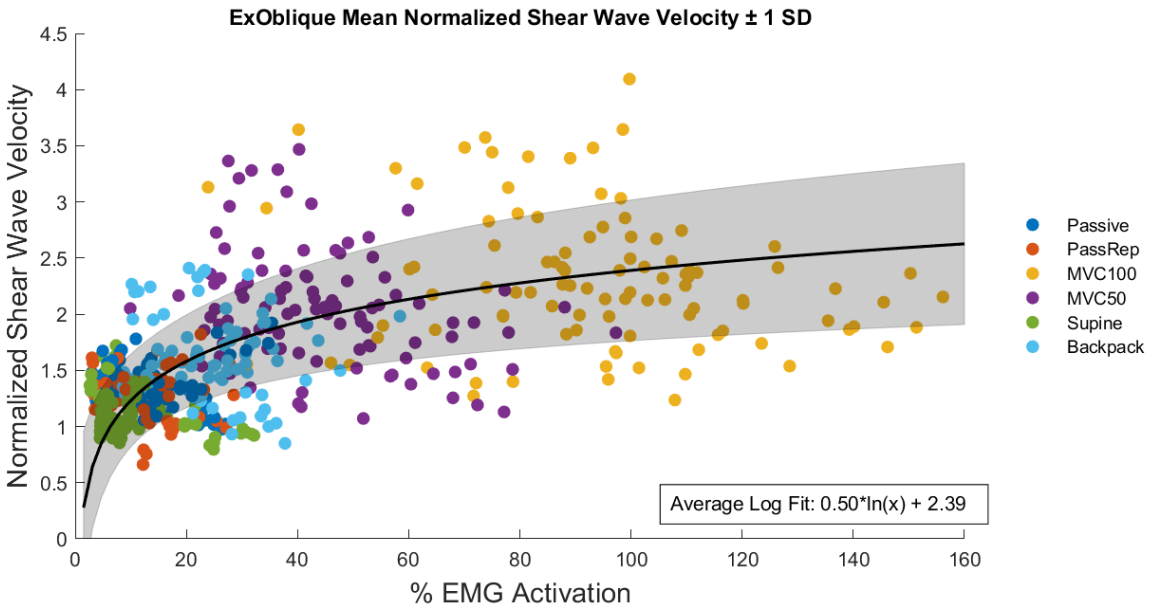

Figure 9: The average normalized shear wave velocity and muscle activation functions for pectoralis major and external oblique

Cadaver Results

Shear wave elastography measurements were taken bilaterally on all cadaver torsos. There was no signification difference between the right and left muscles of the cadavers in either the seated or the supine/prone positions (Figure 10). There was also no significant difference in shear wave velocity between the supine/prone position and the seated position for any muscle location. For the cadaver and volunteer comparisons, the cadaver right side SWE averages were compared to the matched right side measurements in the volunteers.

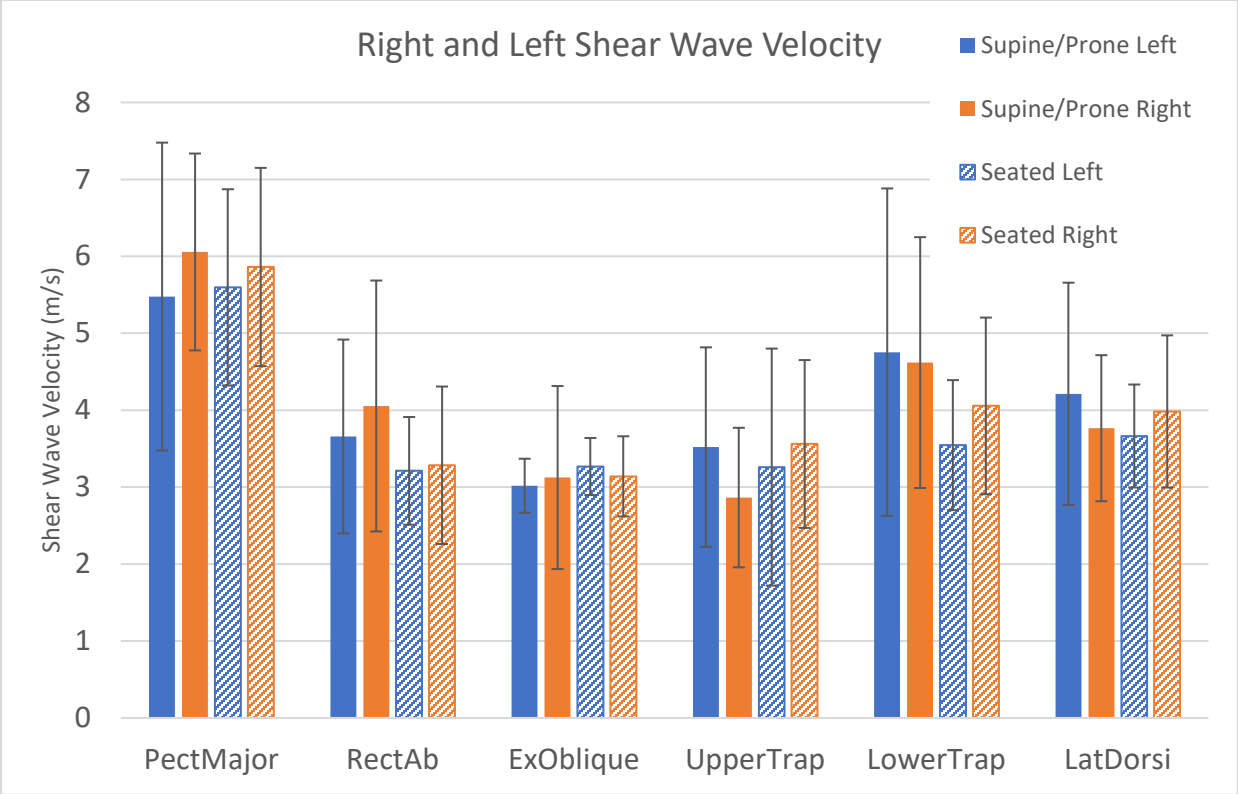

Figure 10: The average shear wave velocity for right and left muscles during the seated, supine, and prone positions

The average shear wave velocity for the PMHS in both seated or the supine/prone position (depending on anterior or posterior muscles) was higher than the volunteer velocities in the supine and passive conditions, with the exception of the upper trapezius (Figure 11 and Figure 12).

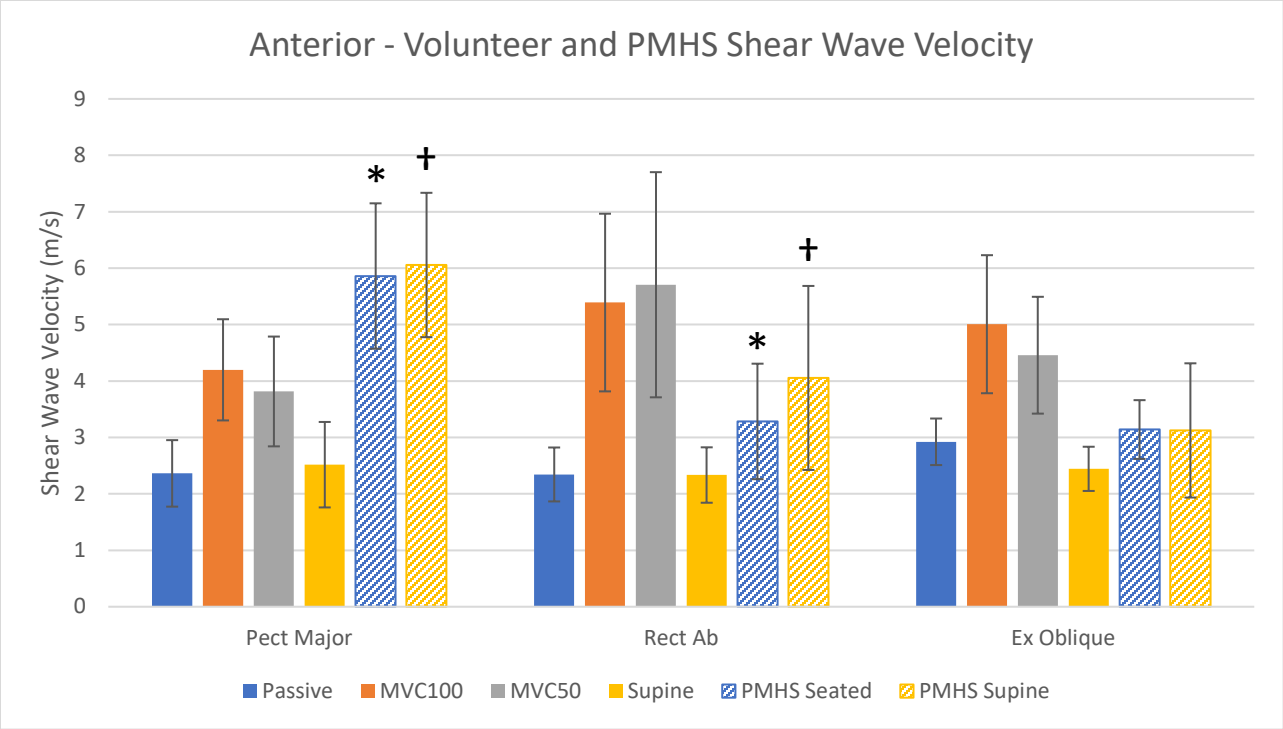

Figure 11: The average shear wave velocities for the anterior muscles for both the volunteer and PMHS subjects. (= significantly different from volunteer passive, † = significantly different from volunteer supine)*

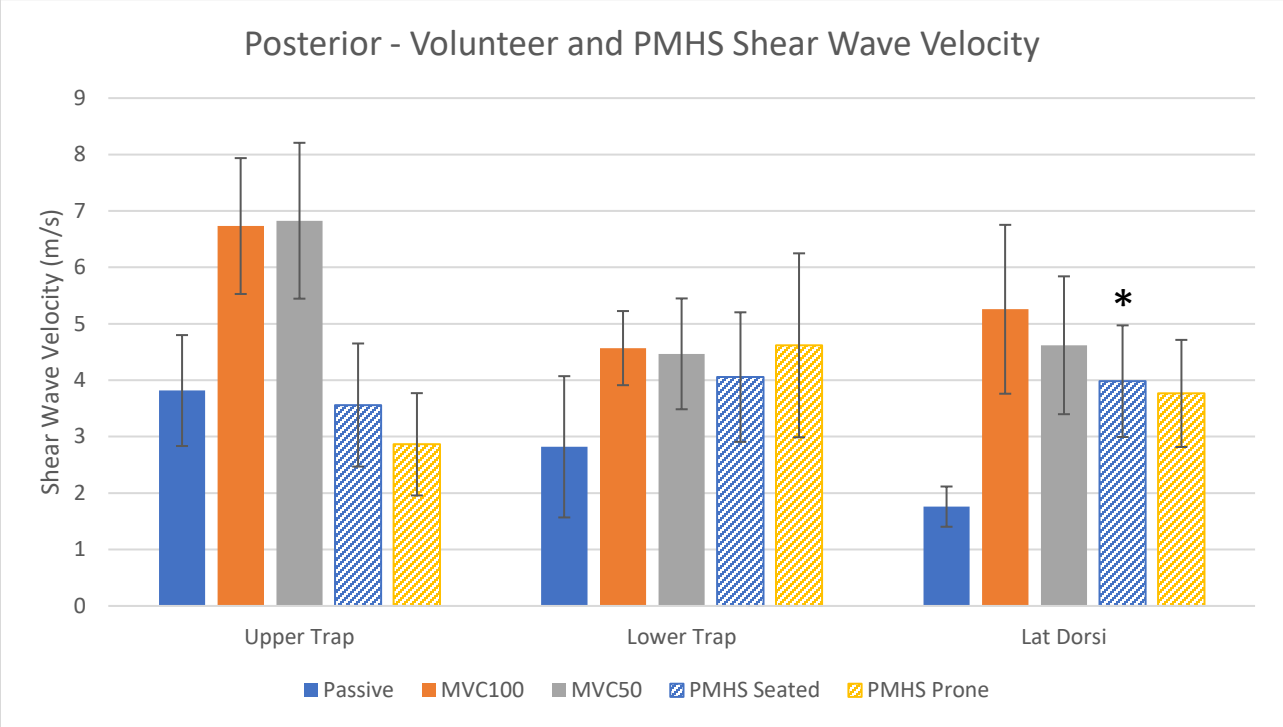

Figure 12: The average shear wave velocities for the posterior muscles for both the volunteer and PMHS subjects. (= significantly different from volunteer passive)*

The average shear wave velocities measured in the PMHS were larger than the volunteers' for passive muscle, liver, and subcutaneous fat; however, the average active muscle (100% and 50% combined conditions) shear wave velocity was greater for the volunteers than the atonic cadaveric tissue (Figure 13).

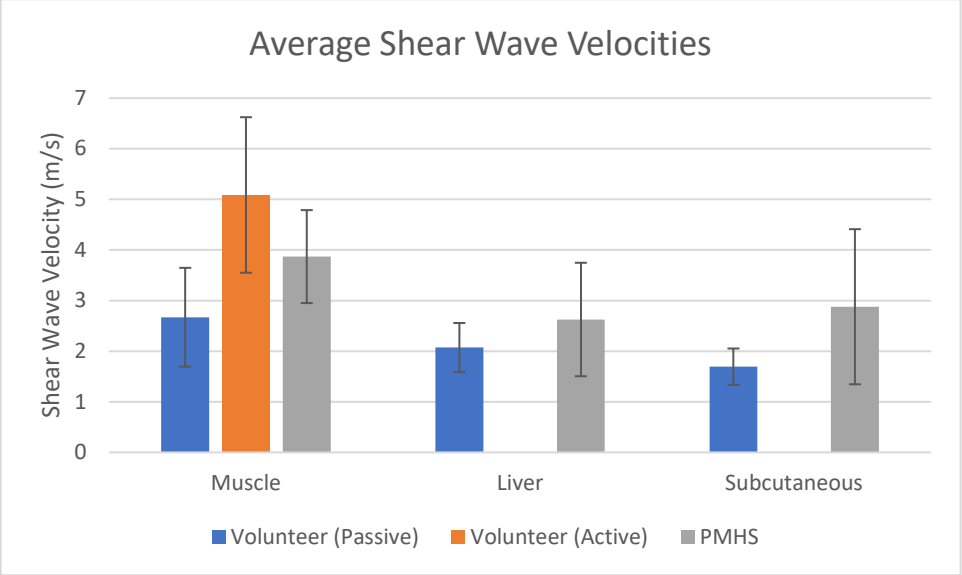

Figure 13: The average shear wave velocity for volunteer and PMHS across all tissues

Conclusions

Activation of thorax musculature was achieved using the cable weight system, with significant increases in EMG signal during the weighted tasks as well as the active tasks. Activation also increased during the dynamic tasks (walking, running, and jumping). The activation led to significantly increased tissue stiffness, as measured by SWE, in both the weighted and standing-while-laden tasks compared to the passive stiffness. The increase in stiffness as a function of action was described using logarithmic relationships for each muscle. This relationship allows prediction of muscle stiffness during dynamic tasks for which SWE was not recorded. SWE of liver and subcutaneous fat showed that both tissues were less stiff than passive muscle.

In general, cadaver tissue was stiffer than passive living tissue. In certain locations, PMHS tissue was analogous to contracted muscle tissue. The liver and subcutaneous fat was likewise stiffer in PMHS than in the volunteers. This indicates that some of the soft tissue properties currently implemented in human body models, which have been based on previous PMHS tests, may overestimate tissue stiffness.

Aim 2: Low-severity impacts in volunteers and cadaveric tissue, and higher-severity impacts in cadaveric tissue

Overview

Using the same isometric activations and passive postures as Aim 1, soft tissue response to impact was measured using a custom-built indenter device on both volunteers and cadaveric subjects. The handheld indenter was spring-power, stroke-limited and allowed a free-flight projectile to impact the torso of both volunteers and cadavers. The projectile was instrumented with an accelerometer to measure projectile accelerations, which allowed for calculation of force and displacement values. These low-severity impacts were designed to be non-injurious to the volunteers, and the test conditions were then repeated on cadavers. Additionally, the cadavers were impacted with a higher-severity impact.

Methods

Test Subjects

The volunteer study was approved by both the University of Virginia Institutional Review Board for Health Sciences Research (IRB-HSR) and the Department of Navy Human Research Protection Official (HRPO), and all volunteers supplied written consent before beginning the study. Ten healthy male volunteers completed this study, and these subjects were a subset of the 20 who completed the SWE volunteer study. Inclusion criteria again included no history of thoracic injury or surgery, BMI of 20 to 30kg/m^2, aged 18 to 40 years, capable of completing moderate amounts of exercise, and capable of receiving a torso MRI.

The cadaver study was approved by the UVA Center for Applied Biomechanics cadaver protocol committee and the University of Virginia IRB-HSU. The impactor study included the same four male PMHS used in the SWE study.

Testing Procedure

Volunteer Testing Procedure

For the impactor volunteer study, testing was completed over two separate appointments: a pre-test MRI and the impactor-testing day. Each subject completed a torso MRI scan prior to any impacts, and the medical scans were read by a licensed radiologist to ensure the absence of pre-existing conditions that would warrant exemption from the study. The MRI protocol included a large field of view axial T1-scan, a large field of view coronal STIR scan (detects inflammation), and coronal and axial Dixon scans (highlights fat and muscle). After scans were read and approved by the medical doctor, the volunteers completed the second day of testing, which included the non-injurious impacts.

During the impactor testing, the same six muscles were investigated: pectoralis major, rectus abdominis, external oblique, upper trapezius, lower trapezius, and latissimus dorsi. Again, all measurements occurred on the right side of the body. For each muscle of interest, the subject was asked to lift the same maximum weight estimated during the SWE testing to ensure the weight was still manageable and comfortable. All subjects used the same maximum and 50% weights during both halves of the volunteer study. Each impact location was matched to the SWE measurement locations using the same anthropometric measurements taken during Aim 1.

All of the impacts were delivered using a custom-built impactor that measured the projectile acceleration using an attached accelerometer and initial velocity using an attached optical velocity gate. The projectile was in free-flight before impact and was stroke limited, ensuring the projectile did not leave the indenter device. The spring compression was calibrated to deliver a 5.5m/s impact during all test conditions (5.6 ± 0.1m/s). The first set of impacts occurred with the volunteer supine, and the anterior three muscles were impacted. The subjects were instructed to remain passive. Two impacts were delivered to each muscle location. Before each impact, a research team member asked if the subject was ready and okay to proceed. At any point during the study, volunteers were able to remove themselves from the testing for any reason. No subjects exited the study early.

After supine testing, the volunteer switched to a prone position, and the three posterior muscles were impacted two times each. The subjects were instructed to remain passive while prone. The next set of impacts occurred with the subjects passively standing. While passive, all six muscles were impacted two times each.

The next measurements occurred during the isometric muscle activations. For a single muscle, the subject completed two 100% lifts and impacts, then two 50% lifts and impacts, and finally two repeated passive impacts. This process was then completed for the remaining five muscles. These isometric muscle activation impacts were delivered in the same order as the isometric SWE recordings, and the same order was used for all subjects. Rectus abdominis was the final muscle for the isometric contractions, and an additional pair of bracing impacts were delivered to the rectus abdominis. The bracing instructions were the same as those given during SWE testing.

After all of the impacts were complete, the subject was given a post-test questionnaire and was asked to complete the questionnaire at six hours, one day, and three days post-test. The questionnaire included questions on visibility, sensitivity, and bruising at the six impact locations (Appendix 11).

The total test matrix for the volunteer low-severity impact conditions explains the data collected for each activity and muscle (Table VII: The test matrix for volunteer impactor study.).

Table VII: The test matrix for volunteer impactor study

Subjects	Activities	Muscle Locations	Repetitions	# Impacts
10 Volunteers	Supine	3 Anterior muscles	2	6
	Prone	3 Posterior muscles	2	6
	Passive	6 muscles	2	12
	100% MVC	6 muscles	2	12
	50% MVC	6 muscles	2	12
	Passive Repeat	6 muscles	2	12
	Bracing	Rectus Abdominis	2	2
Total Measurements				**620**

PMHS Testing Procedure

Prior to any SWE or impactor testing, each of the cadavers completed the same MRI scan protocol as the volunteers after being completely thawed and brought to room temperature (approximately 65°F).

The PMHS testing protocol matched the volunteer protocol, but the PMHS had only three testing positions, supine, prone, and seated, matched to the volunteer supine, prone, and passive positions, respectively. All of the 5.5m/s (5.4 ± 0.2m/s) low-severity impacts were done on the right side of each cadaver, with the exception of PMHS 3A. Because of the ostomy bag on the right side, the low-severity impact (5.5 m/s) was delivered to the left rectus abdominis for PMHS 3A. This was done to ensure the best data for the matched condition between the volunteer and the PMHS tests. Additionally, the cadavers were also impacted with a higher-severity 11m/s (11.0 ± 0.2m/s) on the left side of the body. Again, this was switched for PMHS 3A, with the higher-severity (11m/s) impact delivered to the right rectus abdominis.

To ensure that varying temperatures did not have an effect on the stiffness of the muscle or superficial flesh, the superficial tissue temperature was recorded at each location prior to impactor and SWE tests. This was completed with the subjects in all three positions, and all of the recorded temperatures are provided in Appendix 12. The average tissue temperature during SWE and impacts was 59.8 ± 2°F.

All the impacts occurred after the SWE testing was complete in each position. The first set of impacts occurred with the subject in the supine position. After all of the SWE supine measurements were complete, the three right anterior muscle locations were each impacted three times per muscle with the 5.5m/s impact, and the three left anterior muscles locations were each impacted three times per muscle with the 11m/s impact. The cadaver was then hoisted into the seated position; again, after all of the SWE seated measurements were complete, the six right muscle locations were each impacted three times with the 5.5m/s impact, and the six left muscle locations were each impacted three times with the 11m/s impact. Finally, with the cadaver prone, each of the three right posterior muscle locations were impacted three times with the 5.5m/s impacts, and the three left posterior muscle locations were impacted three times with the 11m/s impacts.

The total test matrix for the PMHS impact conditions explains the data collected for each position, muscle, and severity (Table VIII).

Table VIII: The test matrix for the PMHS impactor study

Subjects	Position	Muscle Locations	Severity	Repetitions	# Impacts
4 PMHS	Supine	3 **Right** anterior muscles	5.5m/s	3	9
		3 **Left** anterior muscles	11m/s	3	9
	Passive/Seated	6 **Right** muscles	5.5m/s	3	18
		6 **Left** muscles	11m/s	3	18
	Prone	3 **Right** posterior muscles	5.5m/s	3	9
		3 **Left** posterior muscles	11m/s	3	9

Subjects	Position	Muscle Locations	Severity	Repetitions	# Impacts
Total Measurements					**288**

Equipment

Impactor Device

All impacts were delivered using a custom-built impactor device. This handheld, spring controlled, stroke-limited indenter device was designed to be easily maneuverable and allow for quick, repeated impacts (Figure 14). The capped barrel established a pre-determined maximum indentation depth to prevent unintended tissue damage or penetration. The impactor operator was able to move the device to be normal (i.e., perpendicular) and flush to each impact location on the torso to ensure repeatability of impact. The 3D-printed projectile (40mm diameter, 40g mass) was instrumented with a single direction accelerometer sensor (AC 7264B-2000T; Meggitt Sensing Systems) to measure the projectile's acceleration during each impact; the sensor gave the acceleration time history before, during, and after impact. Acceleration data was collected at 50,000Hz. The impactor device was also equipped with an optical velocity gate, which included an LED emitter-detector sensor pair (LTE-302, LTE-301; LiteOn Electronics Inc.). The projectile included an external fin, which passed between the emitter-detector sensor pair and shortly blocks the transmitted light; while the light is obstructed, the sensor shows a large and sharp drop in the measured voltage. The time of this obstructed light can later be used to calculate the initial velocity of the projectile before impact with the torso.

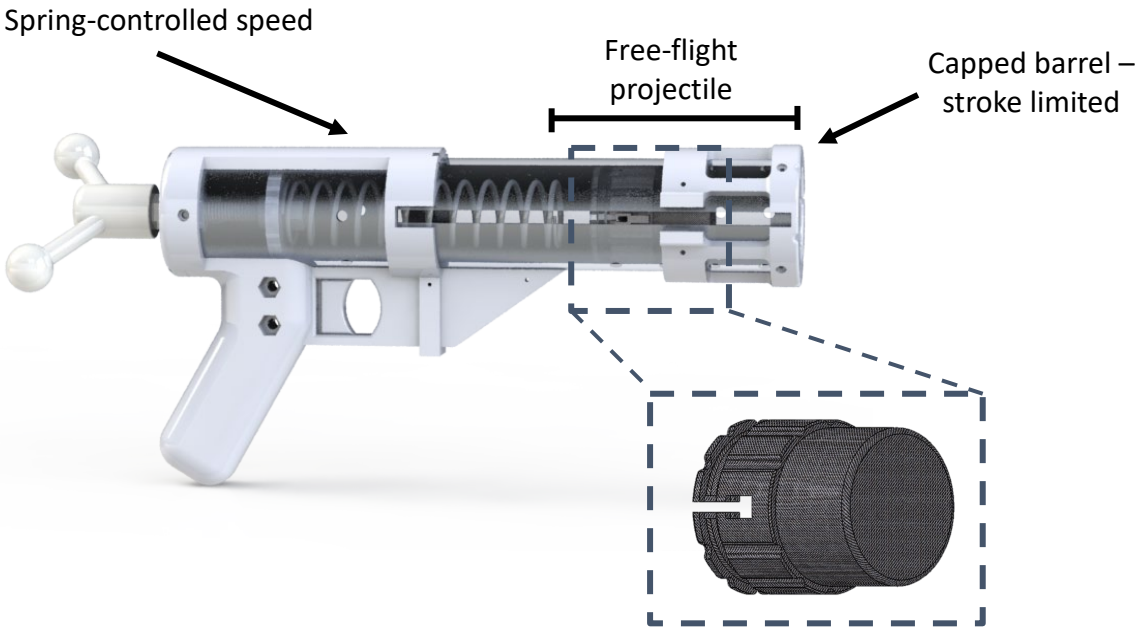

Figure 14: The custom-built impactor device used for all volunteer and PMHS impacts. This device was used for both low- and high-speed impacts by changing the spring

The impact device was validated to ensure the accuracy of the accelerometer in the projectile and the velocity calculated by the velocity gate (Figure 15). All validation was performed at the

highest impact speed (11m/s). The accelerometer reading was validated by impacting a load cell through two layers of Confor foam. The average discrepancy in peak force was 2.3% (10N) across 10 trials. The velocity gate was separately validated against high-speed video tracking. Over four trials, the velocity measured by the gate was 10.6 ± 0.4m/s, while the video tracking showed a true velocity of 10.8 ± 0.2m/s. The average error between velocity gate and video tracked velocity was 2.7%.

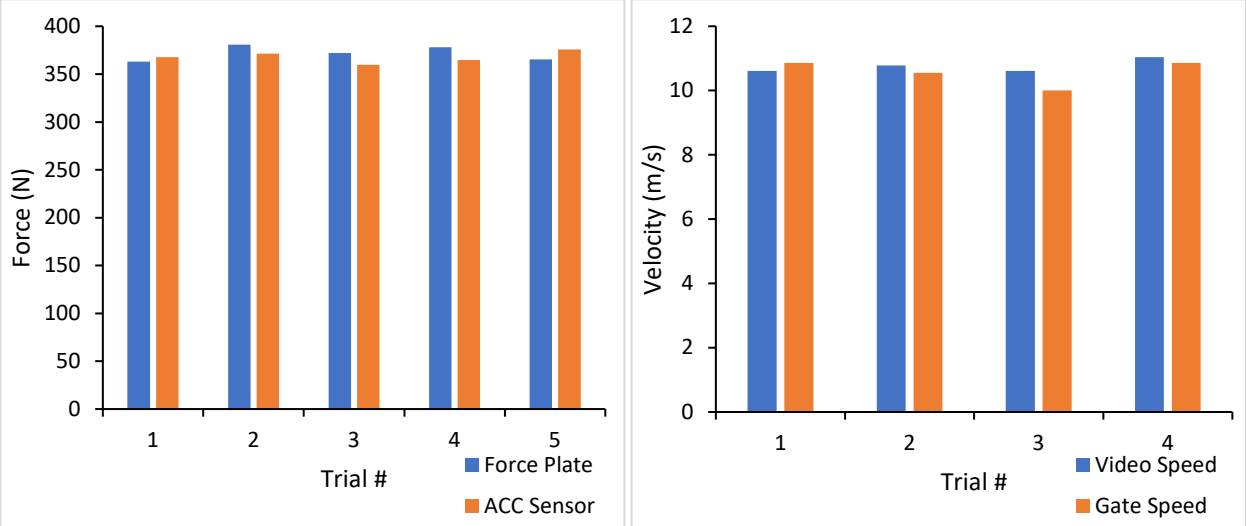

Figure 15: Validation of impactor data. (Left) Peak force measured by the accelerometer was validated against an external load cell. (Right) The velocity measured by the velocity gate was validated against high-speed video

Exercise Equipment

The cable weight system used for isometric contractions was the same system previously used with the SWE volunteer study (Aim 1).

Data Analysis

Impactor Device

Volunteer and PMHS acceleration data from the indenter were processed using custom Matlab code. The acceleration time history was filtered using a 4th-order Butterworth high-pass filter at 0.5Hz to remove bias and drift, and then filtered using a 4th-order Butterworth low-pass filter at 4000Hz. The choice of cutoff frequency was based on spectrum analysis. The filtered acceleration data was used to calculate force by multiplying by the known mass of the projectile (40g).

Initial contact with the skin was defined by the maximum of the second derivative of acceleration. Time was set to zero at this contact point to align all of the data traces. The acceleration signal was integrated to calculate the velocity of the projectile. Due to drift in the integrated signal, the initial velocity, calculated from the velocity gate, was used to correct the velocity of the projectile immediately before impact. The initial velocity at the gate was calculated by dividing the known length between fins (6.38mm) by the time the fin was blocking the LED signal between the emitter-detector sensor pair.

Displacement of the projectile was calculated as the integral of the corrected velocity signal. Indentation was defined as displacement after impact. To limit the effect of error inherent to double integration of acceleration data, final displacement was defined when the measured force dropped below a preset force threshold. This force threshold was defined as 150% of the noise floor.

The resulting force-time, displacement-time, and force-displacement curves were used to find the average response for each muscle and condition. Force-time and displacement-time corridors were generated as plus/minus one standard deviation from the mean at each time point. All acceleration time histories, from both 5.5 and 11m/s impacts, were analyzed using the same process explained above.

For statistical analysis of impact forces and depths between the volunteers, two-sample paired t-tests were used to compare statistically significant differences between all activities and the passive response ($\alpha = 0.05$). Paired t-tests were also used to evaluate differences between postures in the four PMHS. Finally, unpaired t-tests were used to compare passive and supine/prone volunteers to the matched seated and supine/prone PMHS, respectively.

Tissue Thickness

Tissue thicknesses were measured from the ultrasound B-mode images for each muscle at each different activity. Tissue depths were determined for skin, fat, and muscle. The average of each of these thicknesses was based on points taken from the B-mode images. Three distinct measurements were averaged on each picture to compute an average tissue thickness for that individual trial. This was repeated for the five trials at each activity (or three trials for repeated passive). The tissue thicknesses from the five trails were averaged to find the mean tissue thickness for skin, fat, and muscle for each subject at every muscle and activity combination.

Results

Volunteer Results

Across the volunteer impacts at 5.5m/s, indentation depths ranged from 3.4 to 18.4mm, with peak contact forces of 112 to 480N. Average passive indentation depths for the pectoralis major, upper trapezius, and lower trapezius (7.5 ± 1.6, 6.6 ± 1.6, 7.4 ± 0.8mm, respectively) were significantly lower than those in the rectus abdominis, external oblique, and latissimus dorsi (13.4 ± 1.7, 12.3 ± 1.5, 11.8 ± 1.5mm, respectively). Additionally, the indentation of in rectus abdominis was significantly greater than the latissimus dorsi. Conversely, the peak forces in the passive pectoralis major, upper trapezius, and lower trapezius (252.9 ± 83.4, 285.1 ± 58.6, 291.4 ± 41.3N, respectively) were significantly higher than those in the rectus abdominis, external oblique, and latissimus dorsi (161.6 ± 29.0, 188.4 ± 50.4, 179.8 ± 36.7N, respectively). In general, increasing activation led to significantly decreased indentation depth in the latissimus dorsi and lower trapezius, but 50% contraction of the pectoralis major increased indentation depth. Peak contact force was significantly decreased with activation in the pectoralis major and upper trapezius but significantly increased in the rectus abdominis (Figure 16).

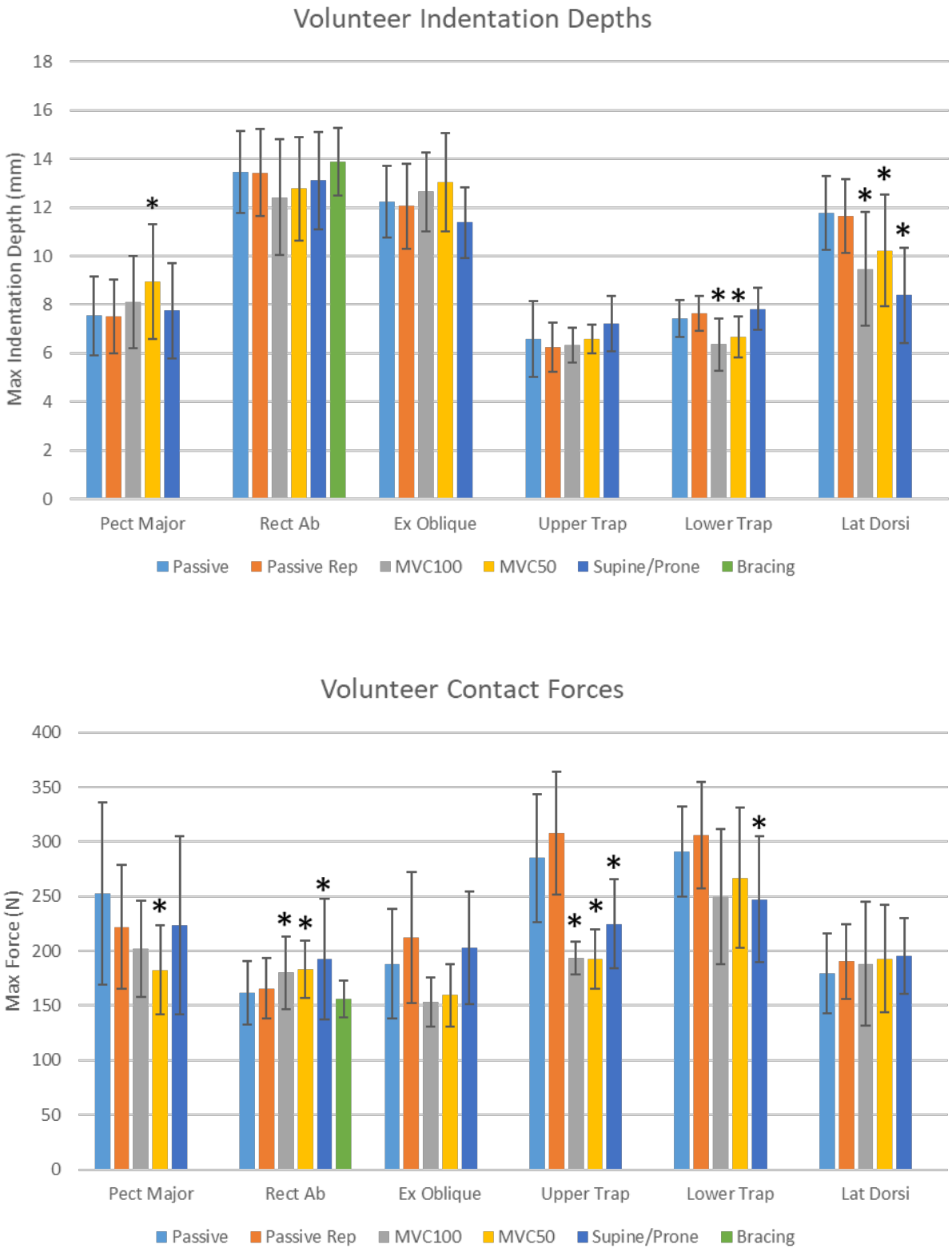

Figure 16: Average (mean ± 1 SD) peak indentation depth and contact force for volunteer impacts at 5.5m/s (= significantly different from passive for each muscle)*

Additionally, there were significant differences between passive and supine/prone positions (indentation depth: latissimus dorsi, contact force: rectus abdominis, upper trapezius, and lower trapezius). A complete tabulation of the maximum forces and displacements for each subject and condition are in Appendix 13.

For each volunteer, force and displacement histories were calculated as described above. An example dataset is shown below in Figure 17. Selected force-time and force-displacement curves are shown in Figure 18 below, with the full set of curves in Appendix 16 (force-time corridors) and Appendix 17 (force-displacement curves).

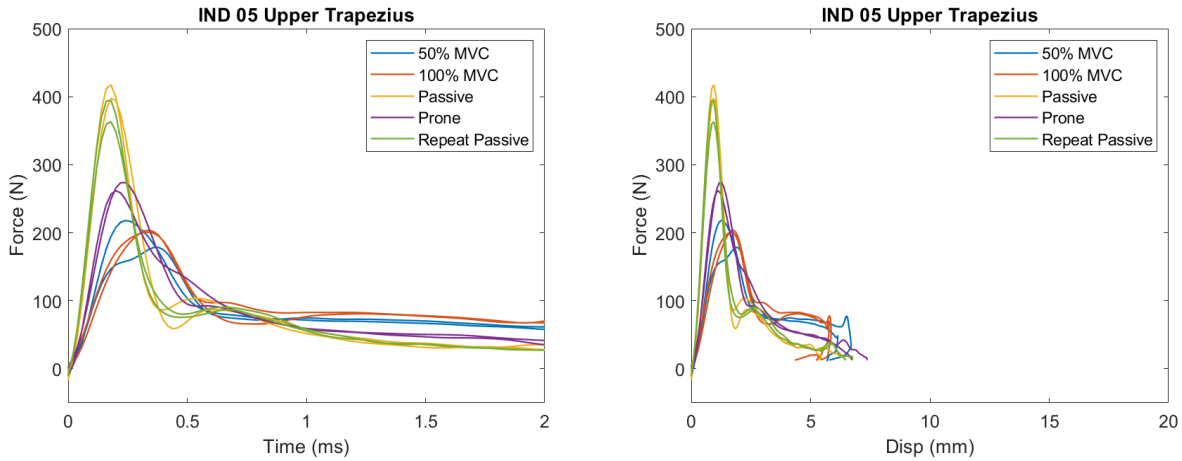

Figure 17: Example force-time and force-displacement curves for the upper trapezius of a single subject

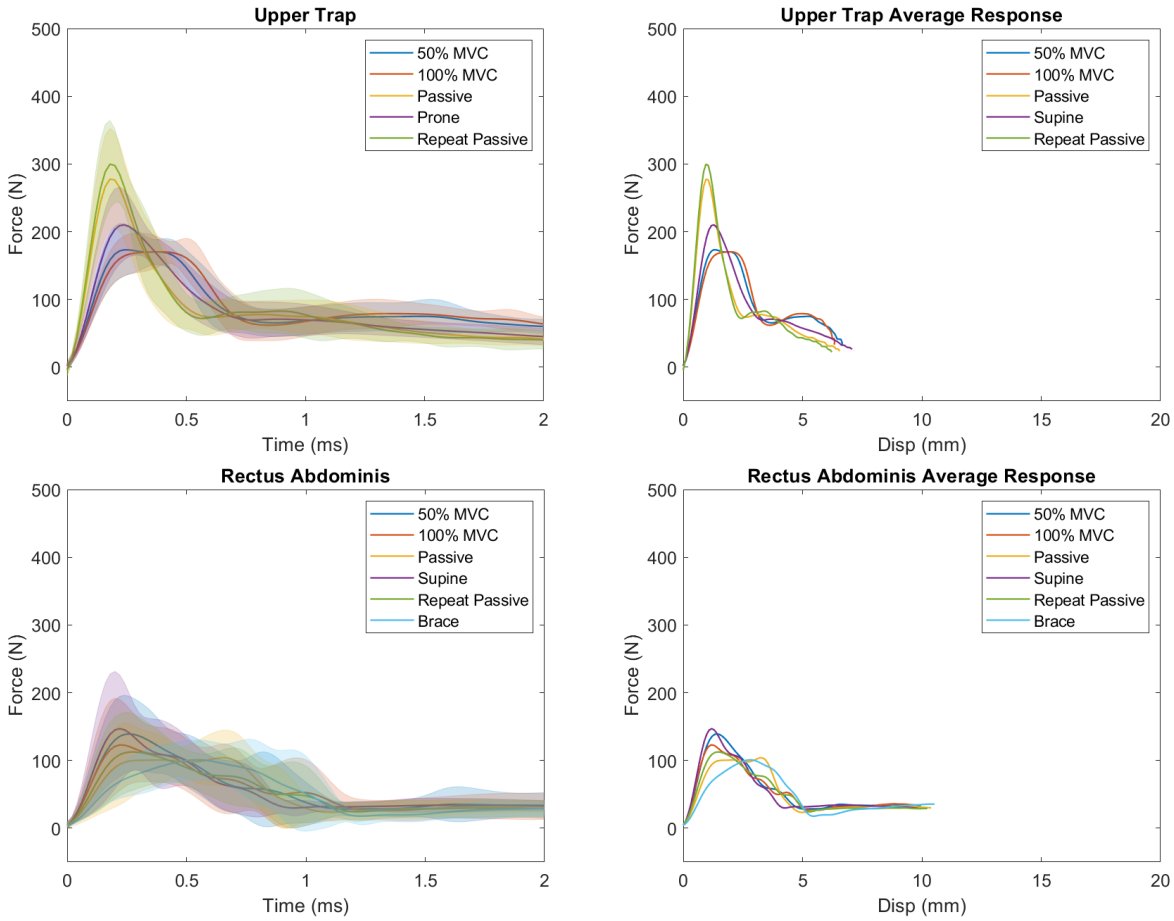

Figure 18: Force-time corridors and average force-displacement curves for the upper trapezius (top) and rectus abdominis (bottom)

Cadaver Results

In the PMHS impacts at 5.5m/s, indentation depths ranged from 2.1 to 12.7mm, with peak contact forces ranging from 103 to 633N. There were significant differences in impact conditions between testing postures. The indentation depth was significantly greater in the seated (10.1 ± 1.6mm) than prone (7.2 ± 1.3mm) position for the latissimus dorsi, but significantly less in seated (8.5 ± 0.3mm) than supine (9.2 ± 0.5mm) for the external oblique. There was a significantly higher max contact force in the prone/supine positions than seated for the rectus abdominis (supine: 247.2 ± 47.7N; seated: 151.0 ± 19.8N) and latissimus dorsi (prone: 205.3 ± 47.8N; seated: 177.6 ± 46.5N).

At the higher impact speed of 11m/s, indentation depths ranged from 5.3 to 23.4mm, while peak contact forces ranged from 438 to 1198N. There was significantly more indentation in the seated than prone positions for the latissimus dorsi (seated: 15.7 ± 3.1mm; prone: 10.0 ± 2.6mm) and lower trapezius (seated: 10.2 ± 3.7mm; prone: 8.7 ± 3.7mm). No significant differences were found in peak force between positions for any muscle site. The peak values for all PMHS are included in Appendix 13.

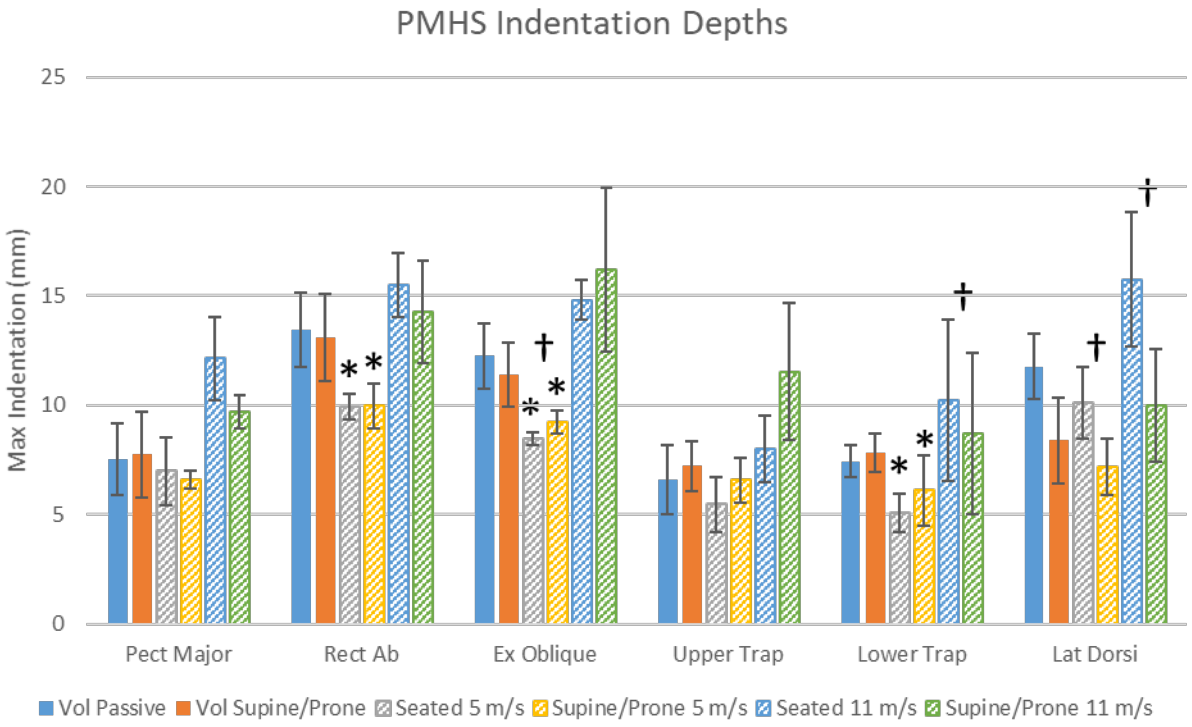
PMHS Indentation Depths
Max Indentation (mm)
25
20
15
10
5
0
Pect Major
Rect Ab
Ex Oblique
Upper Trap
Lower Trap
Lat Dorsi
Vol Passive
Vol Supine/Prone
Seated 5 m/s
Supine/Prone 5 m/s
Seated 11 m/s
Supine/Prone 11 m/s

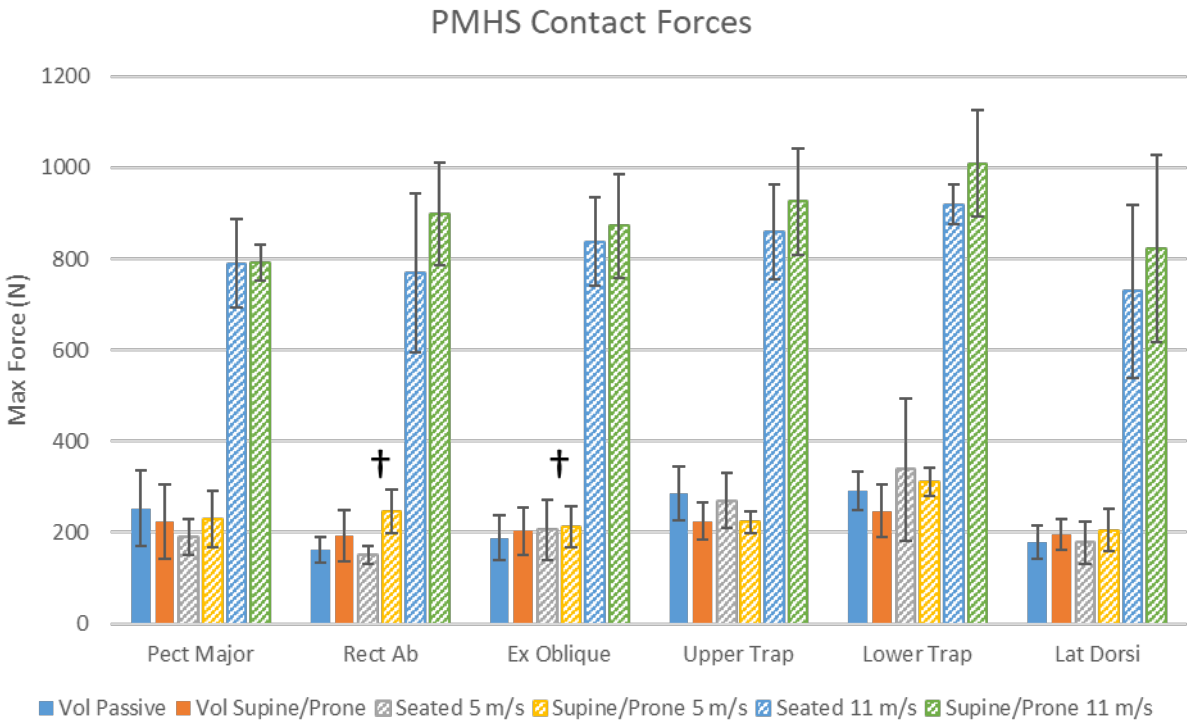
PMHS Contact Forces
Max Force (N)
1200
1000
800
600
400
200
0
Pect Major
Rect Ab
Ex Oblique
Upper Trap
Lower Trap
Lat Dorsi
Vol Passive
Vol Supine/Prone
Seated 5 m/s
Supine/Prone 5 m/s
Seated 11 m/s
Supine/Prone 11 m/s

Figure 19: Average (mean ± 1 SD) peak indentation depth and contact force for PMHS impacts compared at 5.5m/s and 11m/s (= significantly different from matched volunteer test, † = significantly different between seated and supine/prone)*

There were also significant differences in the response of the musculature between locations in the PMHS. In the seated position at 5.5m/s indentation speed, the lower trapezius (5.1 ± 0.9mm) had significantly lower displacement than the pectoralis major, external oblique, rectus abdominis, and latissimus dorsi (7.0 ± 1.6mm, 8.5 ± 0.3mm, 9.9 ± 0.6mm, 10.1 ± 1.6mm). The upper trapezius (6.6 ± 1.0mm) displaced significantly less than the external oblique, rectus abdominis, and latissimus dorsi. There was also a significant difference in peak indentation between the external oblique and the rectus abdominis. The only significant difference in peak force from PMHS was between the rectus abdominis and upper trapezius. Sample PMHS force-displacement curves are shown below in Figure 20, with the complete set of force-time and force-displacement curves included in Appendix 18. Figure 21 below shows a comparison between PMHS and volunteer corridors for the 5.5m/s impact conditions, with the additional force-time corridors, force-displacement average curves, and comparisons to volunteers in Appendix 19, Appendix 20, and Appendix 21, respectively.

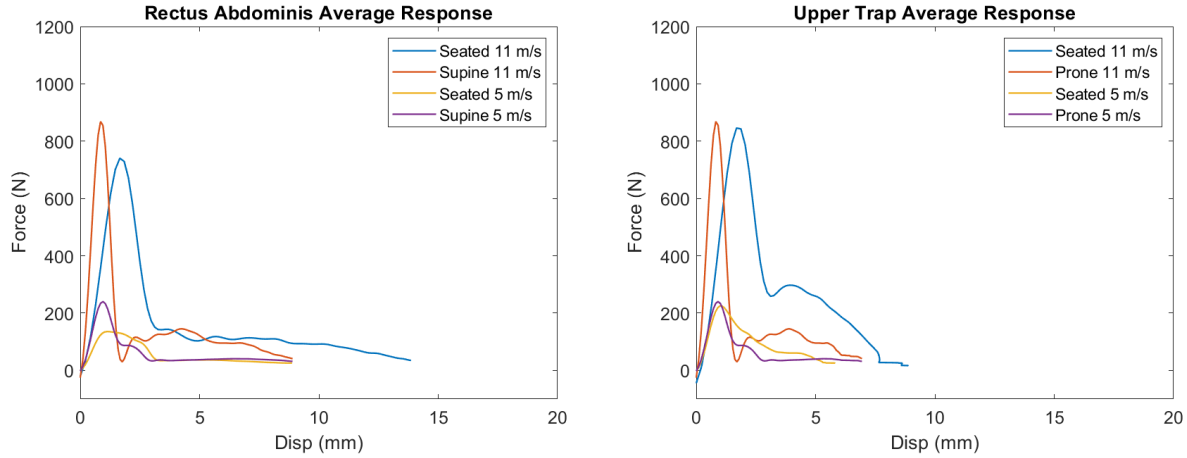

Figure 20: PMHS force-displacement curves for seated, supine, and prone positions under 5.5 and 11m/s impact conditions

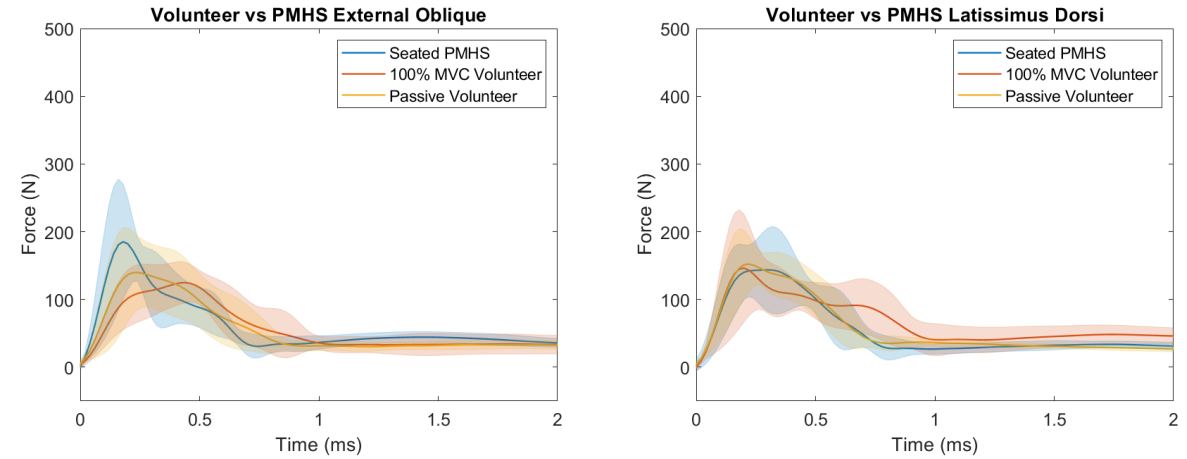

Figure 21: Comparison of 5.5m/s force-time corridors of seated PMHS, passive volunteers, and maximally contracted volunteers

Tissue Thicknesses

Skin, fat, and muscle thicknesses were calculated for each muscle during all of the shear wave elastography activities, and the results for the 10 impactor subjects are reported. The average anterior skin thickness, 1.85 ± 0.30mm, was thinner than the average posterior skin thickness, 2.36 ± 0.29mm, for the passive conditions. For the pectoralis major, there was no significant difference between the passive skin thickness and any activity; however, the fat thickness was significantly different between the passive and supine conditions, and the muscle thickness was different between the passive 50% MVC (Figure 22). All of the tissue thicknesses per muscle and activity are included in Appendix 14.

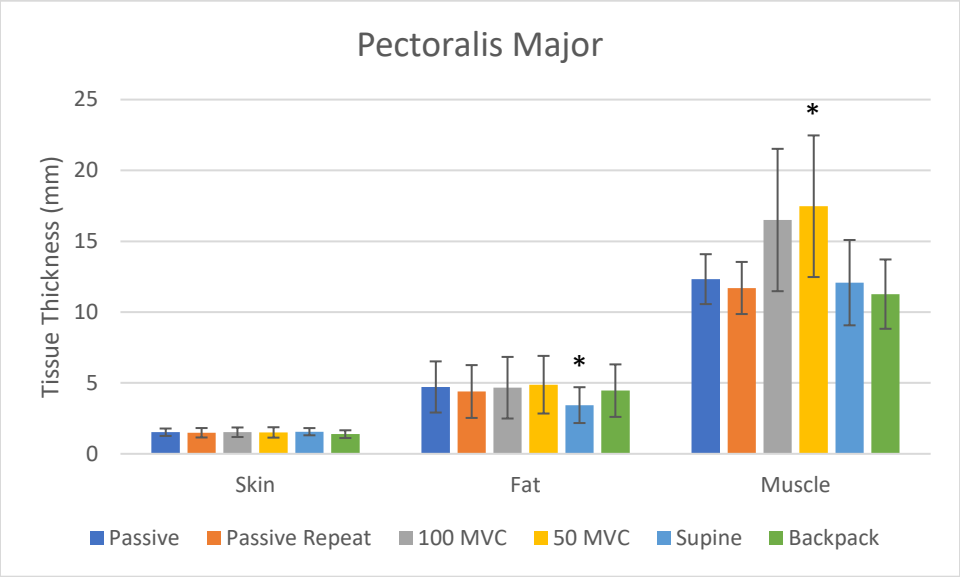

Figure 22: The average tissue thickness (± 1 standard deviation) for the pectoralis major during each SWE muscle activation level

Post-Test Survey

Volunteers were asked to complete a three-part post-test survey. Subjects listed impact locations that were visible, sensitive, or bruised six hours, one day, and three days post-impact test day (Figure 23). All subjects listed the external oblique impact location as visible at both six hours and one day, and four out of ten listed it as visible at three days post. At six hours post, the external oblique was also listed as sensitive by four out of ten and bruised by seven out of ten. The latissimus dorsi was also listed as visible by a majority of the subjects at both six hours and one day post-impact.

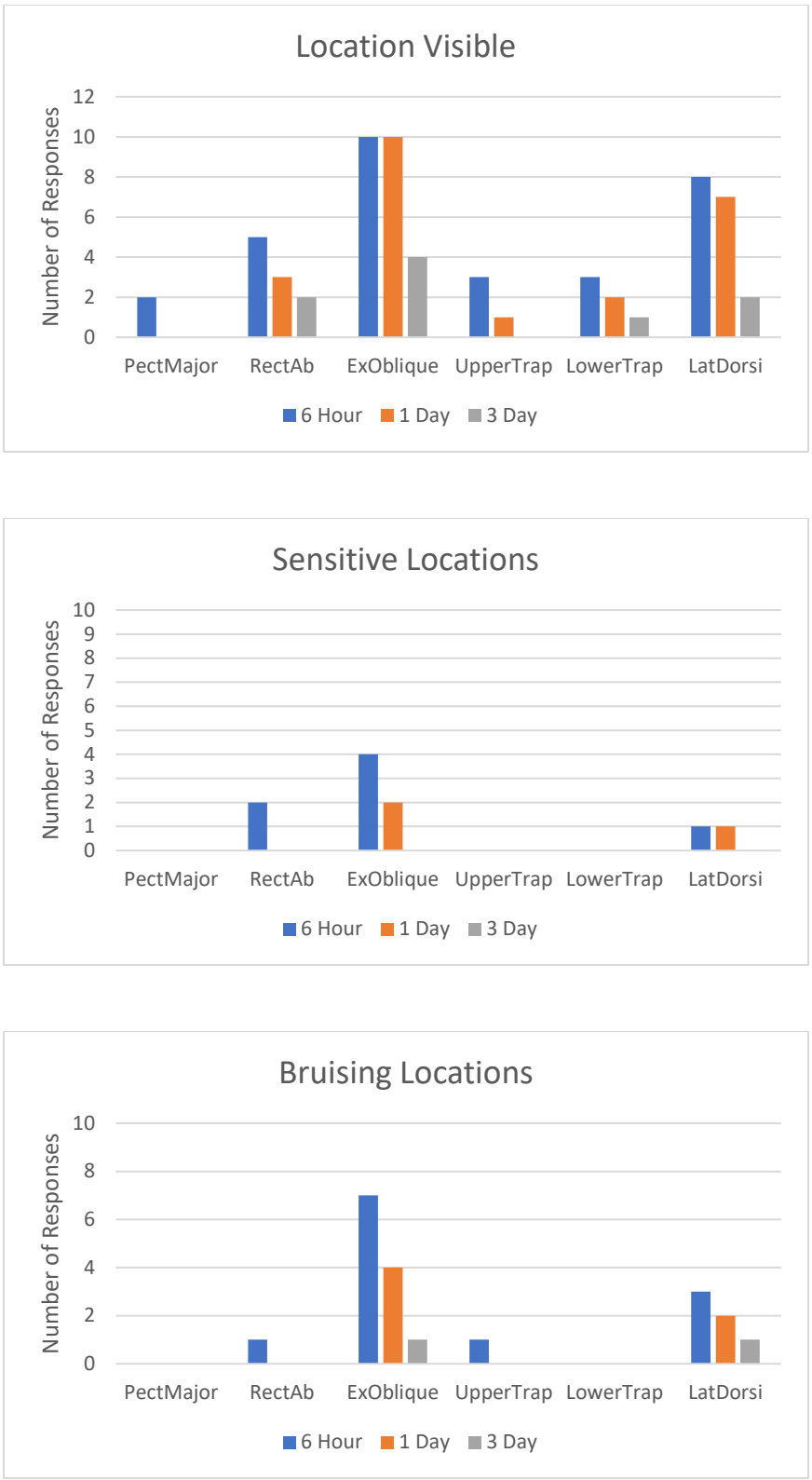

Figure 23: The survey results for the number of subjects with visible (top), sensitive (middle), and bruised (bottom) impact locations per muscle

Conclusions

Force-time and force-displacement curves were created for each impact and averaged across subjects for each impact condition. The force-time and force-displacement curves showed pronounced initial peaks within 0.5ms of contact that were driven by the inertial response of the tissue, followed by a longer-duration response as the tissue compressed.

There were significant differences in the volunteer impact response across different locations and activation levels. In general, peak contact forces decreased with increasing muscle activation. Changes to peak impact force from impact were likely dominated by the inertial response of the soft tissue, with the contracted musculature acting to change the total effective mass of the loose tissue, as well as the boundary condition on the internal face. However, there was not a clear directional trend of peak indentation depth across muscles. The lack of a clear trend is likely due to confounding effect of changing soft tissue thickness with both activation and posture. It can be seen from SWE (Aim 1) that the contracted musculature is stiffer than relaxed, which would result in a decrease in indentation depth for the same tissue. However, in many locations, the total tissue thickness of both the fat and muscle were increased in the contracted state, which would be expected to increase the indentation depth.

Peak indentation depths were significantly smaller in the PMHS than the volunteer for three of the six muscle sites tested (rectus abdominis, external oblique, and lower trapezius). There were no significant differences in impact force between the volunteers and the matched PMHS conditions. Additionally, the posture (prone/supine versus seated) of the PMHS tests had a significant effect on the peak contact force and impact depth in several locations, demonstrating the effect of posture and tissue thickness independent of muscle activation. The difference in indentation depth between PMHS and volunteers may suggest a potential caveat when using PMHS tissue for internal injury prediction under blunt impact.

As expected, the 11m/s impacts had significantly increased contact force and indentation depth compared to the 5.5m/s impacts in either the PMHS or volunteer data sets.

Aim 3: High-rate, high-deformation mechanical tests on *ex situ* in cadaveric tissue

Overview

Additional mechanical testing was completed on excised cadaveric tissue. Tissue was removed from the low-severity impact locations (right-side muscles), and using a drop tower, step-hold mechanical tests were used to characterize the nonlinear, viscoelastic properties of the passive tissue. The force-relaxation relationship of the tissue was recorded using a load cell below the tissue, and displacement of the tissue interaction was recorded from high-speed video.

Methods

Test Subjects/Samples

The same four PMHS used in both the SWE and impactor studies were again used in the drop tower mechanical characterization tests. However, the tissue mechanically tested was first excised from the torso. Anterior tissue samples were removed first. For the anterior muscle locations (pectoralis major, rectus abdominis, and external oblique), a y-shaped incision was drawn and cut along the breastplate and abdomen. Additional lines were drawn to ensure the tissue sample would not be affected by any incisions. The anterior tissue slabs included all the superficial tissue down to either the ribcage (pectoralis major) or the organ wall (rectus abdominis and external oblique). Additional incision lines were drawn on the posterior, and the tissue slabs were removed without interfering with the tissue samples. The posterior tissue slabs included all of the superficial tissue down to the both the ribcage (latissimus dorsi and lower trapezius) and all muscle below the upper trapezius (Figure 24).

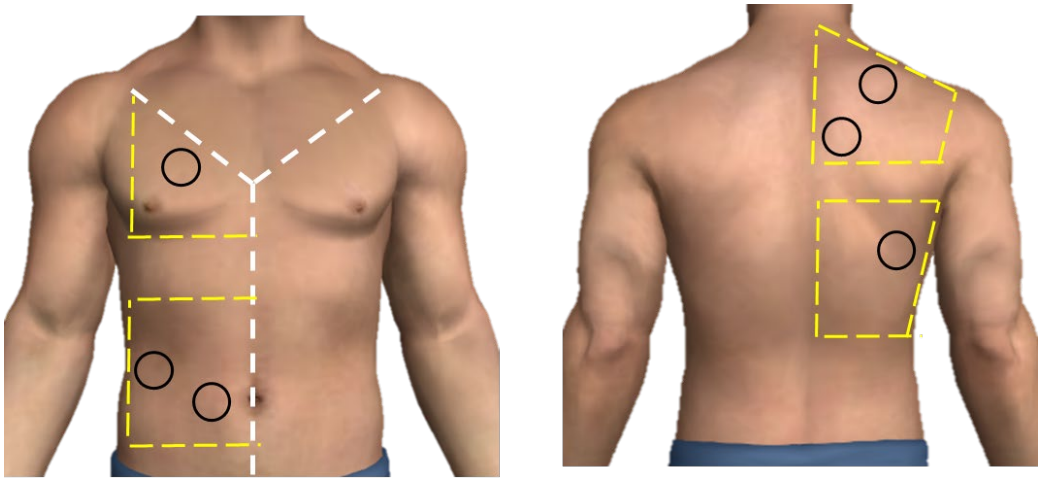

Figure 24: The anterior and posterior tissue samples (black circles), y-shaped incision (white dashed line), and tissue slab edges (yellow dashed line)

Once all of the tissue slabs were removed, the tissue samples were cut into 3in diameter cylinders, with the tissue depth determining height. A 3in diameter metal tube was used as a guide, and a scalpel was used to remove the cylindrical tissue sample from the tissue slab. The cylindrical tissue samples were kept in cylindrical polycarbonate dishes (Figure 25: Excised tissue samples in polycarbonate cylindrical dish).

Figure 25: Excised tissue samples in polycarbonate cylindrical dish

Testing Procedure

To control the temperature, the tissue was double-bagged and placed in a 60°F water bath. Each sample was kept in the water bath until immediately before testing. The tissue and dish were placed within the drop tower assembly, and the pre-test superficial tissue temperature was recorded, with average tissue temperature 60.4 ± 2.6°F (Appendix 22). Each tissue sample was impacted at 4.5m/s (4.2 ± 0.1m/s) with a cylindrical indenter (15.25mm diameter, 0.78kg mass) to 50% total compressive depth (Figure 26). Magnets within the drop tower assembly created a step-hold displacement profile. Overall tissue height was calculated for each sample by averaging four depth measurements taken around the polycarbonate dish. Each tissue was tested a single time; the force was measured using a load cell below the tissue, and displacement was determined from high-speed video analysis.

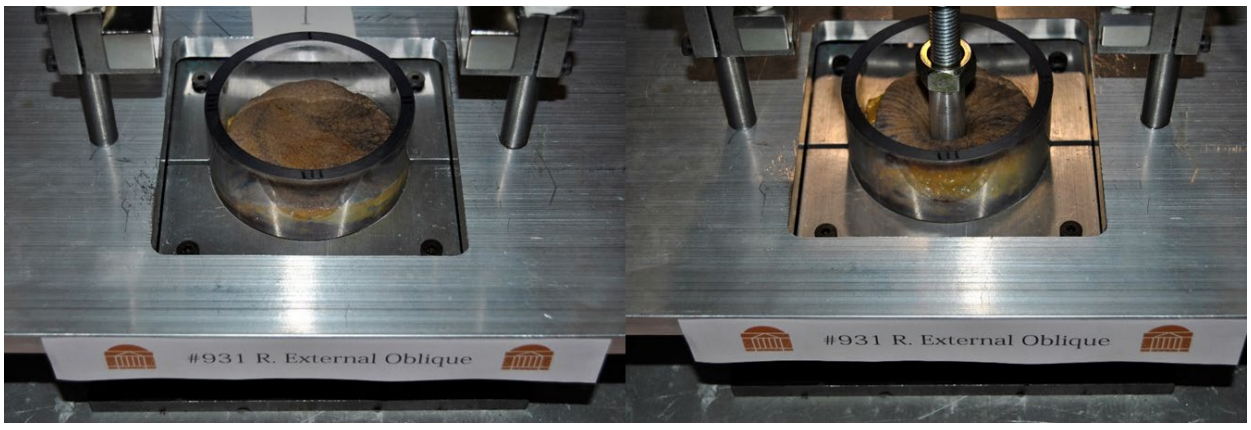

Figure 26: (Left) A tissue sample prior to a drop tower test and (Right) post-test with the indenter at a 50% compressive depth.

Equipment

Drop Tower

The drop tower includes two separate impactor masses: the drop tower mass (energy source) and the intermediate indenter that interacts with the tissue (Figure 27). The original drop tower mass height was selected to ensure the intermediate indenter impacted the tissue at 4.5m/s. The energy source interacted with the intermediate cylindrical indenter (15.25mm diameter, 0.78kg mass); the intermediate indenter then dropped into the tissue and attached to magnets to create a step-hold displacement profile.

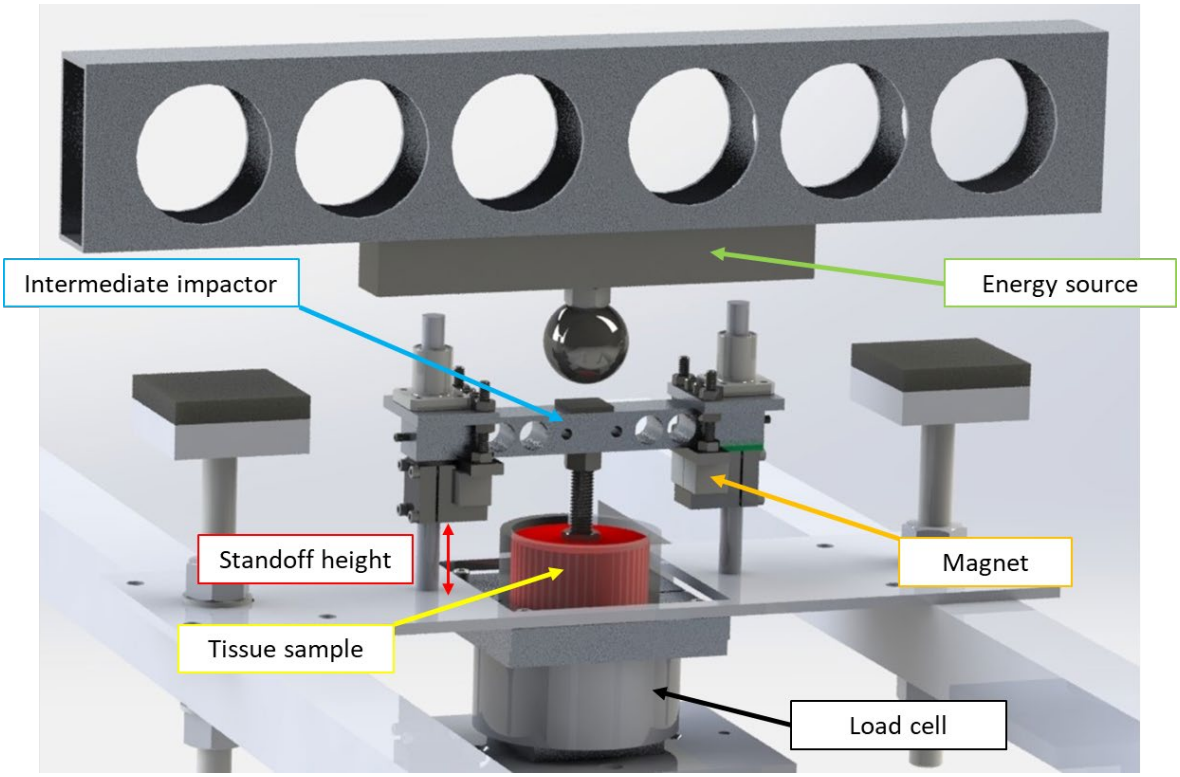

Figure 27: Drop tower assembly used for mechanical testing of excised cadaver tissue samples

Data Acquisition

The force was recorded using a load cell (Model No. 5024J, Humanetics Innovative Solutions) below the tissue sample. The load cell recorded force for 15 seconds to capture the relaxation of fat with a sample frequency of 20kHz. Displacement data was calculated from video markers on the intermediate impactor. The video recorded at 5kHz.

Data Analysis

The video displacement data was up-sampled to 20kHz using linear interpolation between the data points. The force data along the main axis of loading was debiased and filtered with a 4^{th}-order Butterworth low-pass filter with a cutoff frequency of 800Hz. Cutoff frequency was determined from spectral analysis. Time of initial contact with the tissue was defined as the final time the signal passed through zero force before the maximum peak. Tissue displacement and force were determined from initial contact to 15 seconds post-contact.

Results

The displacement data for a single cadaver across all muscles (PMHS 3A), shown in both linear and log time, highlight the speed of the step-hold system (Figure 28). The average time to peak displacement across all of the subjects and muscle locations was 6.2 ± 8.5ms. Additionally, the force-time history shows the relaxation curve generated from the step-hold input (Figure 29). The average time to peak force was 3.9 ± 0.1ms for all of the samples tested. The remaining cadaver displacement- and force-time histories are provided in Appendix 23.

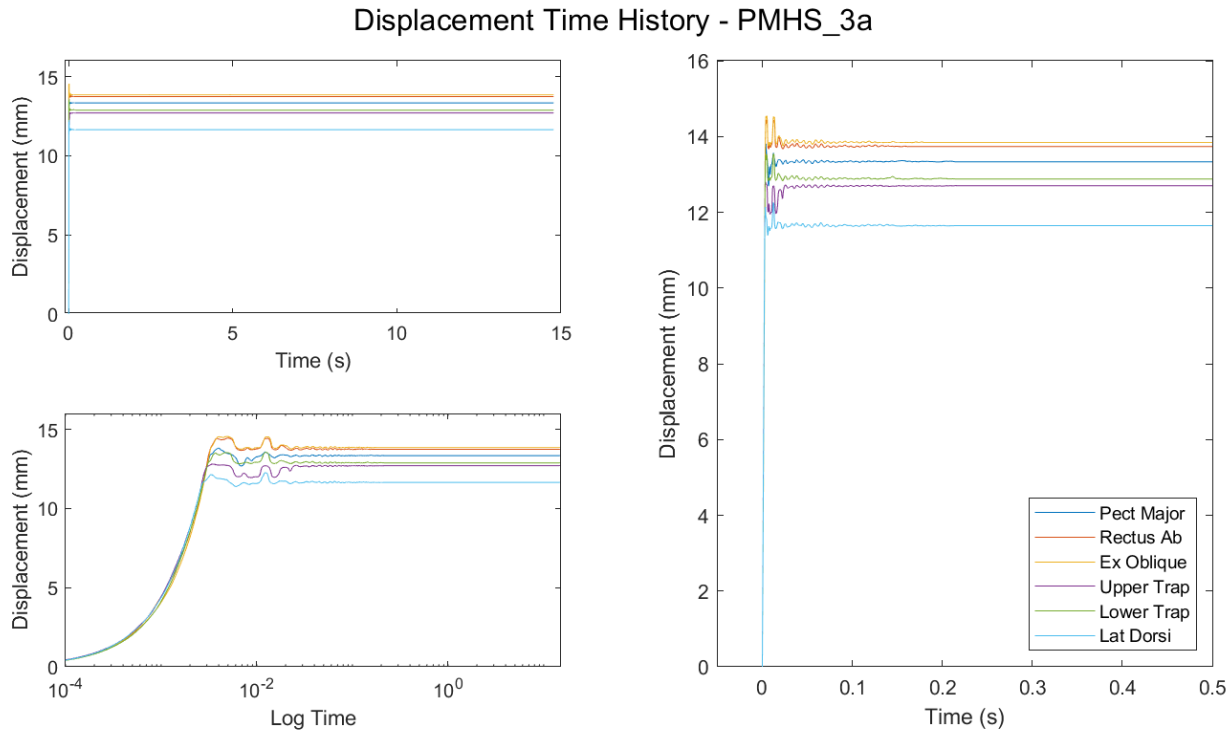

Figure 28: The displacement time histories for all six muscles on a single cadaver, including full linear displacement-time history (top left), initial step in displacement until 0.5s (right), and full log displacement-time history (bottom left).

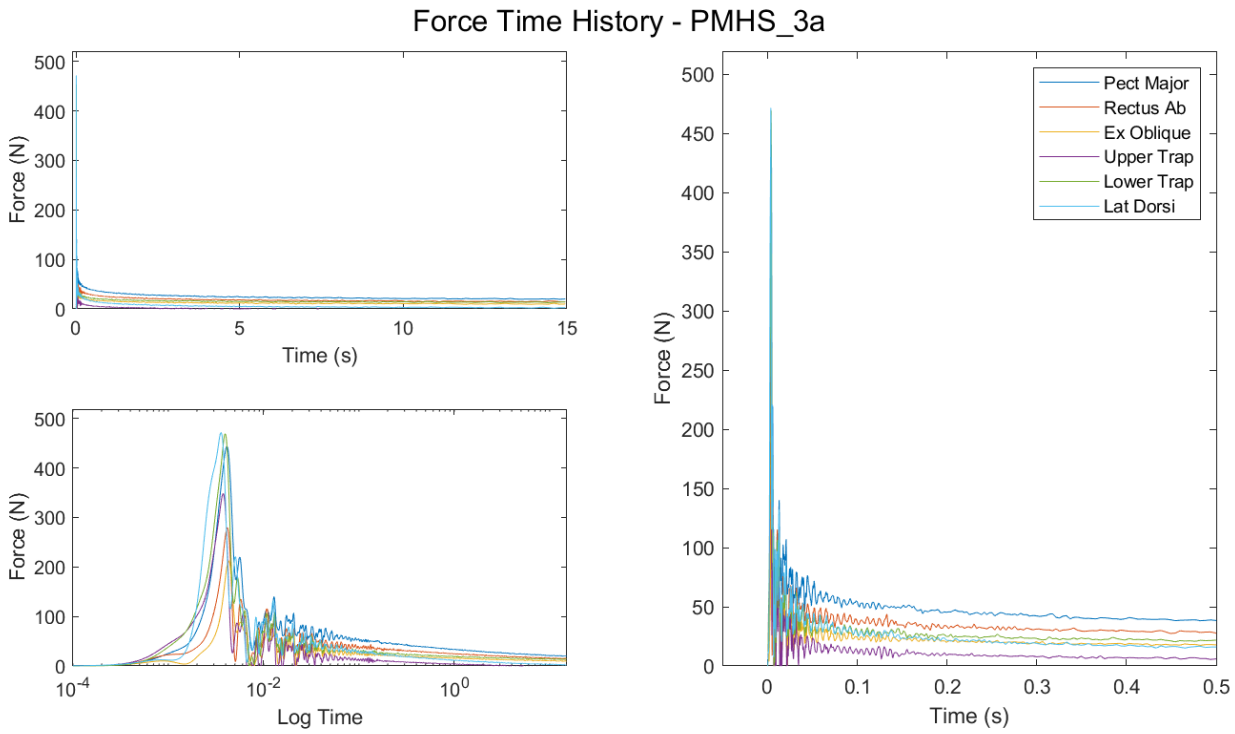

Figure 29: The force time histories for all six muscles on a single cadaver, including full linear force-time history (top left), initial relaxation until 0.5s (right), and full log force-time history (bottom left)

The standoff height was set to achieve 50% strain for the average tissue depth. The average compressive strain and peak force across all of the muscles were 0.53 ± 0.08N and 566.5 ± 262.0N, with each muscle separated in Table IX. For the lower trapezius, the force-compressive strain response is shown for all cadaver tissues (Figure 30), with the remaining muscles shown in Appendix 24.

Table IX: The average (mean ± 1 SD) compressive strain and peak force per muscle between cadaver tissues

Muscle	Compressive Strain (mean ± 1 SD)	Peak Force (N) (mean ± 1 SD)
Pectoralis Major	0.60 ± 0.09	650.2 ± 162.2
Rectus Abdominis	0.51 ± 0.06	345.9 ± 53.0
External Oblique	0.49 ± 0.05	313.2 ± 120.9
Upper Trapezius	0.56 ± 0.10	648.2 ± 283.3
Lower Trapezius	0.55 ± 0.03	863.5 ± 305.7
Latissimus Dorsi	0.51 ± 0.10	577.9 ± 149.2

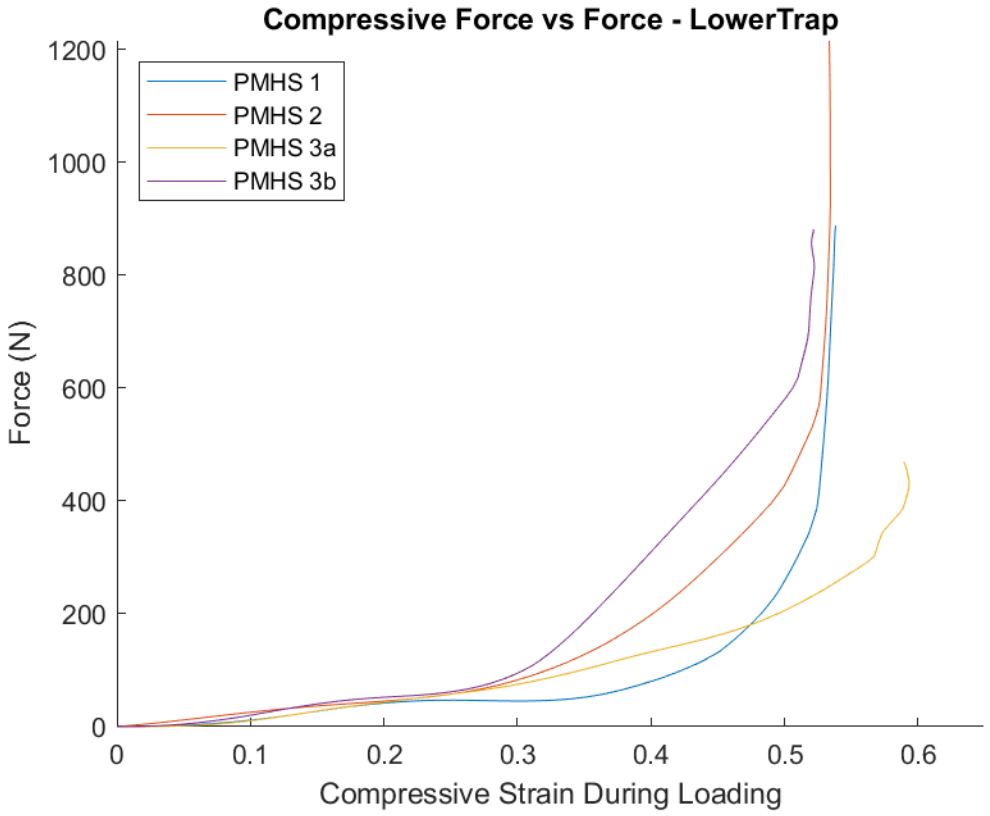

Figure 30: The force-compressive strain response of the lower trapezius during load for each PMHS

Conclusions

Compressive tissue testing was performed on PMHS tissue samples excised from six locations in the thorax. Step-hold relaxation tests involved dynamic, nearly instantaneous tissue compression to 50% strain, followed by a relaxation period at a constant 50% strain. Quasilinear viscoelastic material properties can be computed based on these test results. Viscoelastic materials are dependent on strain history, and with the step-hold test design, displacement history was recorded and incorporated in the model fit for the material. Using all 24 individual models, an average QLV model can be developed for each of the six locations, and these average parameters can be scaled to capture the effect of activation on soft tissue responses. Future validation of both the average PMHS response and scaled volunteer response was completed in Aim 4; additionally, the force-time histories can be used to validate the current soft tissue properties present in human body finite element models.

Aim 4: Constitutive Model Development

Overview

Quasilinear viscoelastic (QLV) theory is used to model the complex, nonlinear behavior that soft tissue exhibits during both the rapid loading and relaxation of a tissue. QLV models incorporate a reduced relaxation function, which captures the stress-relaxation of the tissue; an instantaneous elastic stiffness function, which captures the instant change in stress with an instant step in strain; and the strain history of the material (Equation 1).

$$\sigma(t) = \int_0^t \bar{R}(t-\tau)\frac{d\sigma_0(\varepsilon)}{d\varepsilon}\frac{d\varepsilon}{d\tau}d\tau$$

Equation 1: The governing QLV equation, which includes the reduced relaxation function, the instantaneous elastic stiffness function, and the strain time-history.

The reduced relaxation function is expressed as a Prony series to capture the relaxation of the material based on different time constants (Equation 2). The total stress (Equation 3) is composed of the instantaneous elastic response, modelled using a Fung exponential (Equation 4), and the viscoelastic contributions (Equation 5).

$$\bar{R}(t) = C_\infty + \sum_{i=1}^{n} C_i e^{-t\beta_i}$$

Equation 2: The reduced relaxation function composed of exponential decay terms.

$$\sigma(t) = \sigma_\infty(t) + \sum_{i=1}^{n} \sigma_i(t)$$

Equation 3: The total QLV stress composed of the instantaneous elastic stress and the viscoelastic stress.

$$\sigma_0 = A(e^{B\varepsilon} - 1)$$

Equation 4: The instantaneous elastic function modelled as a Fung exponential.

$$\sigma_{i\,(t)} = \alpha_i\sigma_i(t) + \frac{C_i}{\beta_i}(1-\alpha_i)\left[\frac{\sigma_o(t+\Delta t) - \sigma_0(t)}{\Delta t}\right], where\ \alpha_i = e^{-\Delta t\beta_i}$$

Equation 5: The viscoelastic contributions of stress.

Each sample was fit with a QLV model, and then an average QLV model was developed for each of the six muscle locations. This average model was then scaled to incorporate the difference between atonic cadaver muscle response and the muscle activation of the volunteers taken from SWE in Aim 1. Additionally, these modified models were compared against the force and displacement corridors developed from the low-severity impacts of the volunteers.

Methods

QLV model fits for individual cadaveric test samples

Twenty-four individual models were fit to the test samples. Experimental stress was calculated by dividing the load cell force data by the cylindrical indenter contact area. Compressive strain

was calculated by dividing the tissue displacement by the original average thickness of each individual tissue sample. Using three time constants with three coefficients (C_1, C_2, and C_3) and the Fung exponential instantaneous elastic function with two coefficients (A and B), the optimum QLV model fit was determined using an Excel solver. The optimal solution was defined as the set of coefficients that minimized the weighted sum of squared error between the experimental stress and the predicted QLV model stress and captured the tissue response (Equation 6). The only constraints added to the optimization were that all C_i were greater than zero and C_∞ equaled one less the sum of all C_i.

$$SSE = \sum_{i=1}^{n} w(t)\left[\sigma_{\exp}(t) - \sigma_{model}(t)\right]^2$$

Equation 6: The objective function that was minimized to determine QLV parameters.

Two techniques were used to weight the stress data to optimize the QLV fit. First, the stress and strain experimental data was resampled using log time to prioritize data points taken during the rapid load and quick relaxation; this distributed the experimental data with more samples during the early decades (0.0001 and 0.001s), and fewer samples in the later decades (1 and 10s). Additionally, the weighting factor, *w* in Equation 6, was the experimental stress value at each sample time to assign higher weights to larger values of stress to ensure the QLV model captured the peak stress. This procedure was used to develop 24 unique models, one for each tissue sample.

Average QLV models per cadaveric muscle location

Six average QLV models were developed by combining the four PMHS samples for each muscle location. The optimized parameters (A, B, C_1, C_2, and C_3) were averaged for each muscle. The long-term constant C_∞ was recalculated based on the sum of the average C_1, C_2, and C_3. Because QLV materials and models are strain-history dependent, an average ideal step-hold strain was calculated using the average time to peak displacement and maximum strain for each muscle. Using the average parameters and average strain step-hold, six QLV model responses were generated, one for each muscle. The average QLV constitutive equation developed from cadaveric data can be compared to the cadaveric impact data (Aim 2) at individual muscle locations.

Average QLV models with muscle activation per muscle location

Based on the relationship between cadaver and volunteer tissue response developed from SWE (Aim 1), ratios of average shear wave velocity were calculated for each muscle between PMHS seated and volunteer passive, supine, and 50% and 100% activation. Because stiffness is proportional to velocity squared, the average instantaneous elastic function for each muscle location was then multiplied by the square of the ratio to account for differences between the atonic muscle and active muscle responses.

Comparison of muscle activation QLV fits with cadaver and volunteer impact data

To compare the QLV model with the impact data obtained in Aim 2, force-displacement models were used. A numerical impact model was developed using the initial velocity and mass of the projectile to predict force with the scaled QLV model. Starting with the average initial projectile

velocity, the force was calculated after a small discrete time step (0.00001s). With a known force from the QLV model, the acceleration of the projectile was calculated by dividing by the mass of the projectile (40g). An updated velocity and displacement were calculated using a trapezoidal numerical integration, and these calculations were completed until the force reached zero. The final displacement and peak force from the QLV impact validation were compared to the experimental data.

Validation was completed for the pectoralis major and external oblique for the PMHS 5.5m/s, PMHS 11m/s, volunteer passive, volunteer supine, volunteer 100% MVC, and volunteer 50% MVC impact conditions.

Results

QLV model fits for individual cadaveric test samples

Twenty-four individual QLV constitutive models were fit to the individual stress-strain responses of the test samples. Using the Fung exponential, the instantaneous elastic (IE) response was fit to the experimental stress-strain response. The IE stress response is greater than the experimental stress data to account for the force-relaxation that is inherent to non-idealized experimental data. A true, instant step in strain is impossible, and there will always be a time to peak displacement greater than 0s in experiments; by including an IE function that is larger than the experimental data, the IE function is able to estimate the stress response accounting for the relaxation during the non-instantaneous loading of the tissue.

The reduced relaxation was modelled with a Prony series with three time constants (β = 0.1, 100, and 1000); these were selected to capture the rapid loading of the drop tower and the long-term response of stress. The parameters for each individual fit are supplied in Appendix 25, and the individual experimental data and QLV model fit for an upper trapezius sample are shown in Figure 31 and Figure 32.

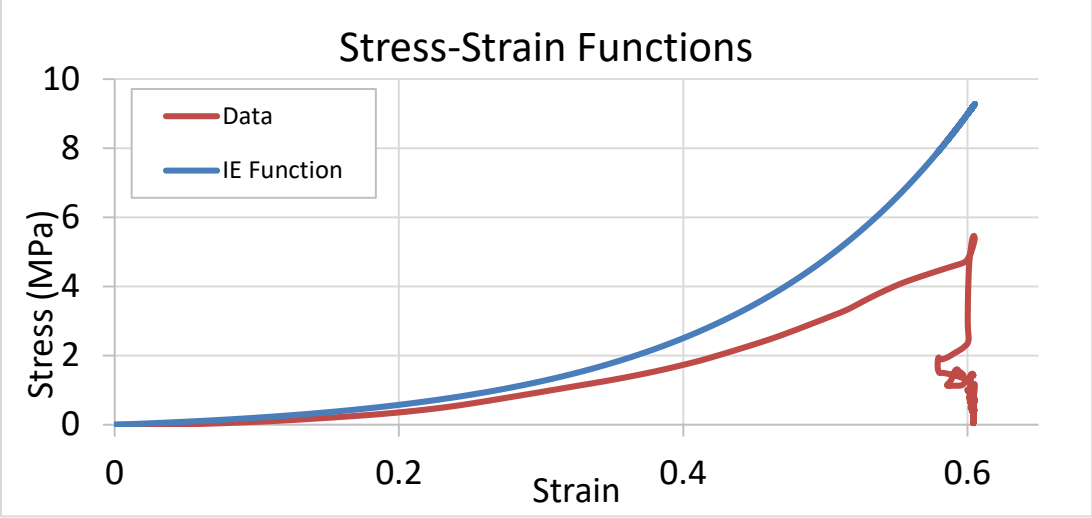

Figure 31: The stress-strain response and instantaneous elastic function for a single upper trapezius sample tissue

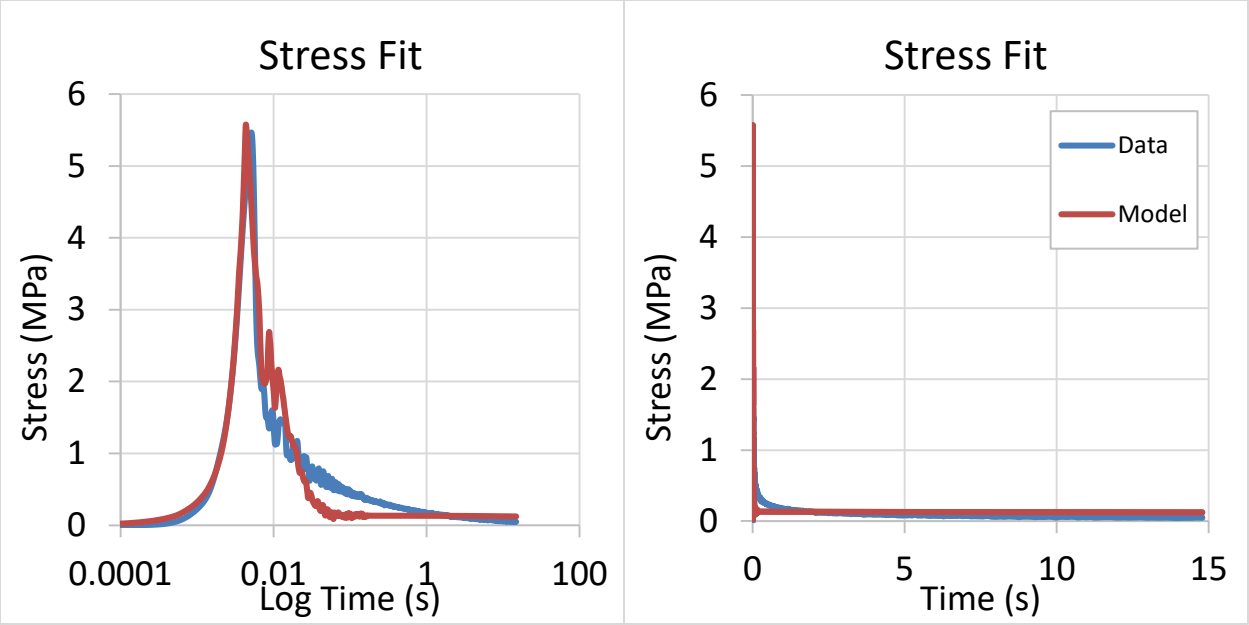

Figure 32: The stress log time-history (left) and linear time-history (right) with an individual QLV fit for the upper trapezius

Average QLV models per cadaveric muscle location

The average (mean ± 1 SD) parameters for each muscle are provided in Appendix 25. Parameters are reported in both stress-strain and force-displacement units. The average time to peak strain and maximum strain values for each muscle were used to build the averaged ideal strain input (Table X). The average strain input plots are included in Appendix 26.

Table X: The average (mean ± 1 SD) maximum strain and time to peak across muscles

	Pectoralis Major	**Rectus Abdominis**	**External Oblique**	**Upper Trapezius**	**Lower Trapezius**	**Latissimus Dorsi**
Max Strain	0.60 ± 0.09	0.51 ± 0.06	0.49 ± 0.05	0.56 ± 0.10	0.55 ± 0.03	0.50 ± 0.10
Time to peak (ms)	3.9 ± 1.1	4.6 ± 1.0	3.4 ± 0.6	4.4 ± 0.8	3.2 ± 0.7	3.0 ± 0.6

With the average QLV parameters and idealized average strain input, the average QLV stress model was computed for each muscle. The average QLV fit for the upper trapezius is plotted against the four PMHS upper trapezius data in both linear and log-time, with the stress-strain response against the IE stress (Figure 33), with all of the muscle fits shown in Appendix 27.

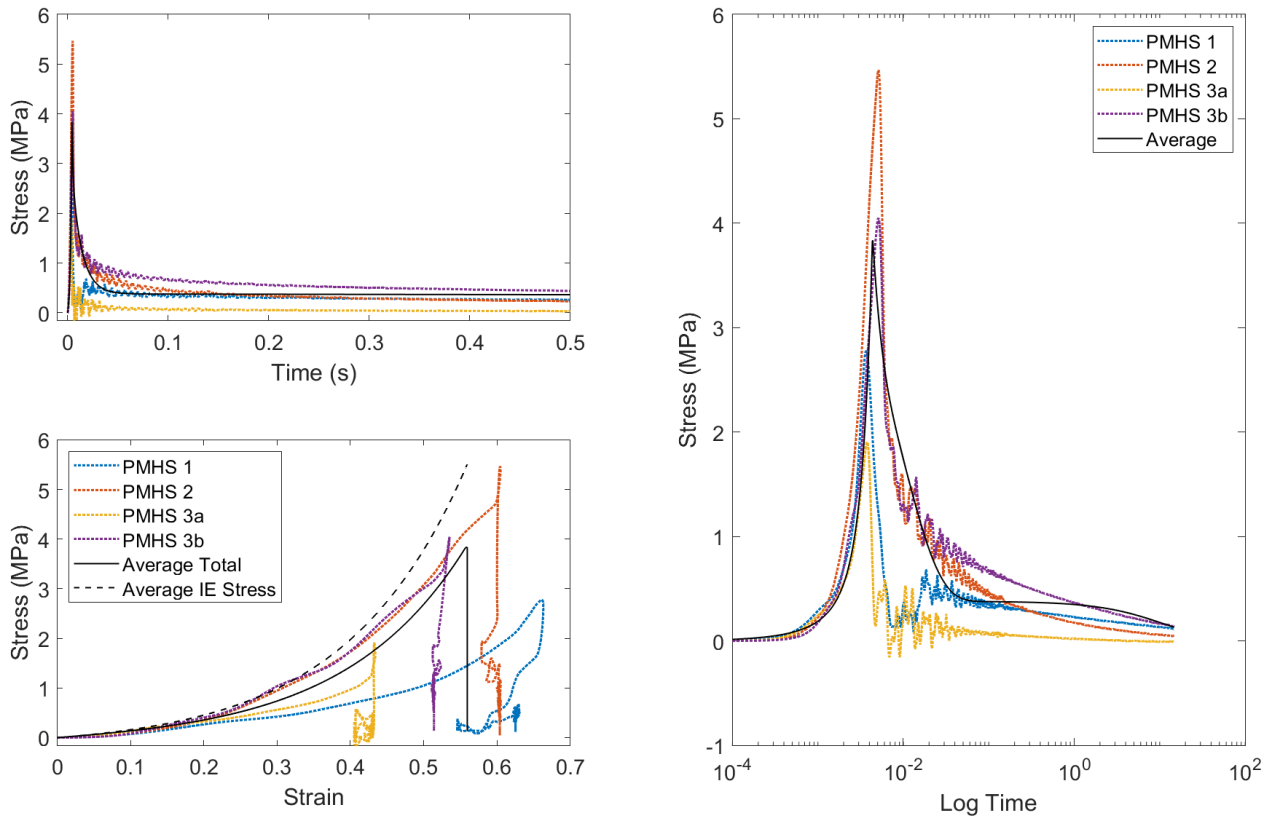

Figure 33: The stress linear time-history (top left), stress log time-history (right), and stress-strain response for the upper trapezius of the four PMHS and the average QLV model

Average QLV models with muscle activation per muscle location

The average PMHS QLV model for each muscle was scaled using ratios developed from the SWE velocity for both PMHS and active volunteer muscles; the scaled instantaneous elastic parameter is provided for both stress-strain and force-displacement units (Appendix 28). Using the same method to develop ideal strain inputs, an ideal average strain input was used for each muscle to compare the average PMHS QLV model to the scaled volunteer models. The predicted QLV model for the external oblique is shown in Figure 34, and the remaining predicted muscle models are shown in Appendix 29.

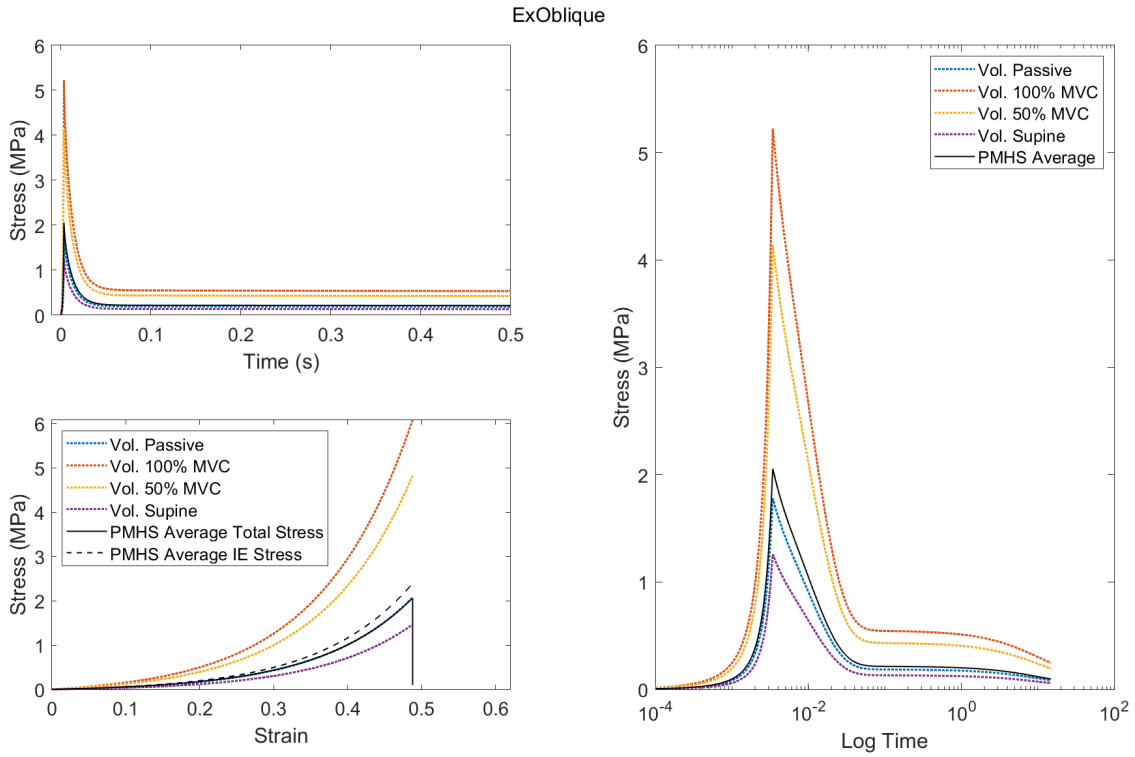

Figure 34: The scaled response for volunteer activities for the external oblique and the average PMHS response, including the linear stress-time history (top left), the log stress-time history (right), and the stress-strain response (bottom left) for passive, 100% MVC, 50% MVC, and supine volunteer conditions

Comparison of muscle activation QLV fits with cadaver and volunteer impact data

The QLV impact model predicted peak forces for the PMHS 5.5 and 11m/s impacts within the spread of the PMHS for the external oblique impacts ($F_{MODEL\ 5.5}$ = 288.8N, $F_{EXP\ 5.5}$ = 206.2 ± 65.6N, and $F_{MODEL\ 11}$ = 882.5N, $F_{EXP\ 11}$ = 837.3 ± 97.5N), with additional measurements shown in Figure 35. The max displacement for the pectoralis QLV model impacts were also similar to the spread of the experimental data ($u_{MODEL\ 5.5}$ = 8.84mm, $u_{EXP\ 5.5}$ = 7.0 ± 1.6mm, and $u_{MODEL\ 11}$ = 11.5mm, $u_{EXP\ 11}$ = 12.1 ± 1.9mm), with additional measurements shown in Figure 36. When comparing the force-time history of the QLV model impact and experimental data, the time of max peaks are not the same because the QLV model impact does not account for the inertia component of the impact (Figure 37).

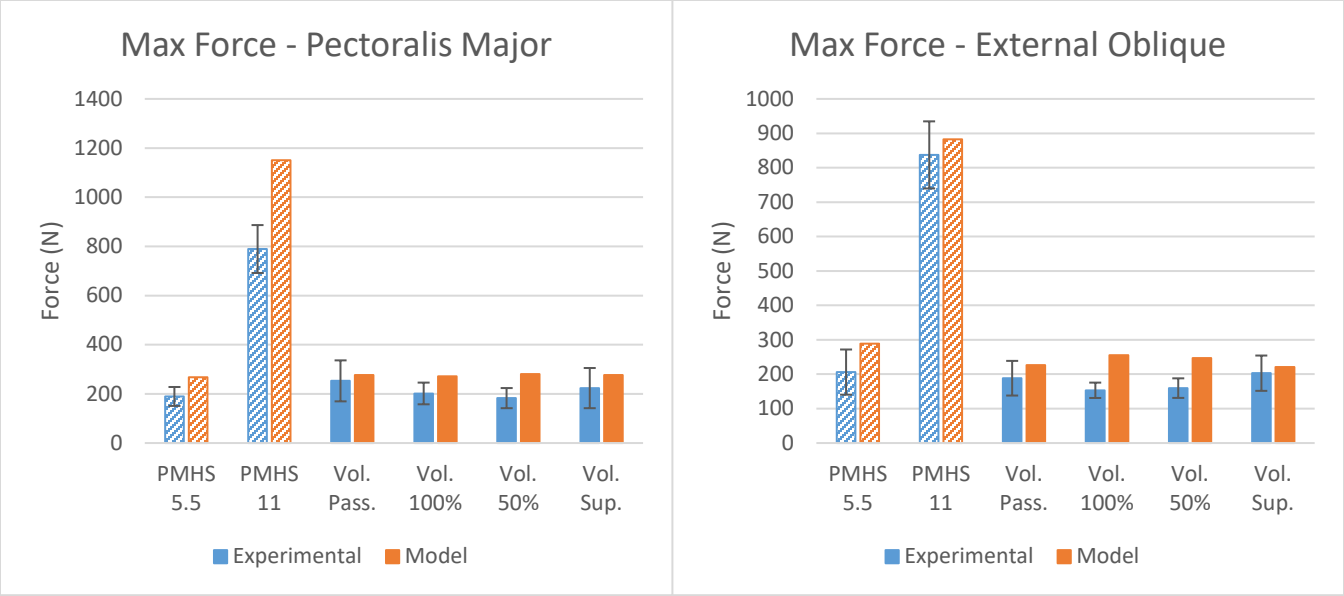

Figure 35: The max force for the pectoralis major and external oblique impact model and experimental data

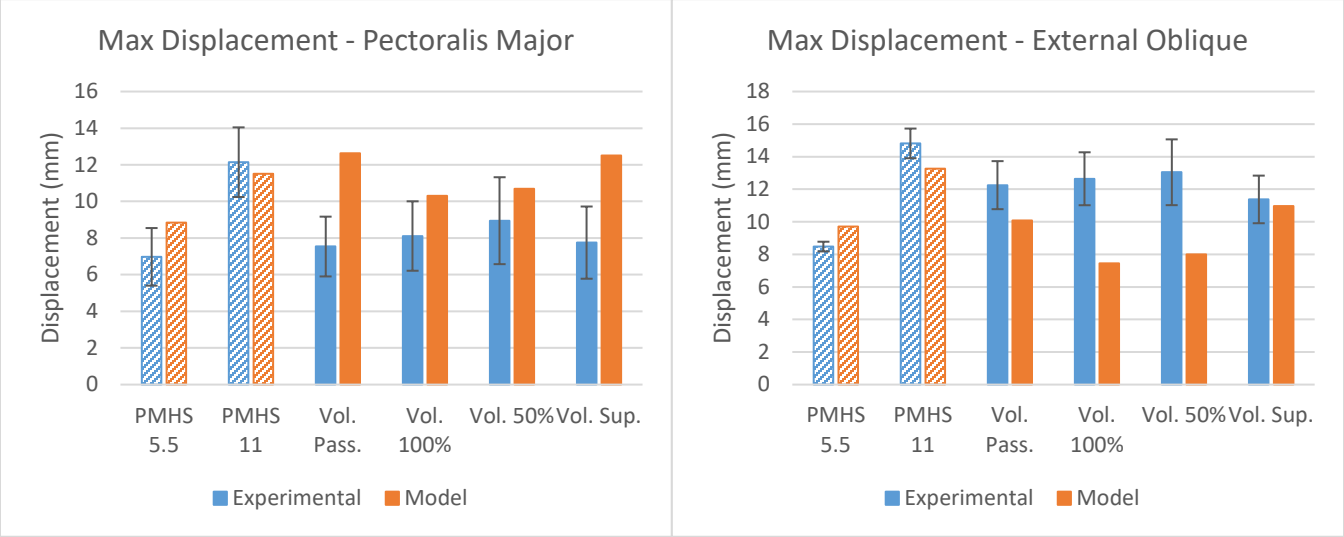

Figure 36: The max displacement for the pectoralis major and external oblique impact model and experimental data

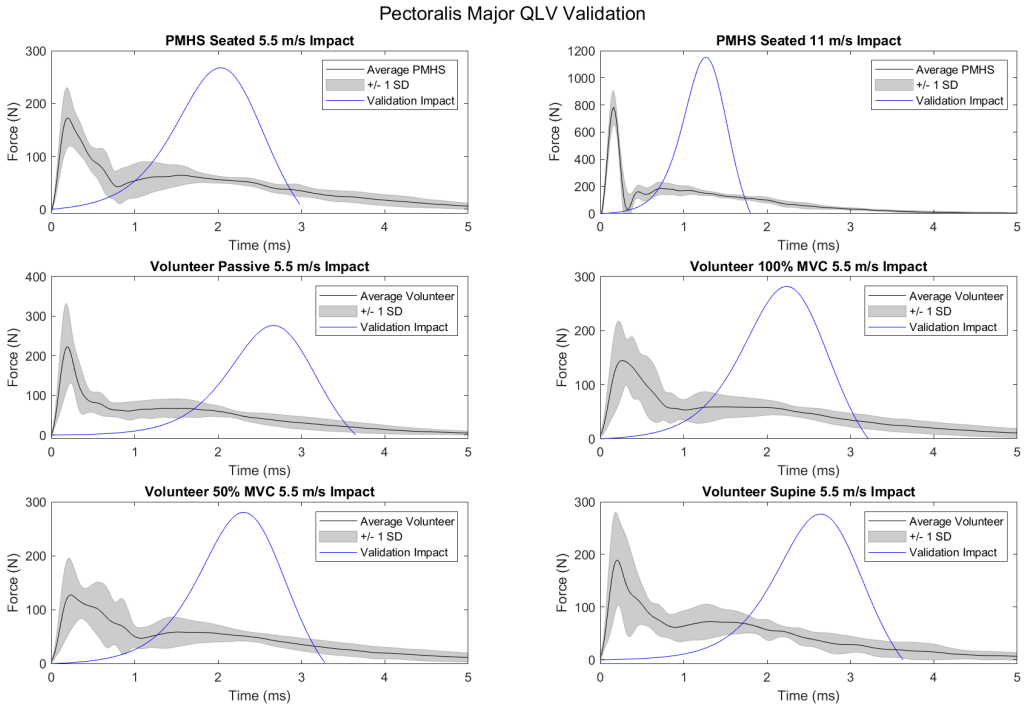

Figure 37: The force time-history of the QLV model impact with the experimental data for the pectoralis major

Conclusions

The results for each high-deformation step hold test in Aim 3 for each PMHS tissue sample were used to develop an individual QLV fit using a Fung exponential form for the instantaneous elastic component, and a three-parameter Prony series for the reduced relaxation. The QLV constants were combined to create an average tissue response at each muscle location. These average PMHS parameters were validated against the PMHS impactor results from Aim 2 at the pectoralis major and external oblique. The average QLV models predicted the peak forces and displacements within the spread of the PMHS data, but time of peak force and displacement did not match the impactor experimental data.

Additionally, the averaged PMHS QLV parameters were then scaled, using stiffness properties determined from SWE testing in Aim 1. Scaled models were developed using SWE stiffness ratios for passive, 50%, and 100% contracted living tissue. The scaled QLV models were validated against the volunteer impactor data for the pectoralis major and external oblique. The QLV model did better to predict the peak force of the supine and passive volunteer conditions at both locations than the peak force of the 100% and 50% activation cases. The QLV model was developed from composite soft tissue (skin, fat, and muscle), but the scaling ratios only included the stiffness change within the muscle. Therefore, the QLV model impact over-predicted the peak force of the muscle activation cases during the impactor volunteer tests because of the significant increase in muscle stiffness, captured with SWE, between passive and active conditions.

Differences in individual tissue layer thicknesses may have introduced variance in the model estimation of displacement.

The time of peak force in the QLV model impact did not match the timing of the impactor data from either the PMHS or the volunteer impacts because the QLV model did not include the inertial response of the tissue. To improve the timing of peak force and displacement, additional information about the tissue needs to be supplied to the impact model. This could be accomplished using an inverse finite element model approach to capture the initial inertia response, and to incorporate changes in thickness between activation conditions.

Discussion

Overall Conclusions

This study provided valuable information for both human body model development and validation for non-injurious blunt impacts. Historically, human body models have been developed using cadaveric soft tissue properties; this study worked to combine the non-injurious testing results from volunteer testing with active musculature with the high-deformation testing using cadaveric tissue to best represent a composite soft tissue response.

The results of this study demonstrated significant differences between the tissue stiffness (Aim 1) and impact response (Aim 2) of PMHS and passive volunteers, and further differences between passive and active volunteers. QLV models for composite skin-fat-muscle tissue were generated (Aims 3 and 4) at six locations in the thorax for PMHS, passive living tissue, and active living tissue. These QLV material models were compared to the forces and displacements measured in both PMHS and volunteers.

Activation levels were described for everyday tasks (standing, standing laden, walking, running) to appropriately prescribe these QLV material models to human body models. Because muscle activation state affects the dynamic tissue response during blunt trauma to the human torso, it will become more important to accurately model the soft tissue response over physiological levels of stiffness.

Overall, the difference between living and post-mortem biomechanics are likely greater at the individual tissue level (i.e., skin, fat, and muscle), than in the combined "flesh" response. Additional work needs to be completed to distinguish the role of each of these tissue levels during a blunt impact to the torso.

Limitations

During our impact testing, there was a decrease in impact force with increasing activation. However, this trend was partially due to the effect of increased tissue thickness during many of the contracted postures. Changing tissue thickness also contributed to the lack of a clear trend in max tissue indentation. For this reason, the impact results should not be interpreted without the accompanying tissue thickness. The force-time corridors and average force-displacement responses may be better validation metrics than the peak forces and displacements alone.

There are inherent differences between atonic cadaver tissue and living human tissue, such as activation; however, during this study and most PMHS experimental testing, the tissues were tested at different temperatures (i.e., non-physiological). To keep the tissue from degrading, the cadaver and soft tissue samples were maintained at about 60°F, but the volunteer human tissue temperature was naturally higher. Throughout this study, all of the cadaveric tissue temperature was tested at similar temperatures, but the effect temperature has on the soft tissue mechanics is not well understood. It is likely that the testing temperature of PMHS tissue contributes to the measured tissue responses. To most accurately compare living and cadaveric tissue, additional experimental work may need to be completed to determine tissue properties with varying temperature.

Additionally, inertia was not accounted for in the validation of the QLV model. The initial peak in the force-time history data, in both volunteer and PMHS, is an inertia effect between the projectile and the tissue; however, the QLV modeled impact does not include any inertia dependence. To better validate and refine the QLV parameters of the different muscles, inverse finite element analysis could be used to include the effect of inertia and optimize parameters.

References

[1] M. Iwamoto, Y. Nakahira, H. Mimpara, T. Sugiyama and K. Min, "Development of Human Body Finite Element Model with Multiple Muscles and Their Controller for Estimating Occupant Motions and Impact Responses in Front Crash Situations," *Stapp Car Crash Journal,* vol. 56, pp. 231-268, 2012.

[2] R. W. Kent, C. R. Bass, W. A. Woods, R. S. Salzar and J. Melvin, "The Role of Muscle Tensing on the Force-Deflection Response of the Thorax and a Reassessment of Front Impact Thoracic Biofidelity Corridors," in *Proceedings of the International Research Council on the Biomechanics of Impact (IRCOBI)*, Lyon, France, 2004.

[3] R. W. Kent, C. R. Bass, W. A. Woods, R. S. Salzar and J. Melvin, "The role of muscle tension on the force-deflection response of the thorax and a reassessment of frontal impact thoracic biofidelity corridors," *Jornal of Automobile Engineering,* vol. 220, no. 7, pp. 853-868, 2006.

[4] C. G. Shaw, D. J. Lessley, J. R. Crandell, R. W. Kent and L. Kitis, "Elimination of Thoracic Muscle Tensing Effects for Frontal Crash Dummies," *SAE Transactions: Journal of Passenger Cars-Mechanical Systems,* vol. 114, no. 2005-01-0307, pp. 205-219, 2005.

[5] M. S. Taljanovic, L. H. Gimber, G. W. Becker, L. D. Latt, A. S. Klauser, D. M. Melvill, L. Gao and R. S. Witte, "Shear-Wave Elastography: Basic Physics and Musculoskeletal Applications," *Radiographics,* vol. 37, no. 3, pp. 855-870, 2017.

[6] S. F. Eby, P. Song, S. Chen, Q. Chen, J. F. Greenleaf and K.-N. An, "Validation of shear wave elastography in skeletal muscle," *Journal of Biomechanics,* vol. 46, no. 14, pp. 2381-2387, 2013.

[7] T. Deffieux, J.-L. Gennisson, L. Bousquet, M. Corouge, S. Cosconea, B. Amroun, S. Tripn, B. Terris, V. Mallet, P. Sogni, M. Tanter and S. Pol, "Investigating liver stiffness and viscosity for fibrosis, steatosis and activity staging using shear wave elastography," *Journal of Hepatology,* vol. 62, no. 2, pp. 317-324, 2015.

[8] A. Guibal, G. Renosi, A. Rode, J. Y. Scoazec, O. Guillaud, L. Chardon, M. Munteanu, J. Dumortier, F. Collin and T. Lefort, "Shear wave elastography: An accurate technique to stage liver fibrosis in chronic liver diseases," *Diagnostic and Interventional Imaging,* vol. 97, no. 1, pp. 91-99, 2016.

[9] Y. C. Fung, Biomechanics: Michanical Properties of Living Tissues, New York: Springer Science & Business Media, 2013.

[10] "ZygoteBody," Zygote Media Group, Inc., 2017. [Online]. Available: https://www.zygotebody.com/. [Accessed 14 January 2020].

Appendices

Appendix 1: Anthropometry Instructions

The measuring instructions are as stated in Gordan et al, 2012 Anthropometric Survey of U.S. Army Personnel: Methods and Summary Statistics.

Acromial Height:
Vertical distance between a standing surface and the *right acromion* landmark

Chest Height:
The vertical distance between a standing surface and the *chest point anterior* landmark

Waist Back Length:
The surface distance between the cervical landmark and the posterior omphalion landmark (measured with tape)

Shoulder Length:
The surface distance between the right trapezius landmark and the right acromion landmark (measured with tape)

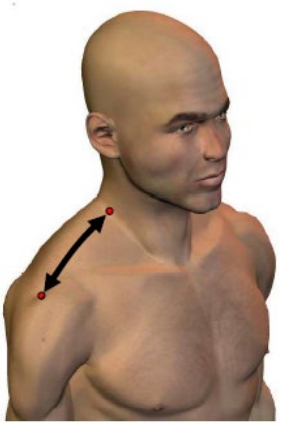

Shoulder Circumference:
The circumference of the shoulders at the level of the right and left deltoid point landmarks (measured with tape)

Chest Circumference:
The maximum horizontal circumference of the chest at the level of the chest point anterior (measured with tape)

Waist Circumference:
The horizontal circumference of the waist passing over all omphalion landmarks (measured with tape)

Biacromial Breadth:
The distance between the right and left acromion landmarks (measured with caliper)

Chest Breadth:
The maximum horizontal breadth of the chest at the level of the chest point anterior landmark (measured with caliper)

Chest Depth:
The horizontal distance between the chest point anterior landmark and the back at the same level (measured with caliper)

Waist Breadth:
The horizontal breadth of the waist at the level of omphalion (measured with caliper)

Waist Depth:
The horizontal distance between the anterior and posterior omphalion landmarks (measured with caliper)

Acromion

Acromion, right and left:
The point of intersection of the lateral border of the acromial process and a line running down the middle of the shoulder from the neck to the tip of the shoulder.

Chest Point

Chest point, anterior*: The most anterior right point on the chest.

Cervicale

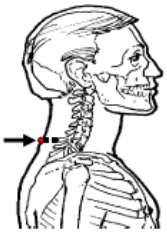

Cervicale*: The most prominent palpable point of the spine of the seventh cervical vertebra.

Omphalion

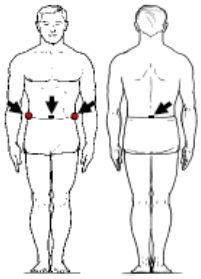

Waist (Omphalion), right, left, anterior, and posterior: The level at the center of the navel.

Trapezius

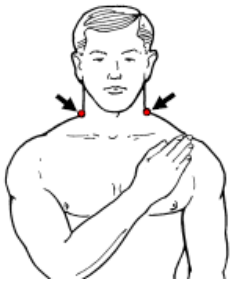

Trapezius, right and left: The point at which the anterior border of the trapezius muscle crosses the neck lateral landmark.

Deltoid

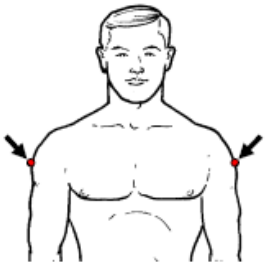

Deltoid point*, right and left: The midpoint of the left and right deltoid muscles.

Appendix 2: Maximum weights per muscle and activity for each subject

The maximum weights used for 100% MVC isometric contractions for each subject and the average.

	Pectoralis Major	Latissimus Dorsi	Lower Trapezius	Upper Trapezius	External Oblique	Rectus Abdominis
SWE_001	40	100	70	70	100	40
SWE_002	25	70	60	110	110	40
SWE_003	60	110	110	140	130	80
SWE_004	40	100	80	130	130	80
SWE_006	50	80	70	90	120	60
SWE_007	20	80	40	90	80	40
SWE_009	30	90	90	120	140	40
SWE_010	50	130	130	190	200	80
SWE_011	40	80	90	100	150	60
SWE_012	40	100	70	70	80	50
SWE_013	30	70	70	70	70	50
SWE_014	40	120	90	125	120	100
SWE_015	40	70	60	70	70	40
SWE_016	40	110	100	180	200	40
SWE_017	30	120	100	130	110	50
SWE_018	30	80	50	100	110	70
SWE_019	50	120	130	170	180	70
SWE_021	40	80	70	150	120	60
SWE_022	30	70	80	100	110	50
SWE_023	40	110	100	110	120	60
Mean	38.3	94.5	83.0	115.8	122.5	58.0
Stand. Dev.	9.6	19.9	24.1	36.5	37.5	17.4

Volunteers were directed to perform the weight lifts and bracing exercise in the following ways. To engage the pectoralis major, the volunteer performed a fly. The volunteer was instructed to hold at the 90° position (exercise itself not described in script, just demonstrated to the volunteer). To engage the rectus abdominis, the volunteer performed a weighted crunch. The volunteer was instructed to lie on his back on a yoga mat, pulled on a rope handle connected to a weight, and contracted enough to lift his shoulders and head off the ground. To additionally engage the rectus abdominis, the volunteer performed a bracing exercise. The volunteer was instructed to brace as if preparing for an impact while imagining that he is expecting to be hit in the stomach by a soccer ball. To engage the external oblique, the volunteer performed a lateral bend. The volunteer was instructed to bend into a vertical neutral position, being maximally contracted while vertical rather than while leaning over. To engage the upper trapezius, the

volunteer performed a cable shrug. The volunteer was instructed to contract a level to lift the weight rather than fully contracting into a “turtle” position (exercise itself not described in script, just demonstrated to the volunteer). To engage the lower trapezius, the volunteer performed bent over rows. The volunteer was instructed to brace his opposing hand against the weight machine if desired, bend to a comfortable level, and pull until his upper arm was parallel to his torso. To engage the latissimus dorsi, the volunteer performed a cable pull down. The volunteer was instructed to hold the weight such that his upper arm was parallel to the floor and his elbow was at a 90° angle.

Appendix 3: EMG sensor locations for each muscle

Upper Trapezius	2cm lateral to the midpoint between C7 spinous process and the acromion	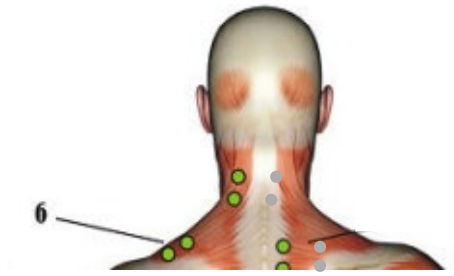
Lower Trapezius	5cm inferomedial from the root of the spine of the scapular at an oblique vertical angle	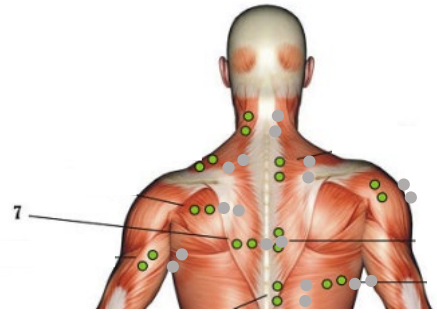
Latissimus Dorsi	1cm lateral to the inferior border of the scapula	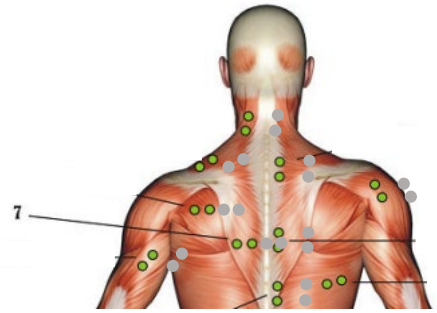
Pectoralis Major	1/3 the distance between the anterior aspect of the acromion and the xiphoid process	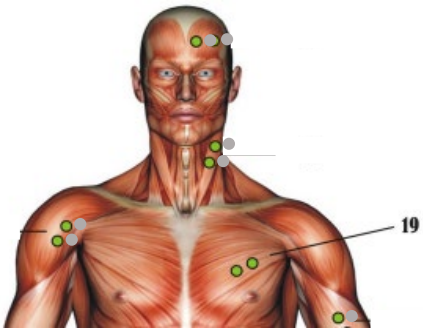
Rectus Abdominis	3cm lateral to the umbilicus in a vertical orientation	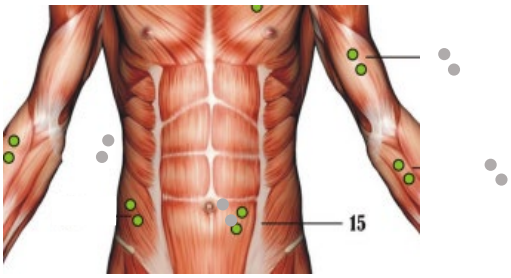

External Oblique	3cm anterior to and mid-way along a line drawn from the lateral pelvic crest to the lateral lower ribcage	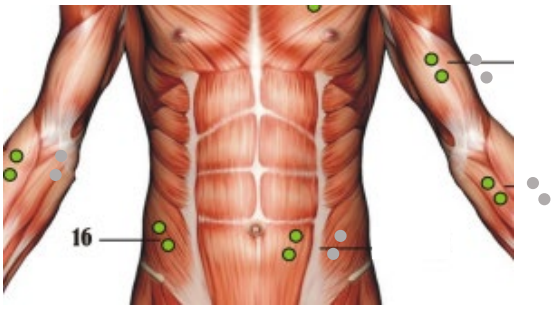

Appendix 4: SWE locations in relation to EMG sensors

SWE measurements were taken across the black line. The triangle indicates direction of probe tip in reference to the torso.

Subject Number: _____

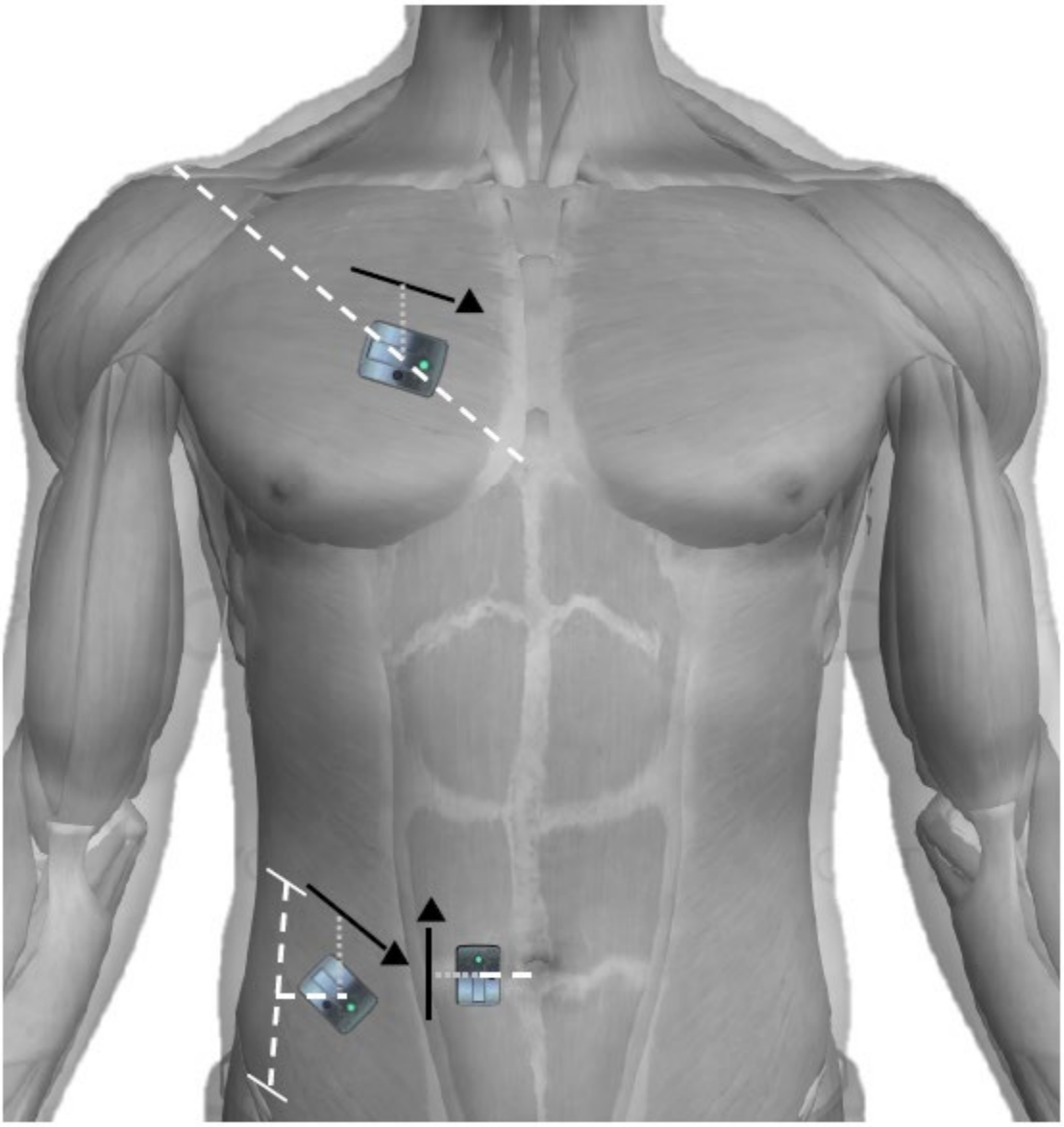

SWE location 4 cm away from center of EMG sensor

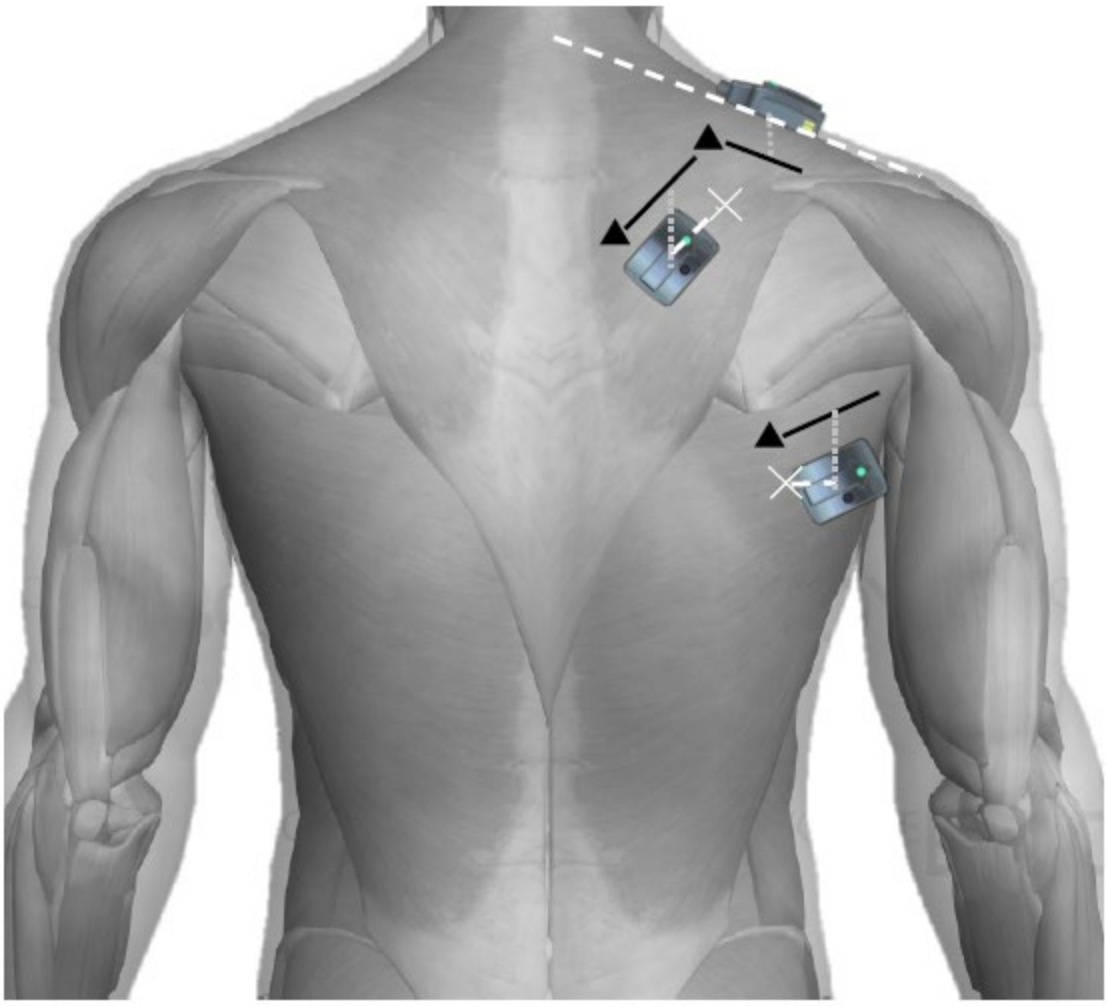

Appendix 5: Average activation across all volunteers per muscle

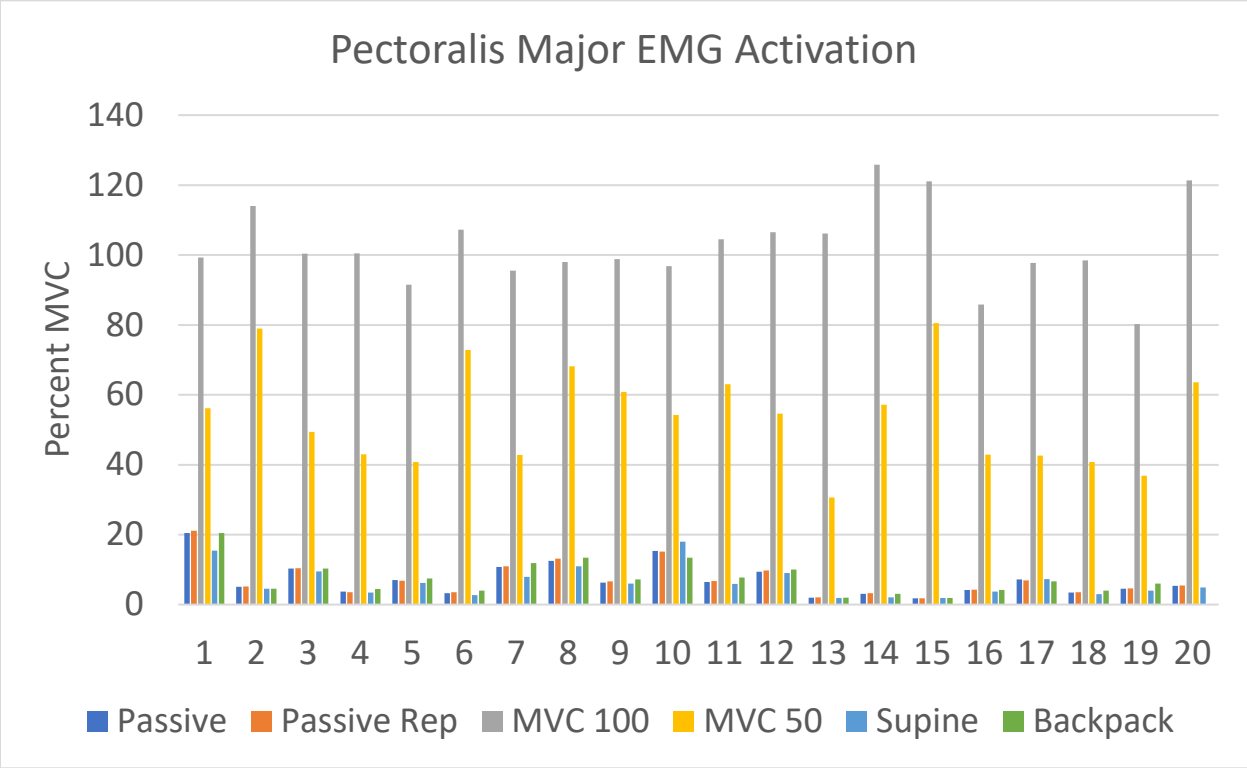

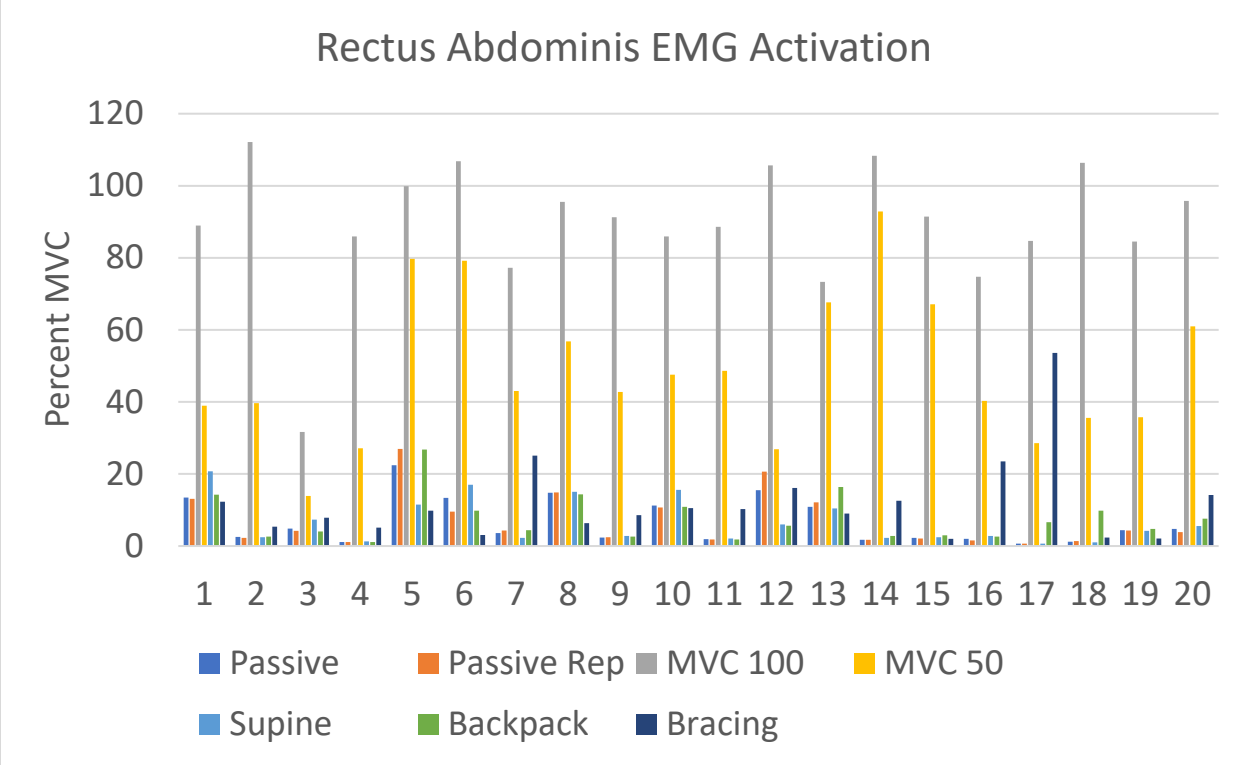

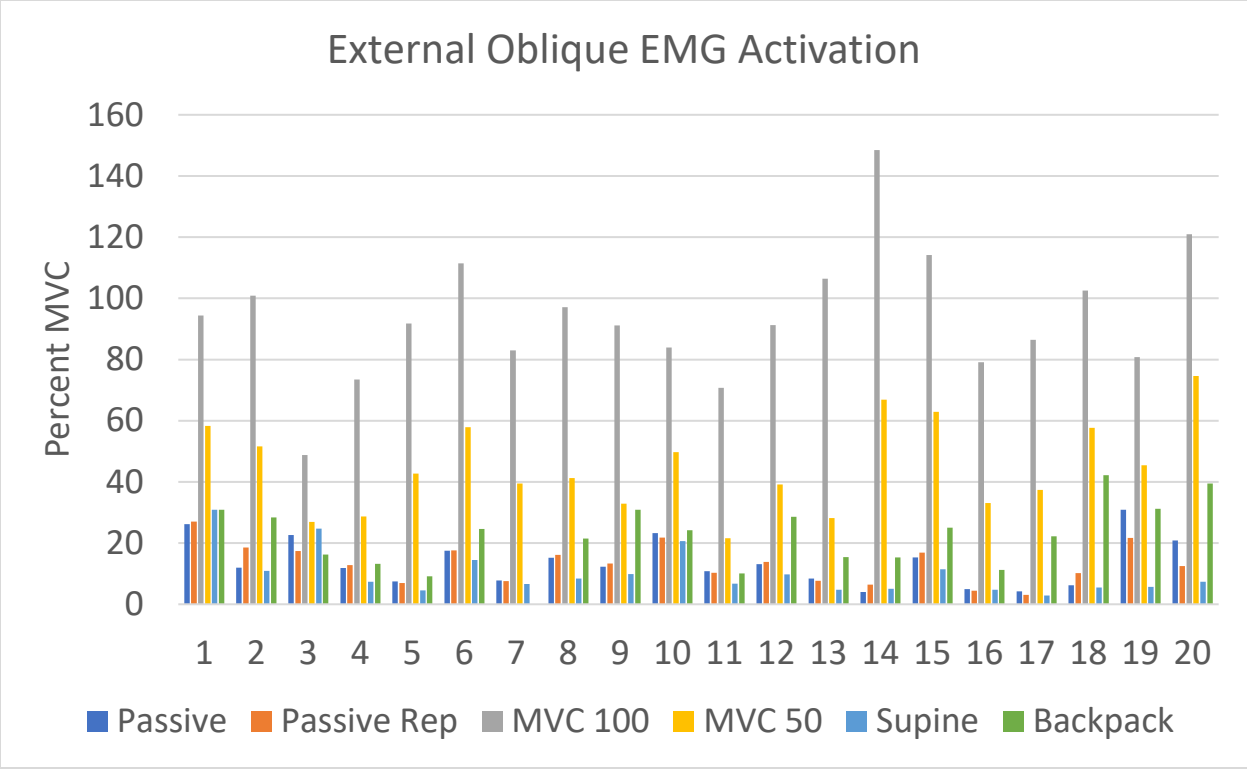
External Oblique EMG Activation
Percent MVC
160
140
120
100
80
60
40
20
0
1 2 3 4 5 6 7 8 9 10 11 12 13 14 15 16 17 18 19 20
Passive
Passive Rep
MVC 100
MVC 50
Supine
Backpack

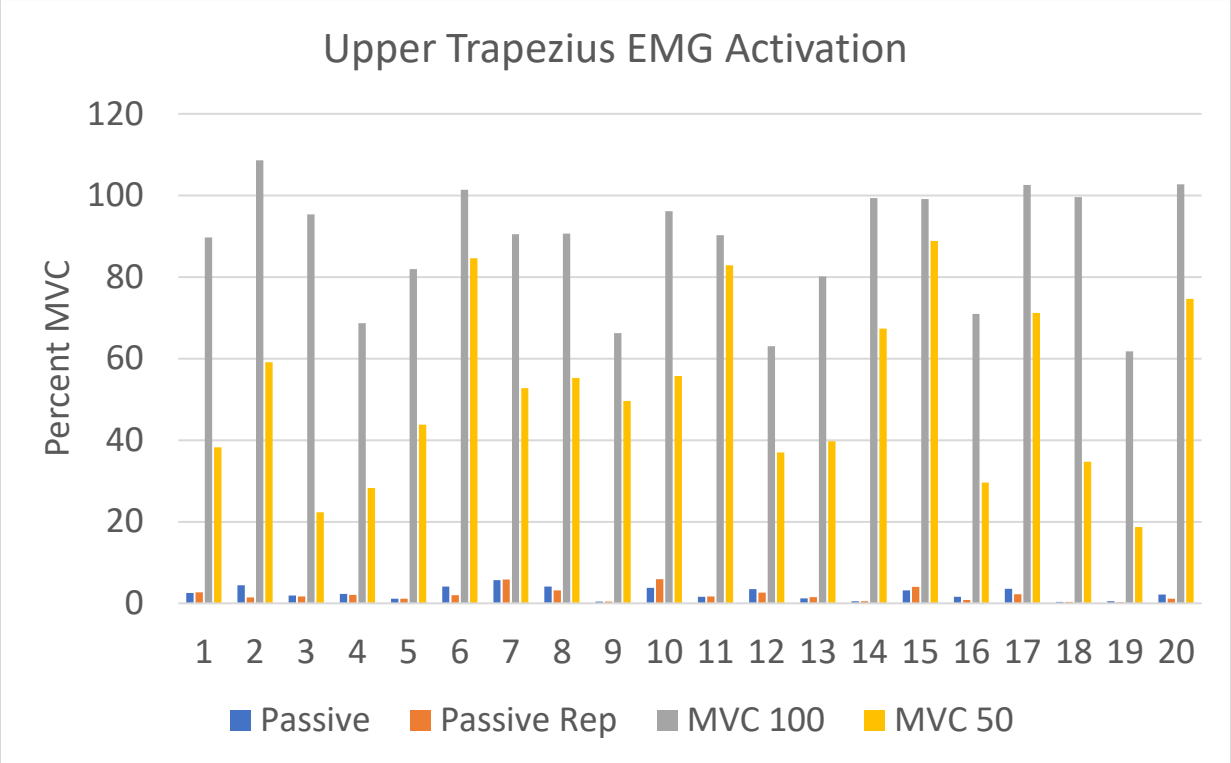
Upper Trapezius EMG Activation
Percent MVC
120
100
80
60
40
20
0
1 2 3 4 5 6 7 8 9 10 11 12 13 14 15 16 17 18 19 20
Passive
Passive Rep
MVC 100
MVC 50

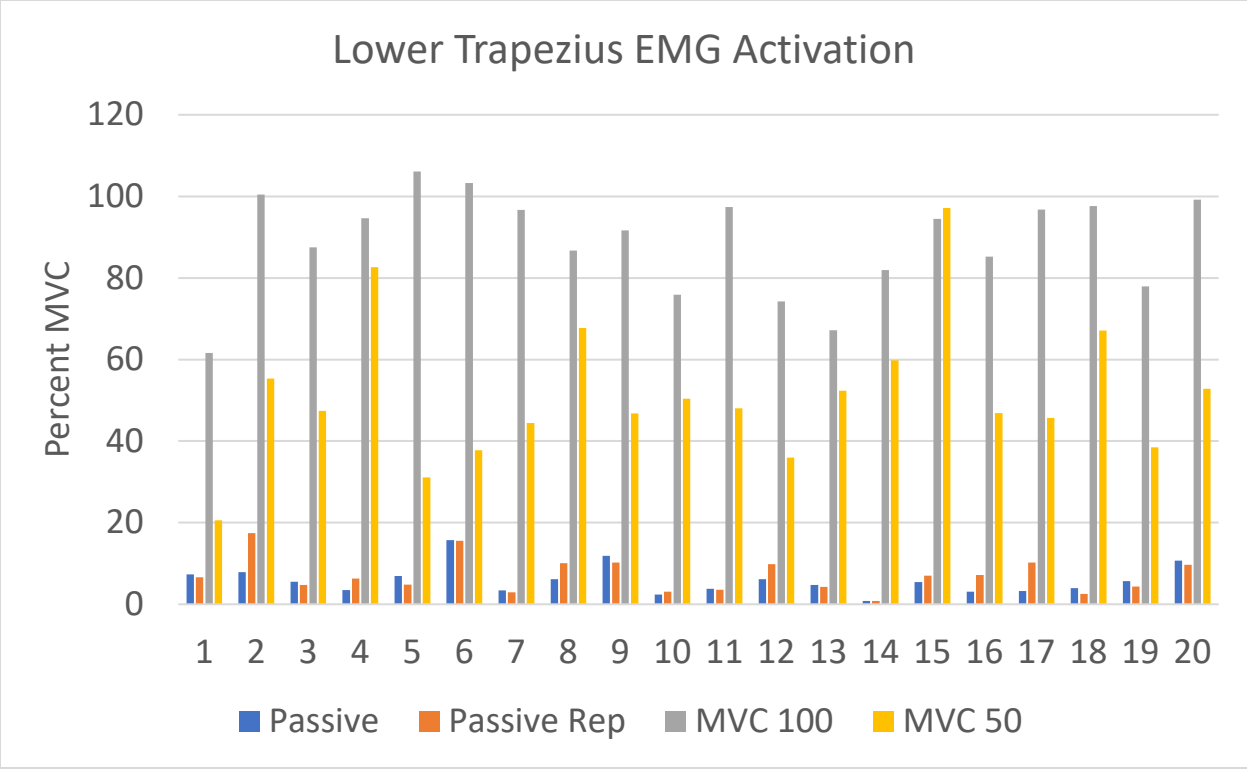
Lower Trapezius EMG Activation
Percent MVC
120
100
80
60
40
20
0
1 2 3 4 5 6 7 8 9 10 11 12 13 14 15 16 17 18 19 20
Passive
Passive Rep
MVC 100
MVC 50

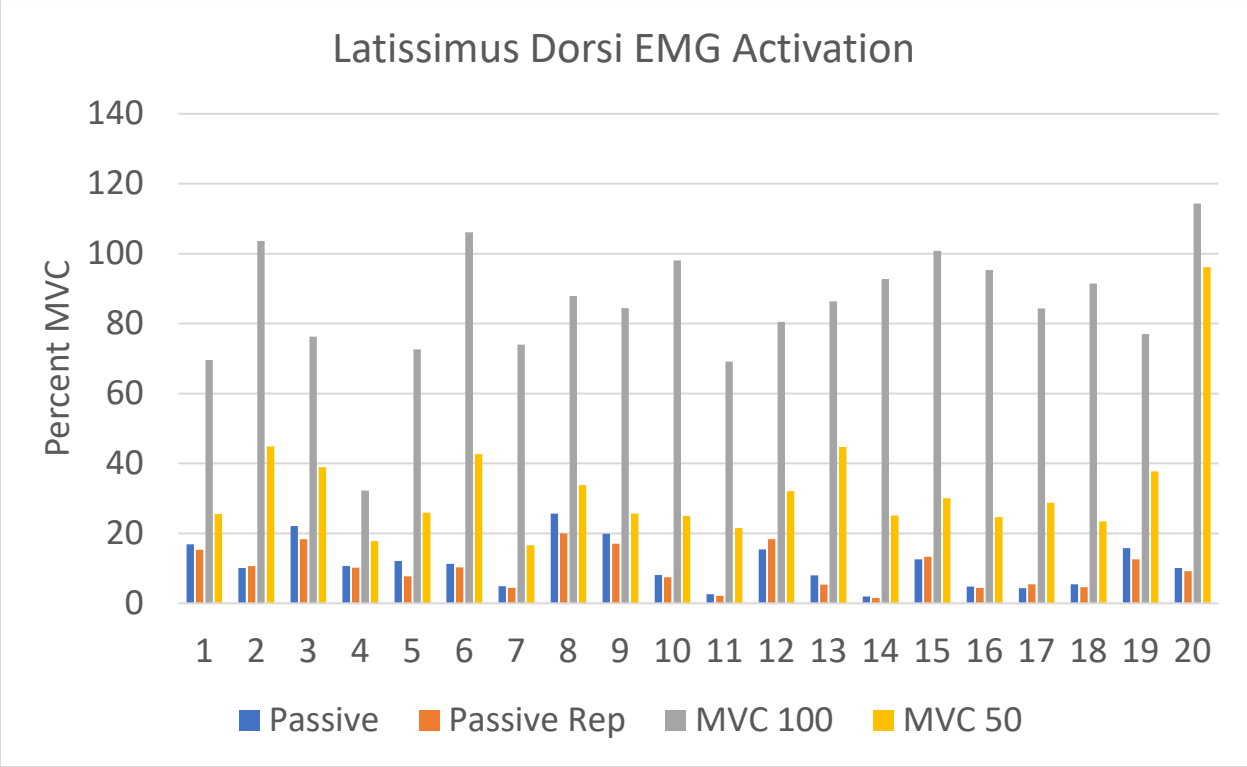
Latissimus Dorsi EMG Activation
Percent MVC
140
120
100
80
60
40
20
0
1 2 3 4 5 6 7 8 9 10 11 12 13 14 15 16 17 18 19 20
Passive
Passive Rep
MVC 100
MVC 50

Appendix 6: Combined average absolute shear wave velocity across all volunteers

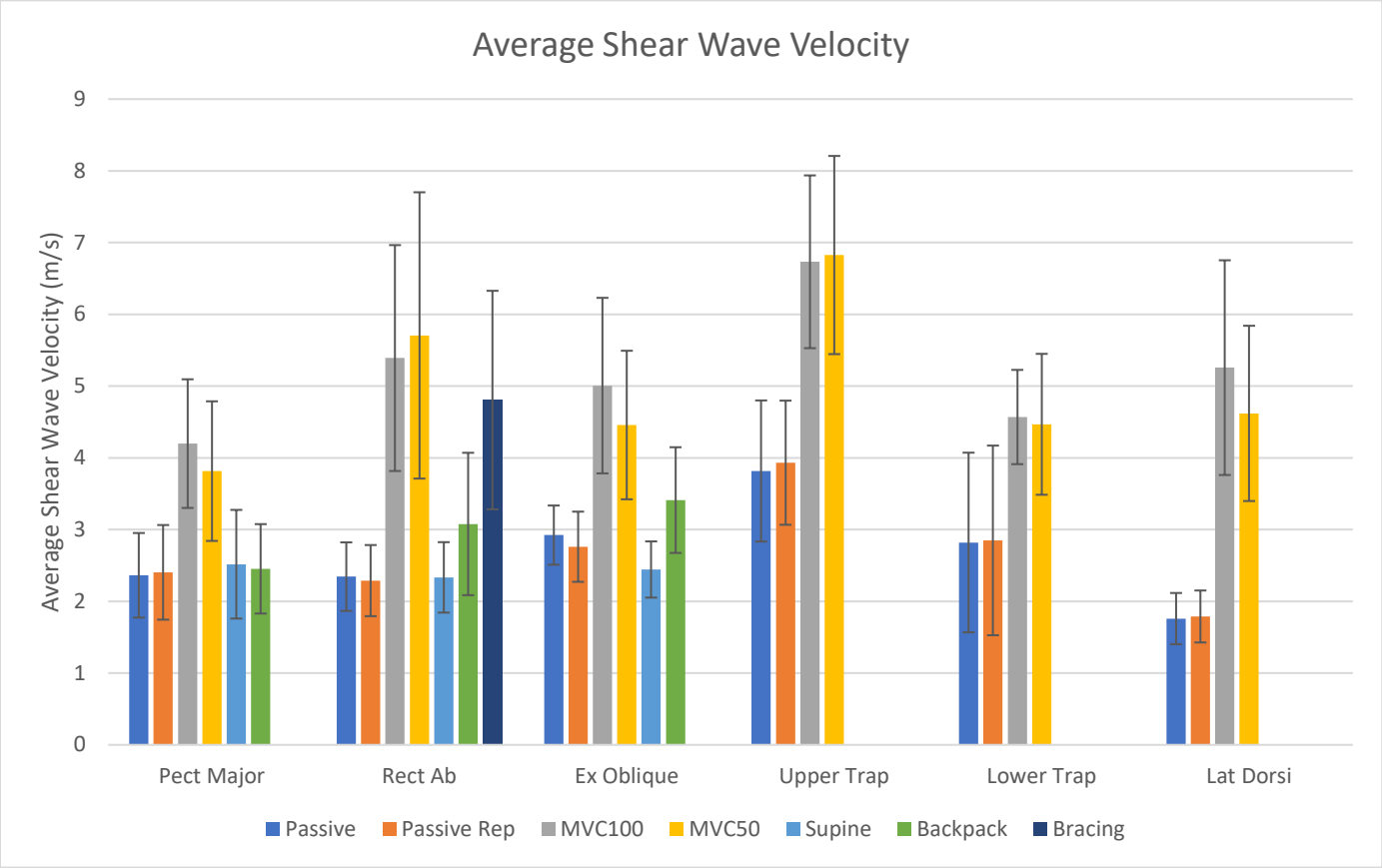

Appendix 7: Individual relationships between muscle activation and absolute shear wave velocity.

$$Shear\ wave\ velocity = a * \ln(\%\ activation) + b$$

The parameters for each individual log fit per subject and muscle using the absolute shear wave velocity; 95% confidence interval included for each parameter.

	Subject Number	a	a CI		b	b CI		R-Squared
Pectoralis Major	SWE_001	1.00	0.82	1.19	3.72	3.46	3.97	0.82
	SWE_002	0.63	0.53	0.73	3.98	3.74	4.21	0.87
	SWE_003	1.12	0.99	1.25	4.37	4.13	4.61	0.93
	SWE_004	0.52	0.43	0.60	4.06	3.84	4.28	0.86
	SWE_006	0.79	0.71	0.88	3.98	3.80	4.16	0.94
	SWE_007	0.35	0.25	0.45	2.99	2.72	3.27	0.67
	SWE_009	0.13	0.06	0.20	1.83	1.67	1.99	0.37
	SWE_010	1.49	1.20	1.77	6.12	5.58	6.65	0.82
	SWE_011	1.56	1.34	1.79	5.91	5.53	6.29	0.89
	SWE_012	0.53	0.39	0.67	3.20	2.89	3.52	0.69
	SWE_013	0.65	0.35	0.94	4.26	3.81	4.70	0.44
	SWE_014	0.59	0.40	0.77	4.55	4.14	4.95	0.62
	SWE_015	0.79	0.59	0.98	4.52	4.15	4.90	0.72
	SWE_016	0.52	0.40	0.64	4.48	4.09	4.87	0.75
	SWE_017	0.20	0.10	0.29	3.09	2.80	3.37	0.39
	SWE_018	0.20	0.10	0.30	3.84	3.52	4.17	0.39
	SWE_019	0.49	0.32	0.66	4.40	3.97	4.84	0.58
	SWE_021	0.96	0.80	1.12	5.15	4.81	5.49	0.86
	SWE_022	0.25	0.05	0.45	4.56	4.01	5.11	0.20
	SWE_023	0.89	0.68	1.11	5.50	4.97	6.03	0.74
Rectus Abdominis	SWE_001	0.69	0.26	1.11	3.92	3.20	4.64	0.26
	SWE_002	1.15	0.92	1.38	7.04	6.35	7.74	0.77
	SWE_003	0.01	-0.29	0.31	2.99	2.19	3.78	0.00
	SWE_004	1.46	1.18	1.74	9.16	8.18	10.15	0.79
	SWE_006	1.36	0.76	1.96	5.96	5.03	6.89	0.41
	SWE_007	0.10	-0.11	0.30	3.69	3.27	4.12	0.03
	SWE_009	0.34	0.20	0.47	2.45	2.14	2.76	0.46
	SWE_010	1.36	1.08	1.64	7.37	6.63	8.11	0.76
	SWE_011	1.04	0.28	1.80	5.95	4.58	7.32	0.20

	Subject Number	a	a CI		b	b CI		R-Squared
	SWE_012	0.51	0.32	0.70	4.38	3.82	4.94	0.48
	SWE_013	0.99	0.46	1.52	4.98	4.01	5.94	0.32
	SWE_014	1.58	1.34	1.82	8.81	8.07	9.54	0.85
	SWE_015	1.13	0.79	1.47	5.38	4.68	6.09	0.60
	SWE_016	1.78	1.17	2.40	6.93	5.80	8.07	0.53
	SWE_017	0.67	0.46	0.87	5.13	4.52	5.75	0.58
	SWE_018	0.41	0.26	0.56	4.44	3.96	4.93	0.49
	SWE_019	1.16	0.88	1.43	7.30	6.49	8.11	0.70
	SWE_021	1.29	1.14	1.44	8.65	8.14	9.16	0.91
	SWE_022	0.87	0.55	1.19	7.59	6.51	8.67	0.50
	SWE_023	0.32	0.16	0.49	4.13	3.67	4.59	0.35
External Oblique	SWE_001	1.56	1.21	1.91	4.23	3.87	4.59	0.77
	SWE_002	0.87	0.72	1.03	4.46	4.23	4.70	0.84
	SWE_003	0.91	0.33	1.49	3.98	3.14	4.81	0.29
	SWE_004	1.50	1.04	1.96	6.56	5.70	7.43	0.63
	SWE_006	0.16	0.00	0.31	3.07	2.73	3.41	0.14
	SWE_007	0.55	0.38	0.72	3.57	3.33	3.81	0.63
	SWE_009	0.69	0.46	0.91	3.67	3.32	4.01	0.60
	SWE_010	1.00	0.78	1.23	5.33	4.87	5.79	0.80
	SWE_011	1.22	0.99	1.45	5.28	4.90	5.65	0.82
	SWE_012	1.92	1.74	2.10	6.66	6.37	6.95	0.95
	SWE_013	2.07	1.76	2.39	5.66	5.27	6.05	0.88
	SWE_014	1.51	1.14	1.87	6.50	5.74	7.26	0.73
	SWE_015	1.25	1.05	1.46	5.66	5.33	5.99	0.86
	SWE_016	0.93	0.73	1.14	5.68	5.24	6.11	0.77
	SWE_017	0.58	0.45	0.72	4.46	4.16	4.75	0.76
	SWE_018	0.48	0.28	0.69	3.68	3.37	3.98	0.47
	SWE_019	1.83	1.60	2.05	8.63	8.11	9.14	0.92
	SWE_021	0.63	0.51	0.74	5.43	5.15	5.70	0.83
	SWE_022	0.72	0.60	0.84	4.86	4.63	5.10	0.85
	SWE_023	1.46	1.00	1.92	6.44	5.73	7.14	0.62
Upper Trapezius	SWE_001	0.73	0.53	0.92	6.67	6.18	7.16	0.80
	SWE_002	1.06	0.96	1.17	7.98	7.70	8.26	0.97
	SWE_003	0.87	0.50	1.24	6.69	5.60	7.78	0.61

	Subject Number	a	a CI		b	b CI		R-Squared
	SWE_004	0.87	0.64	1.11	9.01	8.38	9.65	0.79
	SWE_006	0.89	0.76	1.02	7.94	7.55	8.33	0.93
	SWE_007	0.86	0.71	1.01	7.20	6.85	7.56	0.90
	SWE_009	0.22	0.14	0.30	3.42	3.19	3.64	0.67
	SWE_010	1.24	0.87	1.60	7.99	7.25	8.74	0.76
	SWE_011	1.17	1.00	1.35	8.03	7.63	8.42	0.93
	SWE_012	0.51	0.41	0.61	6.15	5.79	6.50	0.89
	SWE_013	0.79	0.56	1.01	7.11	6.57	7.66	0.77
	SWE_014	0.53	0.39	0.66	5.43	5.05	5.80	0.81
	SWE_015	1.06	0.63	1.50	8.09	7.01	9.16	0.63
	SWE_016	0.68	0.51	0.85	6.61	6.12	7.11	0.82
	SWE_017	0.56	0.39	0.73	6.74	6.14	7.34	0.76
	SWE_018	0.48	0.34	0.62	5.12	4.79	5.44	0.77
	SWE_019	0.42	0.21	0.64	6.98	6.31	7.65	0.52
	SWE_021	0.30	-0.05	0.65	6.68	5.83	7.52	0.17
	SWE_022	0.85	0.60	1.10	8.21	7.26	9.17	0.76
	SWE_023	1.10	0.88	1.31	9.83	8.99	10.68	0.88
Lower Trapezius	SWE_001	1.16	0.71	1.61	5.35	4.41	6.29	0.65
	SWE_002	1.88	1.59	2.16	6.69	6.25	7.12	0.93
	SWE_003	0.65	0.46	0.84	5.01	4.62	5.39	0.76
	SWE_004	0.21	-0.08	0.49	5.83	5.22	6.43	0.13
	SWE_006	1.10	0.75	1.45	5.77	5.07	6.46	0.73
	SWE_007	0.80	0.43	1.17	4.41	3.90	4.92	0.57
	SWE_009	1.30	0.95	1.65	4.01	3.46	4.56	0.79
	SWE_010	0.52	0.33	0.71	4.48	4.02	4.93	0.67
	SWE_011	0.67	0.42	0.92	4.44	3.99	4.88	0.66
	SWE_012	1.10	0.81	1.39	4.30	3.86	4.74	0.81
	SWE_013	0.37	0.05	0.69	4.61	3.81	5.41	0.28
	SWE_014	0.93	0.76	1.09	4.93	4.56	5.29	0.90
	SWE_015	0.41	0.18	0.64	3.62	3.18	4.05	0.47
	SWE_016	0.85	0.61	1.08	4.49	3.99	4.98	0.79
	SWE_017	0.42	0.32	0.52	5.58	5.25	5.91	0.82
	SWE_018	0.86	0.69	1.03	3.98	3.65	4.31	0.88
	SWE_019	-0.02	-0.28	0.24	4.81	4.24	5.38	0.00

	Subject Number	a	a CI		b	b CI		R-Squared
	SWE_021	-0.08	-0.31	0.15	5.08	4.60	5.56	0.03
	SWE_022	-0.23	-0.38	-8.28	3.83	3.48	4.17	0.40
	SWE_023	0.96	0.81	1.12	4.76	4.45	5.08	0.92
Latissimus Dorsi	SWE_001	1.29	0.99	1.58	4.03	3.61	4.45	0.84
	SWE_002	0.98	0.67	1.30	4.34	3.84	4.83	0.73
	SWE_003	1.28	0.80	1.76	4.03	3.45	4.60	0.66
	SWE_004	3.09	2.07	4.11	9.19	7.27	11.12	0.72
	SWE_006	1.02	0.61	1.43	4.56	3.85	5.27	0.63
	SWE_007	1.13	0.61	1.65	4.97	4.17	5.78	0.57
	SWE_009	0.48	0.39	0.58	2.30	2.15	2.44	0.89
	SWE_010	1.40	0.92	1.88	6.62	5.54	7.70	0.71
	SWE_011	2.54	1.33	3.75	6.39	5.02	7.75	0.55
	SWE_012	3.10	2.24	3.96	7.62	6.46	8.77	0.79
	SWE_013	1.01	0.67	1.35	4.66	4.03	5.29	0.71
	SWE_014	1.12	0.68	1.56	7.00	5.82	8.18	0.64
	SWE_015	2.63	2.00	3.26	6.49	5.63	7.35	0.83
	SWE_016	2.06	1.78	2.33	6.90	6.38	7.42	0.94
	SWE_017	0.51	0.42	0.60	3.90	3.66	4.14	0.91
	SWE_018	2.27	1.84	2.71	6.60	5.94	7.26	0.88
	SWE_019	2.19	1.75	2.63	9.09	8.12	10.06	0.87
	SWE_021	1.42	1.18	1.66	6.37	5.85	6.89	0.91
	SWE_022	1.40	0.99	1.81	6.30	5.43	7.17	0.77
	SWE_023	2.51	1.53	3.49	7.65	6.21	9.09	0.65
Rectus Abdominis without Bracing	SWE_001	0.94	0.57	1.30	4.09	3.52	4.67	0.52
	SWE_002	1.17	0.92	1.41	6.97	6.23	7.72	0.78
	SWE_003	0.01	-0.29	0.32	2.97	2.14	3.79	0.00
	SWE_004	1.45	1.17	1.73	8.93	7.91	9.95	0.81
	SWE_006	2.18	1.75	2.61	6.43	5.85	7.02	0.81
	SWE_007	0.18	-0.10	0.46	3.77	3.30	4.25	0.07
	SWE_009	0.33	0.24	0.43	2.32	2.09	2.55	0.66
	SWE_010	1.34	1.06	1.62	7.24	6.46	8.01	0.79
	SWE_011	2.12	1.52	2.72	6.93	5.97	7.88	0.67
	SWE_012	0.50	0.42	0.58	4.16	3.92	4.41	0.86
	SWE_013	1.43	1.18	1.68	5.24	4.80	5.67	0.84

Subject Number	a	a CI		b	b CI		R-Squared
SWE_014	1.57	1.32	1.83	8.68	7.86	9.49	0.86
SWE_015	1.15	0.81	1.48	5.56	4.85	6.28	0.65
SWE_016	2.29	1.79	2.79	7.30	6.44	8.16	0.77
SWE_017	0.63	0.56	0.71	4.71	4.48	4.95	0.92
SWE_018	0.53	0.42	0.63	4.51	4.19	4.83	0.80
SWE_019	1.08	0.84	1.31	6.83	6.10	7.57	0.77
SWE_021	1.26	1.09	1.42	8.48	7.88	9.09	0.90
SWE_022	0.96	0.67	1.26	7.53	6.55	8.50	0.64
SWE_023	0.38	0.18	0.57	4.19	3.70	4.69	0.38

Appendix 8: Individual relationships between muscle activation and normalized shear wave velocity

$$Shear\ wave\ velocity = a * \ln(\%\ activation) + b$$

The parameters for each individual log fit per subject and muscle using the normalized shear wave velocity; 95% confidence interval included for each parameter.

	Subject Number	a	a CI		b	b CI		R-Squared
Pectoralis Major	SWE_001	0.52	0.42	0.62	1.92	1.79	2.05	0.82
	SWE_002	0.32	0.27	0.37	2.05	1.93	2.17	0.87
	SWE_003	0.58	0.51	0.64	2.25	2.13	2.38	0.93
	SWE_004	0.27	0.22	0.31	2.09	1.98	2.21	0.86
	SWE_006	0.41	0.37	0.45	2.06	1.96	2.15	0.94
	SWE_007	0.18	0.13	0.23	1.54	1.40	1.69	0.67
	SWE_009	0.77	0.62	0.92	3.16	2.88	3.43	0.82
	SWE_010	0.81	0.69	0.92	3.05	2.86	3.25	0.89
	SWE_011	0.27	0.20	0.35	1.65	1.49	1.81	0.69
	SWE_012	0.33	0.18	0.48	2.20	1.97	2.43	0.44
	SWE_013	0.30	0.21	0.40	2.35	2.14	2.56	0.62
	SWE_014	0.41	0.30	0.51	2.33	2.14	2.53	0.72
	SWE_015	0.27	0.21	0.33	2.31	2.11	2.52	0.75
	SWE_016	0.10	0.05	0.15	1.59	1.45	1.74	0.39
	SWE_017	0.10	0.05	0.16	1.98	1.82	2.15	0.39
	SWE_018	0.25	0.17	0.34	2.27	2.05	2.50	0.58
	SWE_019	0.49	0.41	0.58	2.66	2.48	2.83	0.86
	SWE_021	0.13	0.02	0.23	2.35	2.07	2.64	0.20
	SWE_022	0.46	0.35	0.57	2.84	2.57	3.11	0.74
	SWE_023	0.07	0.03	0.10	0.94	0.86	1.03	0.37
Rectus Abdominis	SWE_001	0.30	0.11	0.49	1.71	1.40	2.02	0.26
	SWE_002	0.50	0.40	0.60	3.07	2.77	3.37	0.77
	SWE_003	0.00	-0.13	0.13	1.30	0.96	1.65	0.00
	SWE_004	0.64	0.51	0.76	3.99	3.56	4.42	0.79
	SWE_006	0.59	0.33	0.85	2.60	2.19	3.00	0.41
	SWE_007	0.04	-0.05	0.13	1.61	1.42	1.79	0.03
	SWE_009	0.15	0.09	0.21	1.07	0.93	1.20	0.46
	SWE_010	0.59	0.47	0.72	3.21	2.89	3.53	0.76
	SWE_011	0.45	0.12	0.78	2.59	1.99	3.19	0.20

	Subject Number	a	a CI		b	b CI		R-Squared
	SWE_012	0.22	0.14	0.31	1.91	1.67	2.15	0.48
	SWE_013	0.43	0.20	0.66	2.17	1.75	2.59	0.32
	SWE_014	0.69	0.59	0.79	3.84	3.52	4.16	0.85
	SWE_015	0.49	0.34	0.64	2.35	2.04	2.65	0.60
	SWE_016	0.78	0.51	1.04	3.02	2.53	3.52	0.53
	SWE_017	0.29	0.20	0.38	2.24	1.97	2.51	0.58
	SWE_018	0.18	0.11	0.25	1.94	1.73	2.15	0.49
	SWE_019	0.50	0.38	0.62	3.18	2.83	3.54	0.70
	SWE_021	0.56	0.50	0.63	3.77	3.55	3.99	0.91
	SWE_022	0.38	0.24	0.52	3.31	2.84	3.78	0.50
	SWE_023	0.14	0.07	0.21	1.80	1.60	2.00	0.35
External Oblique	SWE_001	0.72	0.56	0.88	1.95	1.78	2.11	0.77
	SWE_002	0.40	0.33	0.47	2.06	1.95	2.16	0.84
	SWE_003	0.42	0.15	0.69	1.83	1.45	2.21	0.29
	SWE_004	0.69	0.48	0.90	3.02	2.62	3.42	0.63
	SWE_006	0.07	0.00	0.14	1.42	1.26	1.57	0.14
	SWE_007	0.25	0.18	0.33	1.64	1.53	1.76	0.63
	SWE_009	0.32	0.21	0.42	1.69	1.53	1.85	0.60
	SWE_010	0.46	0.36	0.57	2.46	2.24	2.67	0.80
	SWE_011	0.56	0.46	0.67	2.43	2.26	2.60	0.82
	SWE_012	0.88	0.80	0.97	3.07	2.93	3.20	0.95
	SWE_013	0.95	0.81	1.10	2.61	2.43	2.79	0.88
	SWE_014	0.69	0.52	0.86	2.99	2.64	3.34	0.73
	SWE_015	0.58	0.48	0.67	2.61	2.45	2.76	0.86
	SWE_016	0.43	0.34	0.53	2.62	2.41	2.82	0.77
	SWE_017	0.27	0.21	0.33	2.05	1.91	2.19	0.76
	SWE_018	0.22	0.13	0.32	1.69	1.55	1.83	0.47
	SWE_019	0.84	0.74	0.94	3.97	3.74	4.21	0.92
	SWE_021	0.29	0.24	0.34	2.50	2.37	2.63	0.83
	SWE_022	0.33	0.28	0.39	2.24	2.13	2.35	0.85
	SWE_023	0.67	0.46	0.88	2.96	2.64	3.29	0.62
Upper Trapezius	SWE_001	0.18	0.13	0.22	1.62	1.50	1.74	0.80
	SWE_002	0.26	0.23	0.28	1.94	1.87	2.01	0.97
	SWE_003	0.21	0.12	0.30	1.63	1.36	1.89	0.61

	Subject Number	a	a CI		b	b CI		R-Squared
	SWE_004	0.21	0.15	0.27	2.19	2.04	2.35	0.79
	SWE_006	0.22	0.18	0.25	1.93	1.84	2.03	0.93
	SWE_007	0.21	0.17	0.25	1.75	1.67	1.84	0.90
	SWE_009	0.05	0.03	0.07	0.83	0.78	0.89	0.67
	SWE_010	0.30	0.21	0.39	1.94	1.76	2.13	0.76
	SWE_011	0.29	0.24	0.33	1.95	1.86	2.05	0.93
	SWE_012	0.12	0.10	0.15	1.50	1.41	1.58	0.89
	SWE_013	0.19	0.14	0.25	1.73	1.60	1.86	0.77
	SWE_014	0.13	0.10	0.16	1.32	1.23	1.41	0.81
	SWE_015	0.26	0.15	0.36	1.97	1.71	2.23	0.63
	SWE_016	0.17	0.12	0.21	1.61	1.49	1.73	0.82
	SWE_017	0.14	0.10	0.18	1.64	1.49	1.79	0.76
	SWE_018	0.12	0.08	0.15	1.24	1.16	1.32	0.77
	SWE_019	0.10	0.05	0.16	1.70	1.53	1.86	0.52
	SWE_021	0.07	-0.01	0.16	1.62	1.42	1.83	0.17
	SWE_022	0.21	0.15	0.27	2.00	1.76	2.23	0.76
	SWE_023	0.27	0.21	0.32	2.39	2.19	2.60	0.88
Lower Trapezius	SWE_001	0.67	0.41	0.93	3.10	2.56	3.64	0.65
	SWE_002	1.09	0.92	1.25	3.87	3.62	4.12	0.93
	SWE_003	0.38	0.26	0.49	2.90	2.67	3.12	0.76
	SWE_004	0.12	-0.05	0.28	3.37	3.02	3.72	0.13
	SWE_006	0.64	0.43	0.84	3.34	2.94	3.74	0.73
	SWE_007	0.46	0.25	0.68	2.55	2.26	2.85	0.57
	SWE_009	0.75	0.55	0.96	2.32	2.00	2.64	0.79
	SWE_010	0.30	0.19	0.41	2.59	2.33	2.85	0.67
	SWE_011	0.39	0.24	0.53	2.57	2.31	2.83	0.66
	SWE_012	0.64	0.47	0.80	2.49	2.23	2.75	0.81
	SWE_013	0.21	0.03	0.40	2.67	2.21	3.13	0.28
	SWE_014	0.54	0.44	0.63	2.85	2.64	3.06	0.90
	SWE_015	0.24	0.10	0.37	2.09	1.84	2.35	0.47
	SWE_016	0.49	0.36	0.63	2.60	2.31	2.89	0.79
	SWE_017	0.24	0.18	0.30	3.23	3.04	3.42	0.82
	SWE_018	0.50	0.40	0.60	2.31	2.12	2.50	0.88
	SWE_019	-0.01	-0.16	0.14	2.79	2.46	3.12	0.00

	Subject Number	a	a CI		b	b CI		R-Squared
	SWE_021	-0.05	-0.18	0.09	2.94	2.66	3.22	0.03
	SWE_022	-0.13	-0.22	-4.80	2.22	2.02	2.41	0.40
	SWE_023	0.56	0.47	0.65	2.76	2.57	2.94	0.92
Latissimus Dorsi	SWE_001	0.89	0.69	1.10	2.80	2.51	3.09	0.84
	SWE_002	0.68	0.46	0.90	3.01	2.67	3.35	0.73
	SWE_003	0.89	0.55	1.22	2.80	2.40	3.19	0.66
	SWE_004	2.14	1.44	2.85	6.38	5.04	7.71	0.72
	SWE_006	0.71	0.42	0.99	3.16	2.67	3.65	0.63
	SWE_007	0.79	0.43	1.15	3.45	2.89	4.01	0.57
	SWE_009	0.34	0.27	0.40	1.59	1.49	1.69	0.89
	SWE_010	0.97	0.64	1.31	4.59	3.84	5.35	0.71
	SWE_011	1.76	0.93	2.60	4.43	3.48	5.38	0.55
	SWE_012	2.15	1.55	2.75	5.28	4.49	6.08	0.79
	SWE_013	0.70	0.46	0.94	3.23	2.79	3.67	0.71
	SWE_014	0.78	0.47	1.08	4.85	4.04	5.67	0.64
	SWE_015	1.83	1.39	2.26	4.50	3.91	5.10	0.83
	SWE_016	1.43	1.23	1.62	4.79	4.43	5.15	0.94
	SWE_017	0.35	0.29	0.41	2.71	2.54	2.87	0.91
	SWE_018	1.58	1.27	1.88	4.58	4.12	5.04	0.88
	SWE_019	1.52	1.22	1.83	6.30	5.63	6.98	0.87
	SWE_021	0.99	0.82	1.15	4.42	4.06	4.78	0.91
	SWE_022	0.97	0.69	1.25	4.37	3.77	4.97	0.77
	SWE_023	1.74	1.06	2.42	5.31	4.31	6.31	0.65
Rectus Abdominis without Bracing	SWE_001	0.41	0.25	0.57	1.78	1.53	2.03	0.52
	SWE_002	0.51	0.40	0.62	3.04	2.72	3.36	0.78
	SWE_003	0.01	-0.13	0.14	1.29	0.93	1.65	0.00
	SWE_004	0.63	0.51	0.75	3.89	3.45	4.34	0.81
	SWE_006	0.95	0.76	1.14	2.80	2.55	3.06	0.81
	SWE_007	0.08	-0.04	0.20	1.64	1.44	1.85	0.07
	SWE_009	0.15	0.10	0.19	1.01	0.91	1.11	0.66
	SWE_010	0.58	0.46	0.71	3.15	2.82	3.49	0.79
	SWE_011	0.92	0.66	1.19	3.02	2.60	3.43	0.67
	SWE_012	0.22	0.18	0.25	1.81	1.71	1.92	0.86
	SWE_013	0.62	0.51	0.73	2.28	2.09	2.47	0.84

Subject Number	a	a CI		b	b CI		R-Squared
SWE_014	0.69	0.57	0.80	3.78	3.43	4.14	0.86
SWE_015	0.50	0.35	0.65	2.42	2.11	2.74	0.65
SWE_016	1.00	0.78	1.21	3.18	2.81	3.55	0.77
SWE_017	0.28	0.24	0.31	2.05	1.95	2.16	0.92
SWE_018	0.23	0.18	0.28	1.97	1.83	2.10	0.80
SWE_019	0.47	0.37	0.57	2.98	2.66	3.30	0.77
SWE_021	0.55	0.47	0.62	3.70	3.43	3.96	0.90
SWE_022	0.42	0.29	0.55	3.28	2.85	3.70	0.64
SWE_023	0.16	0.08	0.25	1.83	1.61	2.04	0.38

Appendix 9: Log Fits for Muscle Activation and Normalized Shear Wave Velocities

Average normalized shear wave velocity and activation relationship (mean ± 1 SD)

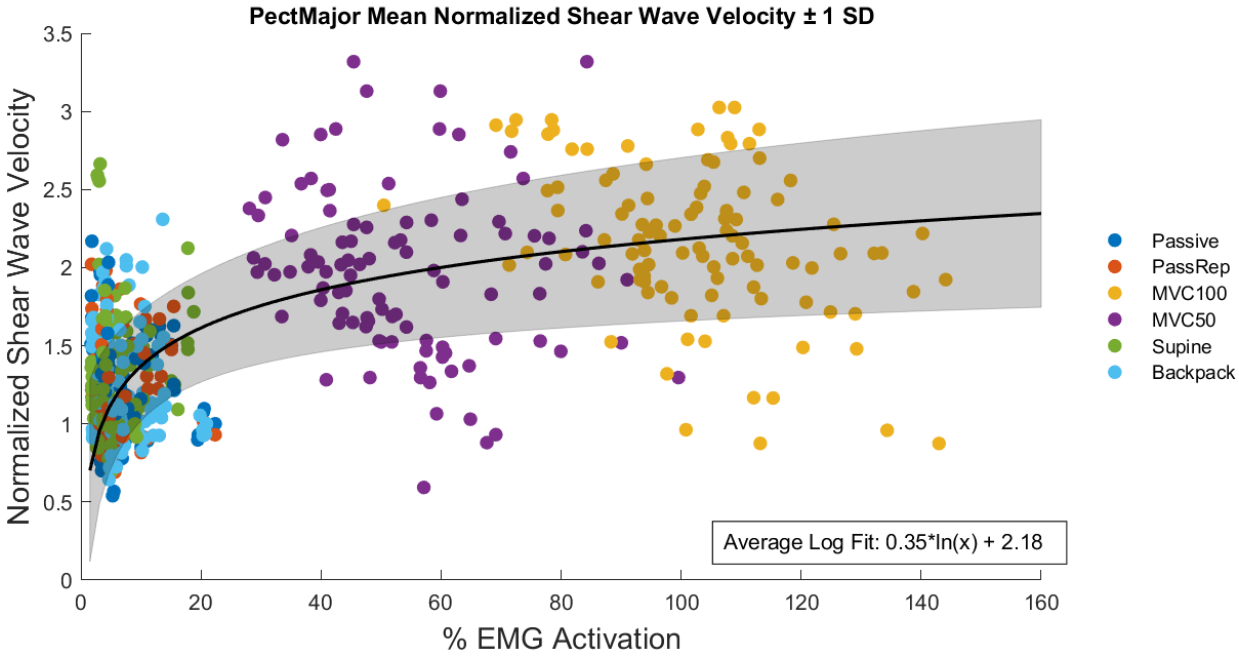

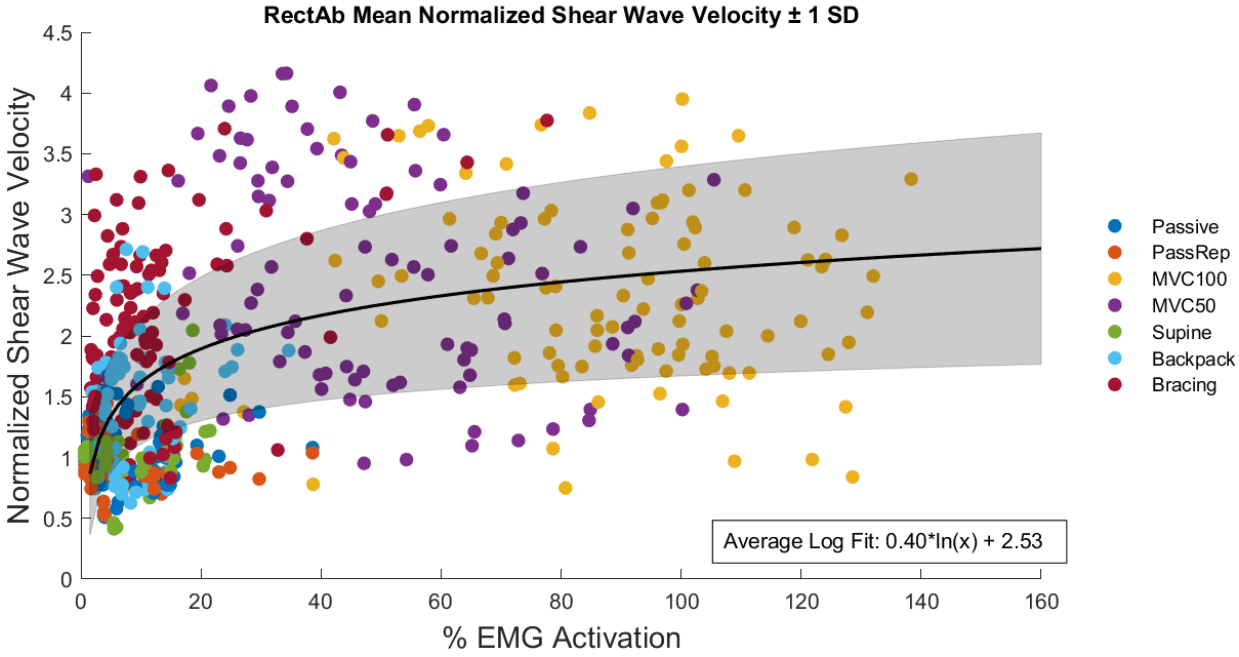

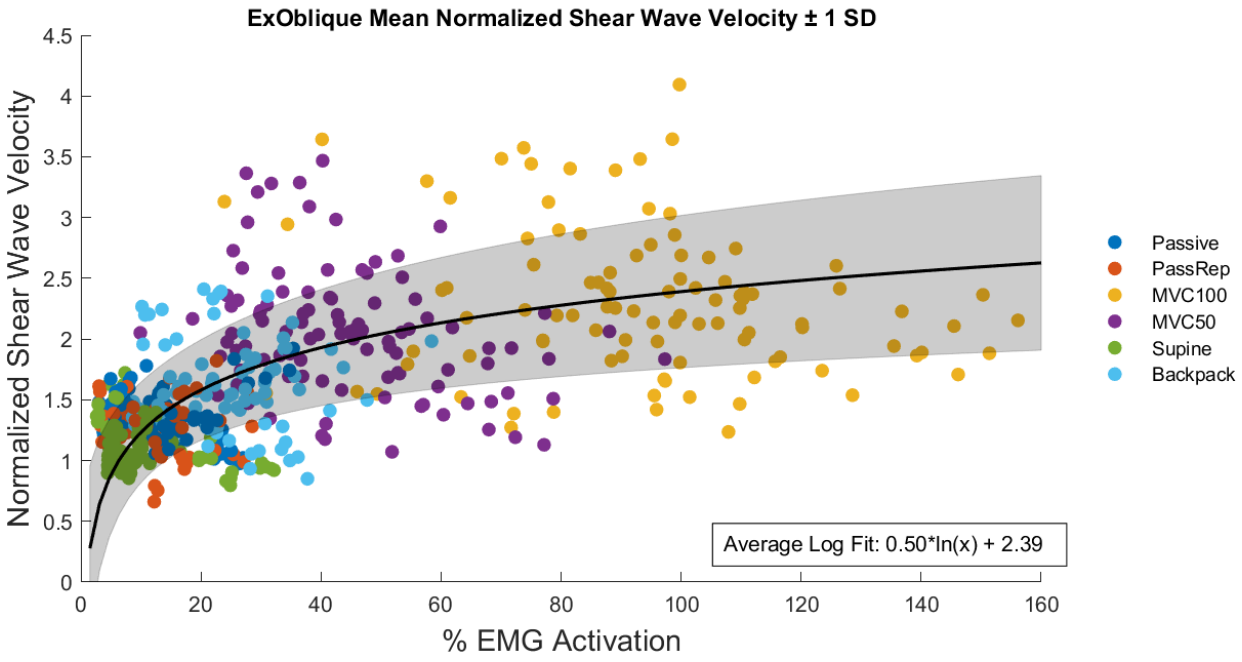
ExOblique Mean Normalized Shear Wave Velocity ± 1 SD
Normalized Shear Wave Velocity
% EMG Activation
Average Log Fit: 0.50*ln(x) + 2.39
Passive
PassRep
MVC100
MVC50
Supine
Backpack

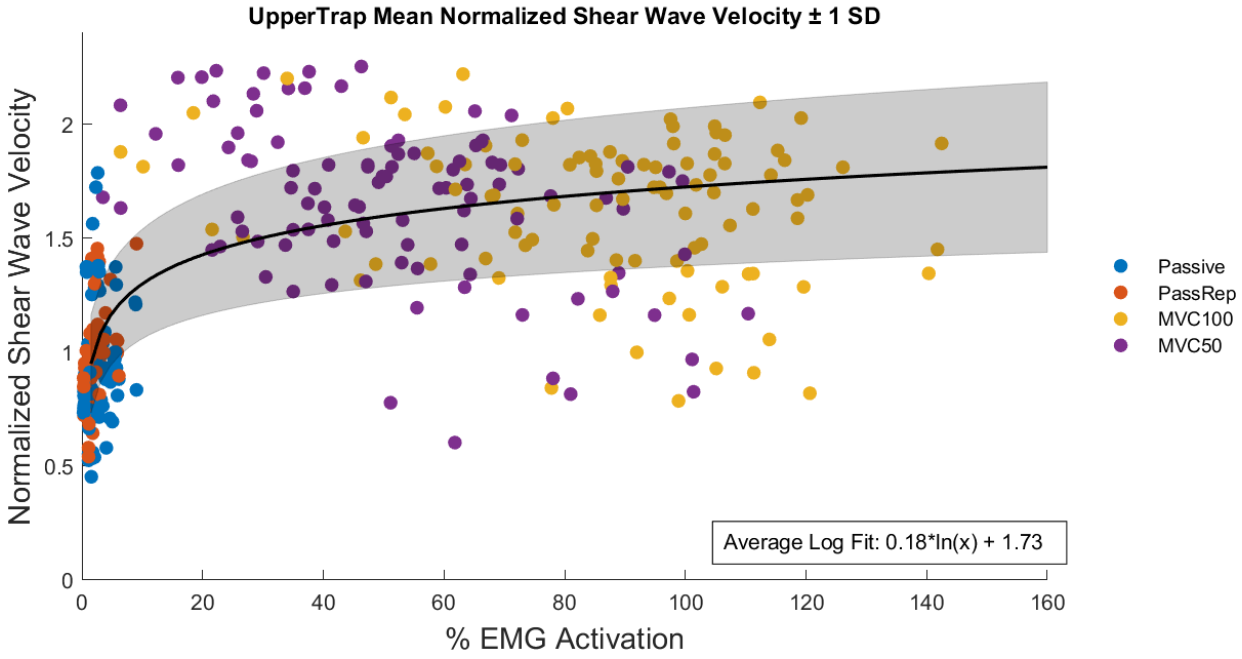
UpperTrap Mean Normalized Shear Wave Velocity ± 1 SD
Normalized Shear Wave Velocity
% EMG Activation
Average Log Fit: 0.18*ln(x) + 1.73
Passive
PassRep
MVC100
MVC50

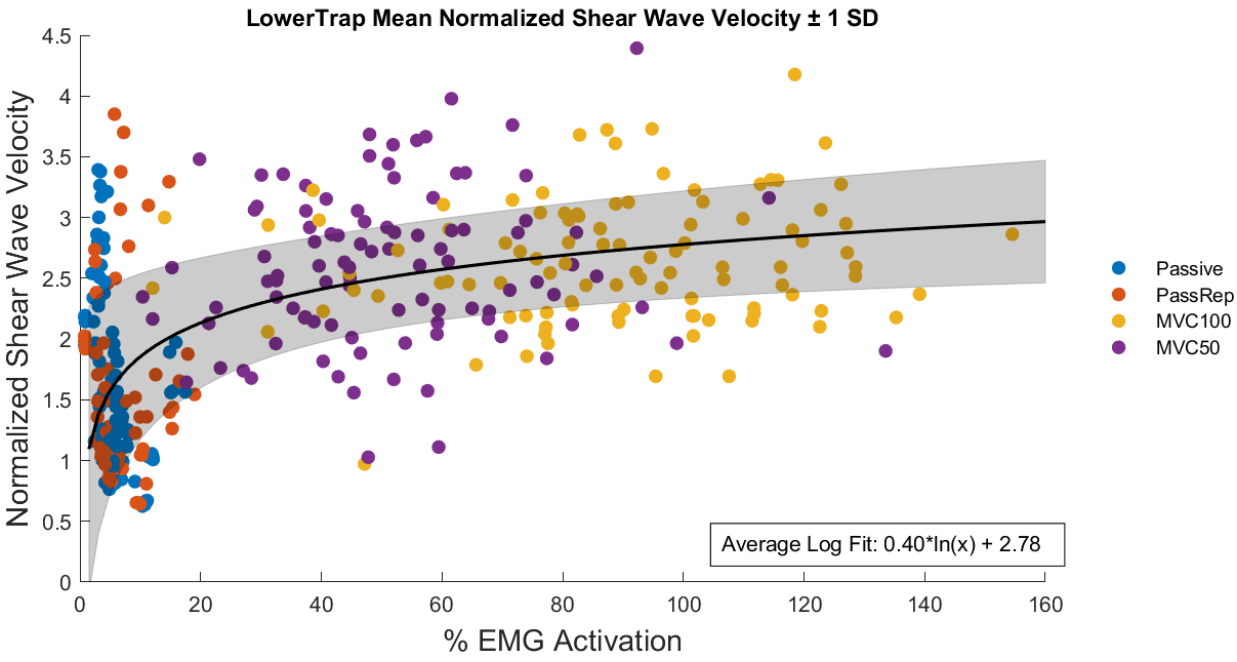
LowerTrap Mean Normalized Shear Wave Velocity ± 1 SD
Normalized Shear Wave Velocity
% EMG Activation
Average Log Fit: 0.40*ln(x) + 2.78
Passive
PassRep
MVC100
MVC50

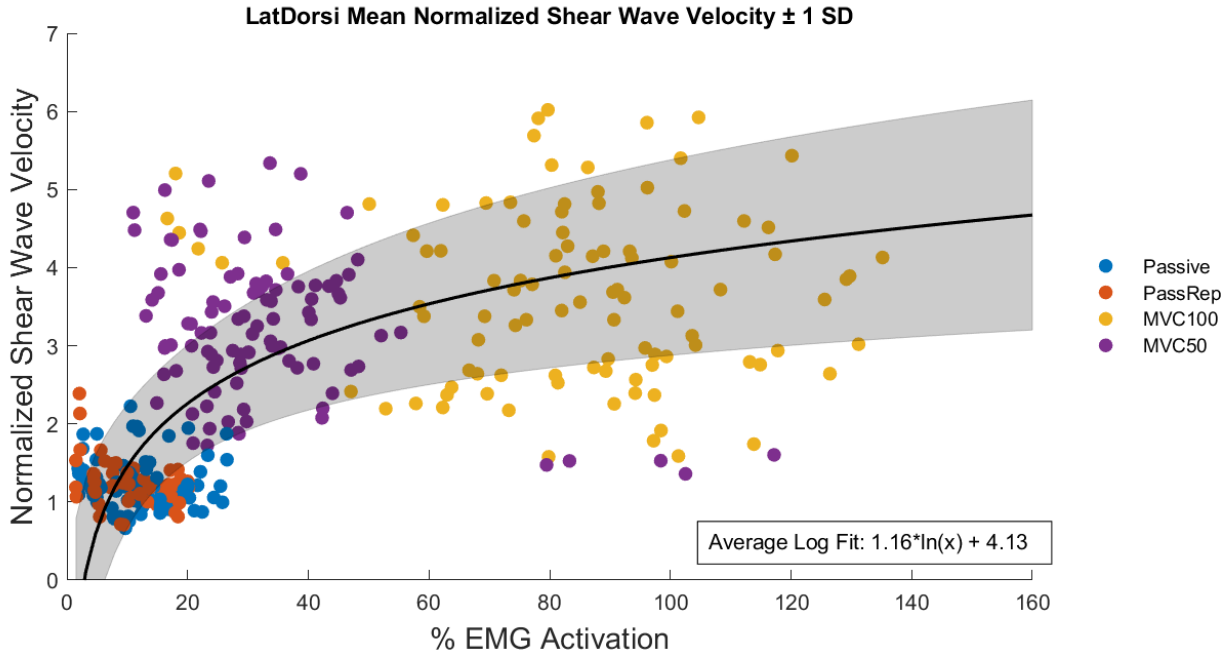
LatDorsi Mean Normalized Shear Wave Velocity ± 1 SD
Normalized Shear Wave Velocity
% EMG Activation
Average Log Fit: 1.16*ln(x) + 4.13
Passive
PassRep
MVC100
MVC50

Average normalized shear wave velocity and activation relationship (mean ± 2 SD)

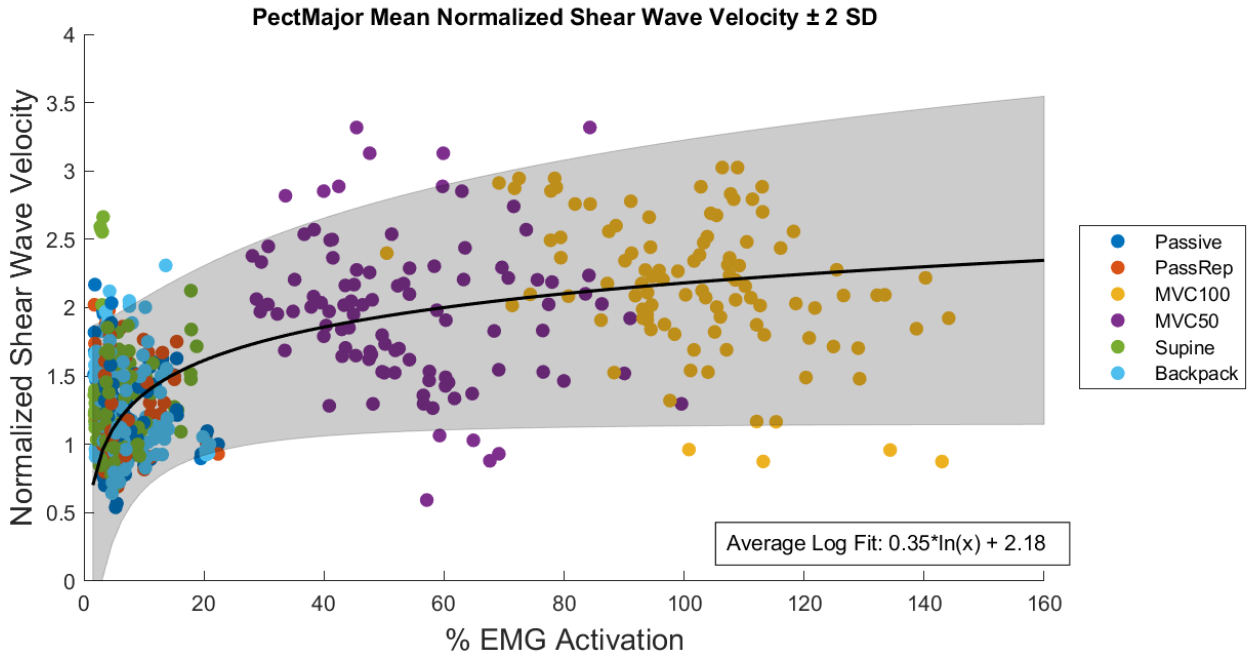

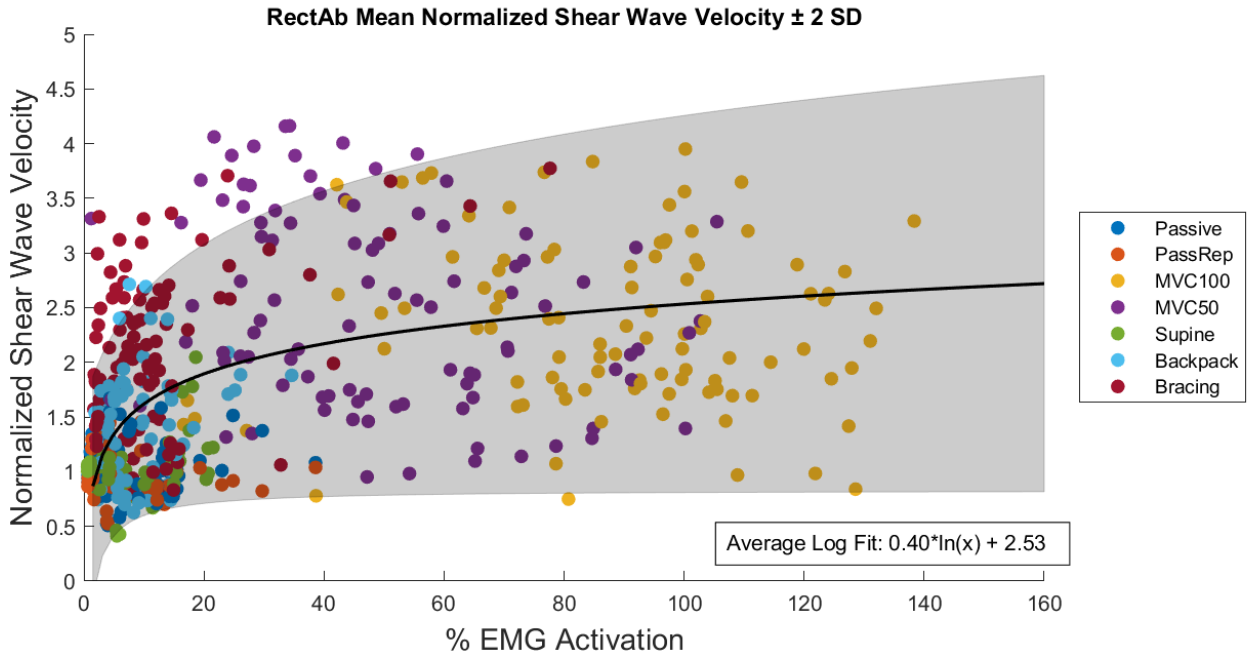

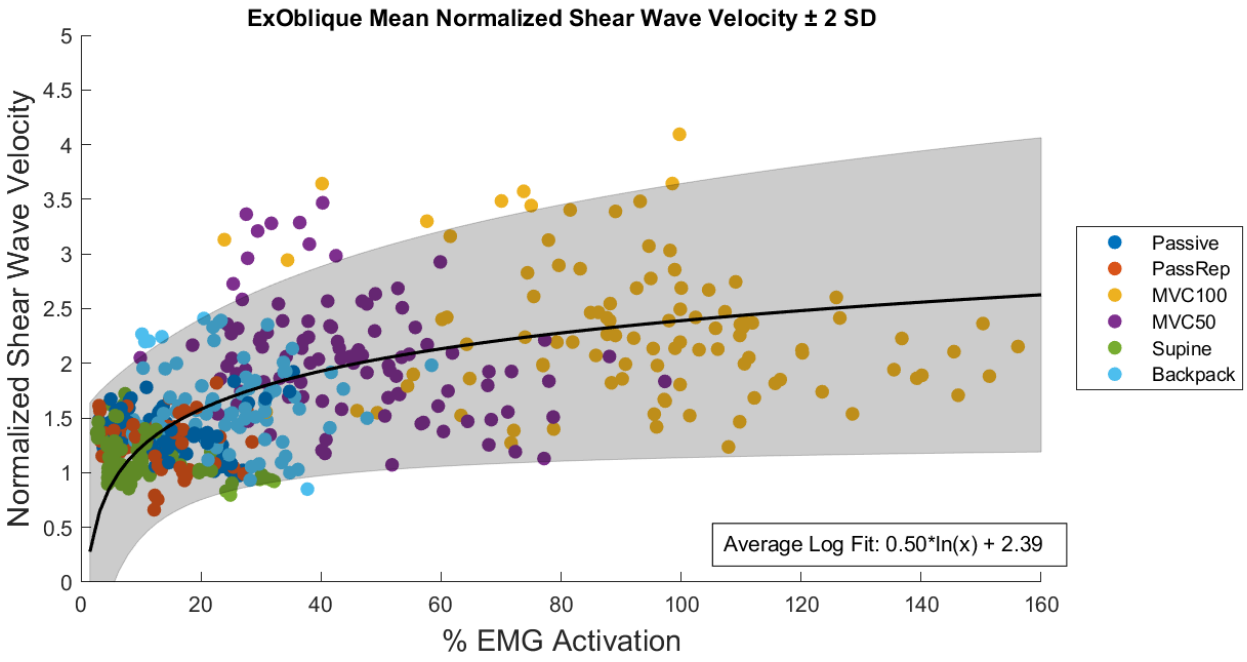
ExOblique Mean Normalized Shear Wave Velocity ± 2 SD
Normalized Shear Wave Velocity
% EMG Activation
Average Log Fit: 0.50*ln(x) + 2.39
Passive
PassRep
MVC100
MVC50
Supine
Backpack

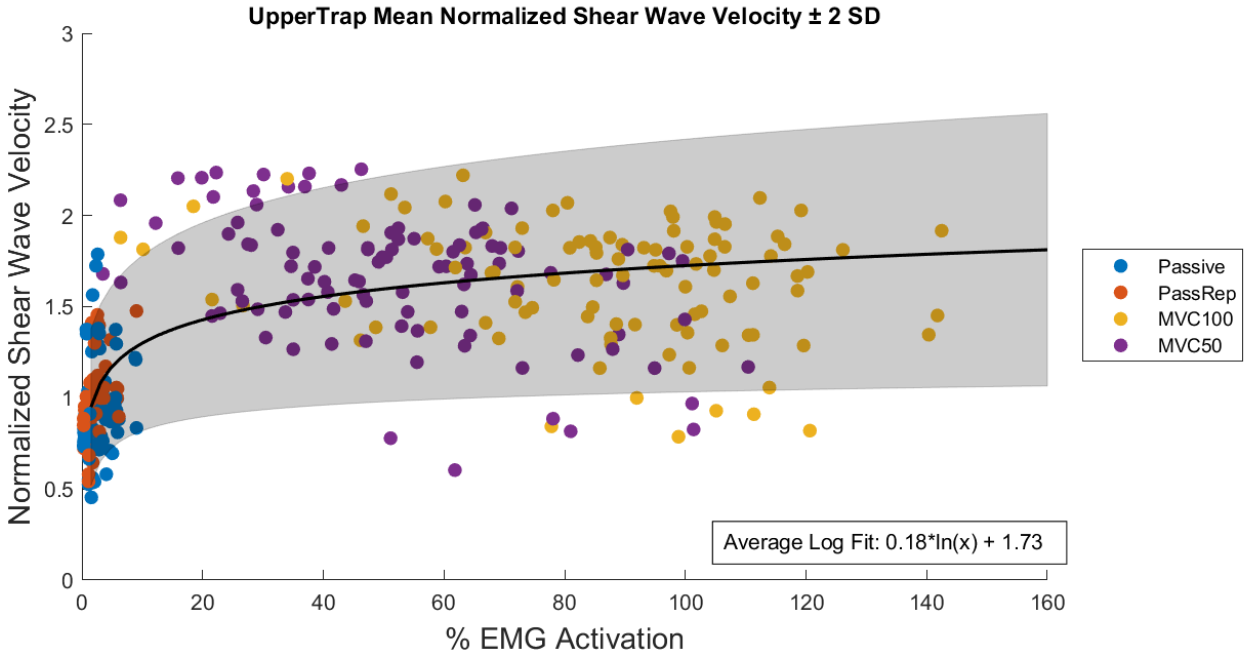
UpperTrap Mean Normalized Shear Wave Velocity ± 2 SD
Normalized Shear Wave Velocity
% EMG Activation
Average Log Fit: 0.18*ln(x) + 1.73
Passive
PassRep
MVC100
MVC50

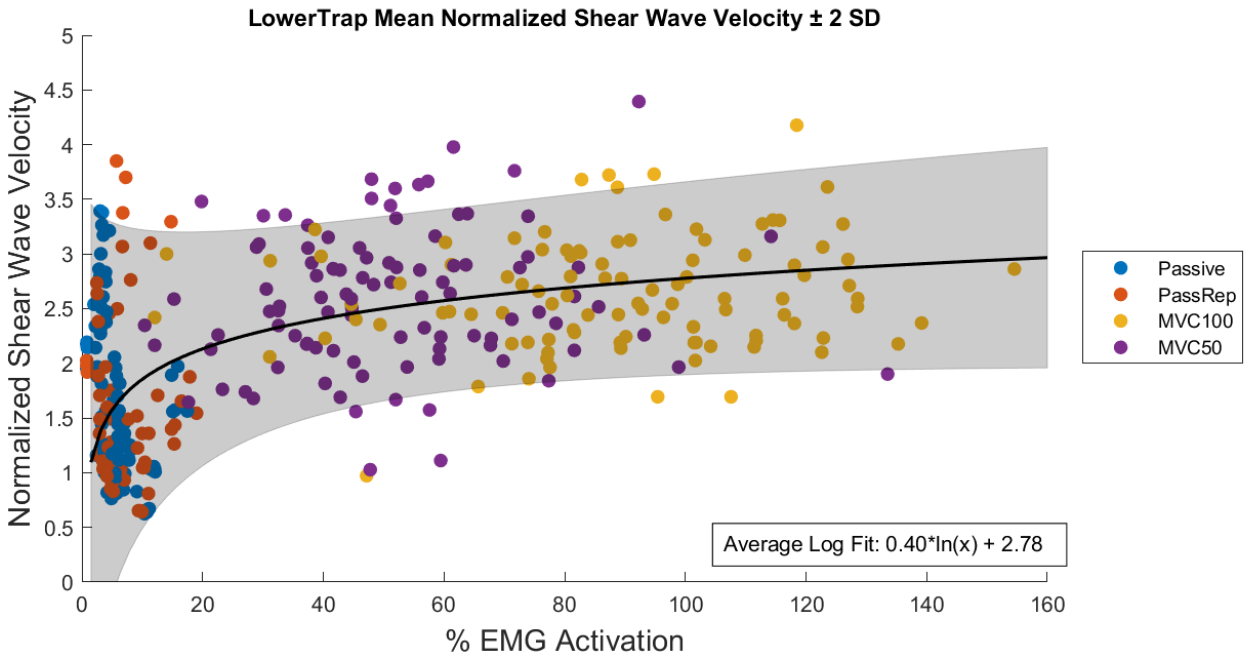
LowerTrap Mean Normalized Shear Wave Velocity ± 2 SD
Normalized Shear Wave Velocity
% EMG Activation
Average Log Fit: 0.40*ln(x) + 2.78
Passive
PassRep
MVC100
MVC50

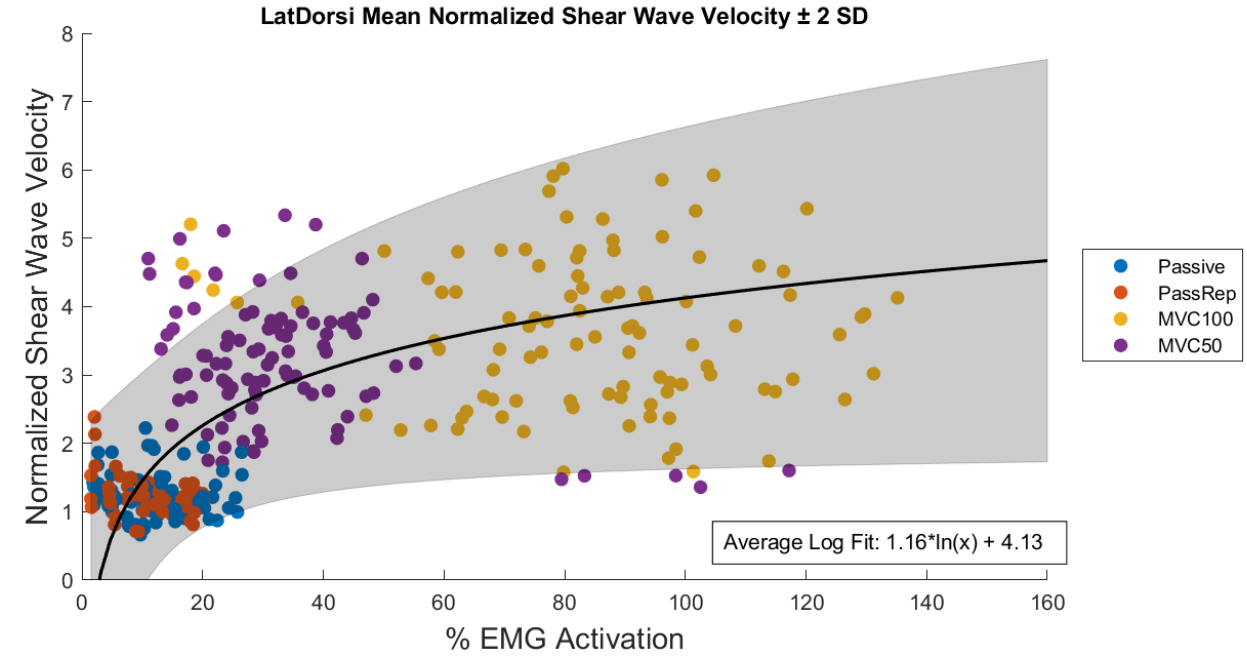
LatDorsi Mean Normalized Shear Wave Velocity ± 2 SD
Normalized Shear Wave Velocity
% EMG Activation
Average Log Fit: 1.16*ln(x) + 4.13
Passive
PassRep
MVC100
MVC50

Appendix 10: Log Fits for Muscle Activation and Absolute Shear Wave Velocities

Average absolute shear wave velocity and activation relationship (mean ± 1 SD)

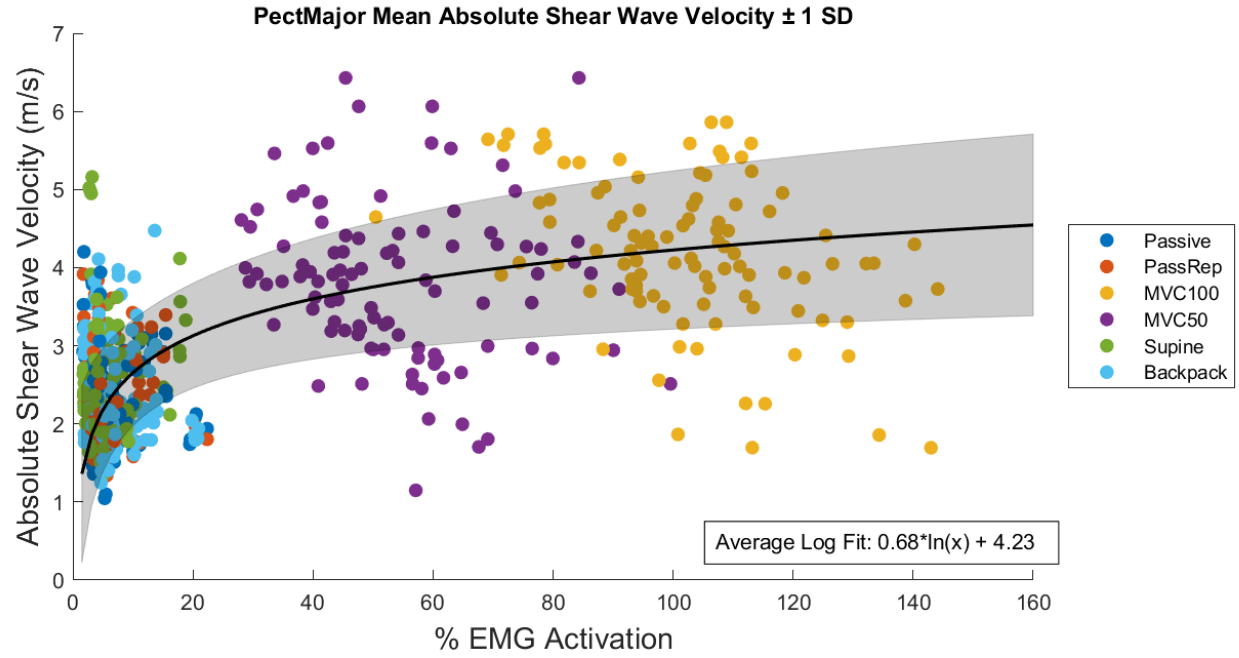

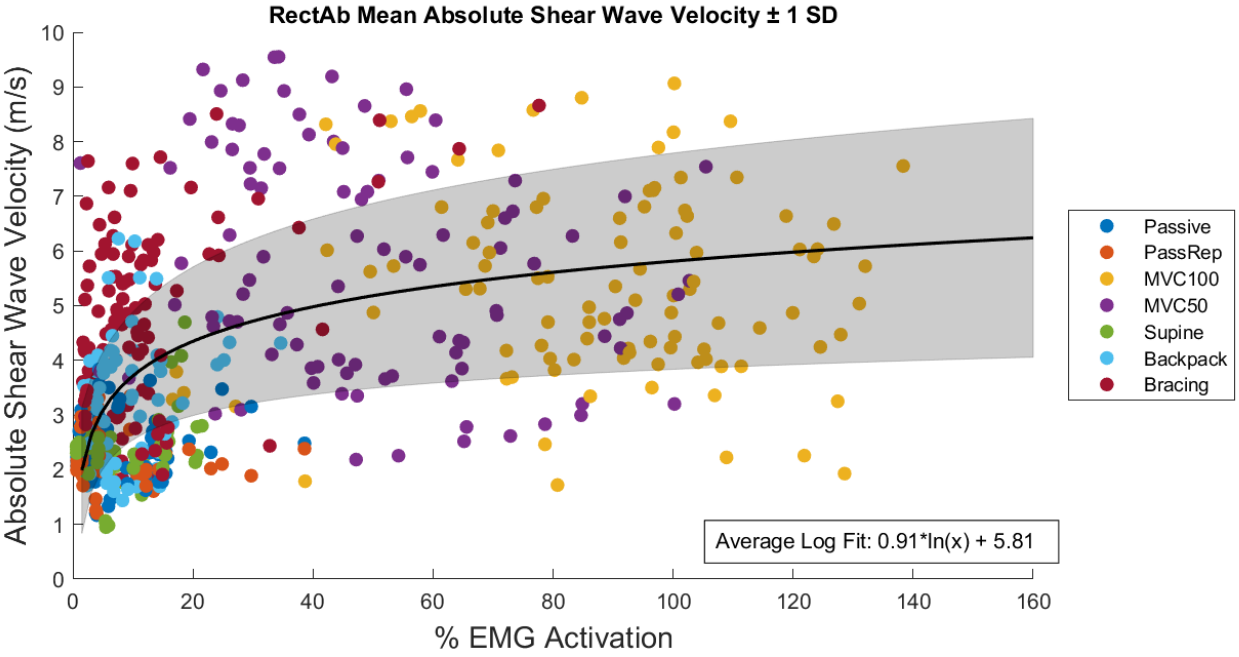

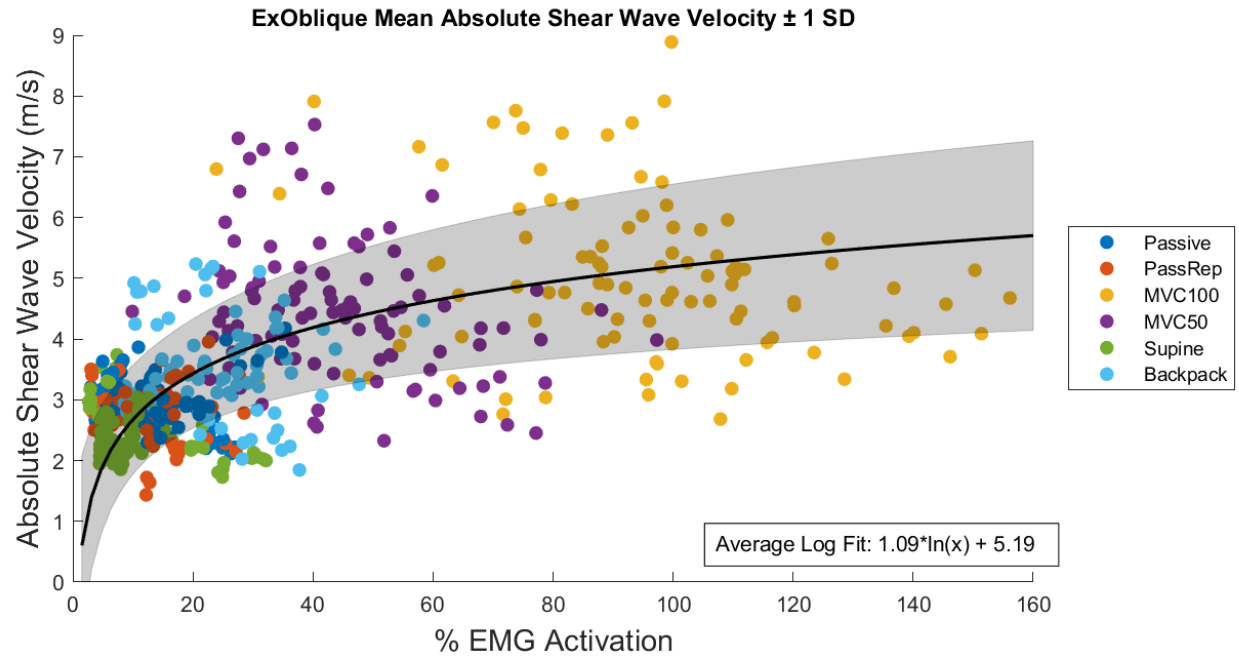
ExOblique Mean Absolute Shear Wave Velocity ± 1 SD
Absolute Shear Wave Velocity (m/s)
% EMG Activation
Average Log Fit: 1.09*ln(x) + 5.19
Passive
PassRep
MVC100
MVC50
Supine
Backpack

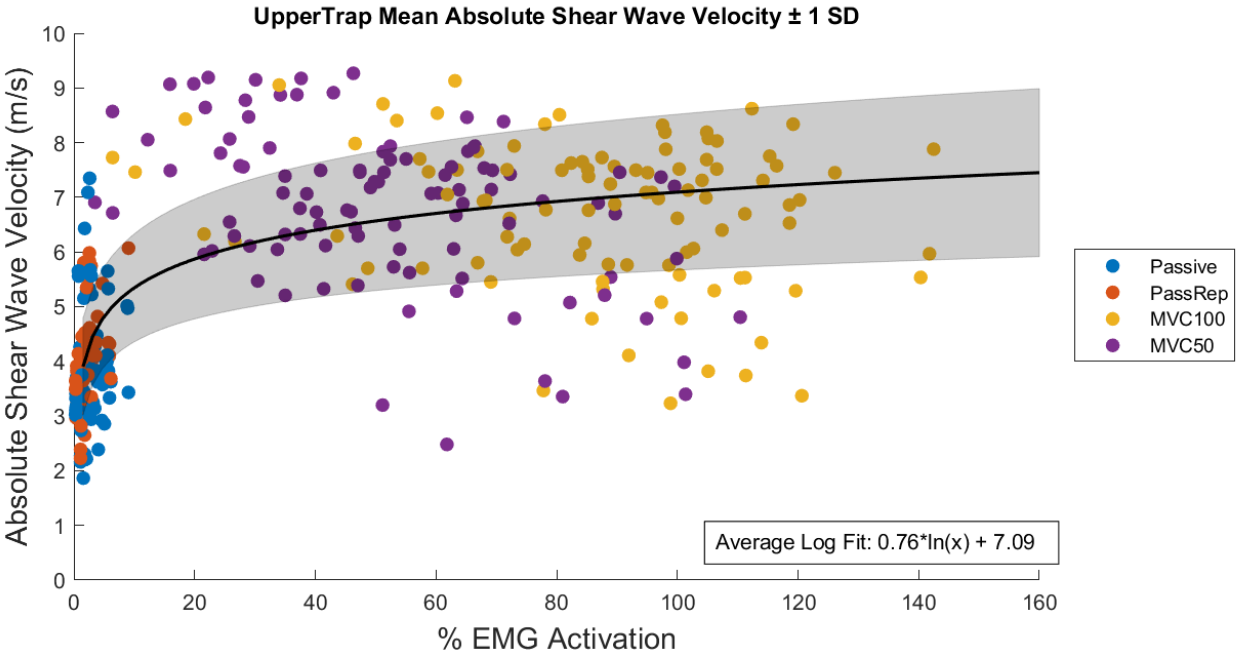
UpperTrap Mean Absolute Shear Wave Velocity ± 1 SD
Absolute Shear Wave Velocity (m/s)
% EMG Activation
Average Log Fit: 0.76*ln(x) + 7.09
Passive
PassRep
MVC100
MVC50

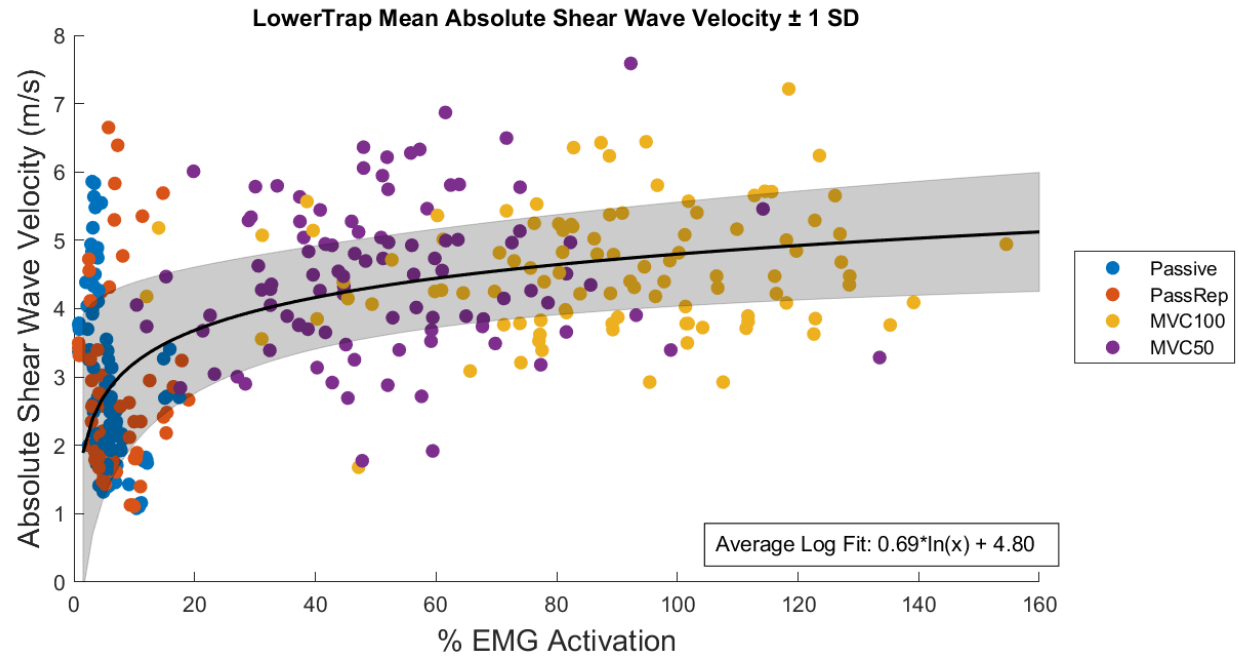
LowerTrap Mean Absolute Shear Wave Velocity ± 1 SD
Absolute Shear Wave Velocity (m/s)
% EMG Activation
Average Log Fit: 0.69*ln(x) + 4.80
Passive
PassRep
MVC100
MVC50

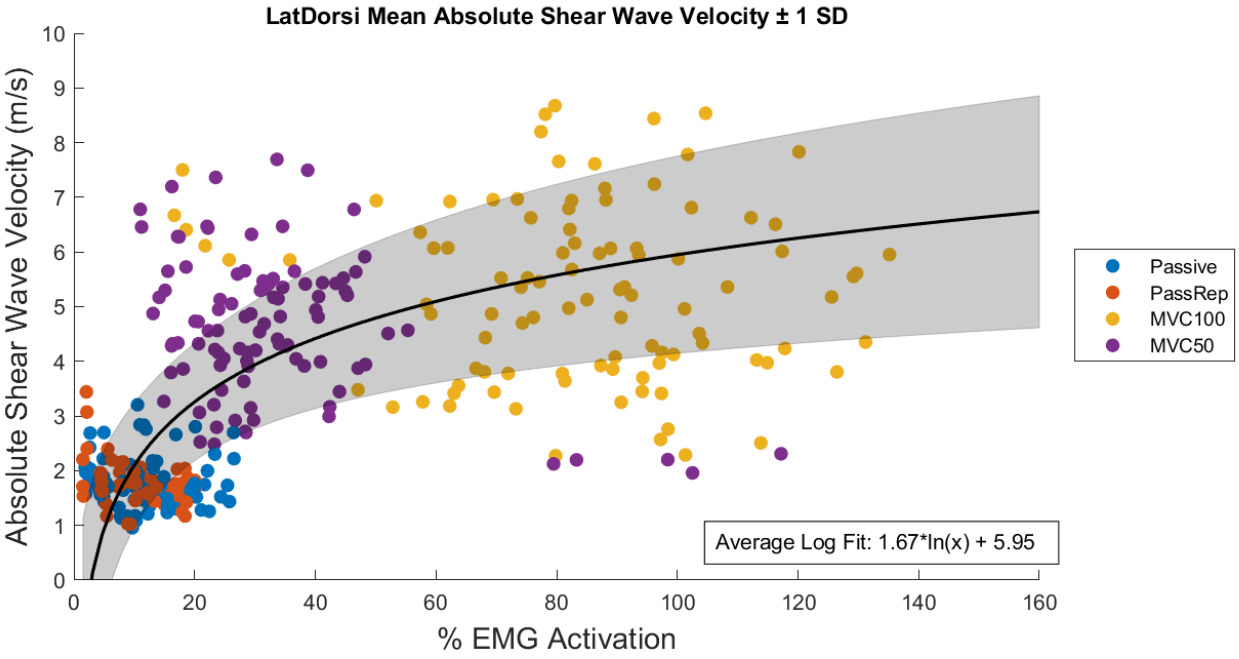
LatDorsi Mean Absolute Shear Wave Velocity ± 1 SD
Absolute Shear Wave Velocity (m/s)
% EMG Activation
Average Log Fit: 1.67*ln(x) + 5.95
Passive
PassRep
MVC100
MVC50

Average absolute shear wave velocity and activation relationship (mean ± 2 SD)

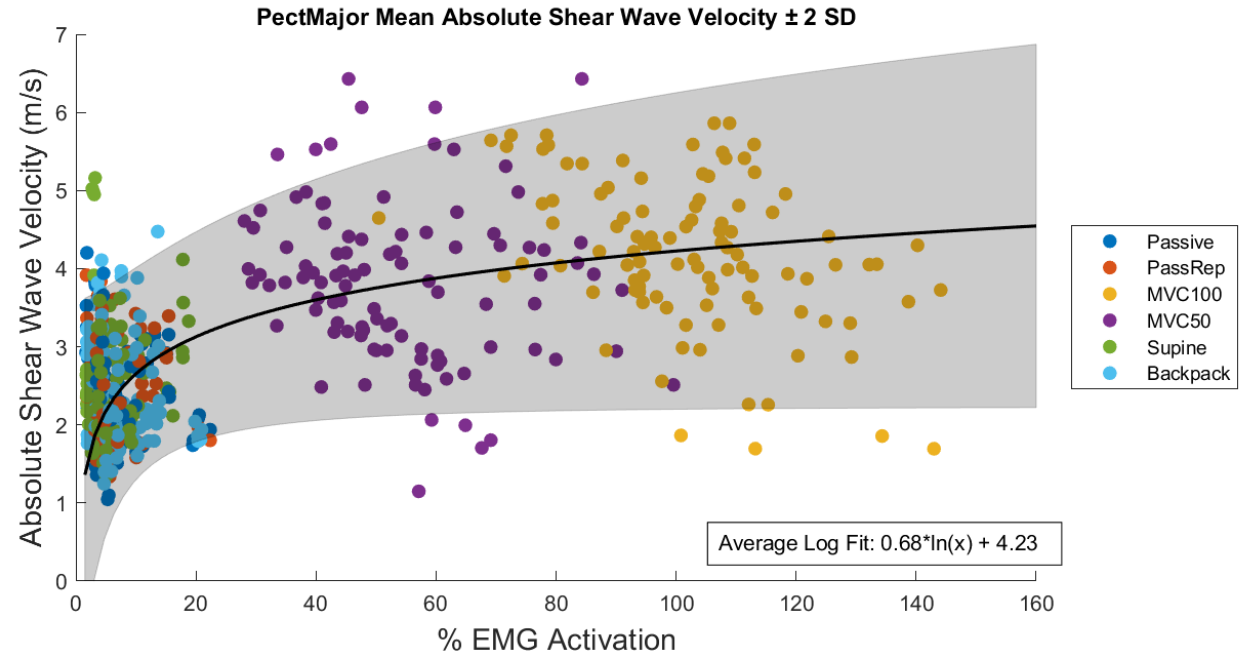

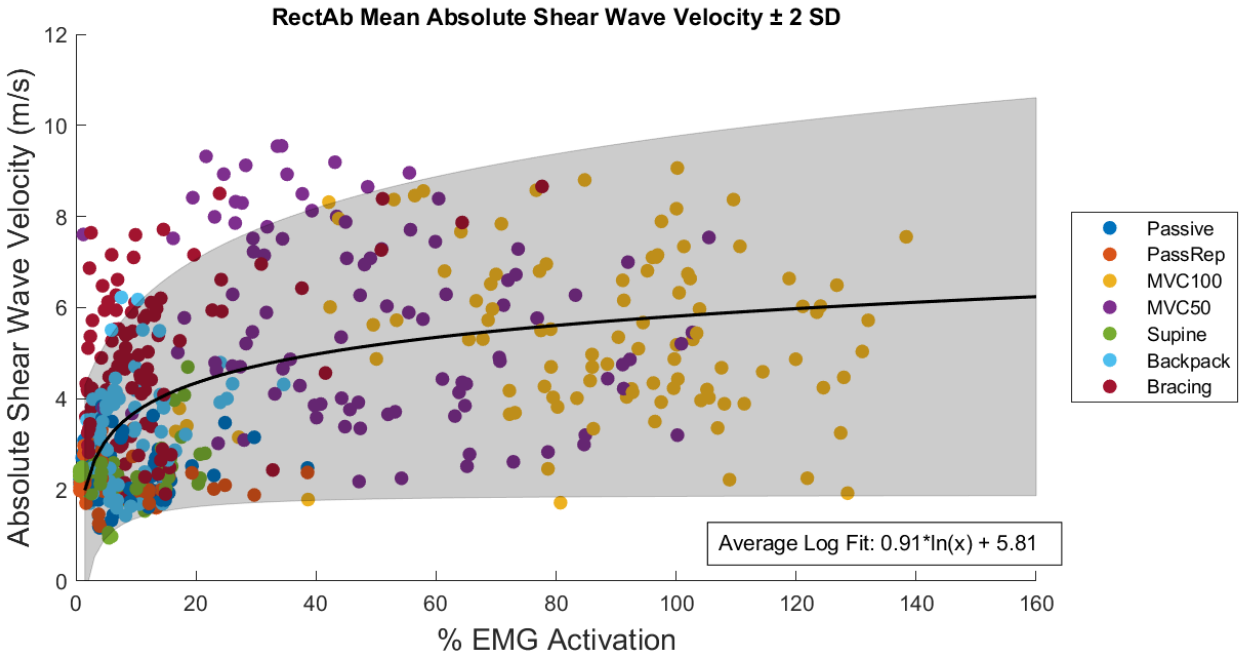

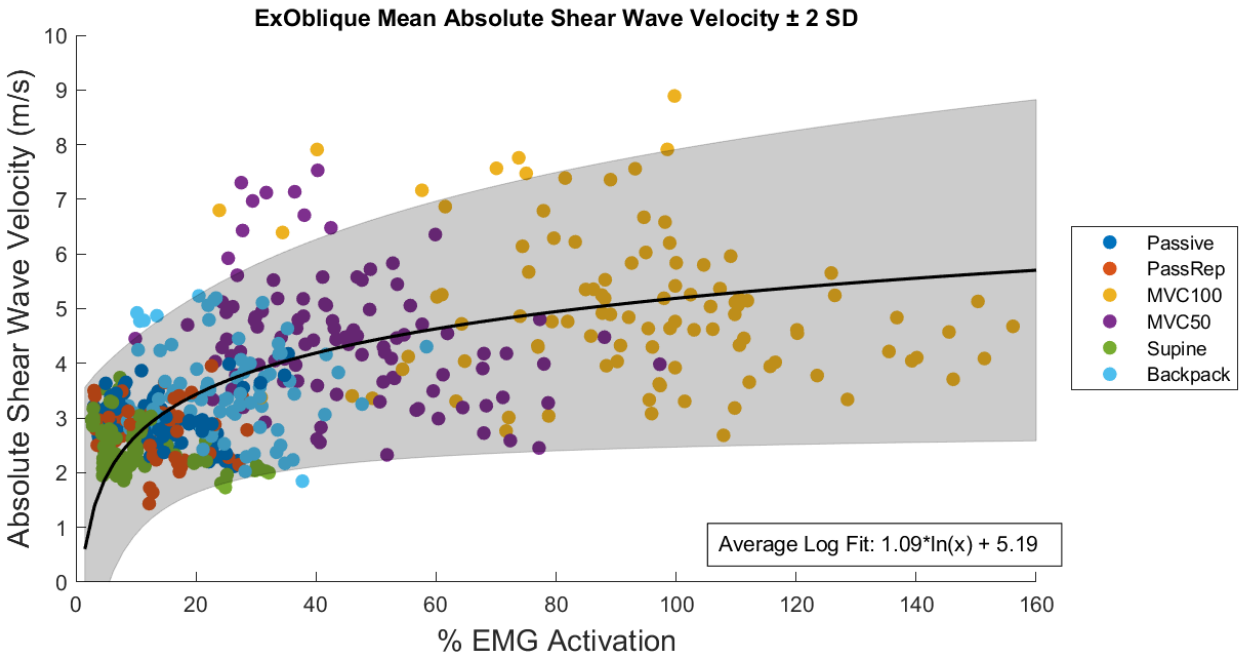
ExOblique Mean Absolute Shear Wave Velocity ± 2 SD
Absolute Shear Wave Velocity (m/s)
% EMG Activation
Average Log Fit: 1.09*ln(x) + 5.19
Passive
PassRep
MVC100
MVC50
Supine
Backpack

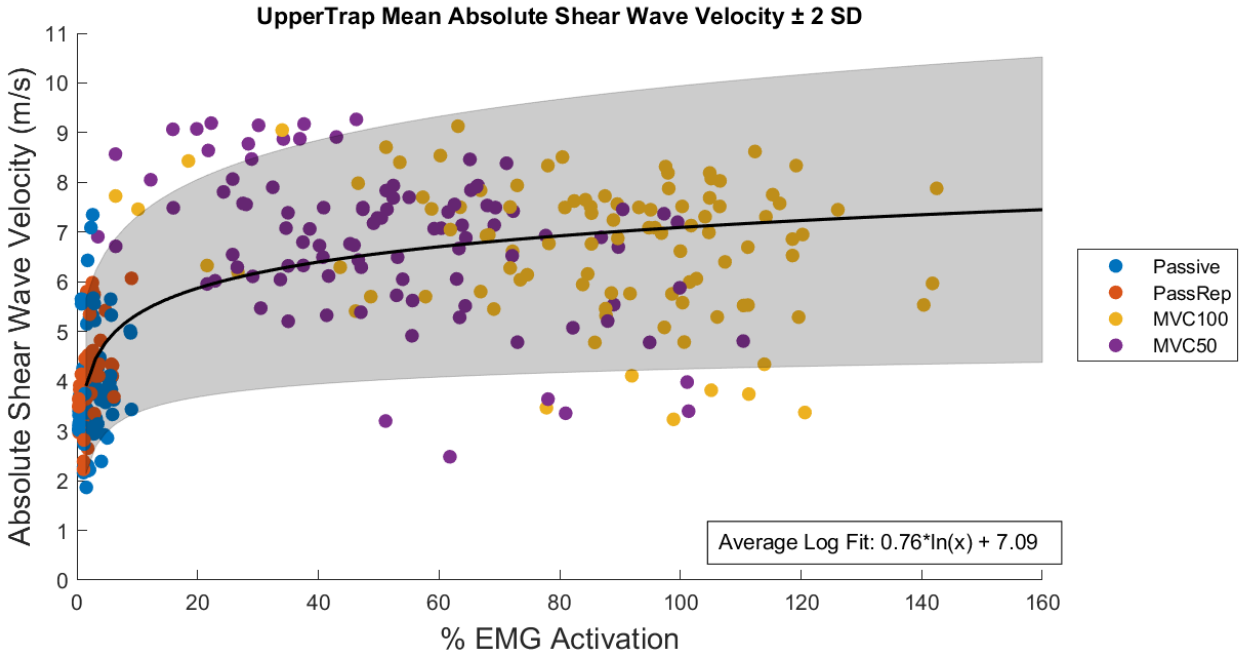
UpperTrap Mean Absolute Shear Wave Velocity ± 2 SD
Absolute Shear Wave Velocity (m/s)
% EMG Activation
Average Log Fit: 0.76*ln(x) + 7.09
Passive
PassRep
MVC100
MVC50

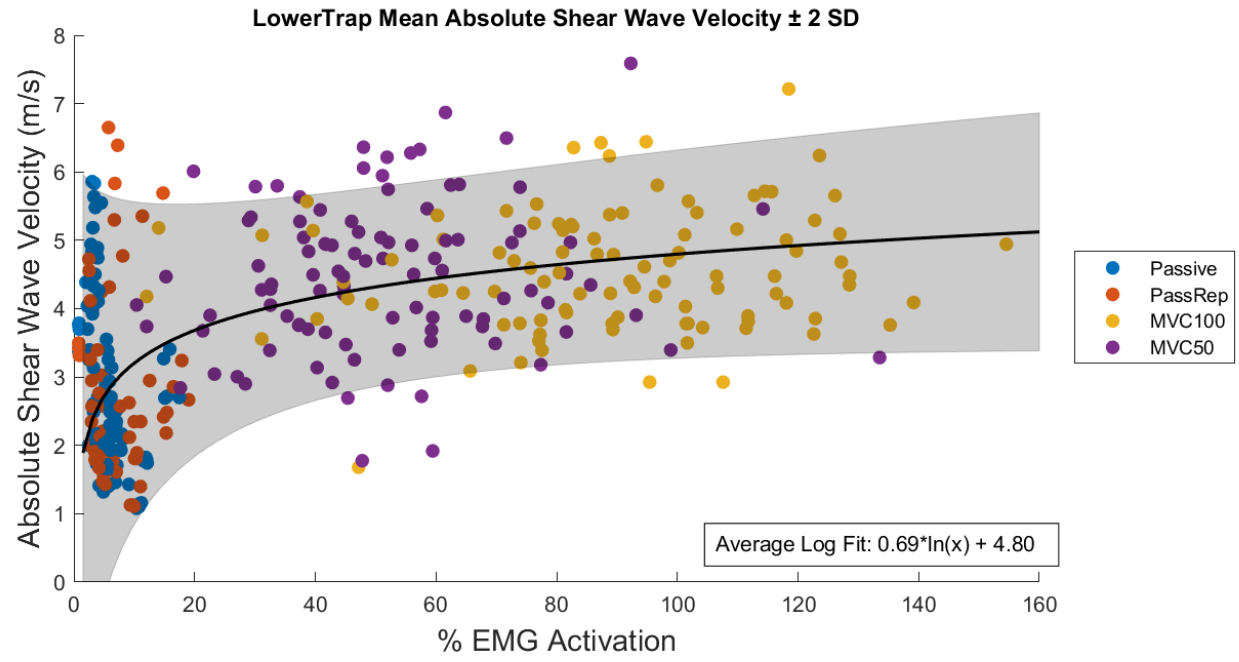
LowerTrap Mean Absolute Shear Wave Velocity ± 2 SD
Absolute Shear Wave Velocity (m/s)
% EMG Activation
Average Log Fit: 0.69*ln(x) + 4.80
Passive
PassRep
MVC100
MVC50

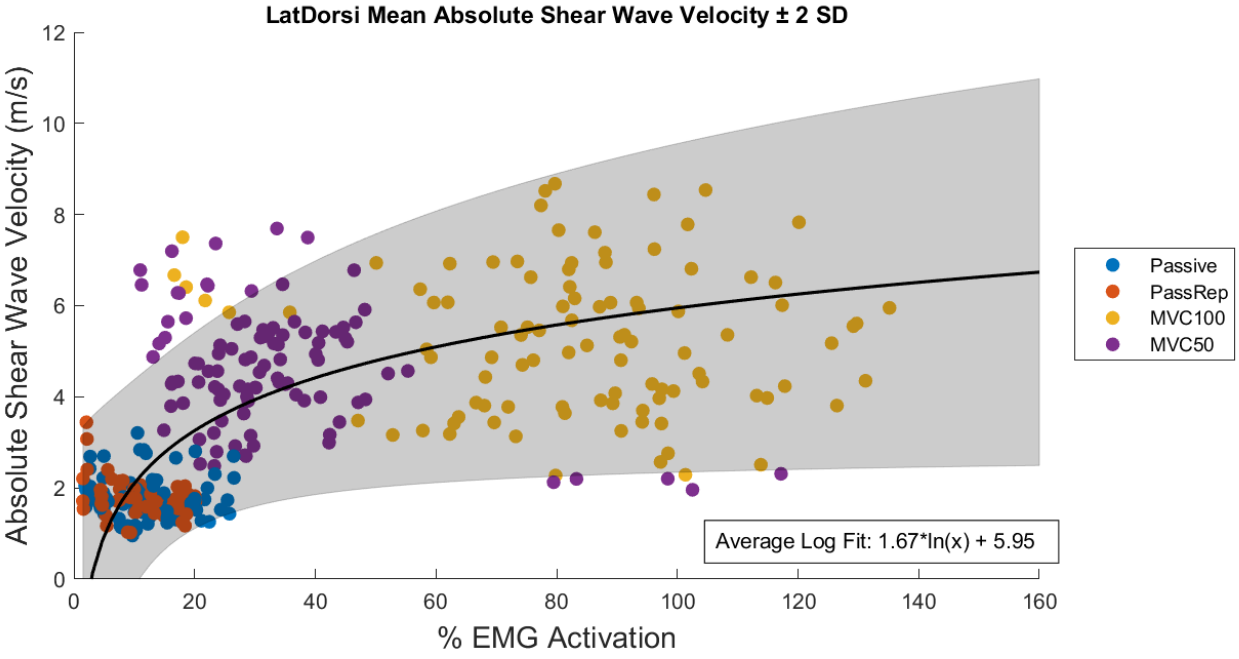
LatDorsi Mean Absolute Shear Wave Velocity ± 2 SD
Absolute Shear Wave Velocity (m/s)
% EMG Activation
Average Log Fit: 1.67*ln(x) + 5.95
Passive
PassRep
MVC100
MVC50

Appendix 11: Volunteer Follow-Up Questionnaire

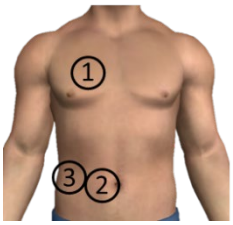

Subject Number: _____

Test Date: _____

---

6 Hour Post

Date: _____ Time: _____

1. Are the marks at impact sites visible? If yes, which location(s)?

2. Are any impact locations sensitive? If yes, which location(s)?

3. Do you have any bruising? If yes, which location(s)?

4. Additional comments for research team.

---

1 Day Post

Date: _____ Time: _____

1. Are the marks at impact sites visible? If yes, which location(s)?

2. Are any impact locations sensitive? If yes, which location(s)?

3. Do you have any bruising? If yes, which location(s)?

4. Additional comments for research team.

---

3 Day Post

Date: _____ Time: _____

1. Are the marks at impact sites visible? If yes, which location(s)?

2. Are any impact locations sensitive? If yes, which location(s)?

3. Do you have any bruising? If yes, which location(s)?

4. Additional comments for research team.

Appendix 12: Superficial temperature recordings for SWE and impactor tests for the PMHS.

PMHS	Position	Muscle	Right or Left	SWE Temperature	Impact Temperature
PMHS 1	Supine	Pectoralis Major	R	60.1	58.5
			L	60.9	59.7
		Rectus Abdominis	R	58.1	56.5
			L	58.3	59.7
		External Oblique	R	58.8	57.3
			L	59.3	59.3
		Subcutaneous Fat	-	57.9	-
		Liver	-	58.5	-
	Seated	Pectoralis Major	R	62.2	-
			L	60.7	-
		Rectus Abdominis	R	57.1	-
			L	60.5	-
		External Oblique	R	60.9	-
			L	61.1	-
		Upper Trapezius	R	62.2	-
			L	62.3	-
		Lower Trapezius	R	61.7	-
			L	61.4	-
		Latissimus Dorsi	R	61.9	-
			L	62.2	-
	Prone	Upper Trapezius	R	64.3	-
			L	63.6	-
		Lower Trapezius	R	63.4	-
			L	62.9	-
		Latissimus Dorsi	R	62.8	-
			L	63.1	-
PMHS 2	Supine	Pectoralis Major	R	62.3	61.2
			L	61.3	59.7
		Rectus Abdominis	R	59.3	59.3
			L	59.7	58.5
		External Oblique	R	59.8	59.1
			L	60.5	59.7
		Subcutaneous Fat	-	59.3	-

PMHS	Position	Muscle	Right or Left	SWE Temperature	Impact Temperature
		Liver	-	59.8	-
	Seated	Pectoralis Major	R	62.6	-
			L	62.7	-
		Rectus Abdominis	R	60.5	-
			L	61.0	-
		External Oblique	R	60.1	-
			L	60.9	-
		Upper Trapezius	R	63.1	-
			L	62.9	-
		Lower Trapezius	R	62.3	-
			L	62.5	-
		Latissimus Dorsi	R	62	-
			L	62.5	-
	Prone	Upper Trapezius	R	63.3	-
			L	62.7	-
		Lower Trapezius	R	62.3	-
			L	62.3	-
		Latissimus Dorsi	R	62.2	-
			L	61.9	-
PMHS 3A	Supine	Pectoralis Major	R	62.0	-
			L	61.7	-
		Rectus Abdominis	R	61.6	-
			L	61.3	-
		External Oblique	R	62.3	-
			L	62.1	-
		Subcutaneous Fat	-	61.6	-
		Liver	-	62.3	-
	Seated	Pectoralis Major	R	60.4	-
			L	60.6	-
		Rectus Abdominis	R	61.3	-
			L	61.3	-
		External Oblique	R	61.2	-
			L	62.0	-
		Upper Trapezius	R	61.9	-
			L	62.9	-

PMHS	Position	Muscle	Right or Left	SWE Temperature	Impact Temperature
		Lower Trapezius	R	62.4	-
			L	62.7	-
		Latissimus Dorsi	R	61.5	-
			L	61.7	-
	Prone	Upper Trapezius	R	61.3	-
			L	61.5	-
		Lower Trapezius	R	62.1	-
			L	61.6	-
		Latissimus Dorsi	R	62.4	-
			L	61.9	-
PMHS 3B	Supine	Pectoralis Major	R	58.3	
			L	57.7	
		Rectus Abdominis	R	57.7	
			L	57.5	
		External Oblique	R	57.9	
			L	57.3	
		Subcutaneous Fat	-	57.7	-
		Liver	-	57.9	-
	Seated	Pectoralis Major	R	59.1	-
			L	58.7	-
		Rectus Abdominis	R	58.7	-
			L	58.7	-
		External Oblique	R	58.2	-
			L	58.6	-
		Upper Trapezius	R	58.5	-
			L	58.3	-
		Lower Trapezius	R	57.3	-
			L	58.1	-
		Latissimus Dorsi	R	57.5	-
			L	58.3	-
	Prone	Upper Trapezius	R	57.7	-
			L	57.8	-
		Lower Trapezius	R	56.7	-
			L	56.2	-
			R	56.3	-

PMHS	Position	Muscle	Right or Left	SWE Temperature	Impact Temperature
		Latissimus Dorsi	L	57.0	-

Appendix 13: Volunteer/PMHS: Peak Impact Force & Indentation Depth

Pectoralis Major Peak Indentation Depths (mm)

VOL	AVG PASSIVE	AVG PASS-REP	AVG MVC100	AVG MVC50	AVG SUPINE
IND 1	9.48	8.78	9.03	9.82	10.80
IND 2	7.18	7.23	7.17	8.36	8.58
IND 3	5.60	6.01	5.87	6.56	5.12
IND 4	7.69	7.54	7.25	7.66	8.42
IND 5	5.30	5.60	6.00	5.99	5.54
IND 6	8.37	9.28	11.48	13.69	8.69
IND 7	8.89	7.93	9.09	9.48	8.79
IND 8	10.03	10.13	10.58	11.69	9.71
IND 9	6.31	6.04	7.95	9.07	6.30
IND 10	6.51	6.58	6.70	7.17	5.56
MEAN	**7.54**	**7.51**	**8.11**	**8.95**	**7.75**
STD	**1.63**	**1.52**	**1.90**	**2.37**	**1.97**

Pectoralis Major Peak Impact Force (N)

VOL	AVG PASSIVE	AVG PASS-REP	AVG MVC100	AVG MVC50	AVG SUPINE
IND 1	421.10	265.46	200.47	194.93	243.06
IND 2	311.05	313.76	257.19	233.34	160.83
IND 3	212.74	174.32	265.47	177.82	178.89
IND 4	247.97	219.93	174.06	208.58	162.34
IND 5	267.91	235.68	171.65	157.23	325.68
IND 6	193.71	159.28	206.82	118.37	372.43
IND 7	138.99	191.07	150.85	193.59	152.88
IND 8	155.53	138.92	133.65	152.85	140.14
IND 9	278.90	284.53	224.42	142.65	294.96
IND 10	301.49	238.10	232.59	248.03	203.86
MEAN	**252.94**	**222.10**	**201.72**	**182.74**	**223.51**
STD	**83.35**	**56.50**	**44.13**	**40.93**	**81.71**

Pectoralis Major Peak Indentation Depth (mm)

PMHS	AVG SEATED 11M/S	AVG SUPINE 11M/S	AVG SEATED 5M/S	AVG SUPINE 5M/S
1	10.04	9.32	5.25	6.15
2	12.64	8.79	6.19	7.04
3A	14.51	10.31	8.82	6.79
3B	11.37	10.31	7.64	6.36

PMHS	AVG SEATED 11M/S	AVG SUPINE 11M/S	AVG SEATED 5M/S	AVG SUPINE 5M/S
MEAN	**12.14**	**9.68**	**6.97**	**6.59**
STD	**1.90**	**0.76**	**1.57**	**0.40**

Pectoralis Major Peak Impact Force (N)

PMHS	AVG SEATED 11M/S	AVG SUPINE 11M/S	AVG SEATED 5M/S	AVG SUPINE 5M/S
1	672.67	804.01	236.58	306.10
2	827.72	799.30	180.62	174.23
3A	756.44	825.51	143.74	186.20
3B	900.27	735.62	197.12	254.14
MEAN	**789.27**	**791.11**	**189.51**	**230.17**
STD	**97.42**	**38.72**	**38.50**	**61.65**

Rectus Abdominis Peak Indentation Depths (mm)

VOL	AVG PASSIVE	AVG PASS-REP	AVG MVC100	AVG MVC50	AVG SUPINE	AVG BRACE
IND 1	14.58	13.15	14.60	14.65	14.02	14.88
IND 2	15.19	15.63	13.73	13.67	13.87	15.64
IND 3	12.82	13.14	8.82	10.61	11.42	12.00
IND 4	12.05	11.55	11.44	11.80	12.16	13.72
IND 5	12.43	12.41	11.76	11.26	11.67	13.80
IND 6	12.88	13.69	14.11	14.58	16.92	15.00
IND 7	12.69	12.83	13.24	13.60	12.58	13.87
IND 8	14.38	14.42	13.78	14.27	14.46	14.08
IND 9	16.56	16.74	14.76	14.86	14.09	14.71
IND 10	10.90	10.74	8.02	8.53	9.85	11.15
MEAN	**13.45**	**13.43**	**12.43**	**12.78**	**13.10**	**13.88**
STD	**1.69**	**1.80**	**2.38**	**2.13**	**1.99**	**1.38**

Rectus Abdominis Peak Impact Force (N)

VOL	AVG PASSIVE	AVG PASS-REP	AVG MVC100	AVG MVC50	AVG SUPINE	AVG BRACE
IND 1	162.04	190.44	163.88	154.48	156.77	150.95
IND 2	142.89	158.02	145.03	160.55	154.15	158.29
IND 3	161.65	127.35	179.69	189.16	212.71	134.97
IND 4	158.56	167.52	200.37	185.02	241.36	160.22
IND 5	133.35	137.55	158.26	177.74	160.00	155.50

VOL	AVG PASSIVE	AVG PASS-REP	AVG MVC100	AVG MVC50	AVG SUPINE	AVG BRACE
IND 6	218.48	208.00	249.33	208.28	254.28	164.66
IND 7	161.10	180.17	214.65	208.77	161.89	194.26
IND 8	143.60	143.54	161.37	169.74	141.68	153.14
IND 9	129.83	148.12	143.64	150.50	145.59	134.01
IND 10	204.27	197.94	183.65	229.59	298.14	156.72
MEAN	**161.58**	**165.86**	**179.99**	**183.38**	**192.66**	**156.27**
STD	**28.96**	**27.44**	**33.44**	**26.02**	**55.07**	**16.74**

Rectus Abdominis Peak Indentation Depth (mm)

PMHS	AVG SEATED 11M/S	AVG SUPINE 11M/S	AVG SEATED 5M/S	AVG SUPINE 5M/S
1	14.63	14.03	10.59	8.53
2	17.43	15.79	9.62	10.36
3A	14.14	11.07	9.27	10.12
3B	15.78	16.16	10.27	10.89
MEAN	**15.49**	**14.26**	**9.94**	**9.98**
STD	**1.46**	**2.32**	**0.60**	**1.02**

Rectus Abdominis Peak Impact Force (N)

PMHS	AVG SEATED 11M/S	AVG SUPINE 11M/S	AVG SEATED 5M/S	AVG SUPINE 5M/S
1	570.29	751.86	137.01	226.68
2	678.82	1021.59	175.02	269.04
3A	923.94	889.14	159.37	192.08
3B	908.56	934.95	132.67	300.93
MEAN	**770.40**	**899.38**	**151.01**	**247.18**
STD	**174.25**	**112.65**	**19.82**	**47.69**

External Oblique Peak Indentation Depths (mm)

VOL	AVG PASSIVE	AVG PASS-REP	AVG MVC100	AVG MVC50	AVG SUPINE
IND 1	11.86	10.91	13.15	13.50	11.36
IND 2	11.89	11.94	12.93	13.73	11.32
IND 3	14.44	13.50	13.29	13.34	11.04
IND 4	12.81	11.93	13.36	14.58	12.26
IND 5	11.03	11.13	13.14	13.44	9.80
IND 6	13.01	13.56	13.20	10.75	14.21

VOL	AVG PASSIVE	AVG PASS-REP	AVG MVC100	AVG MVC50	AVG SUPINE
IND 7	14.02	14.31	13.64	15.82	13.08
IND 8	11.96	12.77	13.55	13.71	10.98
IND 9	12.21	12.33	11.95	12.98	9.63
IND 10	9.26	8.18	8.21	8.57	10.06
MEAN	**12.25**	**12.06**	**12.64**	**13.04**	**11.37**
STD	**1.48**	**1.74**	**1.63**	**2.02**	**1.46**

External Oblique Peak Impact Force (N)

VOL	AVG PASSIVE	AVG PASS-REP	AVG MVC100	AVG MVC50	AVG SUPINE
IND 1	270.15	290.92	164.56	146.16	171.48
IND 2	138.46	137.16	126.07	146.17	196.91
IND 3	179.84	250.51	157.14	218.11	142.70
IND 4	166.00	214.34	176.59	166.74	189.23
IND 5	164.61	174.61	120.91	121.79	201.00
IND 6	174.28	226.83	164.80	192.67	249.19
IND 7	160.27	148.28	190.71	164.03	160.33
IND 8	168.17	136.21	155.96	134.36	155.13
IND 9	169.83	276.25	139.58	162.16	271.82
IND 10	292.16	269.72	136.50	143.68	291.61
MEAN	**188.38**	**212.48**	**153.28**	**159.59**	**202.94**
STD	50.36	59.81	22.32	28.43	51.31

External Oblique Peak Indentation Depth (mm)

PMHS	AVG SEATED 11M/S	AVG SUPINE 11M/S	AVG SEATED 5M/S	AVG SUPINE 5M/S
1	15.87	21.01	8.33	9.11
2	14.07	16.39	8.53	8.71
3A	14.04	11.86	8.19	9.11
3B	15.28	15.60	8.87	9.97
MEAN	**14.81**	**16.21**	**8.48**	**9.22**
STD	**0.91**	**3.76**	**0.30**	**0.53**

External Oblique Peak Impact Force (N)

PMHS	AVG SEATED 11M/S	AVG SUPINE 11M/S	AVG SEATED 5M/S	AVG SUPINE 5M/S
1	764.42	712.28	293.70	152.28
2	752.89	951.28	217.09	257.79
3A	872.64	956.75	169.09	214.23
3B	959.09	866.81	144.81	228.18
MEAN	**837.26**	**871.78**	**206.17**	**213.12**
STD	**97.50**	**114.03**	**65.63**	**44.44**

Upper Trapezius Peak Indentation Depths (mm)

VOL	AVG PASSIVE	AVG PASS-REP	AVG MVC100	AVG MVC50	AVG SUPINE
IND 1	10.25	6.07	6.64	6.87	6.23
IND 2	6.83	6.90	7.08	7.07	8.37
IND 3	6.64	6.85	5.70	6.24	8.32
IND 4	6.13	6.53	6.32	6.38	8.26
IND 5	5.97	6.62	5.81	6.42	7.05
IND 6	7.70	7.88	7.64	7.38	6.88
IND 7	5.23	5.28	6.25	6.11	6.99
IND 8	6.46	5.97	6.79	7.25	6.78
IND 9	6.20	6.29	6.12	6.76	8.39
IND 10	4.44	4.17	5.18	5.44	4.87
MEAN	**6.58**	**6.26**	**6.35**	**6.59**	**7.21**
STD	**1.56**	**1.00**	**0.72**	**0.59**	**1.15**

Upper Trapezius Peak Impact Force (N)

VOL	AVG PASSIVE	AVG PASS-REP	AVG MVC100	AVG MVC50	AVG SUPINE
IND 1	280.36	372.95	179.61	188.73	298.39
IND 2	256.26	263.43	195.92	191.54	214.93
IND 3	335.38	344.30	200.22	188.25	182.32
IND 4	314.89	309.80	214.06	262.24	265.62
IND 5	407.38	378.72	202.27	198.22	267.80
IND 6	266.60	365.64	210.42	200.25	233.12
IND 7	212.91	208.24	164.59	164.13	179.12
IND 8	305.72	271.25	182.74	176.27	188.03
IND 9	215.36	277.94	192.96	192.34	208.12
IND 10	255.99	287.10	192.83	165.53	212.08
MEAN	**285.08**	**307.94**	**193.56**	**192.75**	**224.95**

VOL	AVG PASSIVE	AVG PASS-REP	AVG MVC100	AVG MVC50	AVG SUPINE
STD	**58.61**	**56.27**	**14.84**	**27.46**	**40.52**

Upper Trapezius Peak Indentation Depth (mm)

PMHS	AVG SEATED 11M/S	AVG SUPINE 11M/S	AVG SEATED 5M/S	AVG SUPINE 5M/S
1	8.45	9.35	6.01	7.81
2	6.07	9.84	4.41	6.37
3A	9.68	10.78	6.98	5.30
3B	7.73	16.18	4.46	6.77
MEAN	**7.98**	**11.54**	**5.46**	**6.56**
STD	**1.51**	**3.16**	**1.25**	**1.04**

Upper Trapezius Peak Impact Force (N)

PMHS	AVG SEATED 11M/S	AVG SUPINE 11M/S	AVG SEATED 5M/S	AVG SUPINE 5M/S
1	742.39	764.36	243.26	198.68
2	843.84	1041.18	251.32	228.65
3A	854.89	958.66	223.74	253.95
3B	994.81	937.82	358.42	208.21
MEAN	**858.98**	**925.51**	**269.19**	**222.37**
STD	**103.75**	**116.33**	**60.61**	**24.48**

Lower Trapezius Peak Indentation Depths (mm)

VOL	AVG PASSIVE	AVG PASS-REP	AVG MVC100	AVG MVC50	AVG SUPINE
IND 1	6.47	7.81	6.72	6.53	7.30
IND 2	8.29	9.37	5.88	7.13	6.67
IND 3	8.71	7.61	5.59	6.63	8.54
IND 4	7.23	7.37	5.80	5.86	8.83
IND 5	6.62	6.80	6.89	7.08	7.65
IND 6	7.57	7.30	6.41	7.59	9.13
IND 7	7.96	8.04	7.40	7.50	7.18
IND 8	6.49	6.89	4.52	4.82	7.07
IND 9	7.56	7.50	8.44	7.30	7.33
IND 10	7.51	7.63	6.06	6.22	8.61
MEAN	**7.44**	**7.63**	**6.37**	**6.67**	**7.83**
STD	**0.76**	**0.72**	**1.08**	**0.86**	**0.86**

Lower Trapezius Peak Impact Force (N)

VOL	AVG PASSIVE	AVG PASS-REP	AVG MVC100	AVG MVC50	AVG SUPINE
IND 1	356.30	341.99	213.61	257.58	328.48
IND 2	225.16	206.72	235.28	227.12	258.07
IND 3	261.61	320.17	313.14	285.94	187.06
IND 4	300.90	258.56	268.86	305.13	230.52
IND 5	338.05	312.79	176.11	193.91	353.32
IND 6	278.39	296.92	258.51	228.21	202.46
IND 7	333.43	366.80	177.46	178.00	195.39
IND 8	269.97	337.27	382.44	394.47	194.91
IND 9	256.91	269.16	235.84	287.83	266.09
IND 10	293.29	350.44	236.82	311.29	257.71
MEAN	**291.40**	**306.08**	**249.81**	**266.95**	**247.40**
STD	**41.29**	**49.15**	**62.00**	**64.03**	**57.51**

Lower Trapezius Peak Indentation Depth (mm)

PMHS	AVG SEATED 11M/S	AVG SUPINE 11M/S	AVG SEATED 5M/S	AVG SUPINE 5M/S
1	7.76	5.42	4.42	4.30
2	7.24	6.69	4.22	6.16
3A	10.50	8.90	6.03	8.18
3B	15.33	13.82	5.57	5.73
MEAN	**10.21**	**8.71**	**5.06**	**6.09**
STD	**3.70**	**3.70**	**0.88**	**1.60**

Lower Trapezius Peak Impact Force (N)

PMHS	AVG SEATED 11M/S	AVG SUPINE 11M/S	AVG SEATED 5M/S	AVG SUPINE 5M/S
1	865.25	1096.41	322.00	292.75
2	904.44	886.07	331.52	355.46
3A	949.92	1120.10	157.41	290.31
3B	956.90	933.69	539.13	303.09
MEAN	**919.13**	**1009.07**	**337.52**	**310.40**
STD	**42.79**	**116.57**	**156.38**	**30.55**

Latissimus Dorsi Peak Indentation Depths (mm)

VOL	AVG PASSIVE	AVG PASS-REP	AVG MVC100	AVG MVC50	AVG SUPINE
IND 1	11.03	11.35	8.30	10.60	8.14

VOL	AVG PASSIVE	AVG PASS-REP	AVG MVC100	AVG MVC50	AVG SUPINE
IND 2	10.50	11.96	13.20	12.35	7.51
IND 3	12.68	12.83	8.15	9.61	6.81
IND 4	11.90	10.88	9.60	9.93	11.38
IND 5	12.27	9.79	10.33	11.02	6.57
IND 6	13.01	14.55	11.03	12.89	10.04
IND 7	11.49	11.55	10.27	10.79	9.77
IND 8	10.03	9.83	6.38	6.97	6.59
IND 9	14.85	13.09	11.67	12.24	10.85
IND 10	9.97	10.48	5.76	5.81	6.14
MEAN	**11.77**	**11.63**	**9.47**	**10.22**	**8.38**
STD	**1.51**	**1.52**	**2.33**	**2.29**	**1.96**

Latissimus Dorsi Peak Impact Force (N)

VOL	AVG PASSIVE	AVG PASS-REP	AVG MVC100	AVG MVC50	AVG SUPINE
IND 1	168.94	214.13	200.70	162.37	219.94
IND 2	173.65	172.52	177.40	154.09	158.69
IND 3	143.45	160.95	148.95	167.38	215.47
IND 4	176.86	191.75	141.06	235.69	248.46
IND 5	152.33	143.57	144.22	147.94	150.37
IND 6	204.34	260.85	186.01	223.78	192.19
IND 7	175.70	205.88	162.75	166.81	155.22
IND 8	156.77	165.40	208.08	201.63	170.45
IND 9	172.72	172.34	179.94	164.69	214.05
IND 10	272.90	216.04	335.04	305.29	227.72
MEAN	**179.77**	**190.34**	**188.41**	**192.97**	**195.26**
STD	**36.68**	**34.57**	**56.42**	**49.53**	**34.70**

Latissimus Dorsi Peak Indentation Depth (mm)

PMHS	AVG SEATED 11M/S	AVG SUPINE 11M/S	AVG SEATED 5M/S	AVG SUPINE 5M/S
1	16.51	8.46	12.13	8.42
2	12.02	7.78	10.71	7.41
3A	15.07	10.10	8.84	7.56
3B	19.40	13.60	8.72	5.38
MEAN	**15.75**	**9.99**	**10.10**	**7.19**
STD	**3.07**	**2.60**	**1.63**	**1.29**

Latissimus Dorsi Peak Impact Force (N)

PMHS	AVG SEATED 11M/S	AVG SUPINE 11M/S	AVG SEATED 5M/S	AVG SUPINE 5M/S
1	510.33	515.56	176.91	202.46
2	657.38	928.45	133.24	170.86
3A	955.60	899.67	158.34	174.15
3B	790.38	946.78	242.09	273.72
MEAN	**728.42**	**822.61**	**177.65**	**205.30**
STD	**189.79**	**205.62**	**46.54**	**47.77**

Appendix 14: The average tissue thickness for each muscle during each SWE muscle activation level

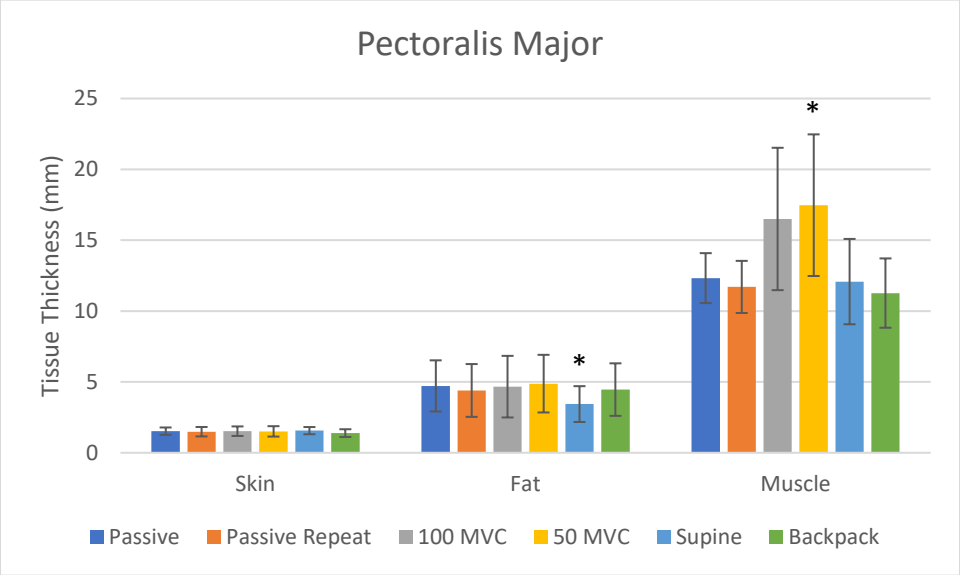

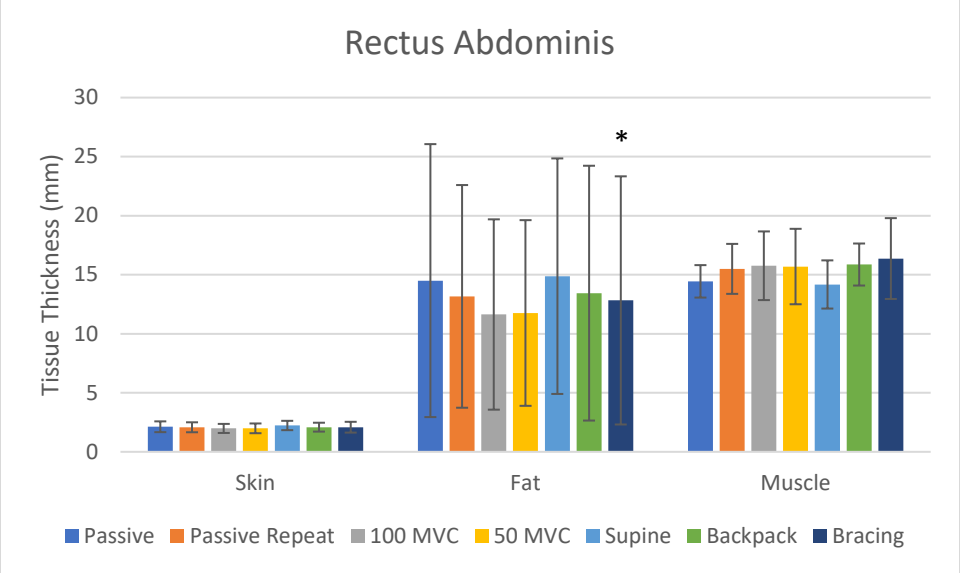

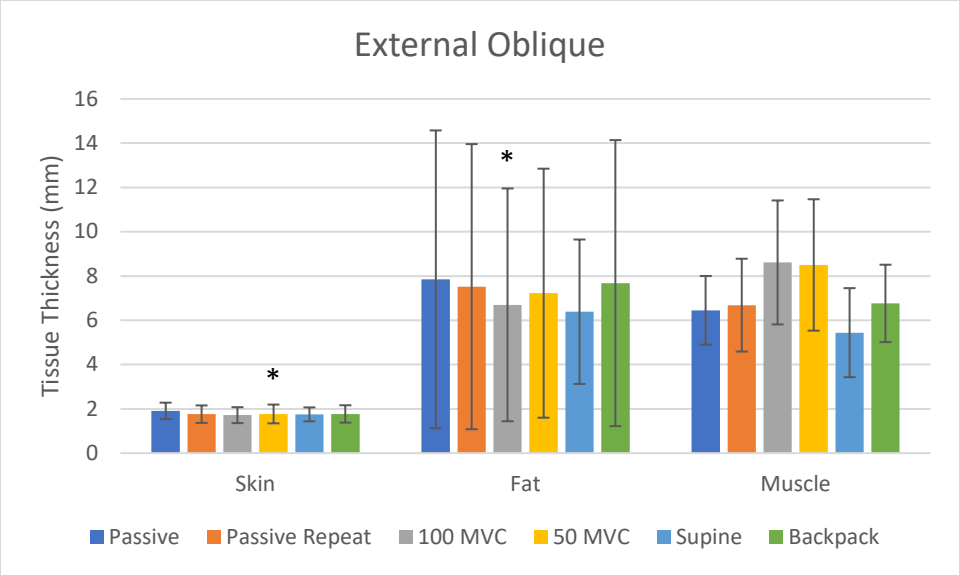
External Oblique
Tissue Thickness (mm)
16
14
12
10
8
6
4
2
0
*
*
Skin
Fat
Muscle
Passive
Passive Repeat
100 MVC
50 MVC
Supine
Backpack

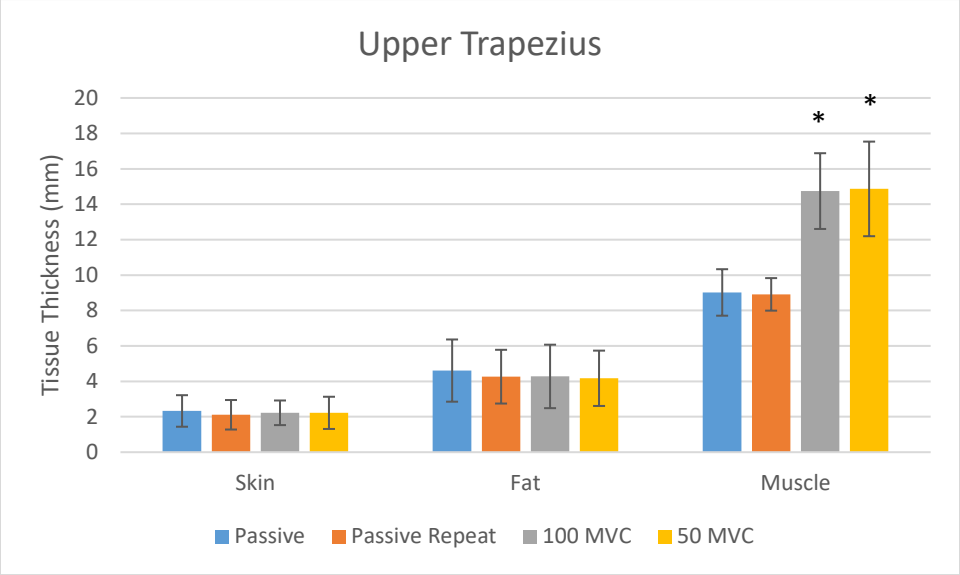
Upper Trapezius
Tissue Thickness (mm)
20
18
16
14
12
10
8
6
4
2
0
*
*
Skin
Fat
Muscle
Passive
Passive Repeat
100 MVC
50 MVC

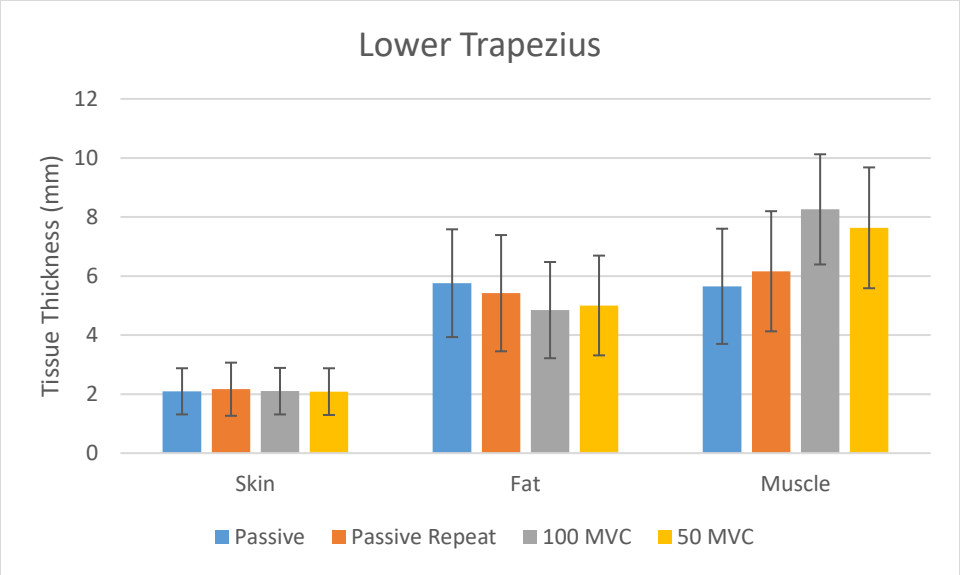
Lower Trapezius
Tissue Thickness (mm)
12
10
8
6
4
2
0
Skin
Fat
Muscle
Passive
Passive Repeat
100 MVC
50 MVC

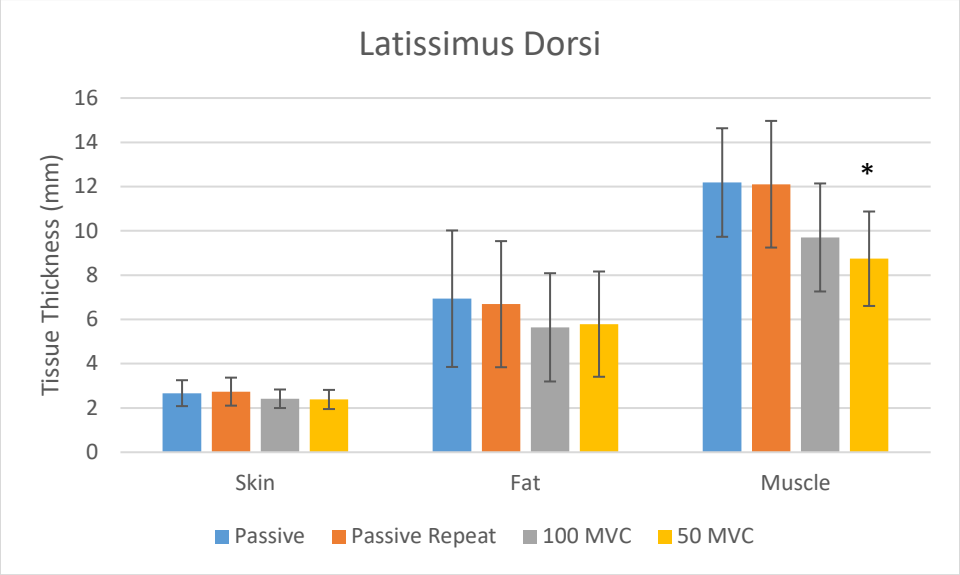
Latissimus Dorsi
Tissue Thickness (mm)
16
14
12
10
8
6
4
2
0
*
Skin
Fat
Muscle
Passive
Passive Repeat
100 MVC
50 MVC

Appendix 15: Volunteer Force-Time and Force-Displacement Curves

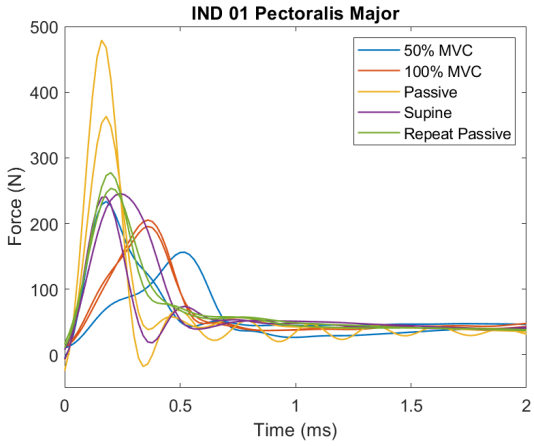

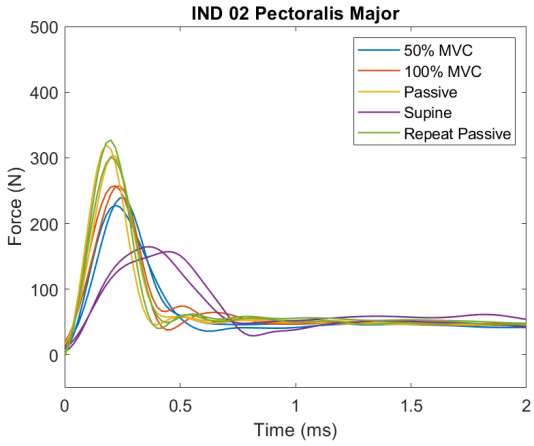

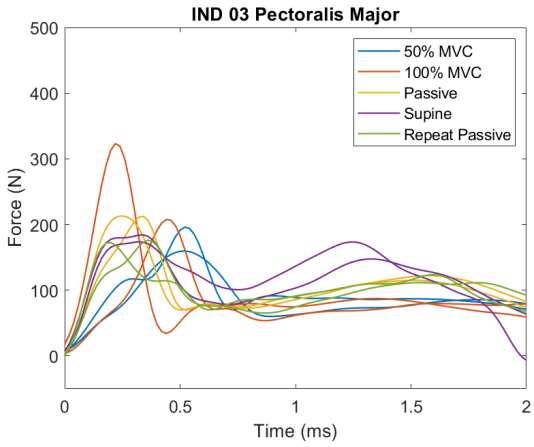

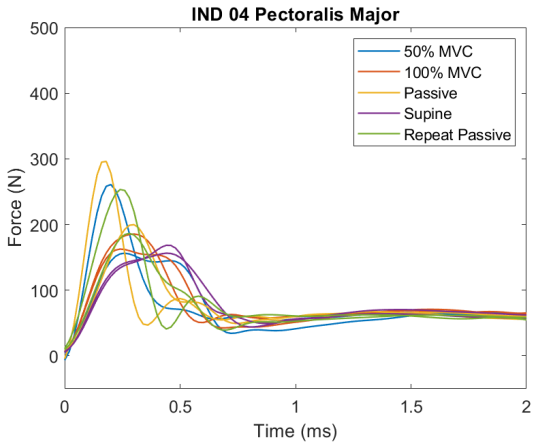

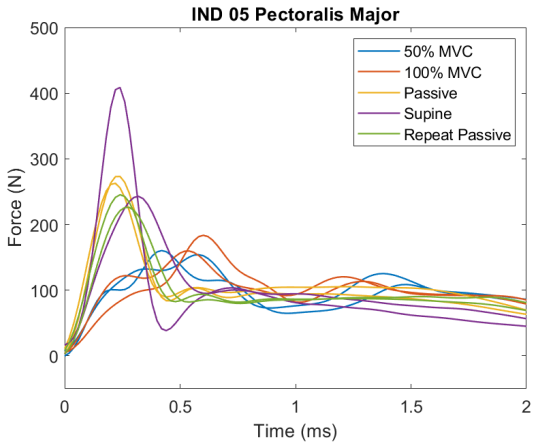

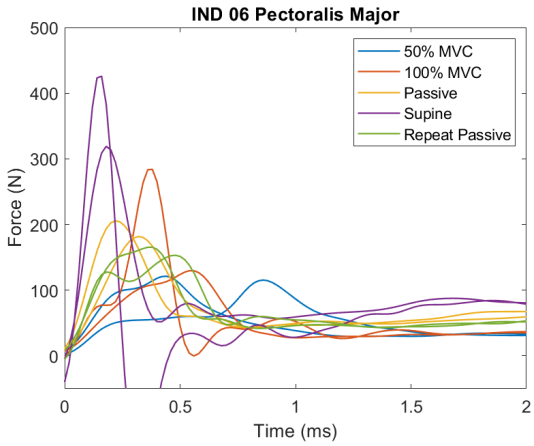

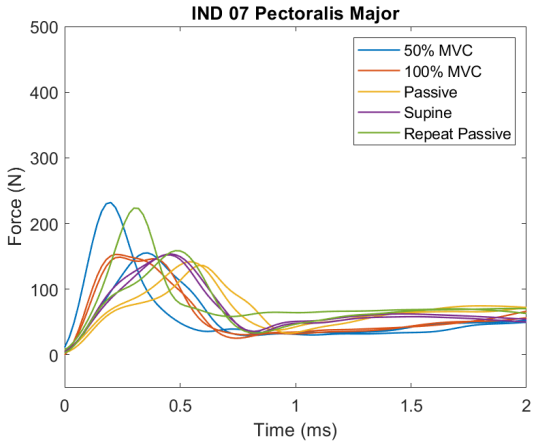
IND 07 Pectoralis Major
50% MVC
100% MVC
Passive
Supine
Repeat Passive
Force (N)
Time (ms)

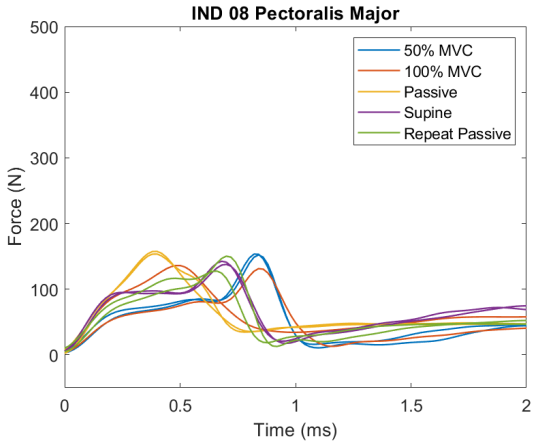
IND 08 Pectoralis Major
50% MVC
100% MVC
Passive
Supine
Repeat Passive
Force (N)
Time (ms)

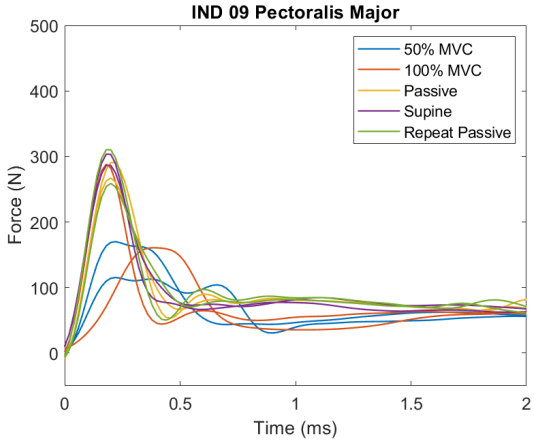
IND 09 Pectoralis Major
50% MVC
100% MVC
Passive
Supine
Repeat Passive
Force (N)
Time (ms)

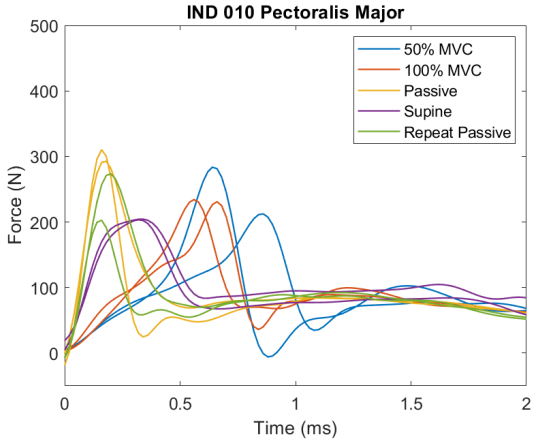
IND 010 Pectoralis Major
50% MVC
100% MVC
Passive
Supine
Repeat Passive
Force (N)
Time (ms)

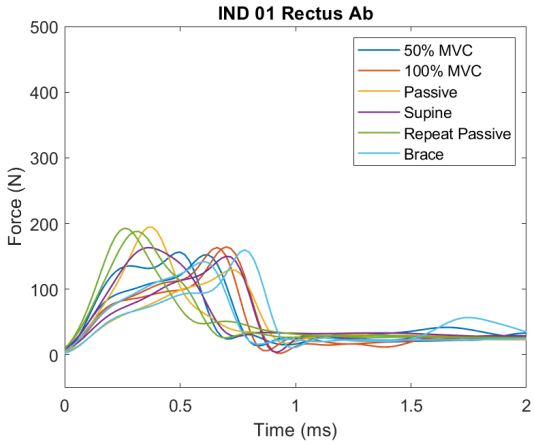
IND 01 Rectus Ab
50% MVC
100% MVC
Passive
Supine
Repeat Passive
Brace
Force (N)
Time (ms)

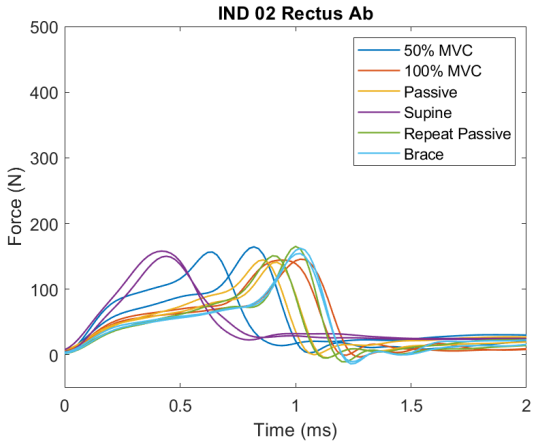
IND 02 Rectus Ab
50% MVC
100% MVC
Passive
Supine
Repeat Passive
Brace
Force (N)
Time (ms)

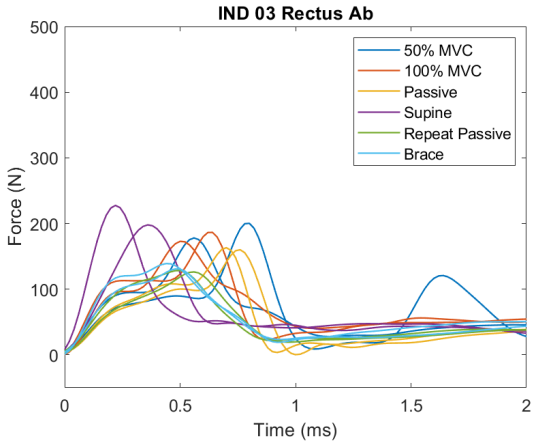
IND 03 Rectus Ab
50% MVC
100% MVC
Passive
Supine
Repeat Passive
Brace
Force (N)
Time (ms)

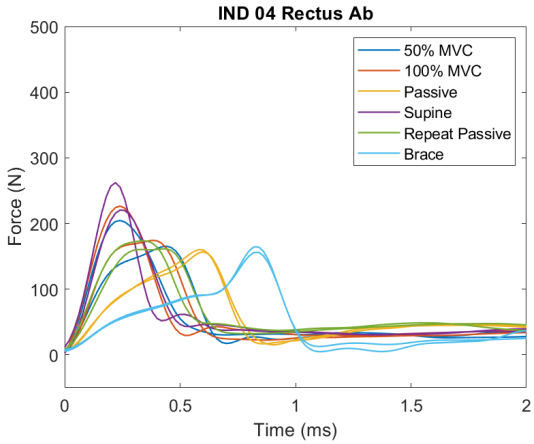
IND 04 Rectus Ab
50% MVC
100% MVC
Passive
Supine
Repeat Passive
Brace
Force (N)
Time (ms)

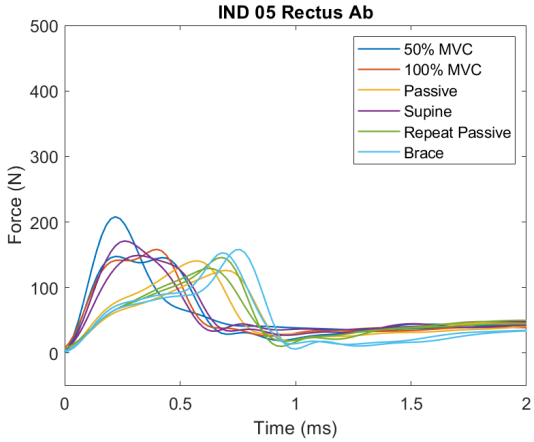
IND 05 Rectus Ab
50% MVC
100% MVC
Passive
Supine
Repeat Passive
Brace
Force (N)
Time (ms)

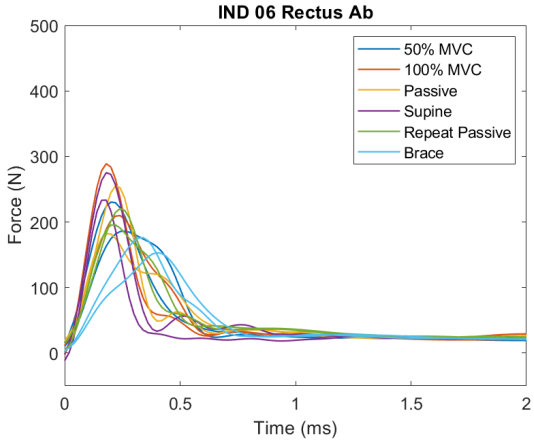
IND 06 Rectus Ab
50% MVC
100% MVC
Passive
Supine
Repeat Passive
Brace
Force (N)
Time (ms)

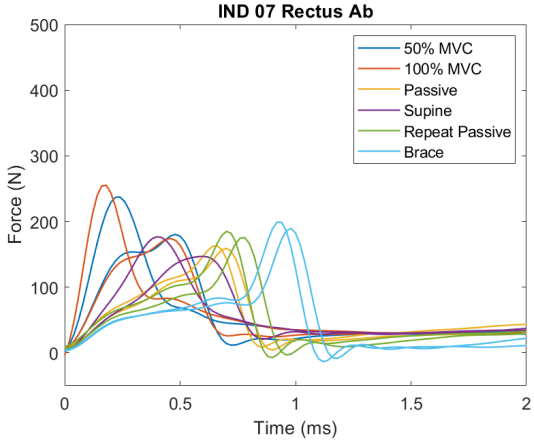
IND 07 Rectus Ab
50% MVC
100% MVC
Passive
Supine
Repeat Passive
Brace
Force (N)
Time (ms)

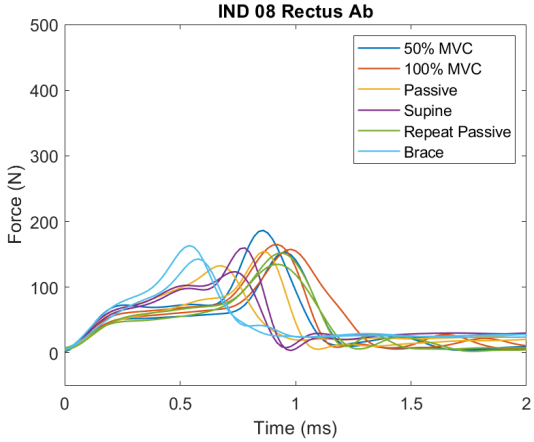
IND 08 Rectus Ab
50% MVC
100% MVC
Passive
Supine
Repeat Passive
Brace
Force (N)
Time (ms)

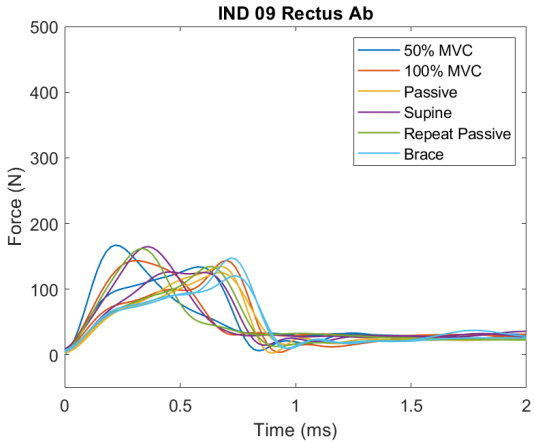
IND 09 Rectus Ab
50% MVC
100% MVC
Passive
Supine
Repeat Passive
Brace
Force (N)
Time (ms)

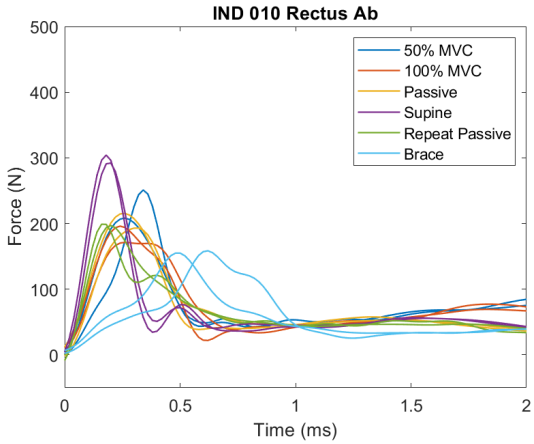
IND 010 Rectus Ab
50% MVC
100% MVC
Passive
Supine
Repeat Passive
Brace
Force (N)
Time (ms)

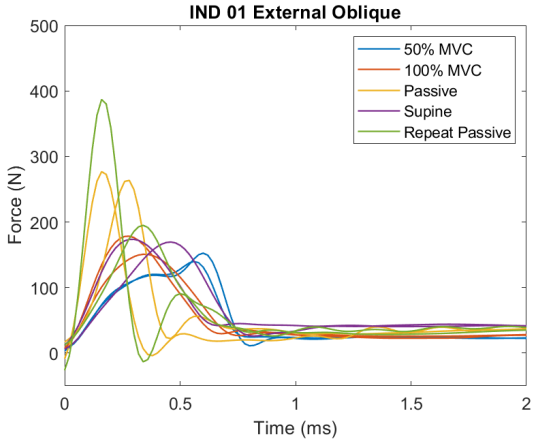
IND 01 External Oblique
50% MVC
100% MVC
Passive
Supine
Repeat Passive
Force (N)
Time (ms)

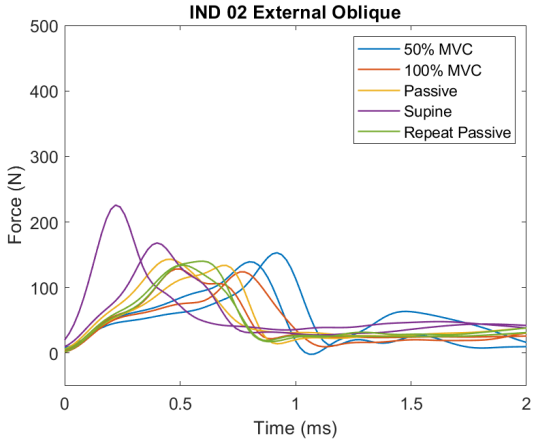
IND 02 External Oblique
50% MVC
100% MVC
Passive
Supine
Repeat Passive
Force (N)
Time (ms)

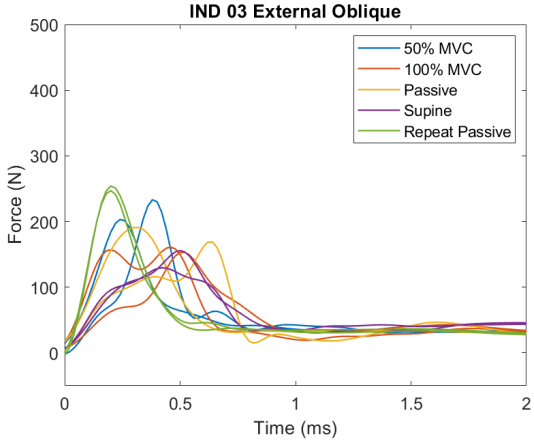
IND 03 External Oblique
50% MVC
100% MVC
Passive
Supine
Repeat Passive
Force (N)
Time (ms)

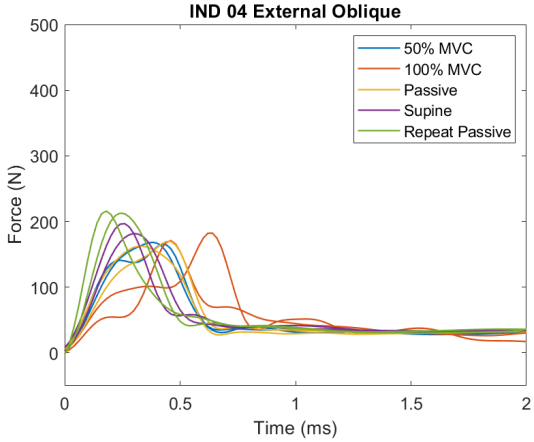
IND 04 External Oblique
50% MVC
100% MVC
Passive
Supine
Repeat Passive
Force (N)
Time (ms)

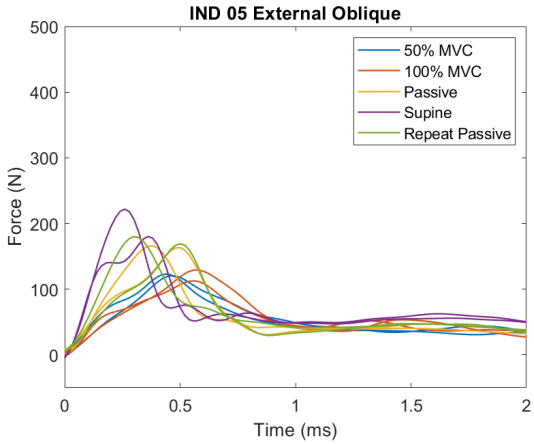
IND 05 External Oblique
50% MVC
100% MVC
Passive
Supine
Repeat Passive
Force (N)
Time (ms)

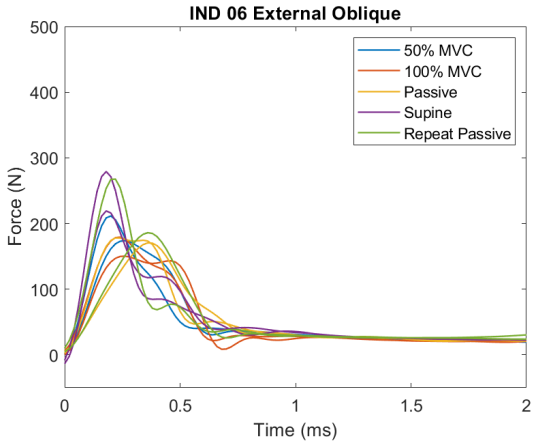
IND 06 External Oblique
50% MVC
100% MVC
Passive
Supine
Repeat Passive
Force (N)
Time (ms)

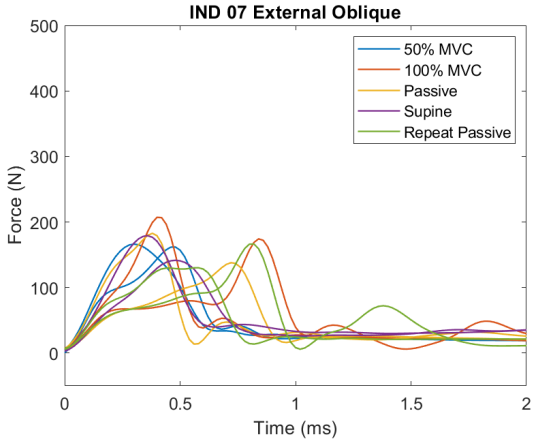
IND 07 External Oblique
50% MVC
100% MVC
Passive
Supine
Repeat Passive
Force (N)
Time (ms)

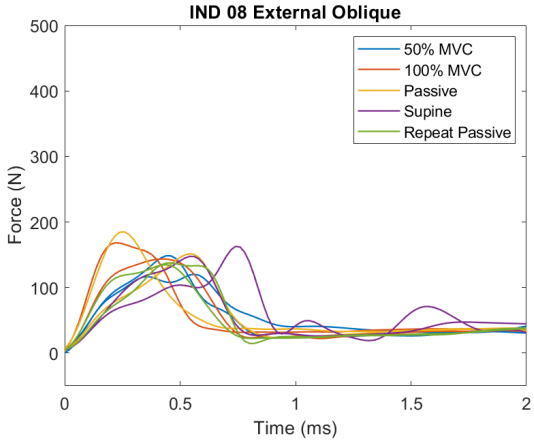
IND 08 External Oblique
50% MVC
100% MVC
Passive
Supine
Repeat Passive
Force (N)
Time (ms)

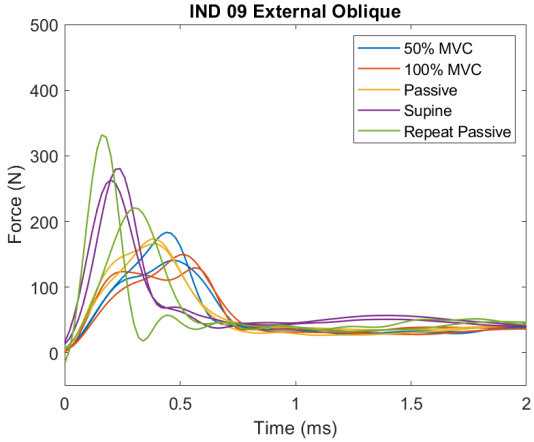
IND 09 External Oblique
50% MVC
100% MVC
Passive
Supine
Repeat Passive
Force (N)
Time (ms)

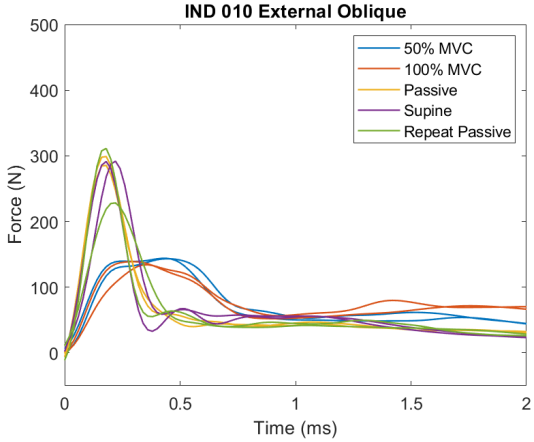
IND 010 External Oblique
50% MVC
100% MVC
Passive
Supine
Repeat Passive
Force (N)
Time (ms)

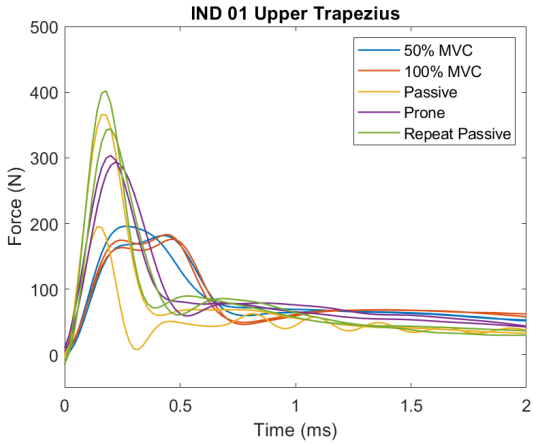
IND 01 Upper Trapezius
50% MVC
100% MVC
Passive
Prone
Repeat Passive
Force (N)
Time (ms)

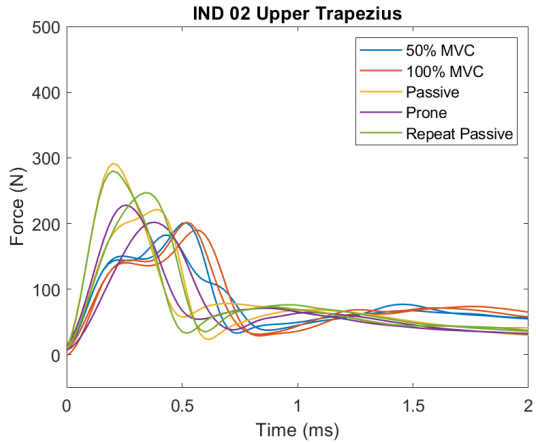
IND 02 Upper Trapezius
50% MVC
100% MVC
Passive
Prone
Repeat Passive
Force (N)
Time (ms)

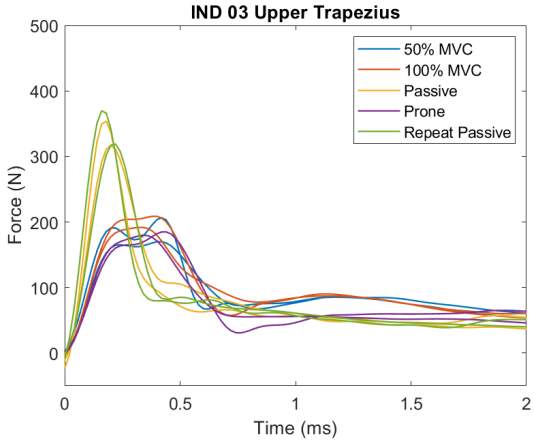
IND 03 Upper Trapezius
50% MVC
100% MVC
Passive
Prone
Repeat Passive
Force (N)
Time (ms)

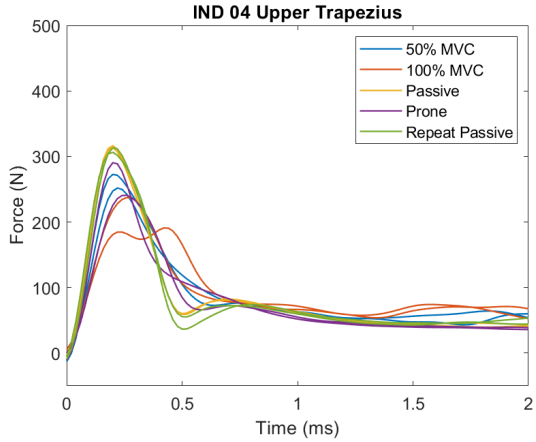
IND 04 Upper Trapezius
50% MVC
100% MVC
Passive
Prone
Repeat Passive
Force (N)
Time (ms)

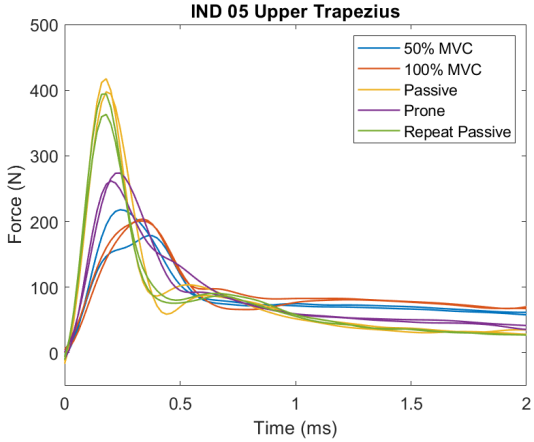
IND 05 Upper Trapezius
50% MVC
100% MVC
Passive
Prone
Repeat Passive
Force (N)
Time (ms)

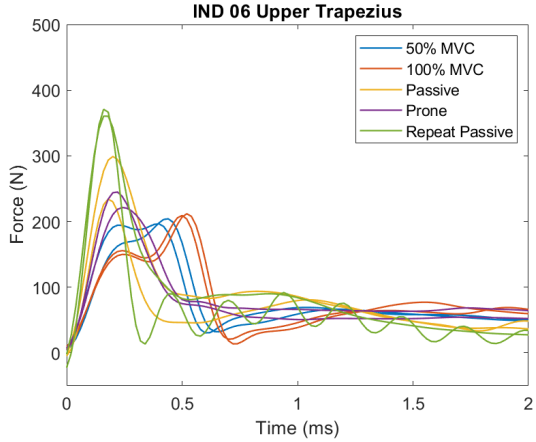
IND 06 Upper Trapezius
50% MVC
100% MVC
Passive
Prone
Repeat Passive
Force (N)
Time (ms)

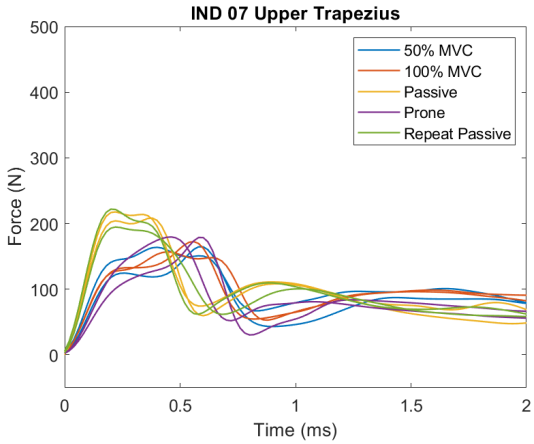
IND 07 Upper Trapezius
50% MVC
100% MVC
Passive
Prone
Repeat Passive
Force (N)
Time (ms)

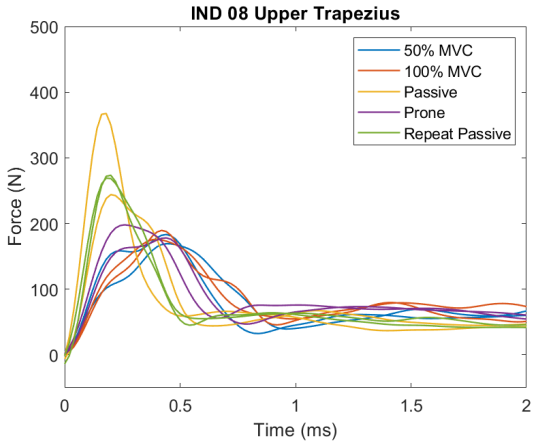
IND 08 Upper Trapezius
50% MVC
100% MVC
Passive
Prone
Repeat Passive
Force (N)
Time (ms)

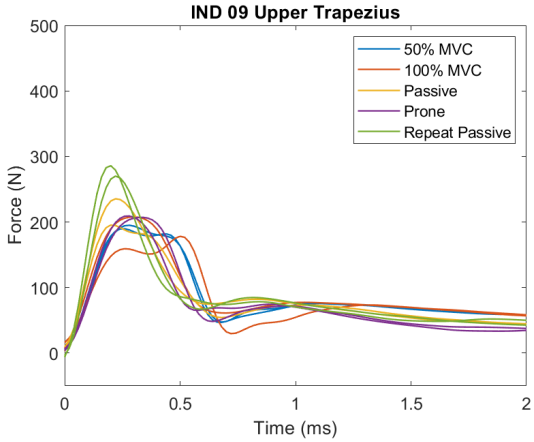
IND 09 Upper Trapezius
50% MVC
100% MVC
Passive
Prone
Repeat Passive
Force (N)
Time (ms)

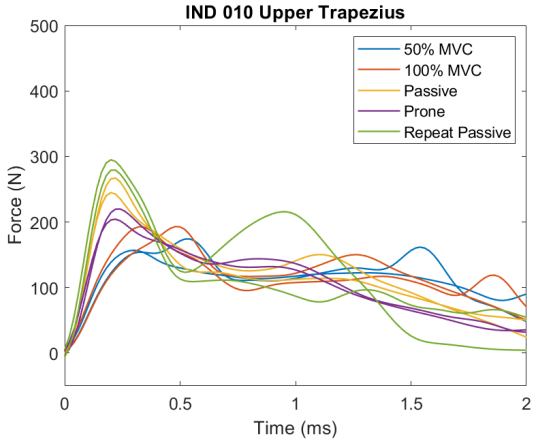
IND 010 Upper Trapezius
50% MVC
100% MVC
Passive
Prone
Repeat Passive
Force (N)
Time (ms)

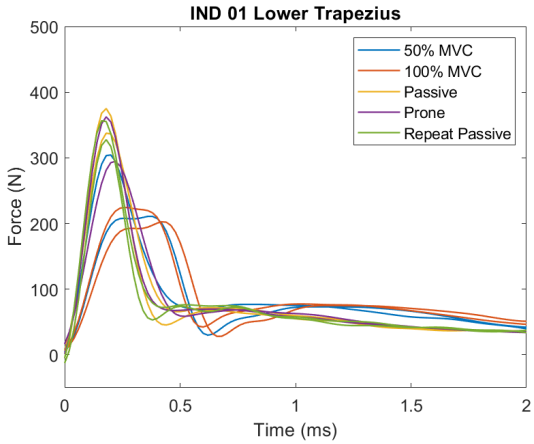
IND 01 Lower Trapezius
50% MVC
100% MVC
Passive
Prone
Repeat Passive
Force (N)
Time (ms)

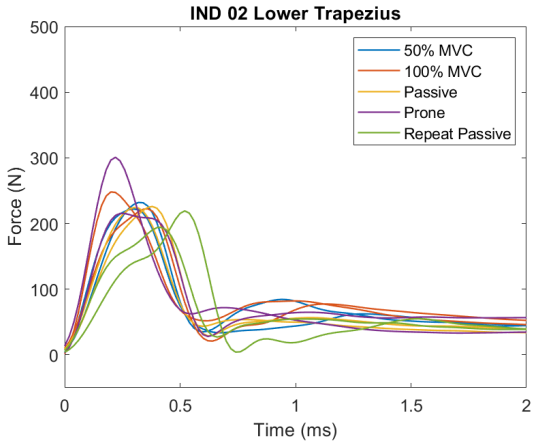
IND 02 Lower Trapezius
50% MVC
100% MVC
Passive
Prone
Repeat Passive
Force (N)
Time (ms)

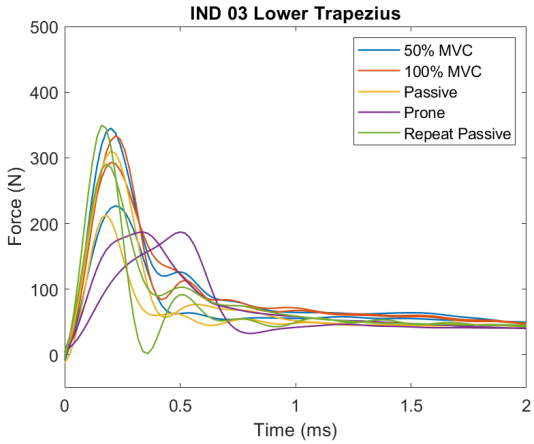
IND 03 Lower Trapezius
50% MVC
100% MVC
Passive
Prone
Repeat Passive
Force (N)
Time (ms)

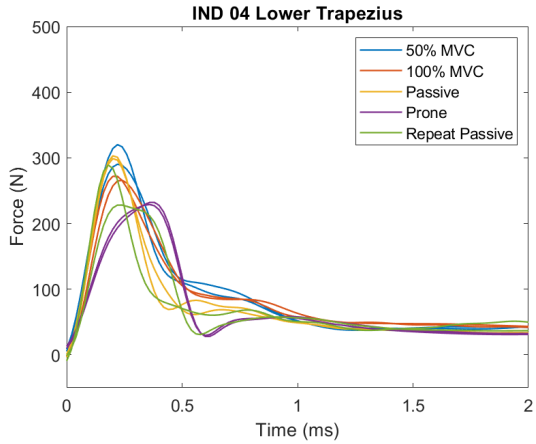
IND 04 Lower Trapezius
50% MVC
100% MVC
Passive
Prone
Repeat Passive
Force (N)
Time (ms)

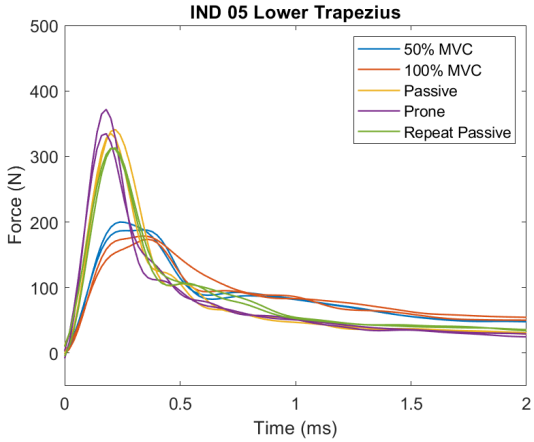
IND 05 Lower Trapezius
50% MVC
100% MVC
Passive
Prone
Repeat Passive
Force (N)
Time (ms)

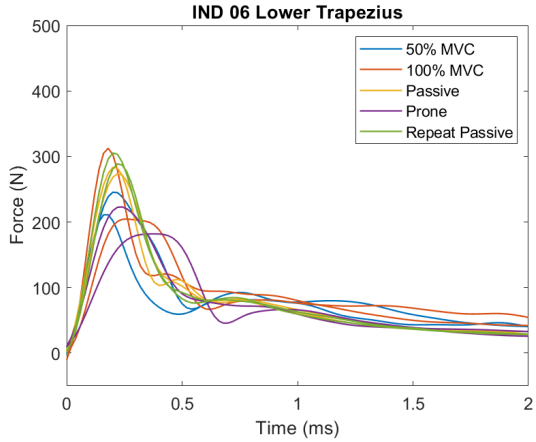
IND 06 Lower Trapezius
50% MVC
100% MVC
Passive
Prone
Repeat Passive
Force (N)
Time (ms)

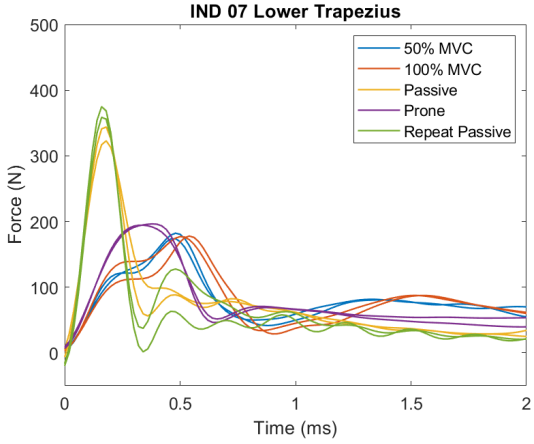
IND 07 Lower Trapezius
50% MVC
100% MVC
Passive
Prone
Repeat Passive
Force (N)
Time (ms)

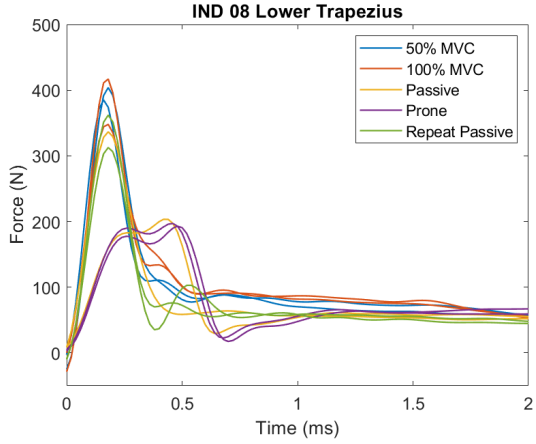
IND 08 Lower Trapezius
50% MVC
100% MVC
Passive
Prone
Repeat Passive
Force (N)
Time (ms)

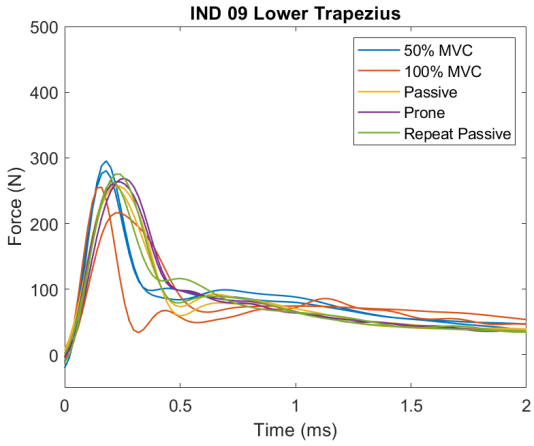
IND 09 Lower Trapezius
50% MVC
100% MVC
Passive
Prone
Repeat Passive
Force (N)
Time (ms)

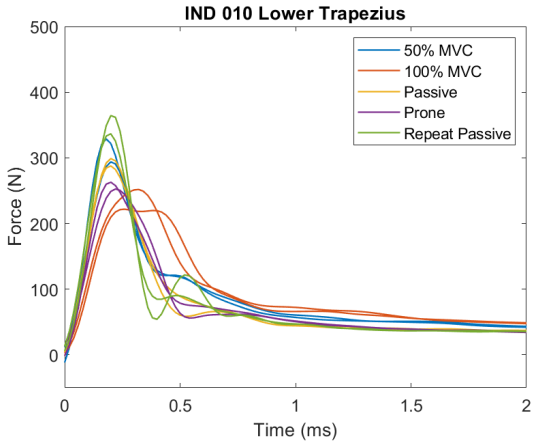
IND 010 Lower Trapezius
50% MVC
100% MVC
Passive
Prone
Repeat Passive
Force (N)
Time (ms)

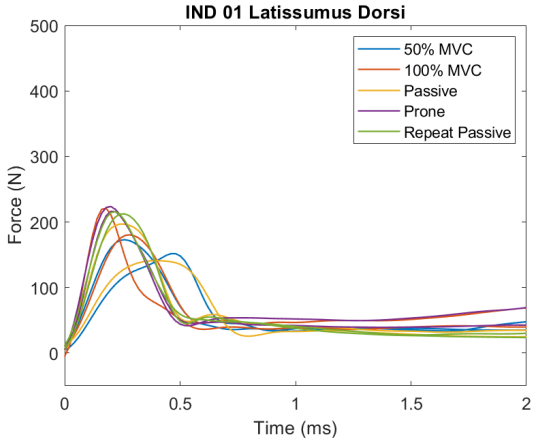
IND 01 Latissumus Dorsi
50% MVC
100% MVC
Passive
Prone
Repeat Passive
Force (N)
Time (ms)

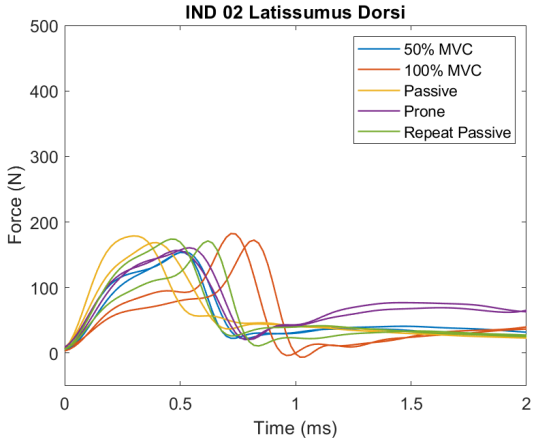
IND 02 Latissumus Dorsi
50% MVC
100% MVC
Passive
Prone
Repeat Passive
Force (N)
Time (ms)

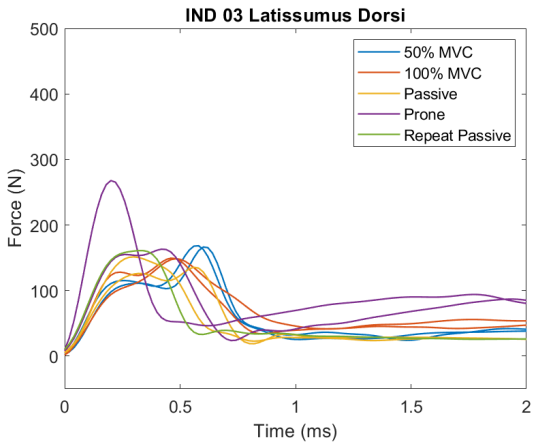
IND 03 Latissumus Dorsi
50% MVC
100% MVC
Passive
Prone
Repeat Passive
Force (N)
Time (ms)

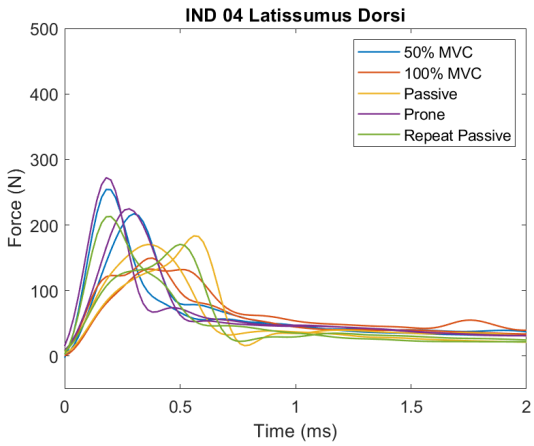
IND 04 Latissumus Dorsi
50% MVC
100% MVC
Passive
Prone
Repeat Passive
Force (N)
Time (ms)

1

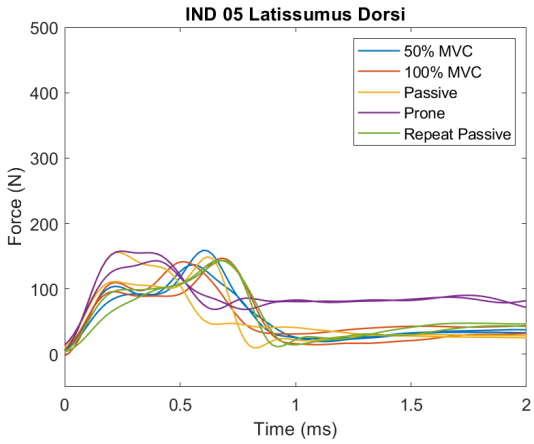
IND 05 Latissumus Dorsi
50% MVC
100% MVC
Passive
Prone
Repeat Passive
Force (N)
Time (ms)

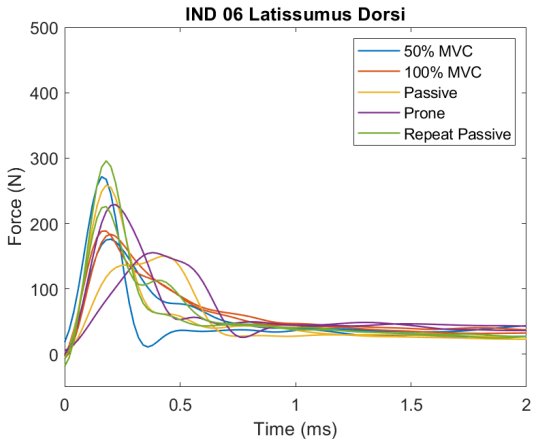
IND 06 Latissumus Dorsi
50% MVC
100% MVC
Passive
Prone
Repeat Passive
Force (N)
Time (ms)

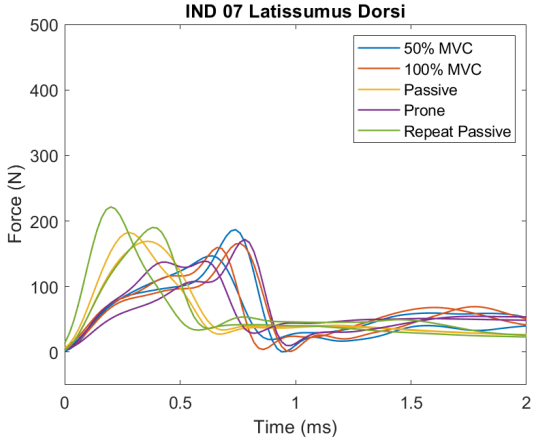
IND 07 Latissumus Dorsi
50% MVC
100% MVC
Passive
Prone
Repeat Passive
Force (N)
Time (ms)

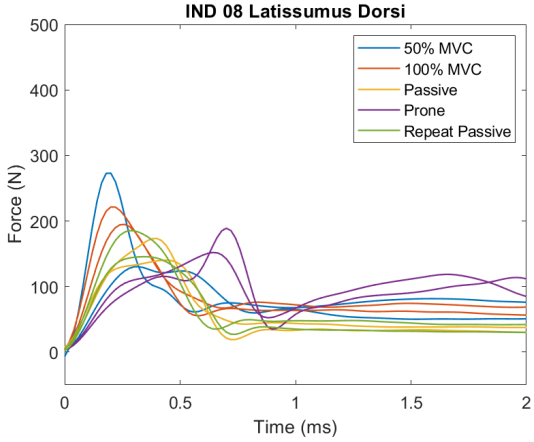
IND 08 Latissumus Dorsi
50% MVC
100% MVC
Passive
Prone
Repeat Passive
Force (N)
Time (ms)

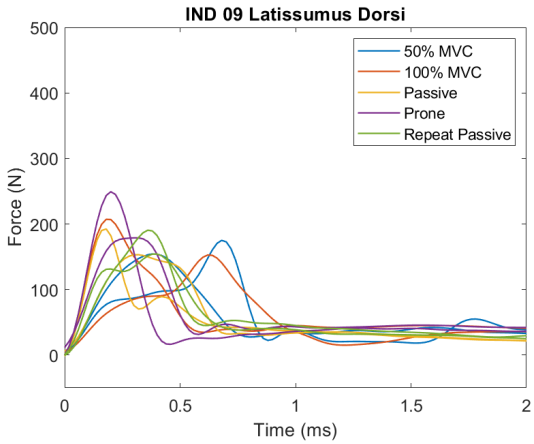
IND 09 Latissumus Dorsi
50% MVC
100% MVC
Passive
Prone
Repeat Passive
Force (N)
Time (ms)

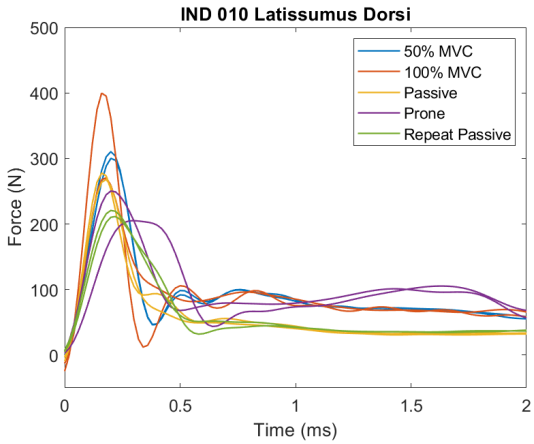
IND 010 Latissumus Dorsi
50% MVC
100% MVC
Passive
Prone
Repeat Passive
Force (N)
Time (ms)

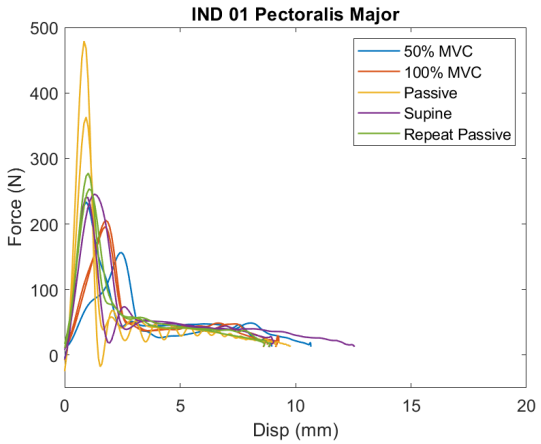
IND 01 Pectoralis Major
50% MVC
100% MVC
Passive
Supine
Repeat Passive
Force (N)
Disp (mm)

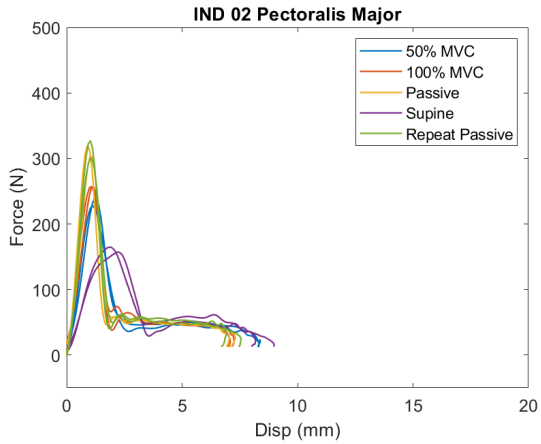
IND 02 Pectoralis Major
50% MVC
100% MVC
Passive
Supine
Repeat Passive
Force (N)
Disp (mm)

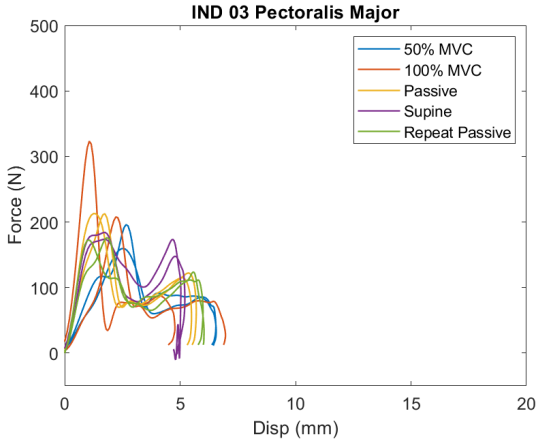
IND 03 Pectoralis Major
50% MVC
100% MVC
Passive
Supine
Repeat Passive
Force (N)
Disp (mm)

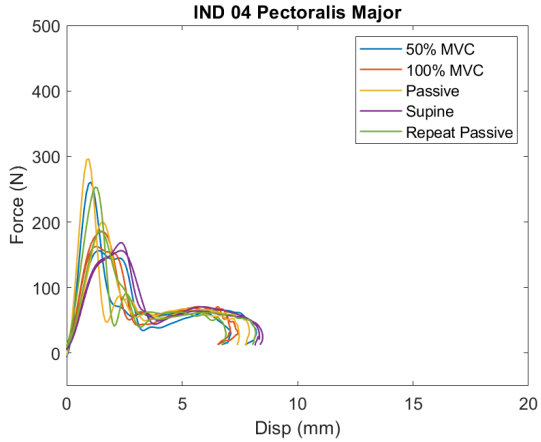
IND 04 Pectoralis Major
50% MVC
100% MVC
Passive
Supine
Repeat Passive
Force (N)
Disp (mm)

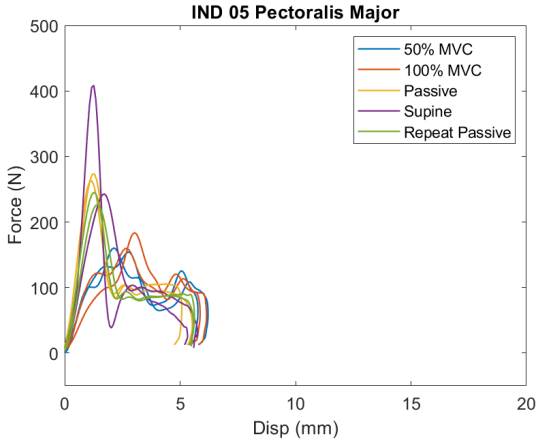
IND 05 Pectoralis Major
50% MVC
100% MVC
Passive
Supine
Repeat Passive
Force (N)
Disp (mm)

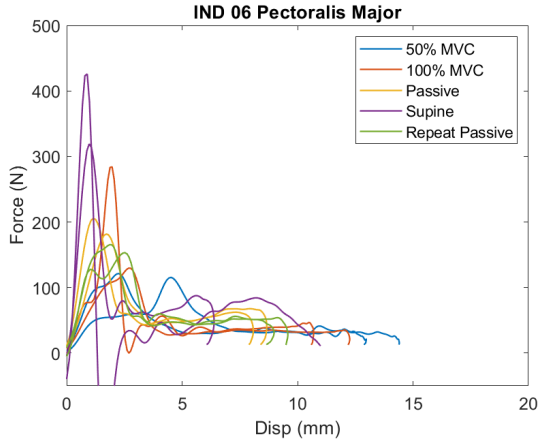
IND 06 Pectoralis Major
50% MVC
100% MVC
Passive
Supine
Repeat Passive
Force (N)
Disp (mm)

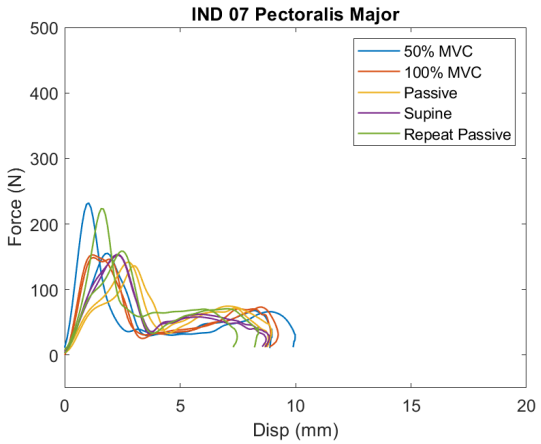
IND 07 Pectoralis Major
50% MVC
100% MVC
Passive
Supine
Repeat Passive
Force (N)
Disp (mm)

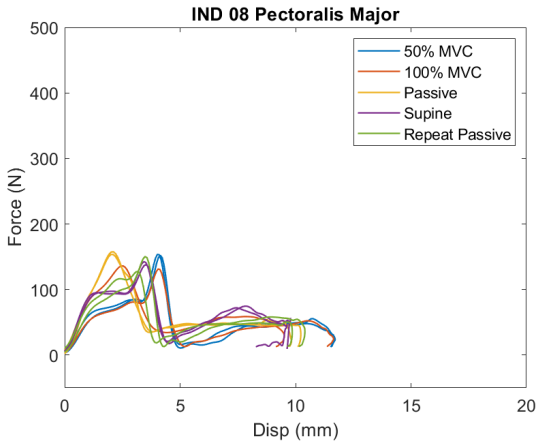
IND 08 Pectoralis Major
50% MVC
100% MVC
Passive
Supine
Repeat Passive
Force (N)
Disp (mm)

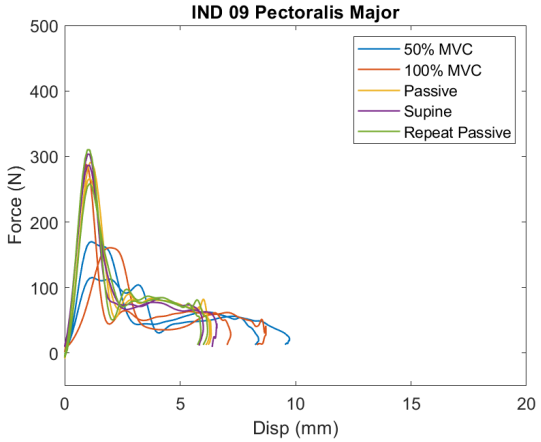
IND 09 Pectoralis Major
50% MVC
100% MVC
Passive
Supine
Repeat Passive
Force (N)
Disp (mm)

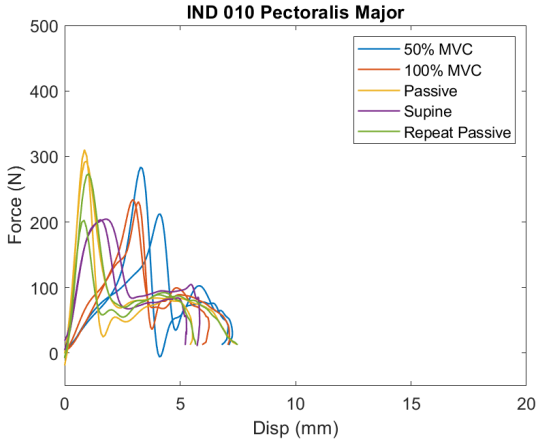
IND 010 Pectoralis Major
50% MVC
100% MVC
Passive
Supine
Repeat Passive
Force (N)
Disp (mm)

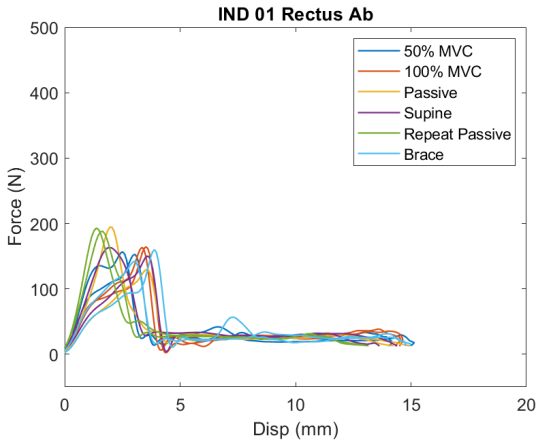
IND 01 Rectus Ab
50% MVC
100% MVC
Passive
Supine
Repeat Passive
Brace
Force (N)
Disp (mm)

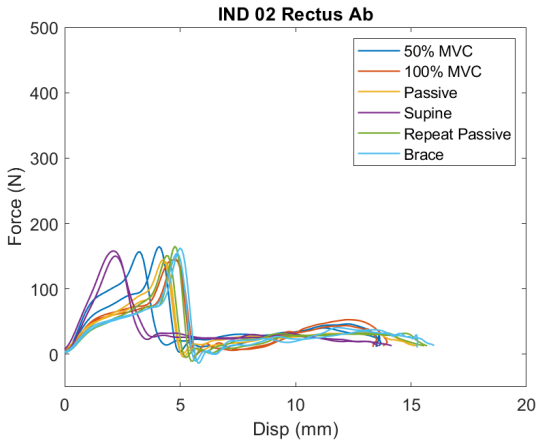
IND 02 Rectus Ab
50% MVC
100% MVC
Passive
Supine
Repeat Passive
Brace
Force (N)
Disp (mm)

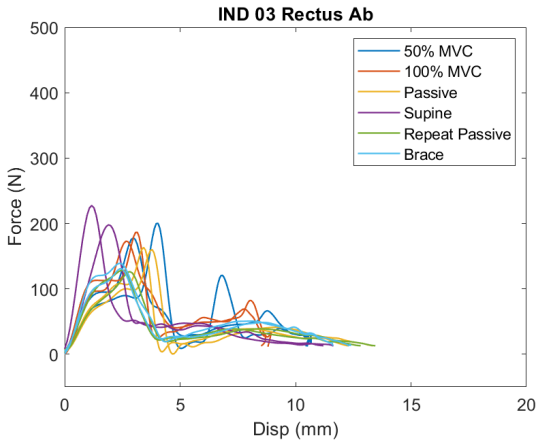
IND 03 Rectus Ab
50% MVC
100% MVC
Passive
Supine
Repeat Passive
Brace
Force (N)
Disp (mm)

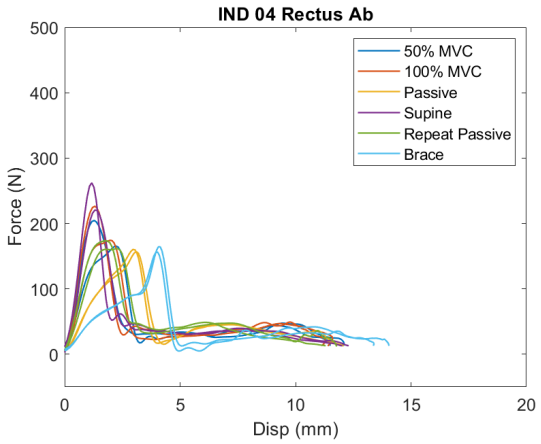
IND 04 Rectus Ab
50% MVC
100% MVC
Passive
Supine
Repeat Passive
Brace
Force (N)
Disp (mm)

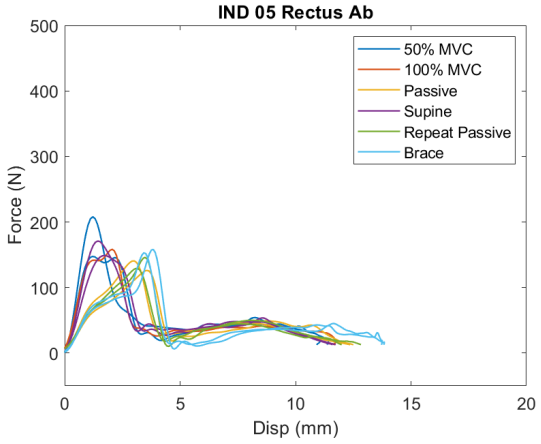
IND 05 Rectus Ab
50% MVC
100% MVC
Passive
Supine
Repeat Passive
Brace
Force (N)
Disp (mm)

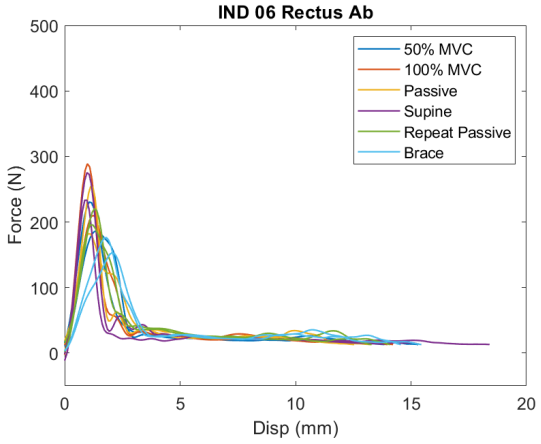
IND 06 Rectus Ab
50% MVC
100% MVC
Passive
Supine
Repeat Passive
Brace
Force (N)
Disp (mm)

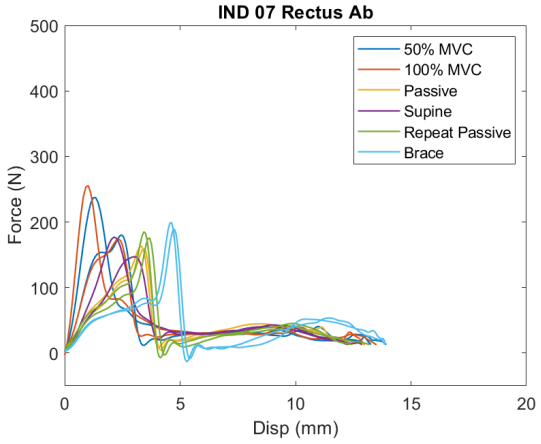
IND 07 Rectus Ab
50% MVC
100% MVC
Passive
Supine
Repeat Passive
Brace
Force (N)
Disp (mm)

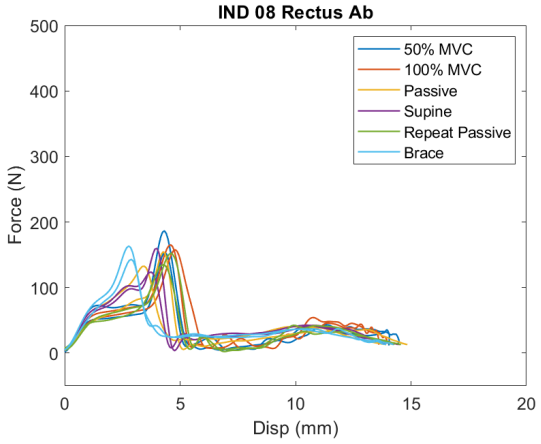
IND 08 Rectus Ab
50% MVC
100% MVC
Passive
Supine
Repeat Passive
Brace
Force (N)
Disp (mm)

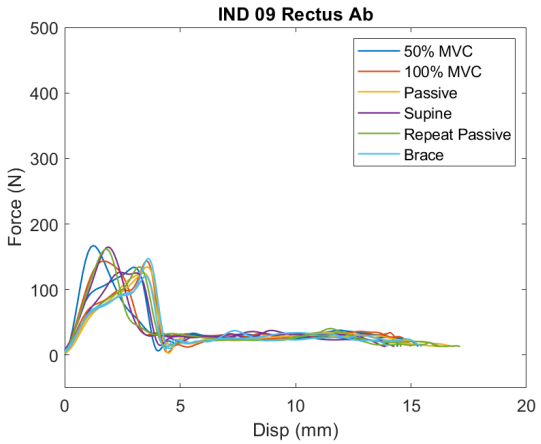
IND 09 Rectus Ab
50% MVC
100% MVC
Passive
Supine
Repeat Passive
Brace
Force (N)
Disp (mm)

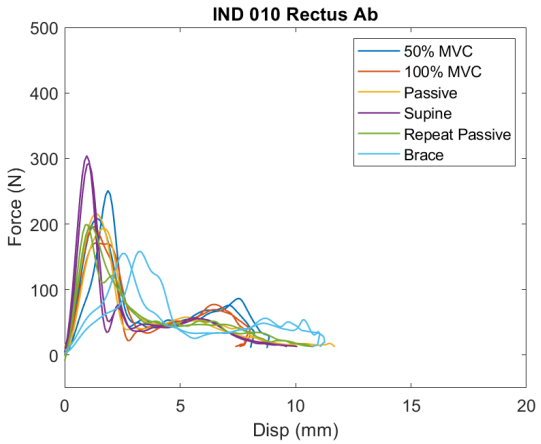
IND 010 Rectus Ab
50% MVC
100% MVC
Passive
Supine
Repeat Passive
Brace
Force (N)
Disp (mm)

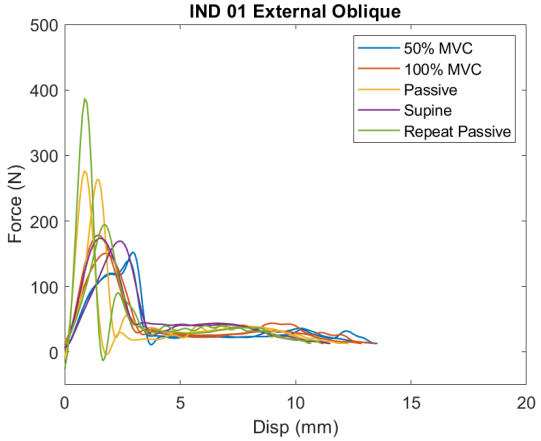
IND 01 External Oblique
50% MVC
100% MVC
Passive
Supine
Repeat Passive
Force (N)
Disp (mm)

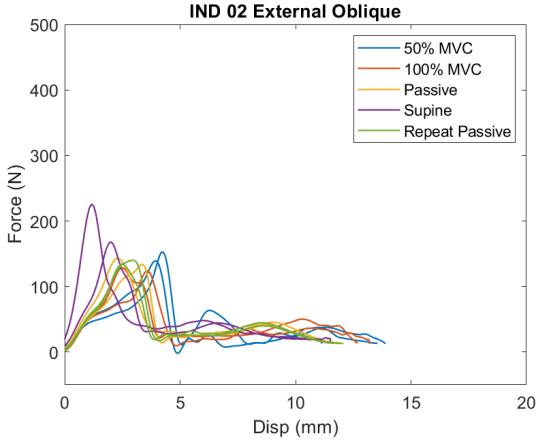
IND 02 External Oblique
50% MVC
100% MVC
Passive
Supine
Repeat Passive
Force (N)
Disp (mm)

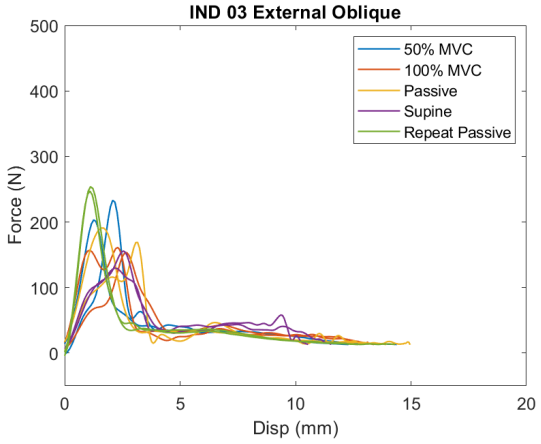
IND 03 External Oblique
50% MVC
100% MVC
Passive
Supine
Repeat Passive
Force (N)
Disp (mm)

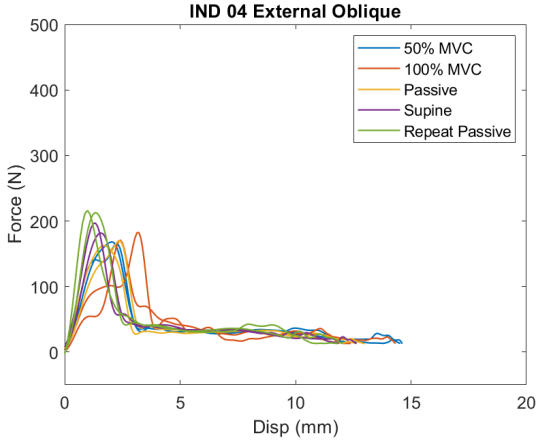
IND 04 External Oblique
50% MVC
100% MVC
Passive
Supine
Repeat Passive
Force (N)
Disp (mm)

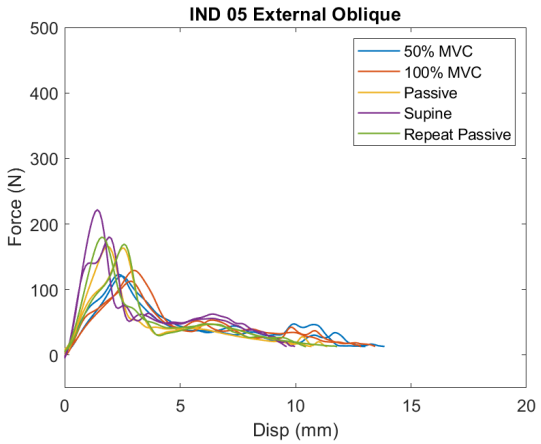
IND 05 External Oblique
50% MVC
100% MVC
Passive
Supine
Repeat Passive
Force (N)
Disp (mm)

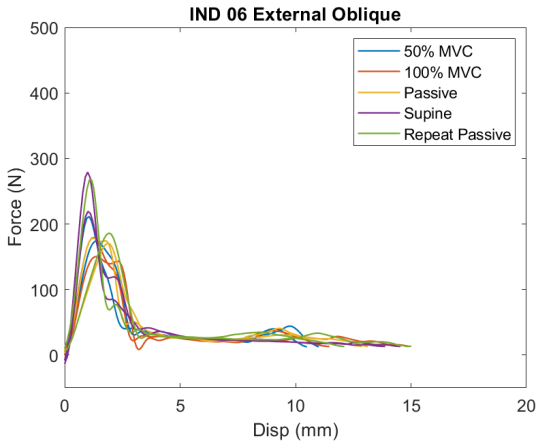
IND 06 External Oblique
50% MVC
100% MVC
Passive
Supine
Repeat Passive
Force (N)
Disp (mm)

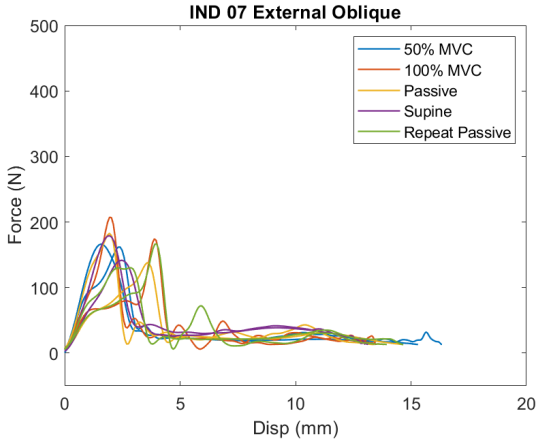
IND 07 External Oblique
50% MVC
100% MVC
Passive
Supine
Repeat Passive
Force (N)
Disp (mm)

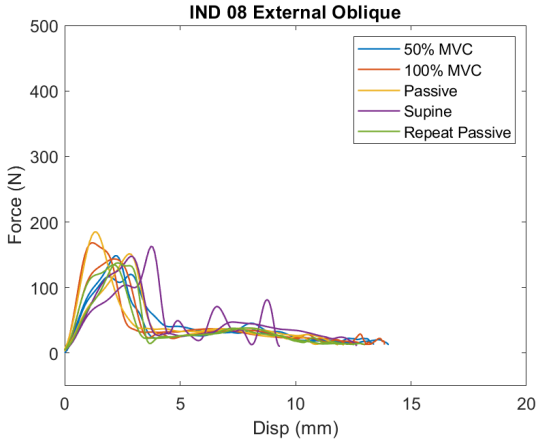
IND 08 External Oblique
50% MVC
100% MVC
Passive
Supine
Repeat Passive
Force (N)
Disp (mm)

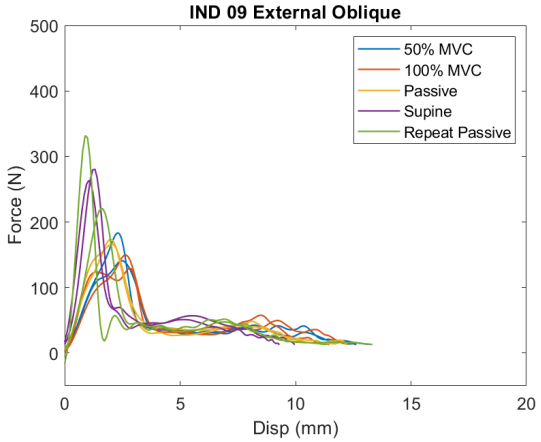
IND 09 External Oblique
50% MVC
100% MVC
Passive
Supine
Repeat Passive
Force (N)
Disp (mm)

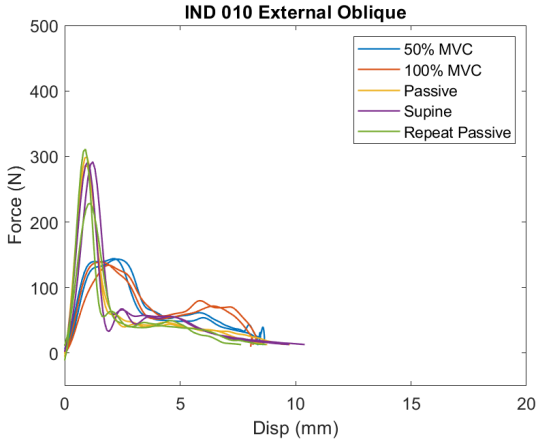
IND 010 External Oblique
50% MVC
100% MVC
Passive
Supine
Repeat Passive
Force (N)
Disp (mm)

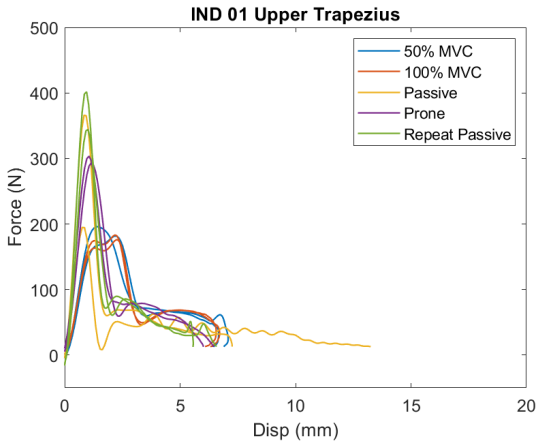
IND 01 Upper Trapezius
50% MVC
100% MVC
Passive
Prone
Repeat Passive
Force (N)
Disp (mm)

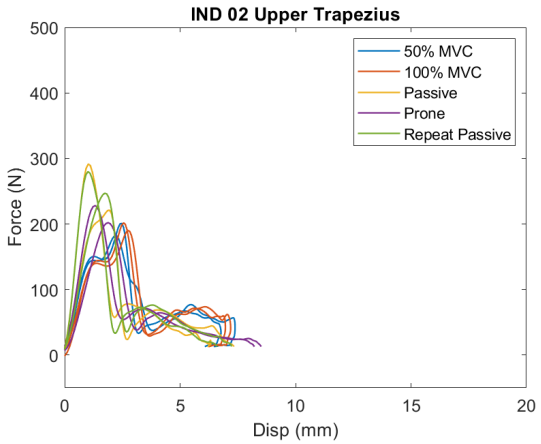
IND 02 Upper Trapezius
50% MVC
100% MVC
Passive
Prone
Repeat Passive
Force (N)
Disp (mm)

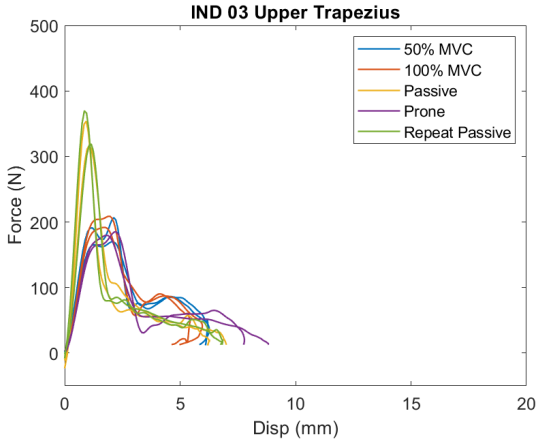
IND 03 Upper Trapezius
50% MVC
100% MVC
Passive
Prone
Repeat Passive
Force (N)
Disp (mm)

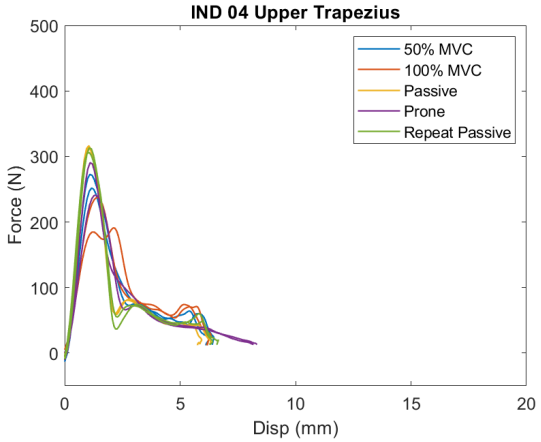
IND 04 Upper Trapezius
50% MVC
100% MVC
Passive
Prone
Repeat Passive
Force (N)
Disp (mm)

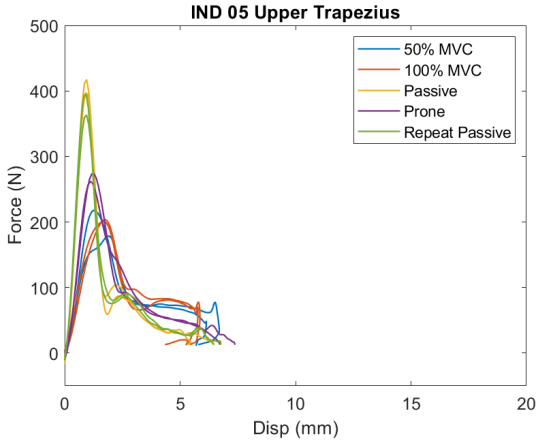
IND 05 Upper Trapezius
50% MVC
100% MVC
Passive
Prone
Repeat Passive
Force (N)
Disp (mm)

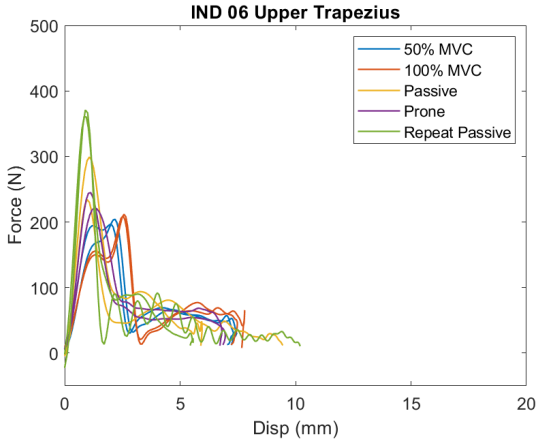
IND 06 Upper Trapezius
50% MVC
100% MVC
Passive
Prone
Repeat Passive
Force (N)
Disp (mm)

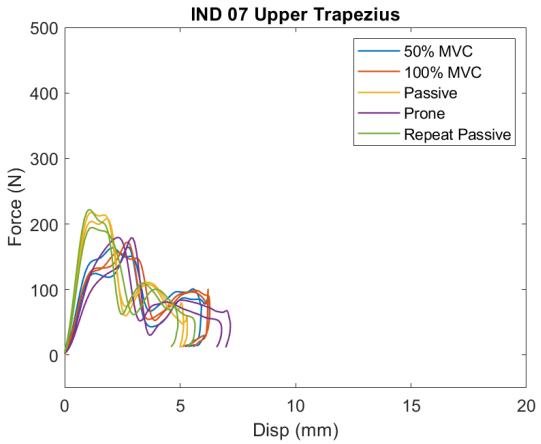
IND 07 Upper Trapezius
50% MVC
100% MVC
Passive
Prone
Repeat Passive
Force (N)
Disp (mm)

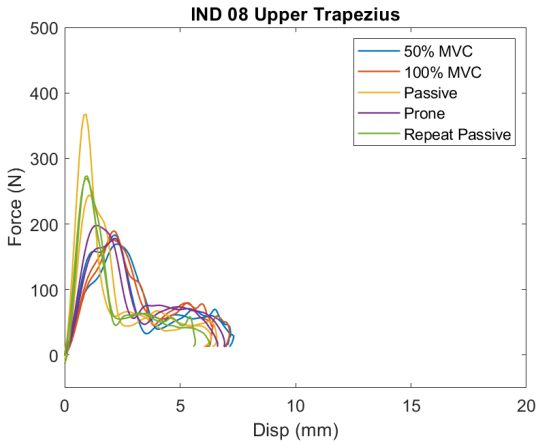
IND 08 Upper Trapezius
50% MVC
100% MVC
Passive
Prone
Repeat Passive
Force (N)
Disp (mm)

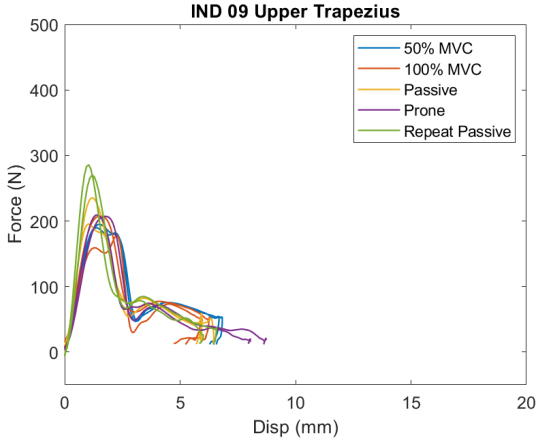
IND 09 Upper Trapezius
50% MVC
100% MVC
Passive
Prone
Repeat Passive
Force (N)
Disp (mm)

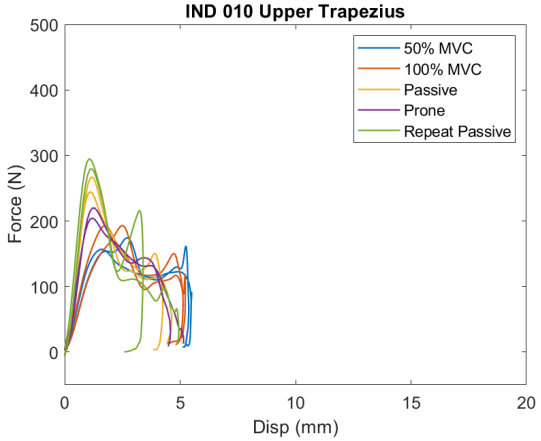
IND 010 Upper Trapezius
50% MVC
100% MVC
Passive
Prone
Repeat Passive
Force (N)
Disp (mm)

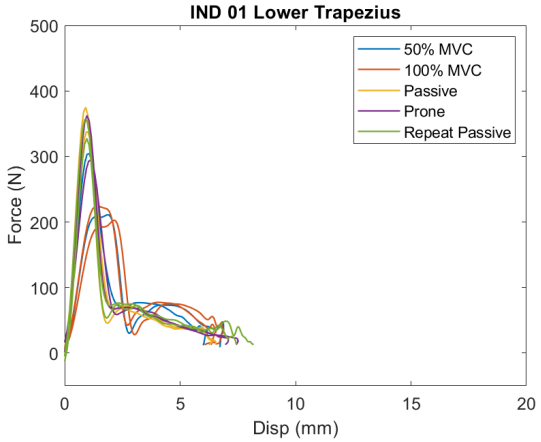
IND 01 Lower Trapezius
50% MVC
100% MVC
Passive
Prone
Repeat Passive
Force (N)
Disp (mm)

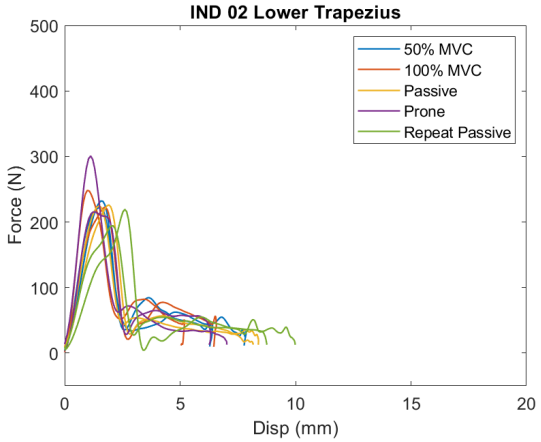
IND 02 Lower Trapezius
50% MVC
100% MVC
Passive
Prone
Repeat Passive
Force (N)
Disp (mm)

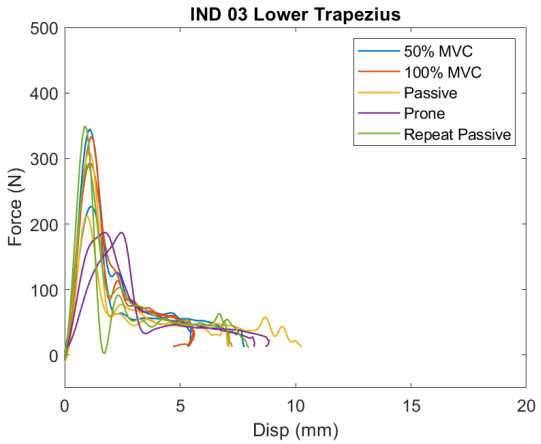
IND 03 Lower Trapezius
50% MVC
100% MVC
Passive
Prone
Repeat Passive
Force (N)
Disp (mm)

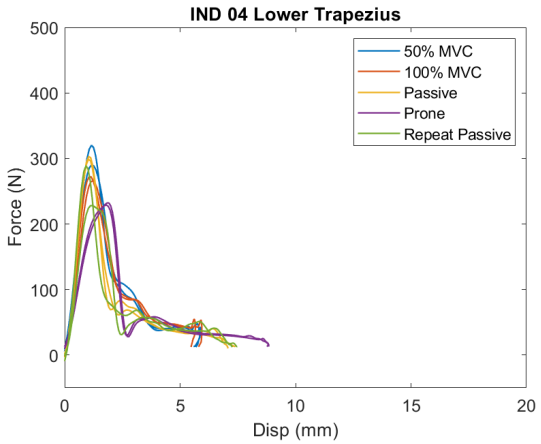
IND 04 Lower Trapezius
50% MVC
100% MVC
Passive
Prone
Repeat Passive
Force (N)
Disp (mm)

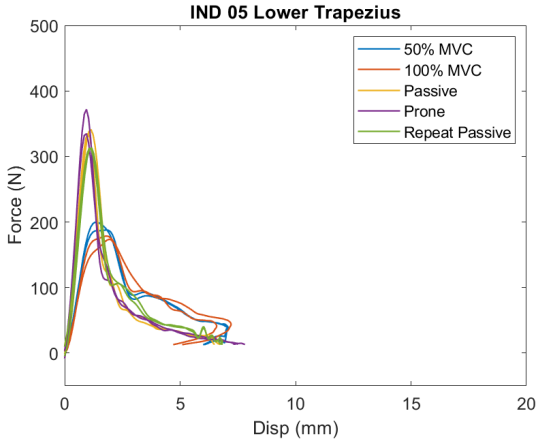
IND 05 Lower Trapezius
50% MVC
100% MVC
Passive
Prone
Repeat Passive
Force (N)
Disp (mm)

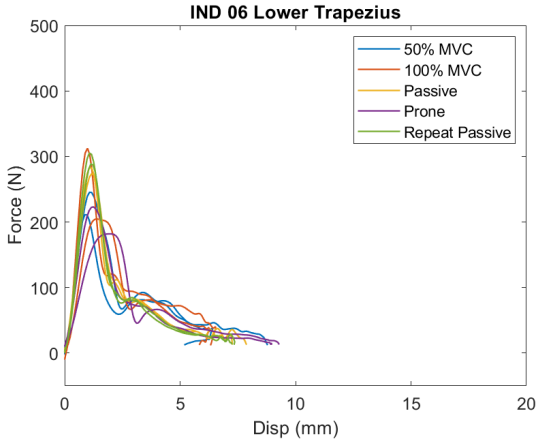
IND 06 Lower Trapezius
50% MVC
100% MVC
Passive
Prone
Repeat Passive
Force (N)
Disp (mm)

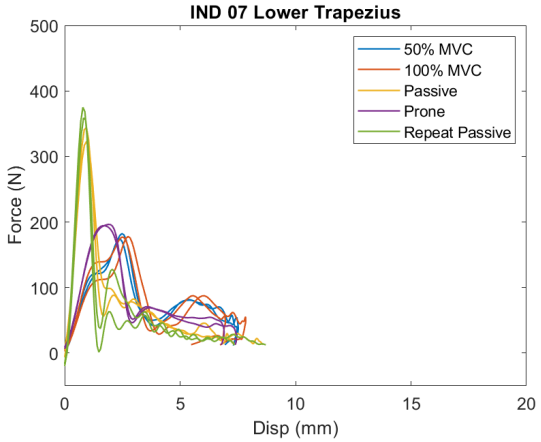
IND 07 Lower Trapezius
50% MVC
100% MVC
Passive
Prone
Repeat Passive
Force (N)
Disp (mm)

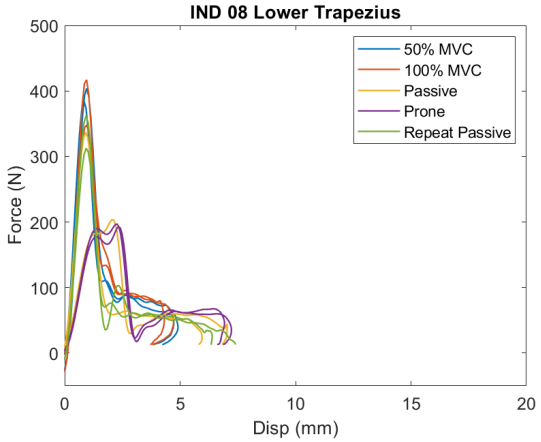
IND 08 Lower Trapezius
50% MVC
100% MVC
Passive
Prone
Repeat Passive
Force (N)
Disp (mm)

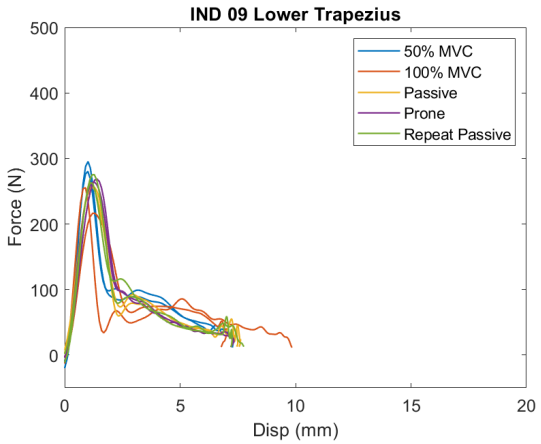
IND 09 Lower Trapezius
50% MVC
100% MVC
Passive
Prone
Repeat Passive
Force (N)
Disp (mm)

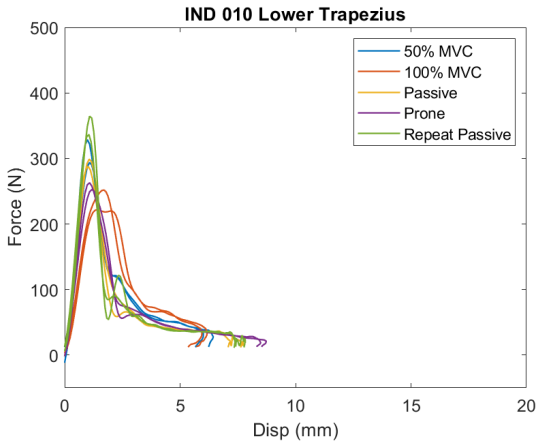
IND 010 Lower Trapezius
50% MVC
100% MVC
Passive
Prone
Repeat Passive
Force (N)
Disp (mm)

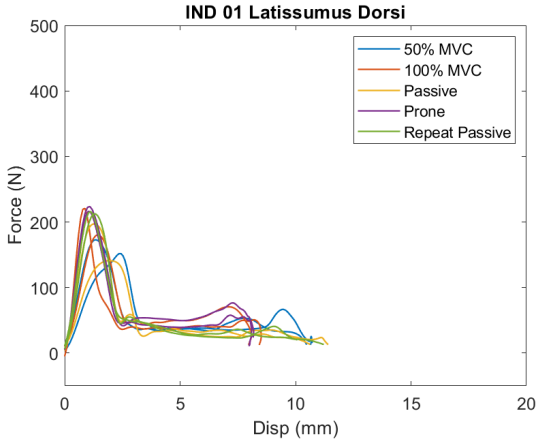
IND 01 Latissumus Dorsi
50% MVC
100% MVC
Passive
Prone
Repeat Passive
Force (N)
Disp (mm)

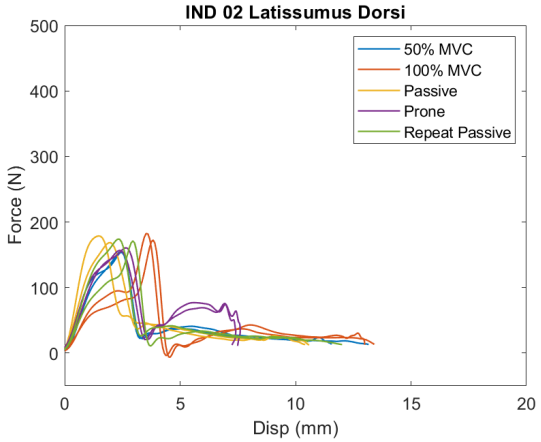
IND 02 Latissumus Dorsi
50% MVC
100% MVC
Passive
Prone
Repeat Passive
Force (N)
Disp (mm)

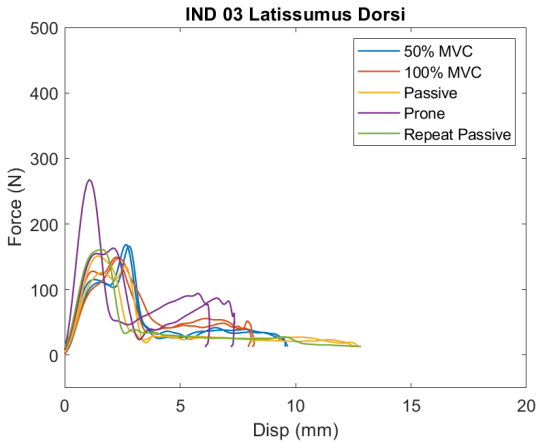
IND 03 Latissumus Dorsi
50% MVC
100% MVC
Passive
Prone
Repeat Passive
Force (N)
Disp (mm)

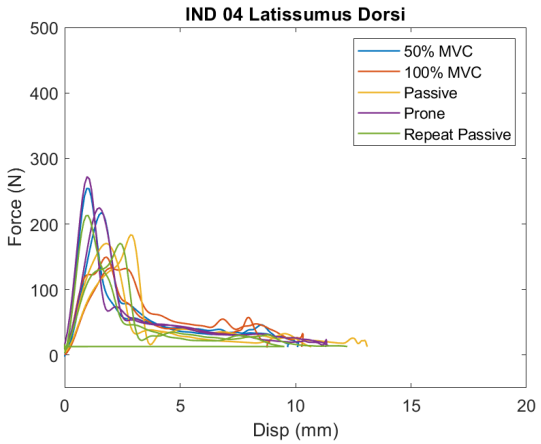
IND 04 Latissumus Dorsi
50% MVC
100% MVC
Passive
Prone
Repeat Passive
Force (N)
Disp (mm)

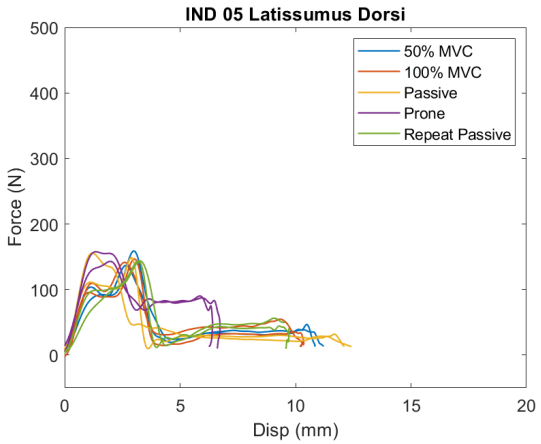
IND 05 Latissumus Dorsi
50% MVC
100% MVC
Passive
Prone
Repeat Passive
Force (N)
Disp (mm)

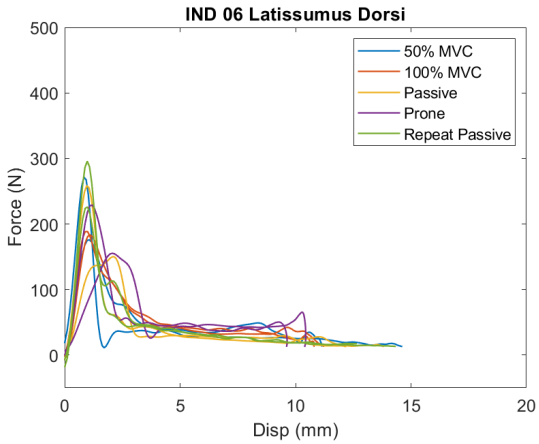
IND 06 Latissumus Dorsi
50% MVC
100% MVC
Passive
Prone
Repeat Passive
Force (N)
Disp (mm)

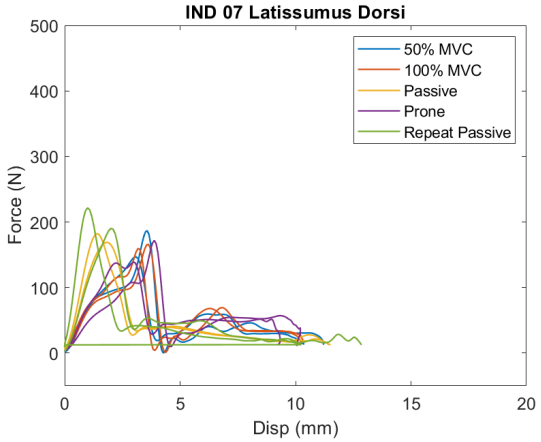
IND 07 Latissumus Dorsi
50% MVC
100% MVC
Passive
Prone
Repeat Passive
Force (N)
Disp (mm)

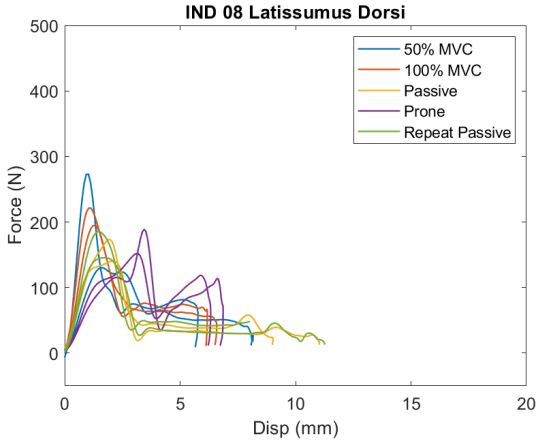
IND 08 Latissumus Dorsi
50% MVC
100% MVC
Passive
Prone
Repeat Passive
Force (N)
Disp (mm)

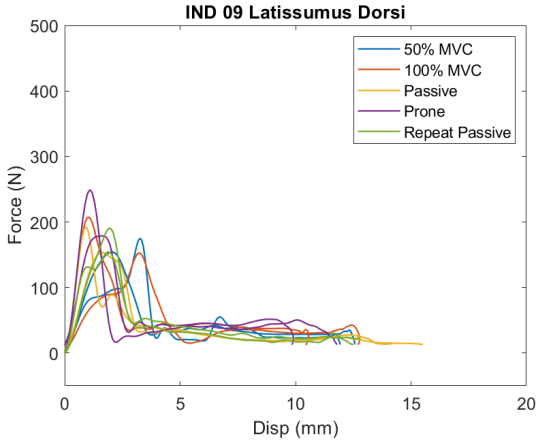
IND 09 Latissumus Dorsi
50% MVC
100% MVC
Passive
Prone
Repeat Passive
Force (N)
Disp (mm)

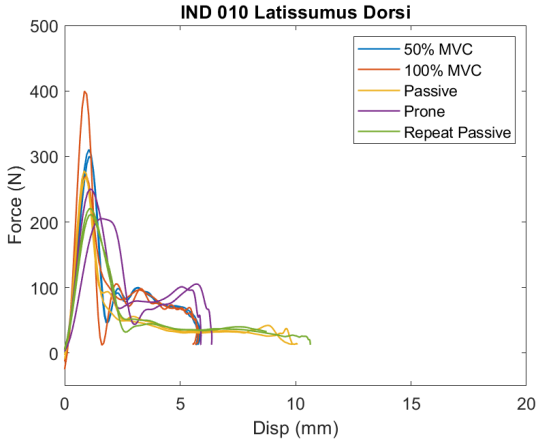
IND 010 Latissumus Dorsi
50% MVC
100% MVC
Passive
Prone
Repeat Passive
Force (N)
Disp (mm)

Appendix 16: Volunteer Force-Time Corridors

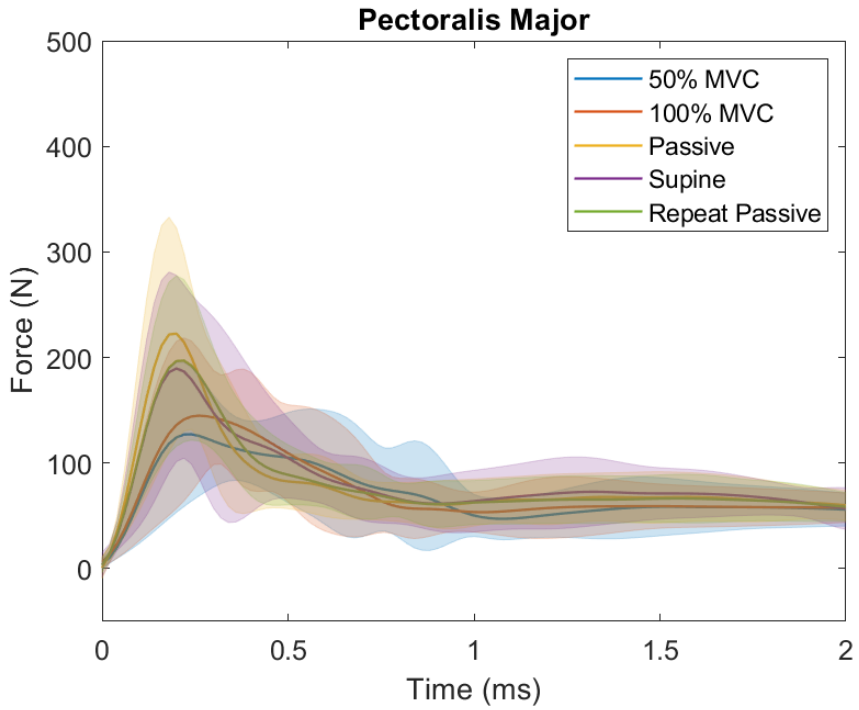

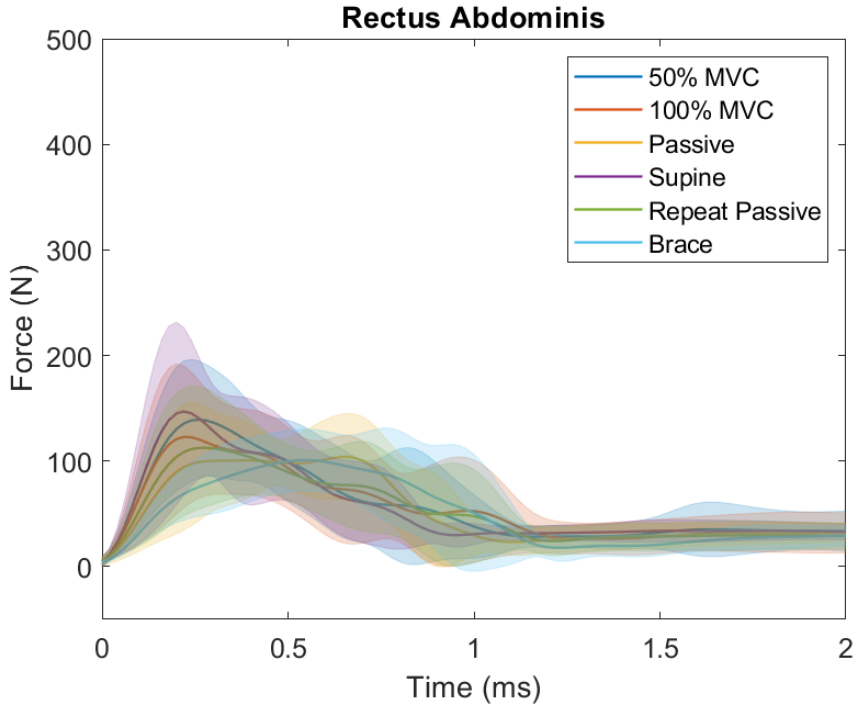

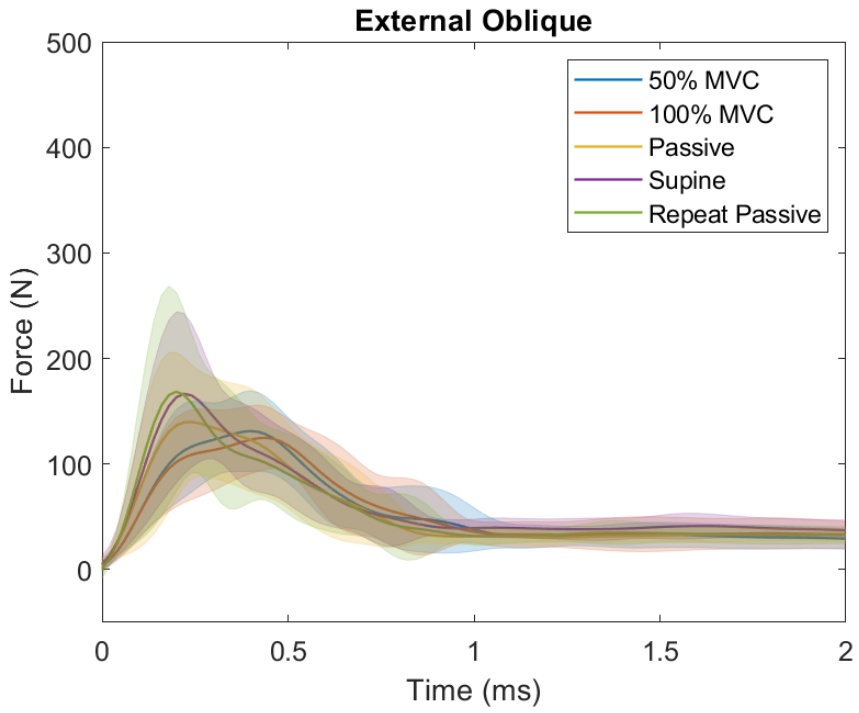
External Oblique
50% MVC
100% MVC
Passive
Supine
Repeat Passive
Force (N)
Time (ms)
0
100
200
300
400
500
0
0.5
1
1.5
2

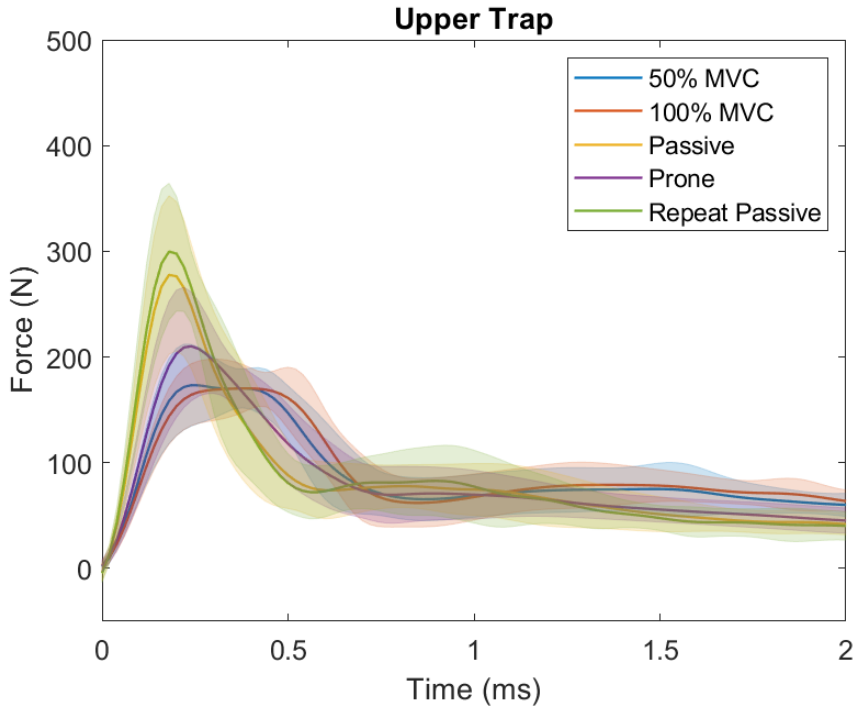
Upper Trap
50% MVC
100% MVC
Passive
Prone
Repeat Passive
Force (N)
Time (ms)
0
100
200
300
400
500
0
0.5
1
1.5
2

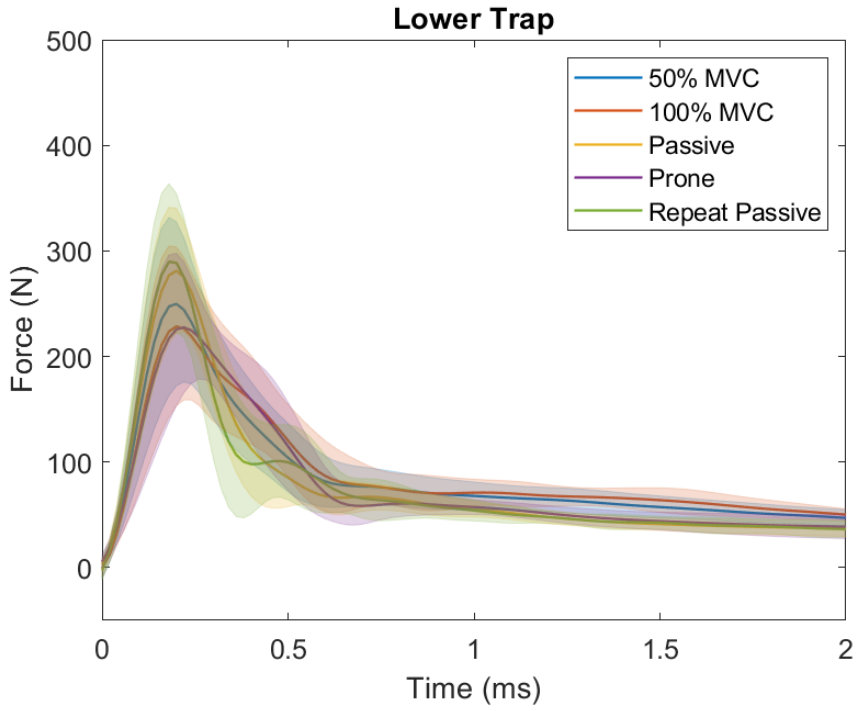
Lower Trap
50% MVC
100% MVC
Passive
Prone
Repeat Passive
Force (N)
Time (ms)
0
100
200
300
400
500
0
0.5
1
1.5
2

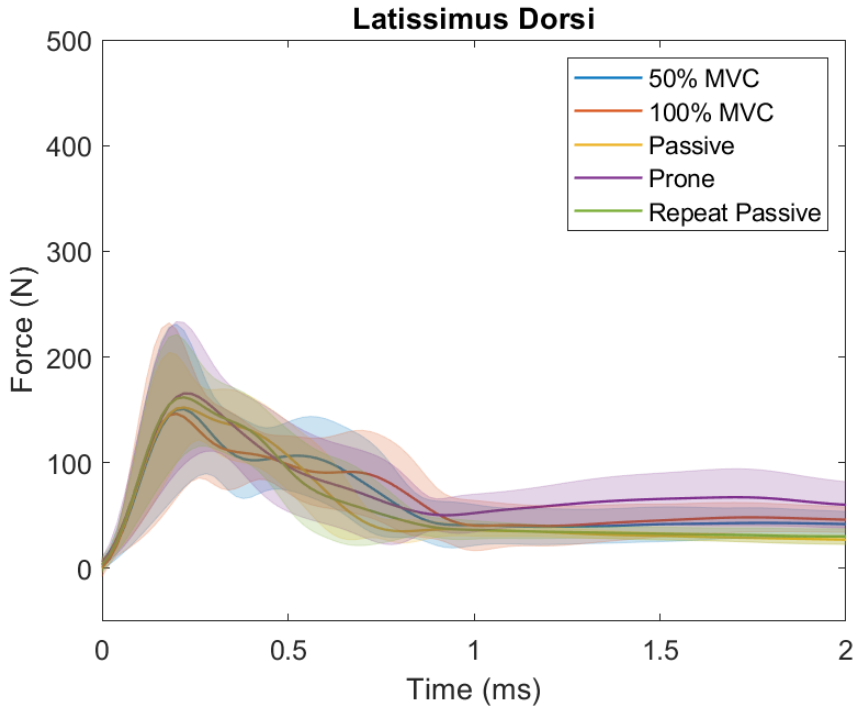
Latissimus Dorsi
50% MVC
100% MVC
Passive
Prone
Repeat Passive
Force (N)
Time (ms)
0
100
200
300
400
500
0
0.5
1
1.5
2

Appendix 17: Volunteer Force-Displacement Average Curves

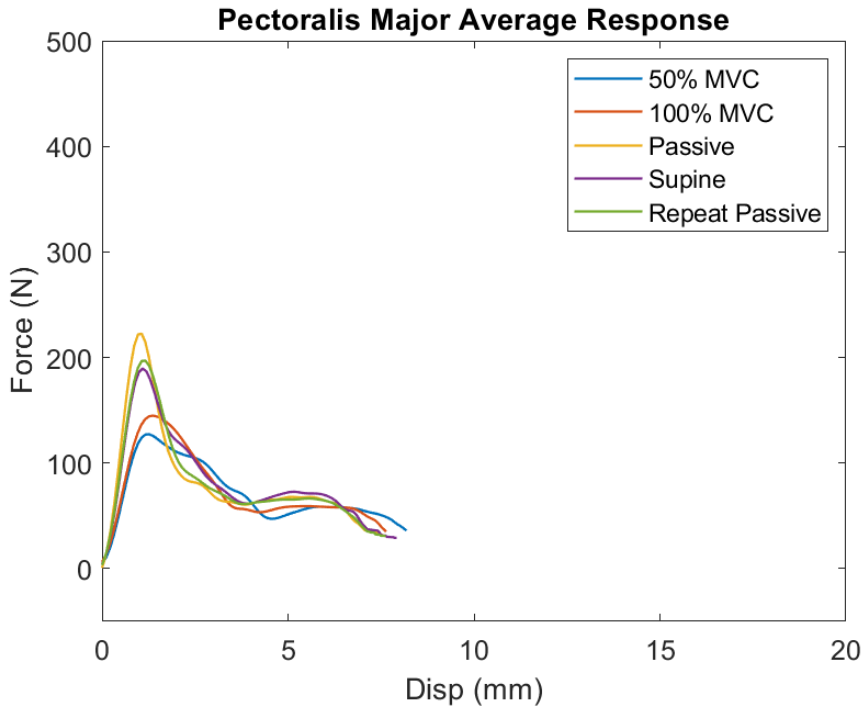

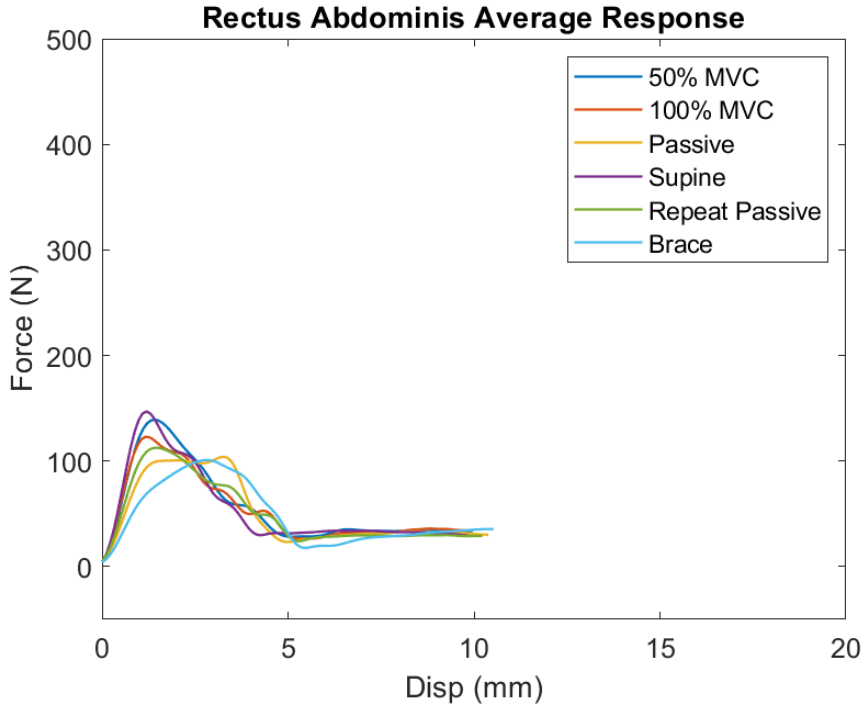

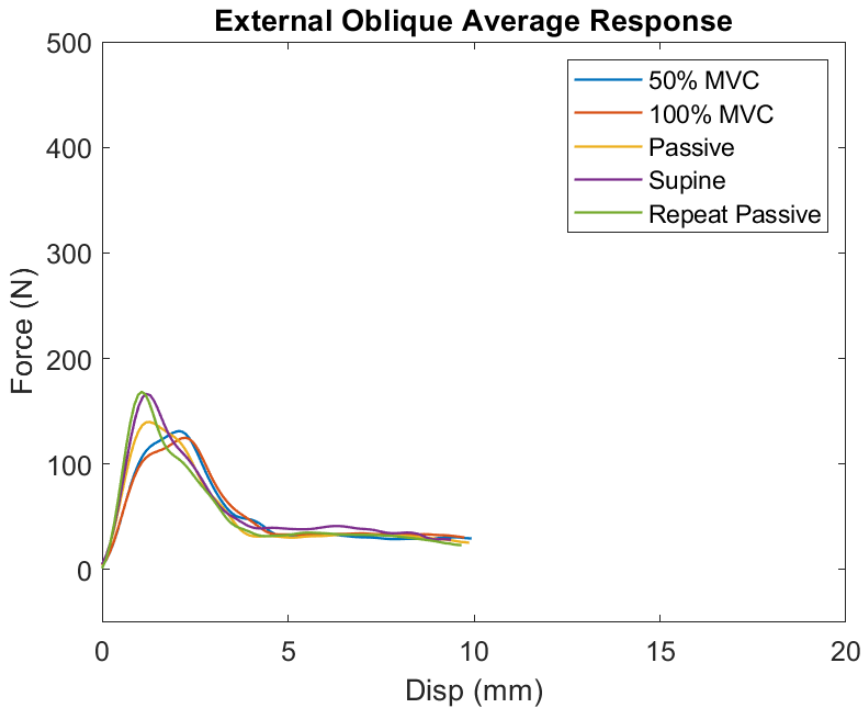
External Oblique Average Response
50% MVC
100% MVC
Passive
Supine
Repeat Passive
Force (N)
Disp (mm)
0
100
200
300
400
500
0
5
10
15
20

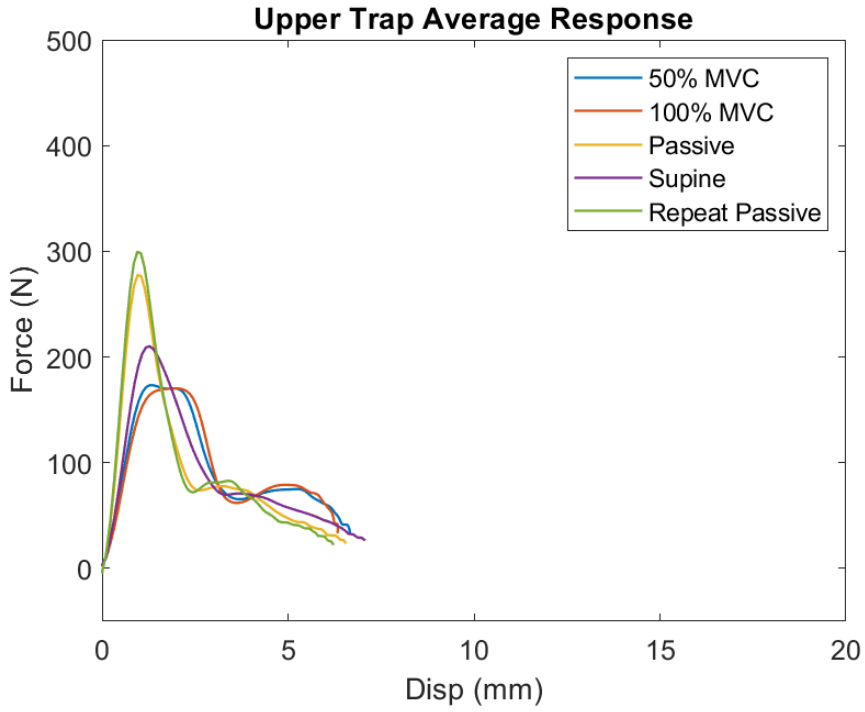
Upper Trap Average Response
50% MVC
100% MVC
Passive
Supine
Repeat Passive
Force (N)
Disp (mm)
0
100
200
300
400
500
0
5
10
15
20

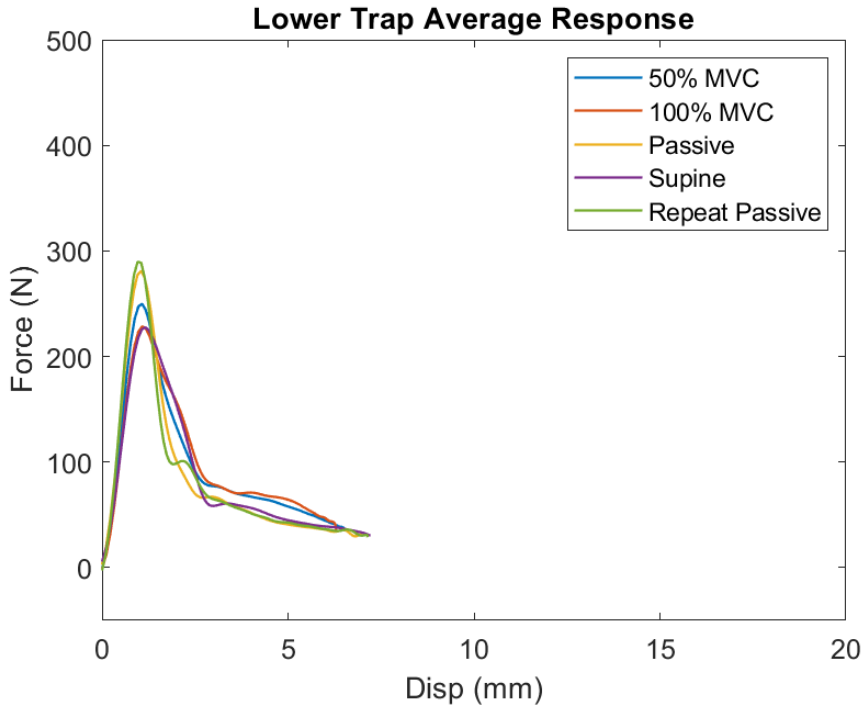
Lower Trap Average Response
50% MVC
100% MVC
Passive
Supine
Repeat Passive
Force (N)
Disp (mm)
0
100
200
300
400
500
0
5
10
15
20

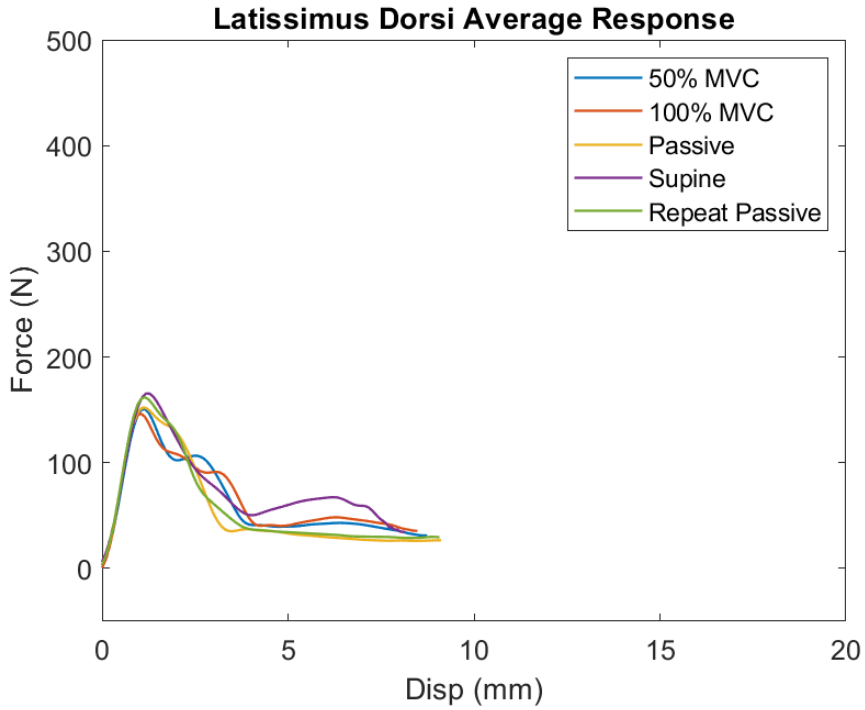
Latissimus Dorsi Average Response
50% MVC
100% MVC
Passive
Supine
Repeat Passive
Force (N)
Disp (mm)
0
100
200
300
400
500
0
5
10
15
20

Appendix 18: PMHS Force-Time and Force-Displacement Curves

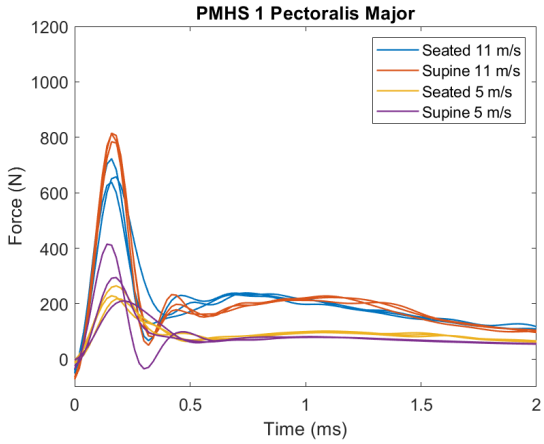

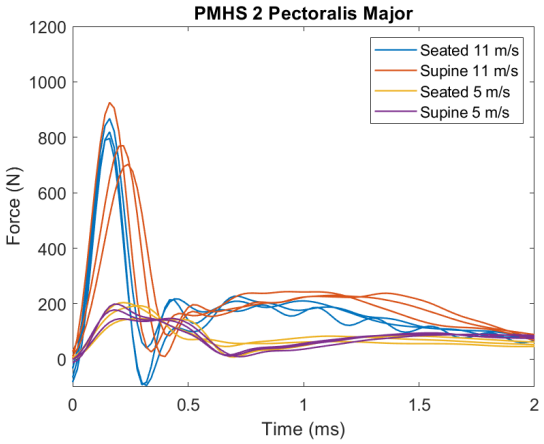

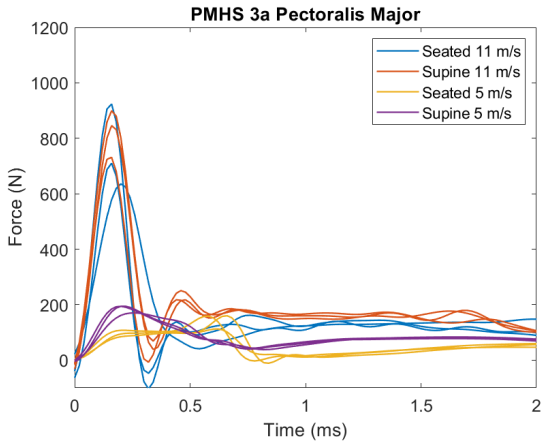

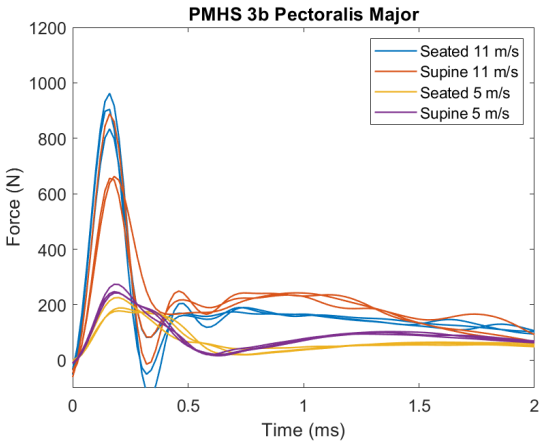

5

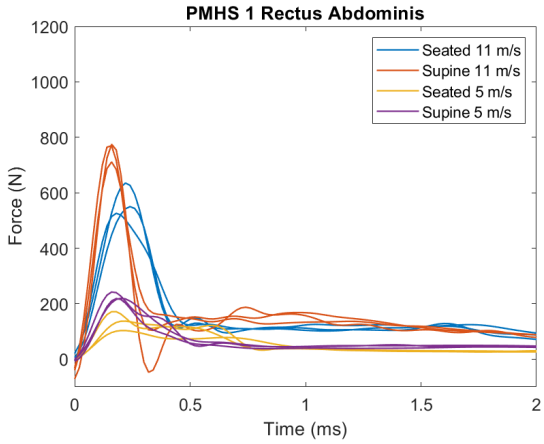

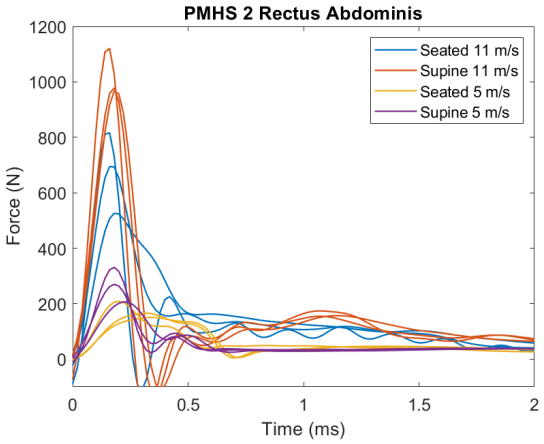

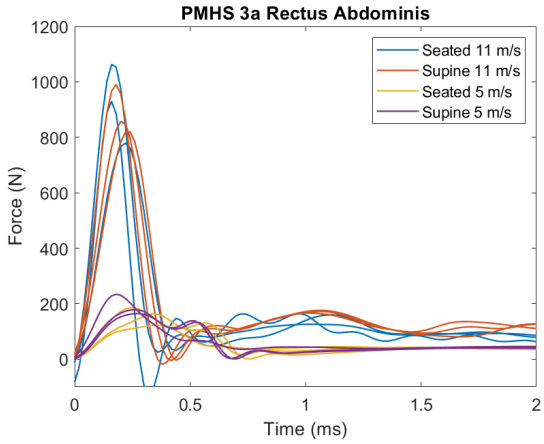
PMHS 3a Rectus Abdominis
Seated 11 m/s
Supine 11 m/s
Seated 5 m/s
Supine 5 m/s
Force (N)
Time (ms)

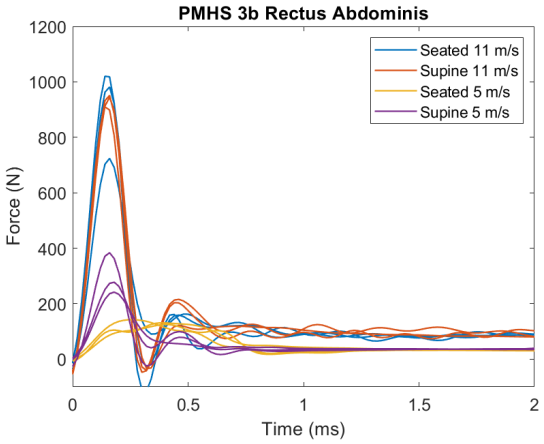
PMHS 3b Rectus Abdominis
Seated 11 m/s
Supine 11 m/s
Seated 5 m/s
Supine 5 m/s
Force (N)
Time (ms)

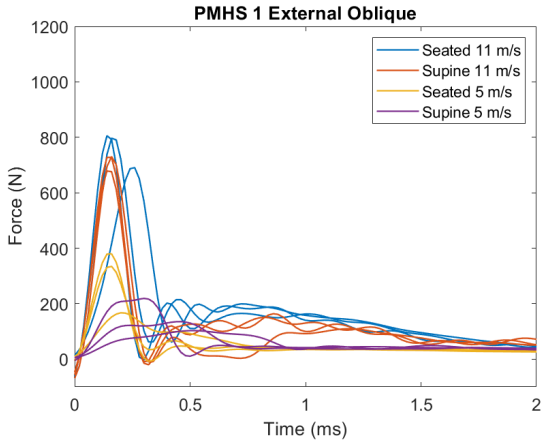
PMHS 1 External Oblique
Seated 11 m/s
Supine 11 m/s
Seated 5 m/s
Supine 5 m/s
Force (N)
Time (ms)

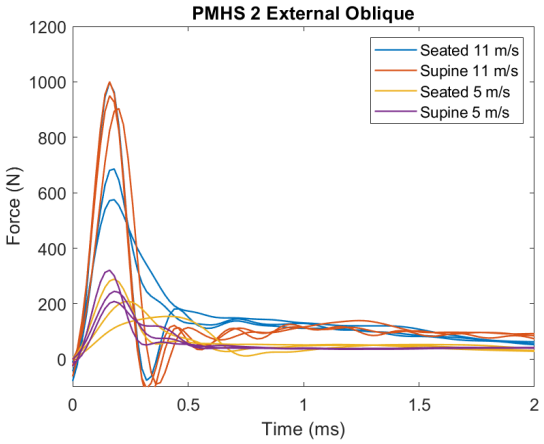
PMHS 2 External Oblique
Seated 11 m/s
Supine 11 m/s
Seated 5 m/s
Supine 5 m/s
Force (N)
Time (ms)

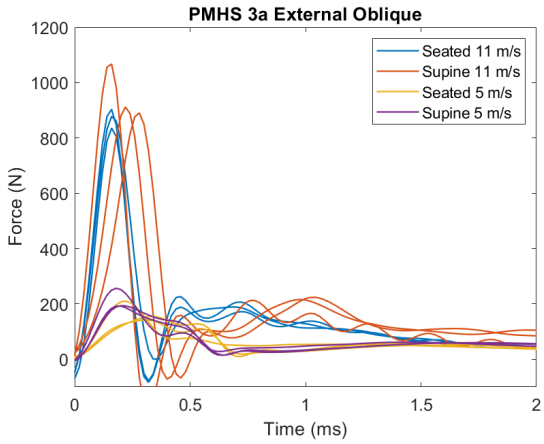
PMHS 3a External Oblique
Seated 11 m/s
Supine 11 m/s
Seated 5 m/s
Supine 5 m/s
Force (N)
Time (ms)

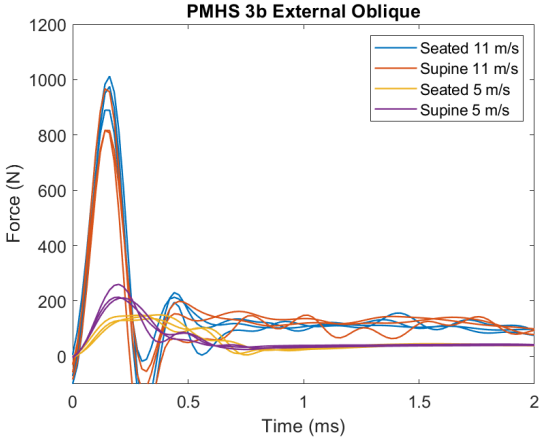
PMHS 3b External Oblique
Seated 11 m/s
Supine 11 m/s
Seated 5 m/s
Supine 5 m/s
Force (N)
Time (ms)

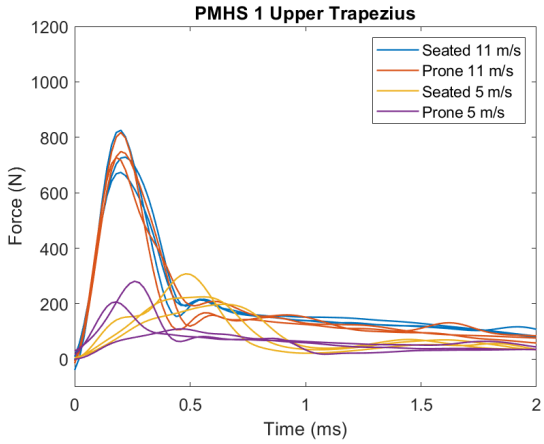
PMHS 1 Upper Trapezius
Seated 11 m/s
Prone 11 m/s
Seated 5 m/s
Prone 5 m/s
Force (N)
Time (ms)

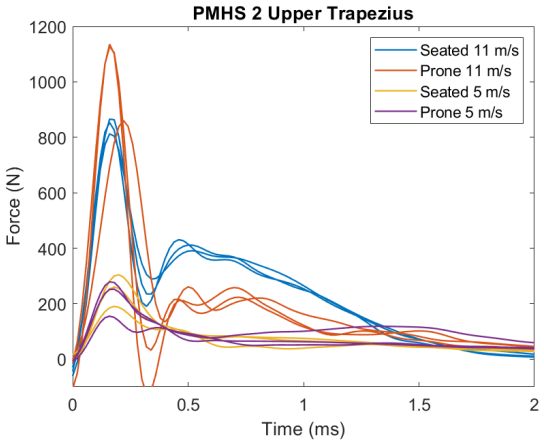
PMHS 2 Upper Trapezius
Seated 11 m/s
Prone 11 m/s
Seated 5 m/s
Prone 5 m/s
Force (N)
Time (ms)

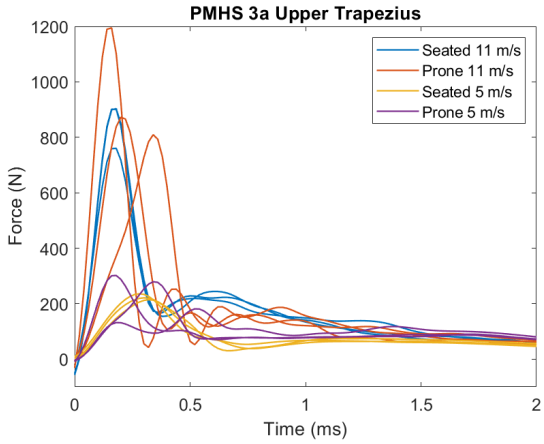
PMHS 3a Upper Trapezius
Seated 11 m/s
Prone 11 m/s
Seated 5 m/s
Prone 5 m/s
Force (N)
Time (ms)

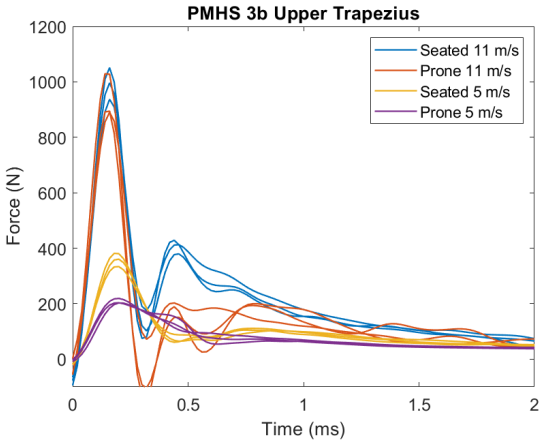
PMHS 3b Upper Trapezius
Seated 11 m/s
Prone 11 m/s
Seated 5 m/s
Prone 5 m/s
Force (N)
Time (ms)

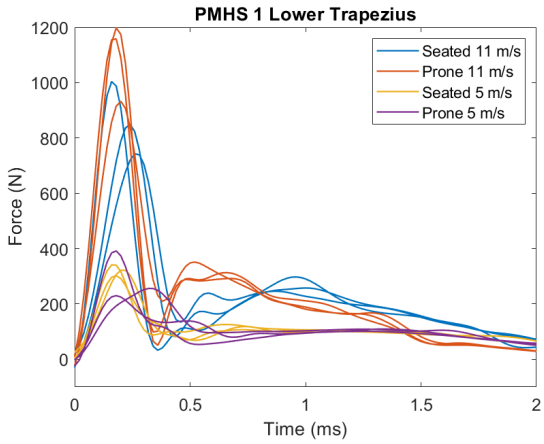
PMHS 1 Lower Trapezius
Seated 11 m/s
Prone 11 m/s
Seated 5 m/s
Prone 5 m/s
Force (N)
Time (ms)

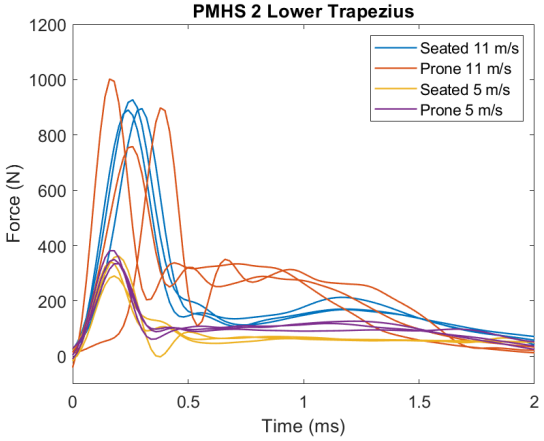
PMHS 2 Lower Trapezius
Seated 11 m/s
Prone 11 m/s
Seated 5 m/s
Prone 5 m/s
Force (N)
Time (ms)

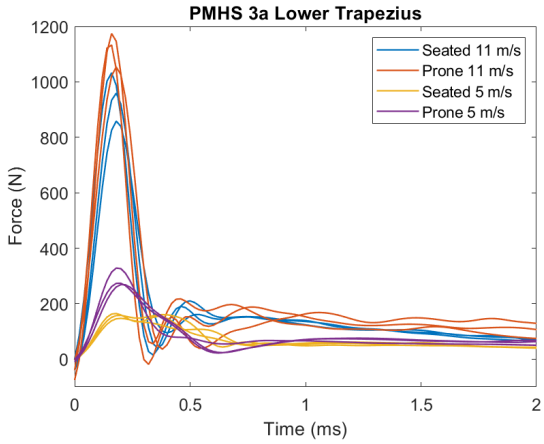
PMHS 3a Lower Trapezius
Seated 11 m/s
Prone 11 m/s
Seated 5 m/s
Prone 5 m/s
Force (N)
Time (ms)

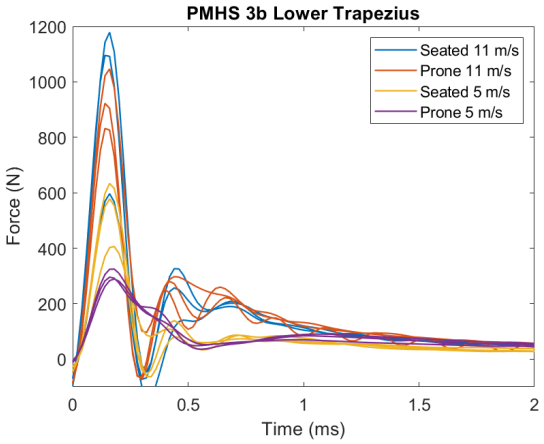
PMHS 3b Lower Trapezius
Seated 11 m/s
Prone 11 m/s
Seated 5 m/s
Prone 5 m/s
Force (N)
Time (ms)

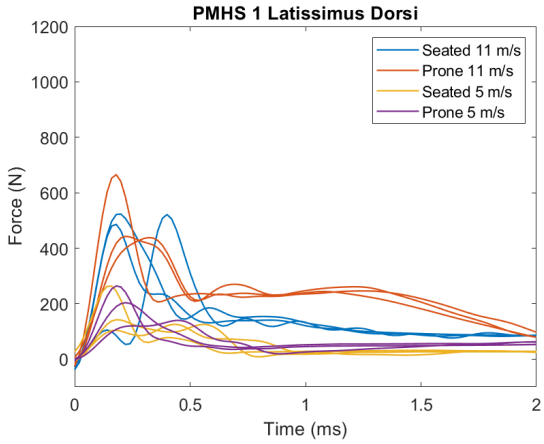
PMHS 1 Latissimus Dorsi
Seated 11 m/s
Prone 11 m/s
Seated 5 m/s
Prone 5 m/s
Force (N)
Time (ms)

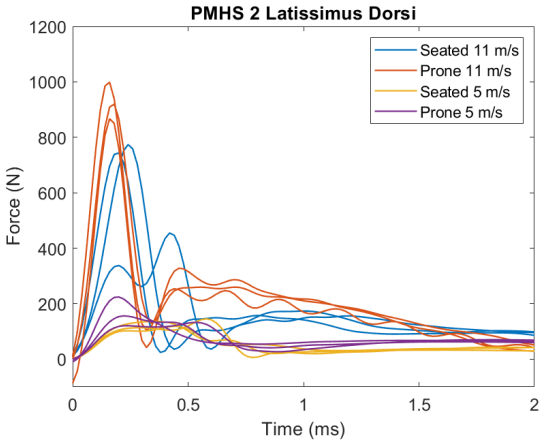
PMHS 2 Latissimus Dorsi
Seated 11 m/s
Prone 11 m/s
Seated 5 m/s
Prone 5 m/s
Force (N)
Time (ms)

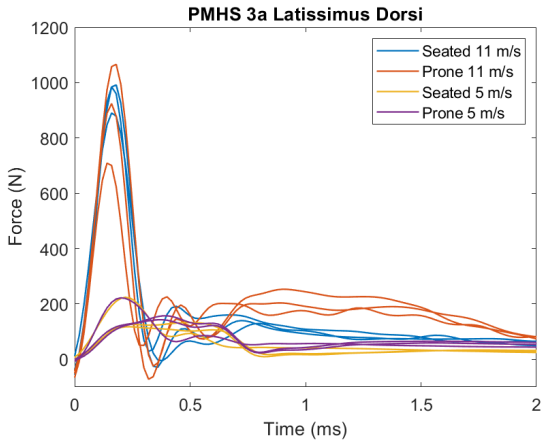
PMHS 3a Latissimus Dorsi
Seated 11 m/s
Prone 11 m/s
Seated 5 m/s
Prone 5 m/s
Force (N)
Time (ms)

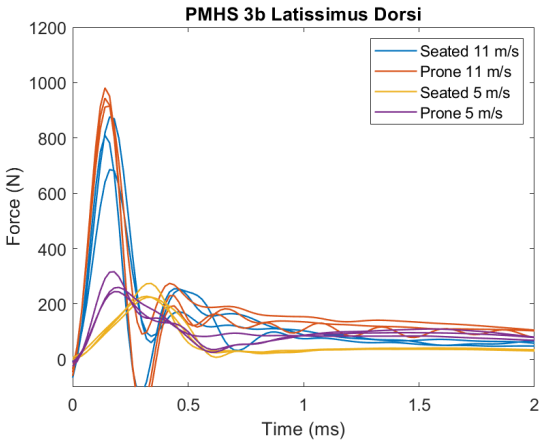
PMHS 3b Latissimus Dorsi
Seated 11 m/s
Prone 11 m/s
Seated 5 m/s
Prone 5 m/s
Force (N)
Time (ms)

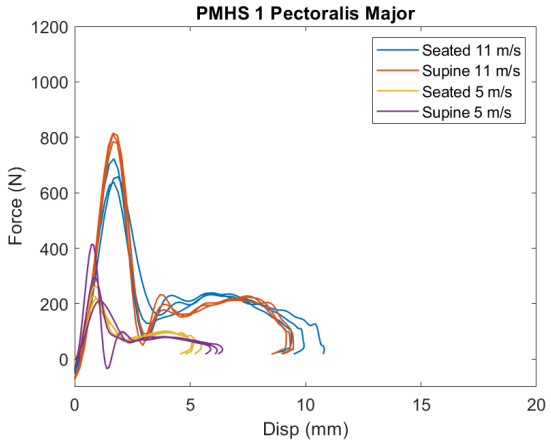
PMHS 1 Pectoralis Major
Seated 11 m/s
Supine 11 m/s
Seated 5 m/s
Supine 5 m/s
Force (N)
Disp (mm)

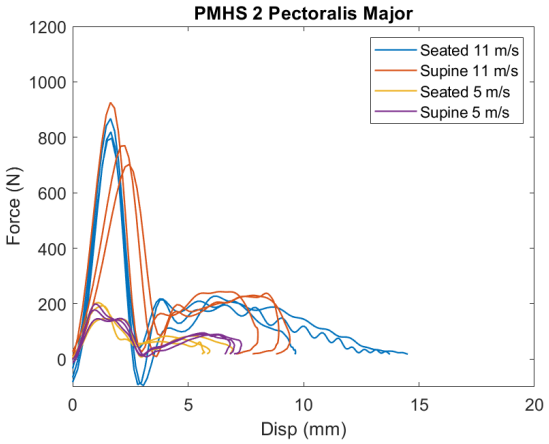
PMHS 2 Pectoralis Major
Seated 11 m/s
Supine 11 m/s
Seated 5 m/s
Supine 5 m/s
Force (N)
Disp (mm)

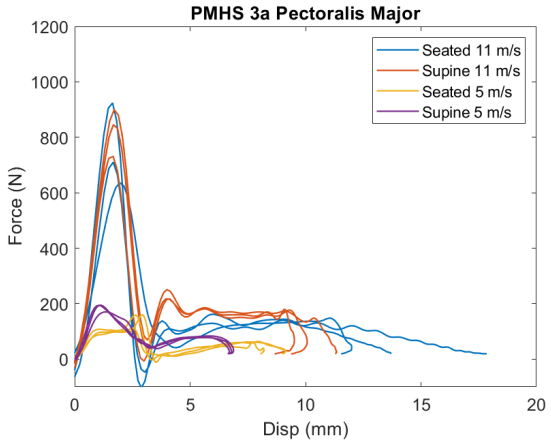
PMHS 3a Pectoralis Major
Seated 11 m/s
Supine 11 m/s
Seated 5 m/s
Supine 5 m/s
Force (N)
Disp (mm)

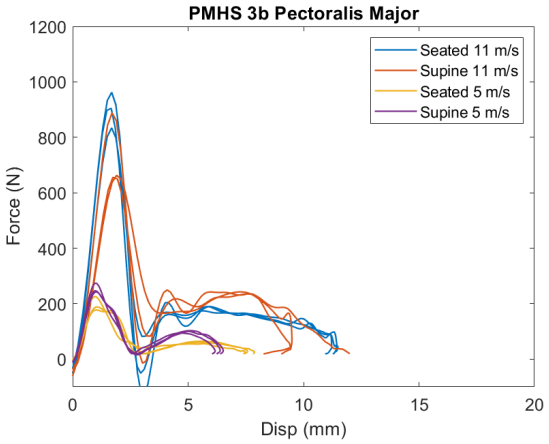
PMHS 3b Pectoralis Major
Seated 11 m/s
Supine 11 m/s
Seated 5 m/s
Supine 5 m/s
Force (N)
Disp (mm)

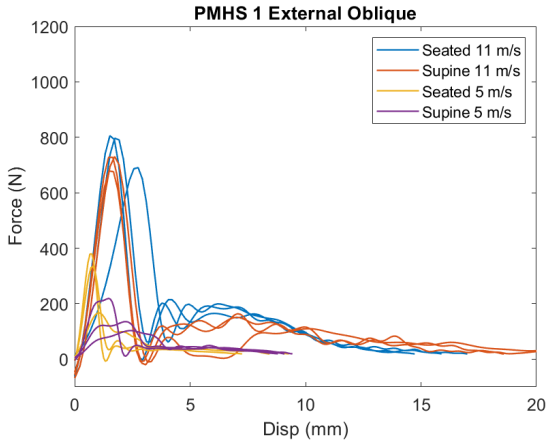
PMHS 1 External Oblique
Seated 11 m/s
Supine 11 m/s
Seated 5 m/s
Supine 5 m/s
Force (N)
Disp (mm)

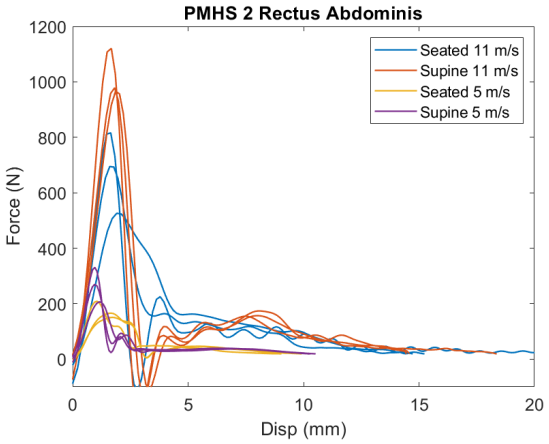
PMHS 2 Rectus Abdominis
Seated 11 m/s
Supine 11 m/s
Seated 5 m/s
Supine 5 m/s
Force (N)
Disp (mm)

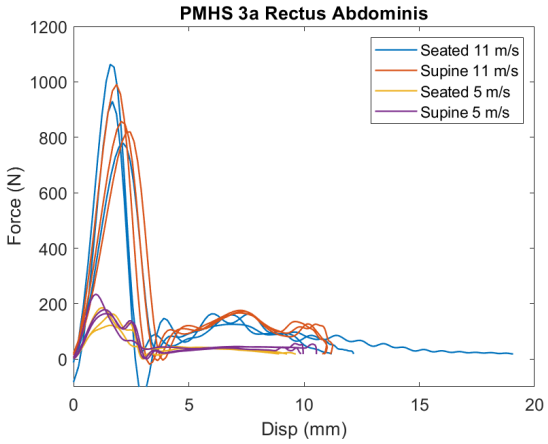
PMHS 3a Rectus Abdominis
Seated 11 m/s
Supine 11 m/s
Seated 5 m/s
Supine 5 m/s
Force (N)
Disp (mm)

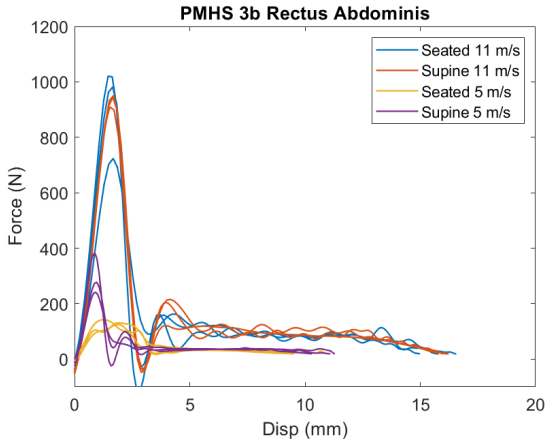
PMHS 3b Rectus Abdominis
Seated 11 m/s
Supine 11 m/s
Seated 5 m/s
Supine 5 m/s
Force (N)
Disp (mm)

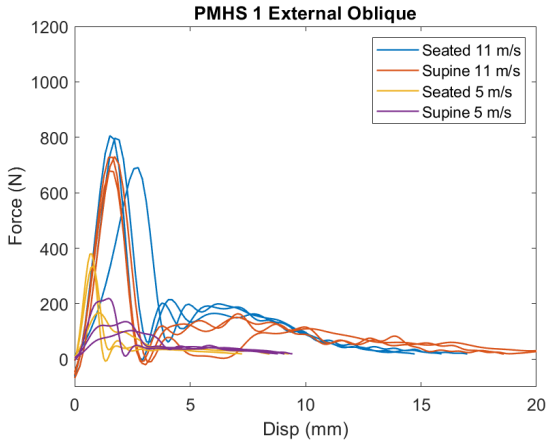
PMHS 1 External Oblique
Seated 11 m/s
Supine 11 m/s
Seated 5 m/s
Supine 5 m/s
Force (N)
Disp (mm)

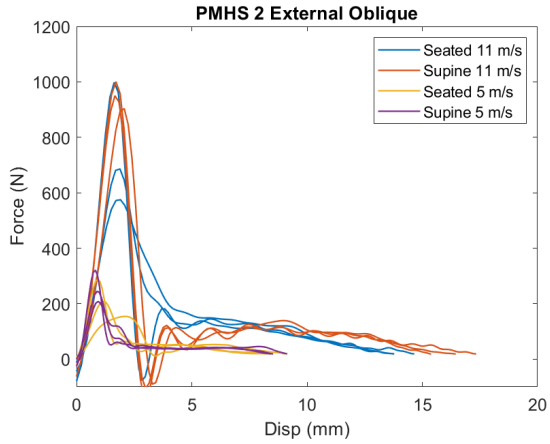
PMHS 2 External Oblique
Seated 11 m/s
Supine 11 m/s
Seated 5 m/s
Supine 5 m/s
Force (N)
Disp (mm)

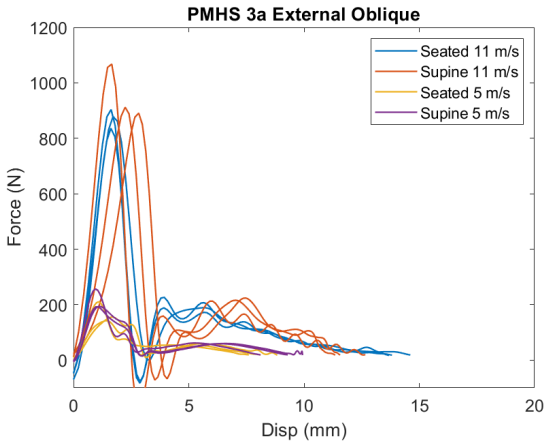
PMHS 3a External Oblique
Seated 11 m/s
Supine 11 m/s
Seated 5 m/s
Supine 5 m/s
Force (N)
Disp (mm)

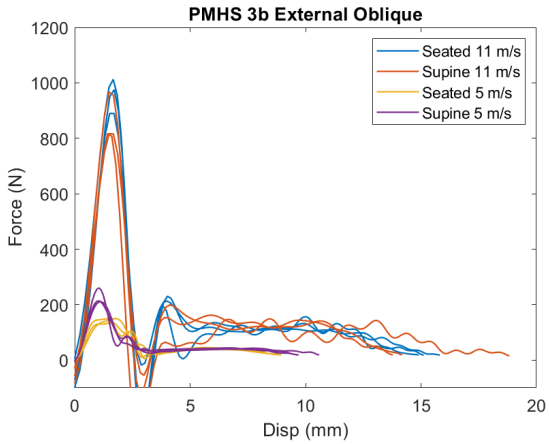
PMHS 3b External Oblique
Seated 11 m/s
Supine 11 m/s
Seated 5 m/s
Supine 5 m/s
Force (N)
Disp (mm)

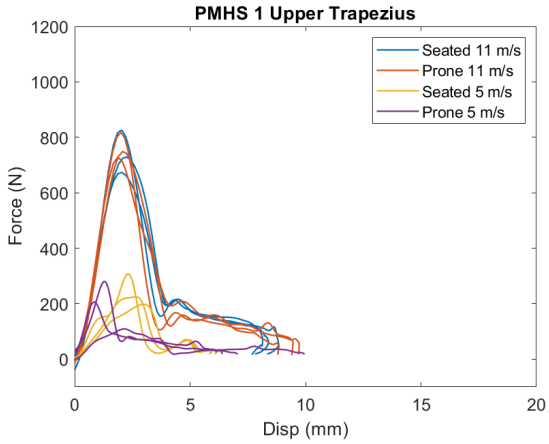
PMHS 1 Upper Trapezius
Seated 11 m/s
Prone 11 m/s
Seated 5 m/s
Prone 5 m/s
Force (N)
Disp (mm)

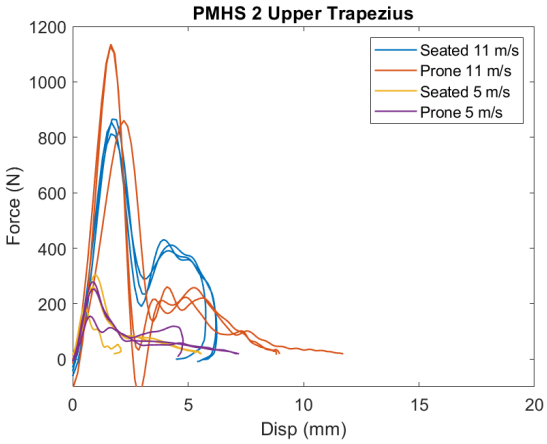
PMHS 2 Upper Trapezius
Seated 11 m/s
Prone 11 m/s
Seated 5 m/s
Prone 5 m/s
Force (N)
Disp (mm)

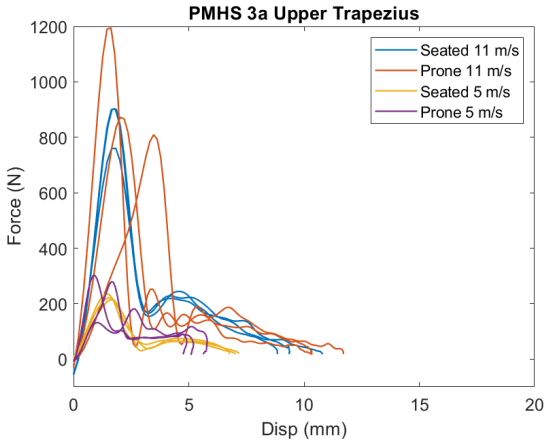
PMHS 3a Upper Trapezius
Seated 11 m/s
Prone 11 m/s
Seated 5 m/s
Prone 5 m/s
Force (N)
Disp (mm)

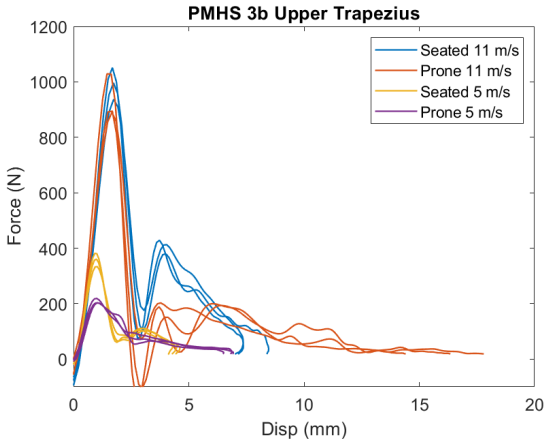
PMHS 3b Upper Trapezius
Seated 11 m/s
Prone 11 m/s
Seated 5 m/s
Prone 5 m/s
Force (N)
Disp (mm)

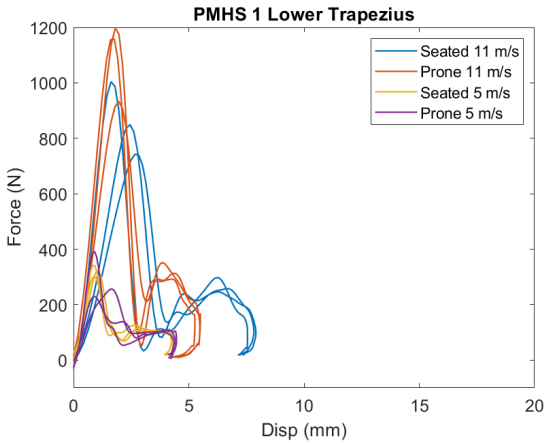
PMHS 1 Lower Trapezius
Seated 11 m/s
Prone 11 m/s
Seated 5 m/s
Prone 5 m/s
Force (N)
Disp (mm)

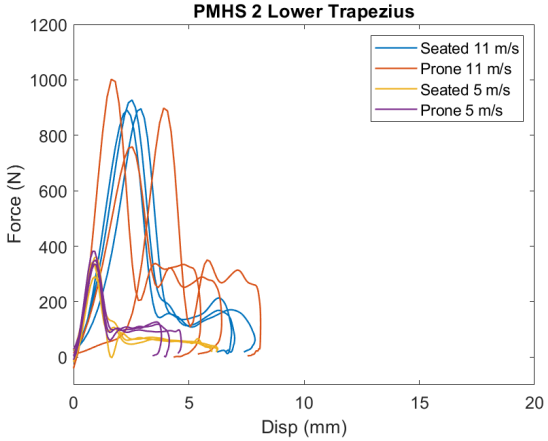
PMHS 2 Lower Trapezius
Seated 11 m/s
Prone 11 m/s
Seated 5 m/s
Prone 5 m/s
Force (N)
Disp (mm)

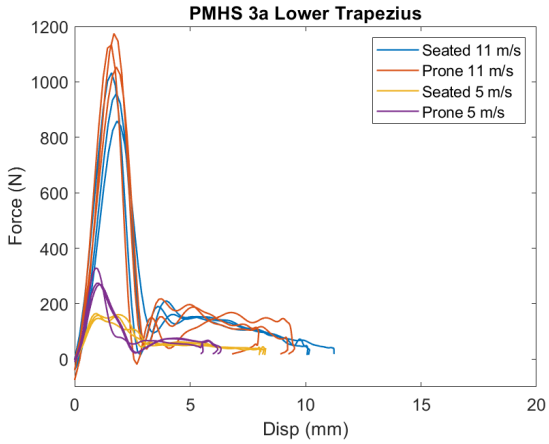
PMHS 3a Lower Trapezius
Seated 11 m/s
Prone 11 m/s
Seated 5 m/s
Prone 5 m/s
Force (N)
Disp (mm)

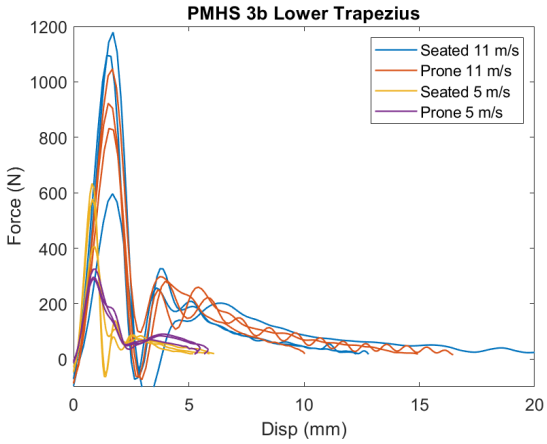
PMHS 3b Lower Trapezius
Seated 11 m/s
Prone 11 m/s
Seated 5 m/s
Prone 5 m/s
Force (N)
Disp (mm)

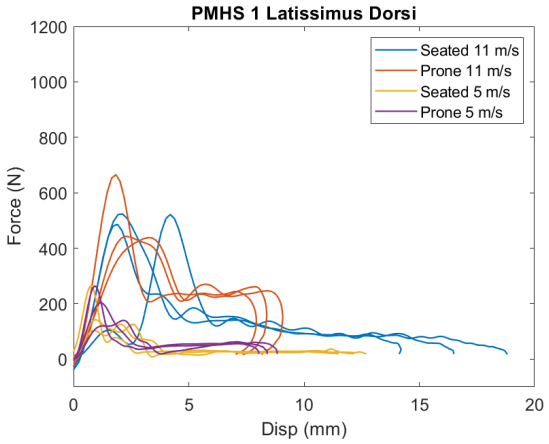
PMHS 1 Latissimus Dorsi
Seated 11 m/s
Prone 11 m/s
Seated 5 m/s
Prone 5 m/s
Force (N)
Disp (mm)

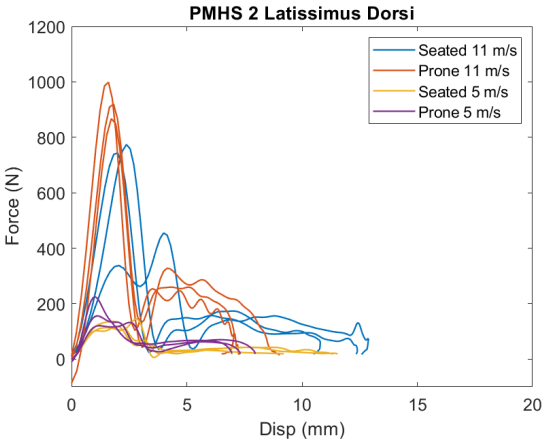
PMHS 2 Latissimus Dorsi
Seated 11 m/s
Prone 11 m/s
Seated 5 m/s
Prone 5 m/s
Force (N)
Disp (mm)

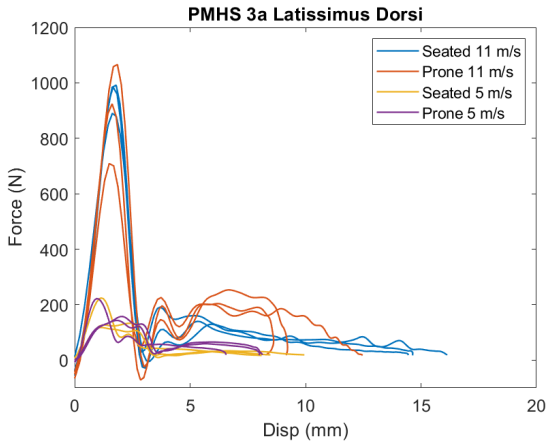
PMHS 3a Latissimus Dorsi
Seated 11 m/s
Prone 11 m/s
Seated 5 m/s
Prone 5 m/s
Force (N)
Disp (mm)

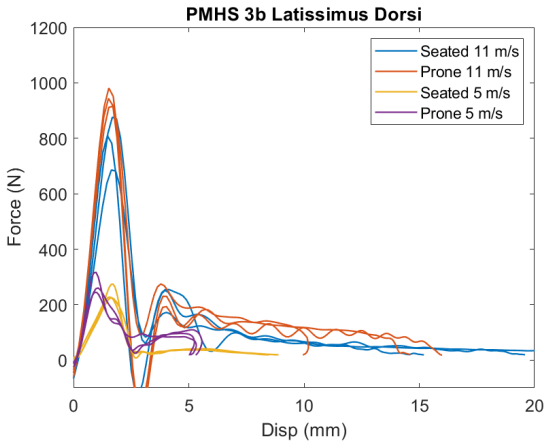
PMHS 3b Latissimus Dorsi
Seated 11 m/s
Prone 11 m/s
Seated 5 m/s
Prone 5 m/s
Force (N)
Disp (mm)

Appendix 19: PMHS Force-Time Corridors

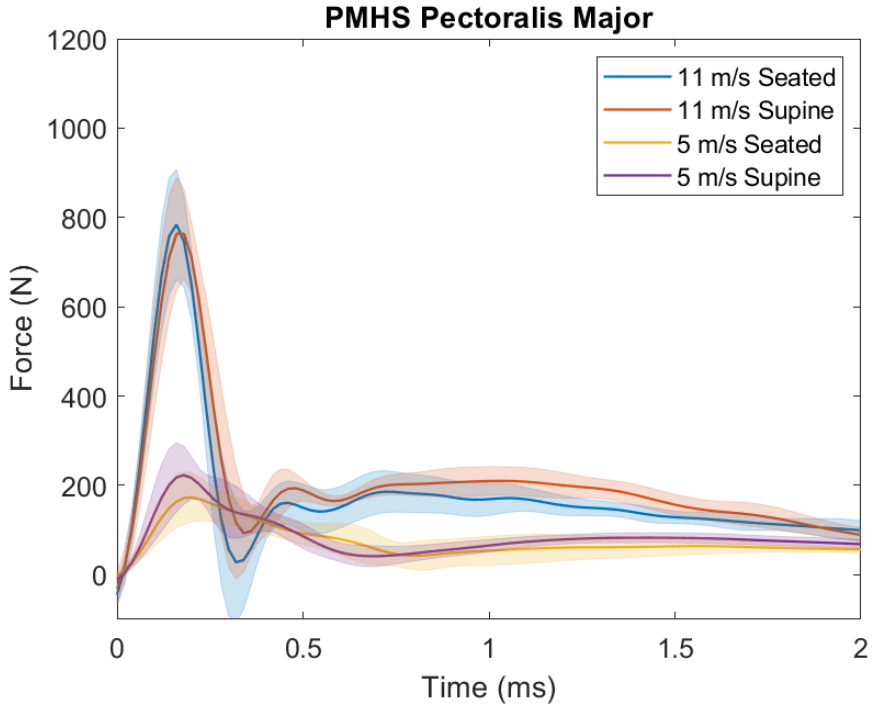

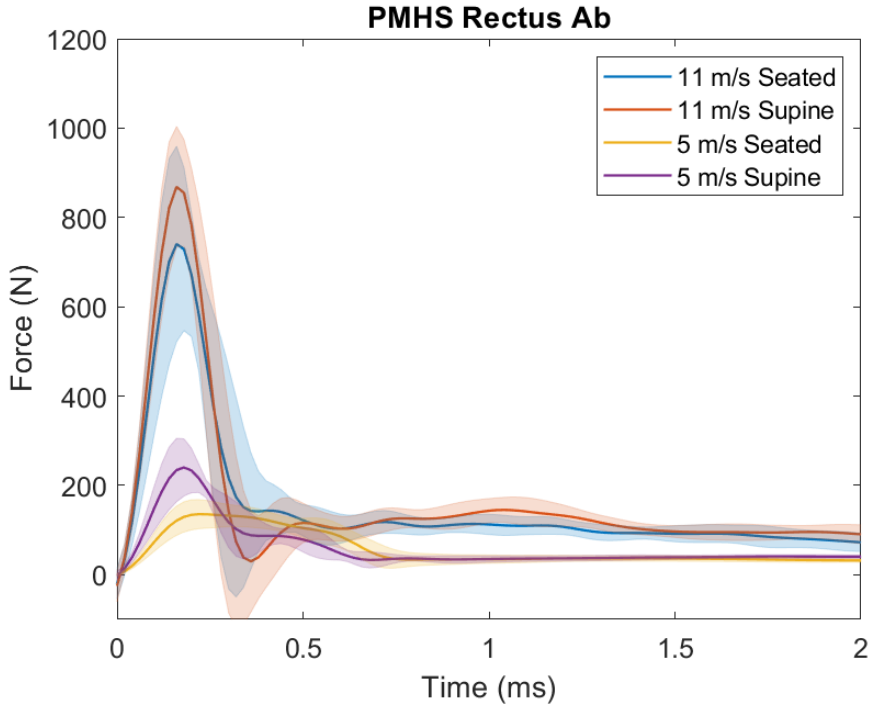

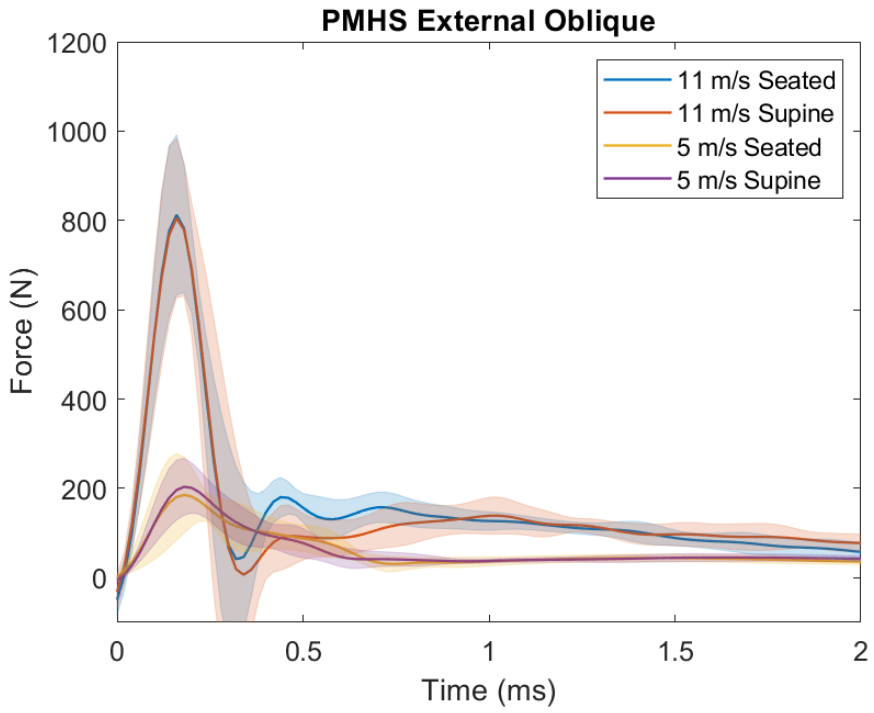
PMHS External Oblique
11 m/s Seated
11 m/s Supine
5 m/s Seated
5 m/s Supine
Force (N)
Time (ms)
0
200
400
600
800
1000
1200
0
0.5
1
1.5
2

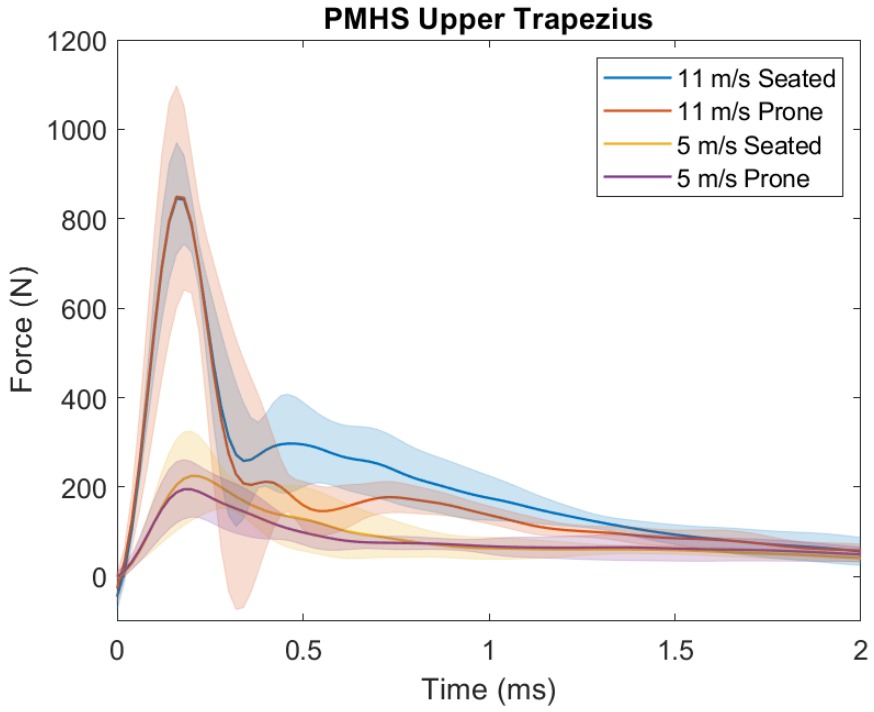
PMHS Upper Trapezius
11 m/s Seated
11 m/s Prone
5 m/s Seated
5 m/s Prone
Force (N)
Time (ms)
0
200
400
600
800
1000
1200
0
0.5
1
1.5
2

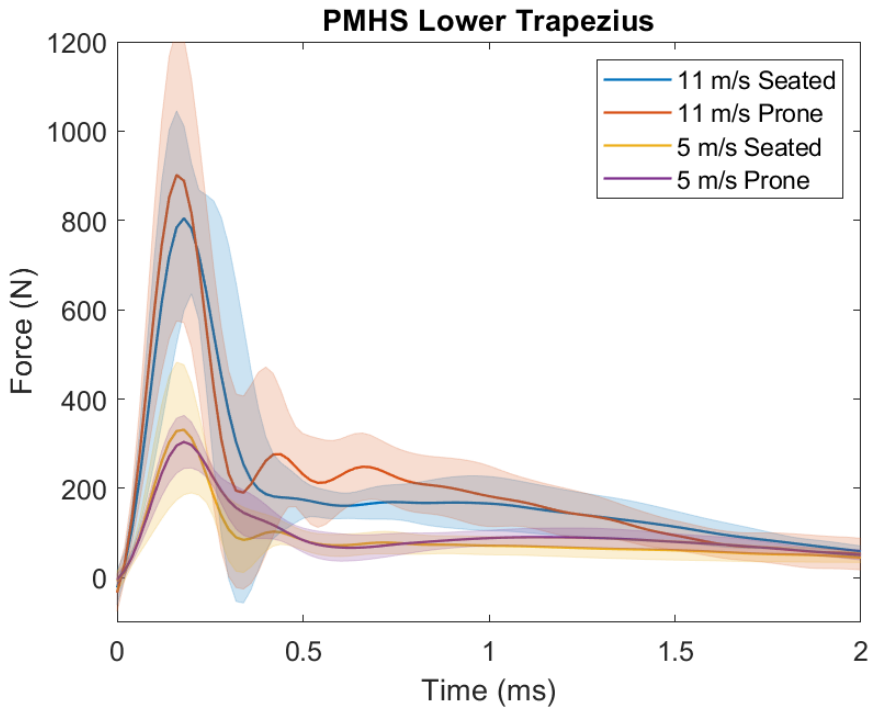
PMHS Lower Trapezius
11 m/s Seated
11 m/s Prone
5 m/s Seated
5 m/s Prone
Force (N)
Time (ms)
0
200
400
600
800
1000
1200
0
0.5
1
1.5
2

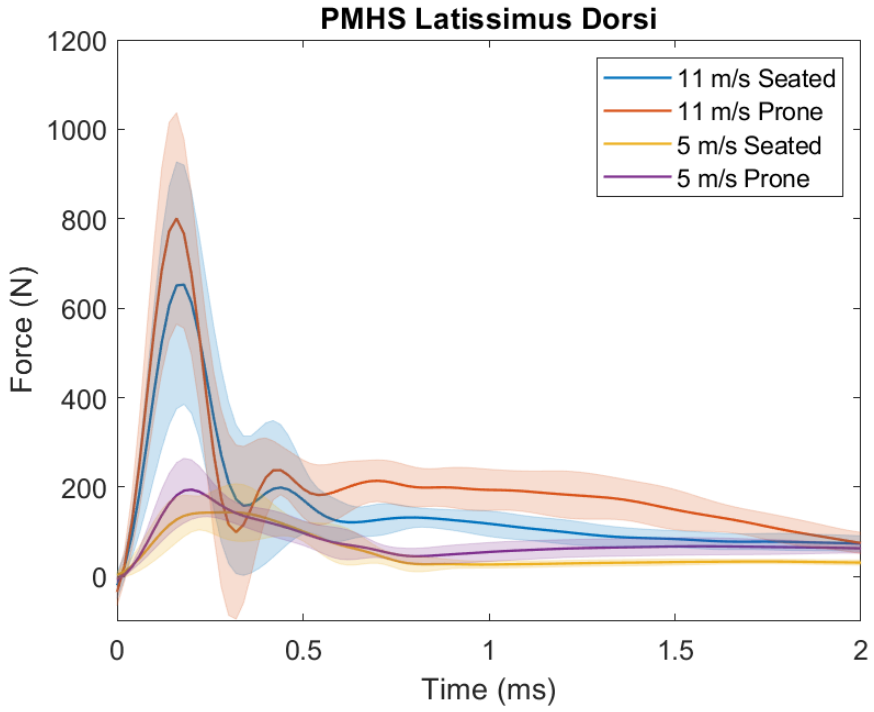
PMHS Latissimus Dorsi
11 m/s Seated
11 m/s Prone
5 m/s Seated
5 m/s Prone
Force (N)
Time (ms)
0
200
400
600
800
1000
1200
0
0.5
1
1.5
2

Appendix 20: PMHS Force-Displacement Average Curves

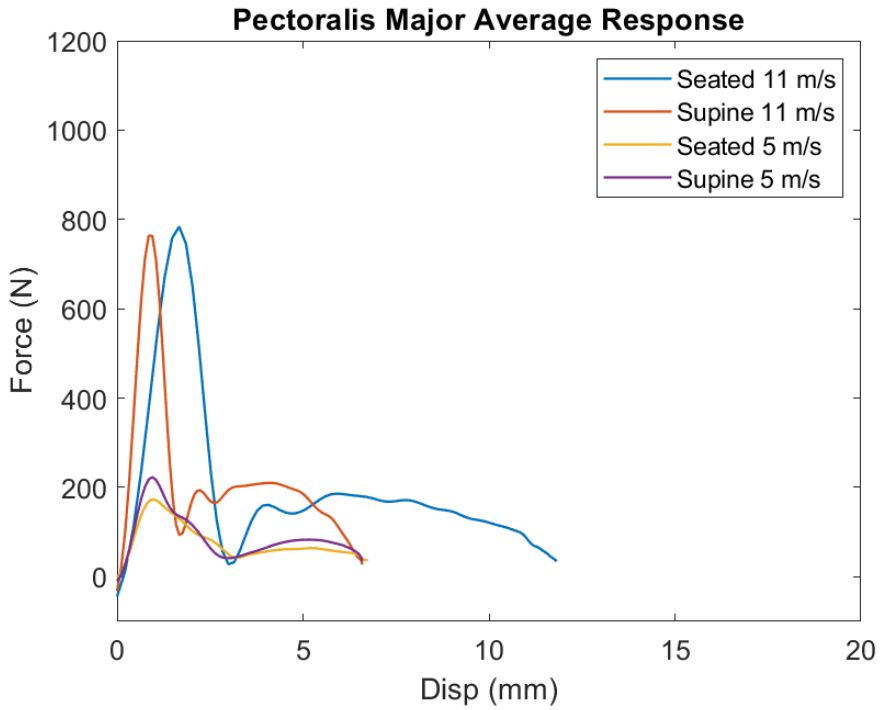

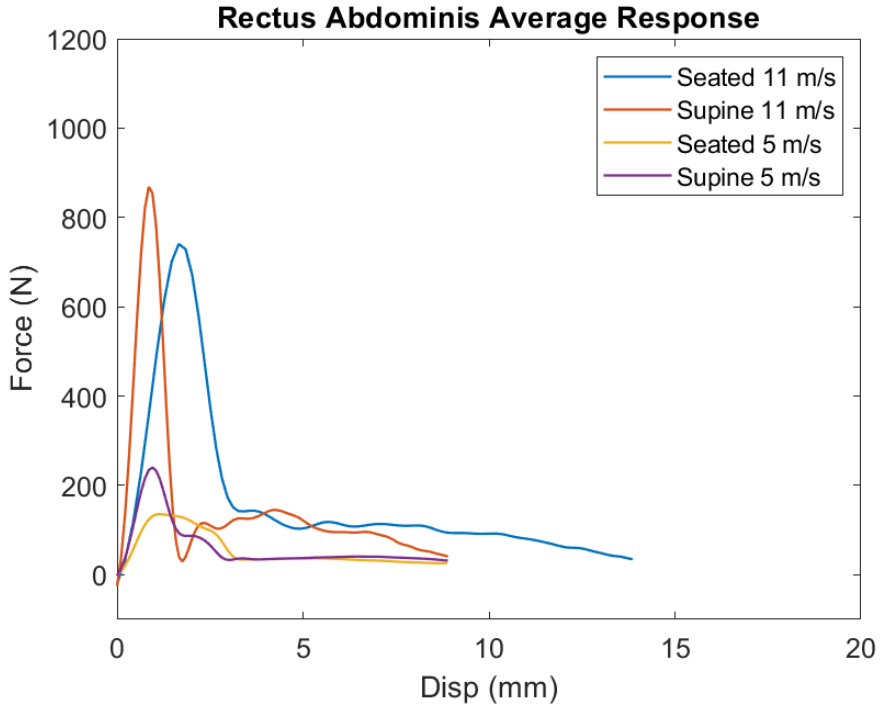

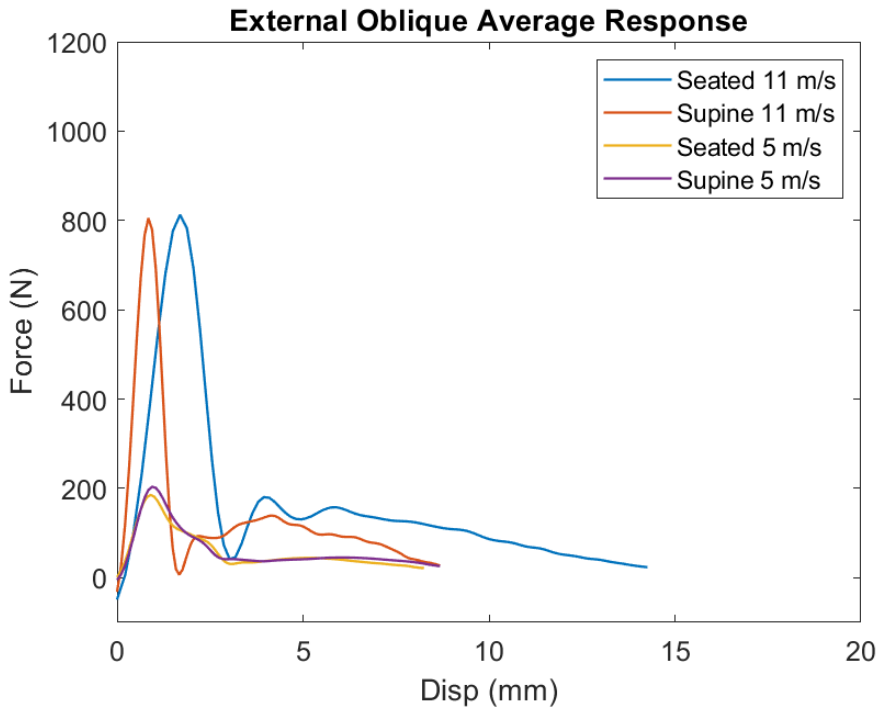
External Oblique Average Response
Seated 11 m/s
Supine 11 m/s
Seated 5 m/s
Supine 5 m/s
Force (N)
Disp (mm)
0
200
400
600
800
1000
1200
0
5
10
15
20

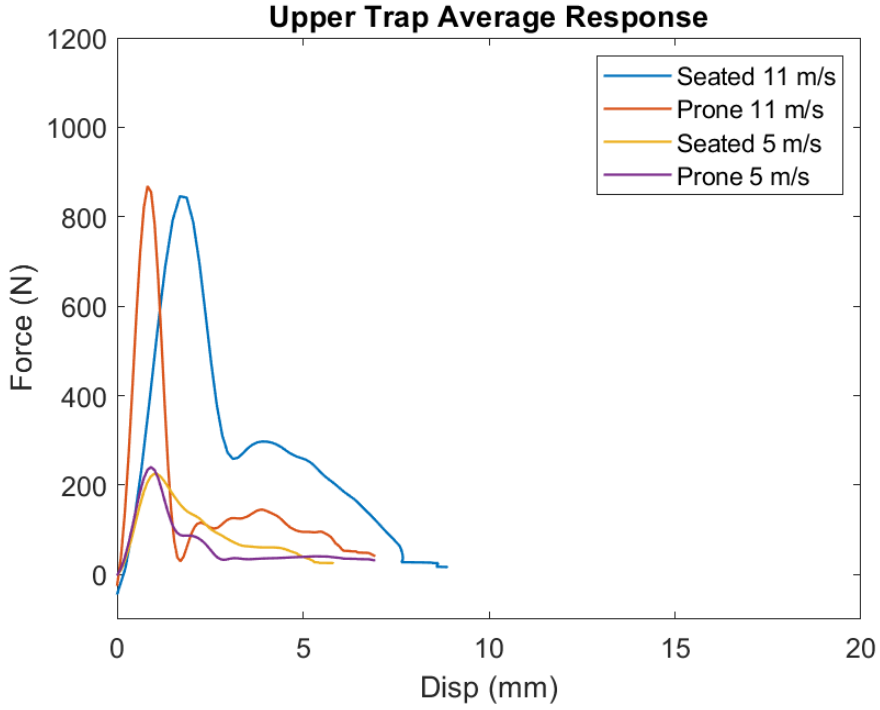
Upper Trap Average Response
Seated 11 m/s
Prone 11 m/s
Seated 5 m/s
Prone 5 m/s
Force (N)
Disp (mm)
0
200
400
600
800
1000
1200
0
5
10
15
20

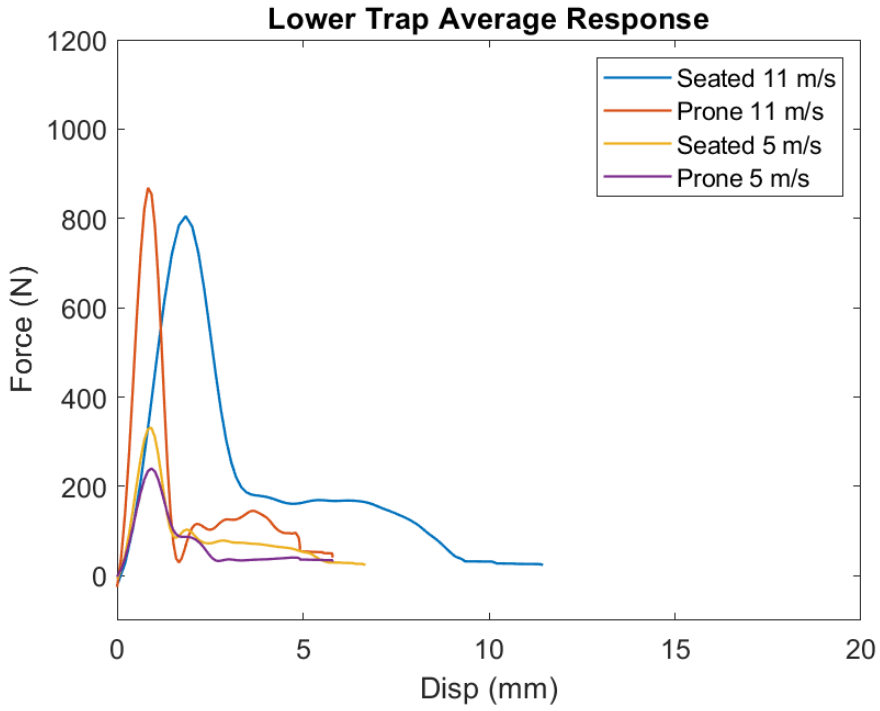
Lower Trap Average Response
Seated 11 m/s
Prone 11 m/s
Seated 5 m/s
Prone 5 m/s
Force (N)
Disp (mm)
0
200
400
600
800
1000
1200
0
5
10
15
20

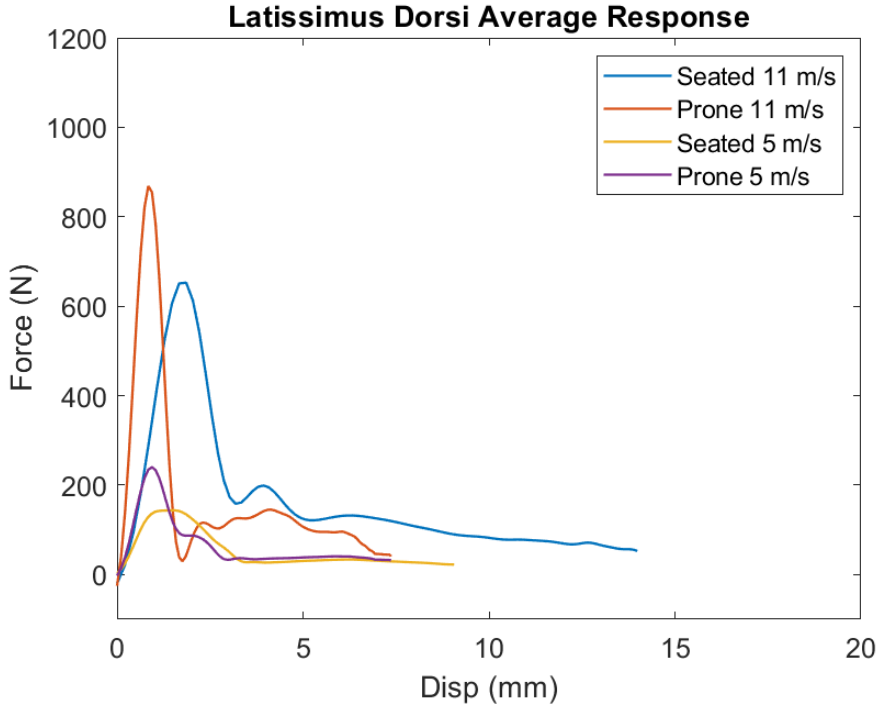
Latissimus Dorsi Average Response
Seated 11 m/s
Prone 11 m/s
Seated 5 m/s
Prone 5 m/s
Force (N)
Disp (mm)
0
200
400
600
800
1000
1200
0
5
10
15
20

Appendix 21: PMHS vs Volunteer Force-Time Corridors

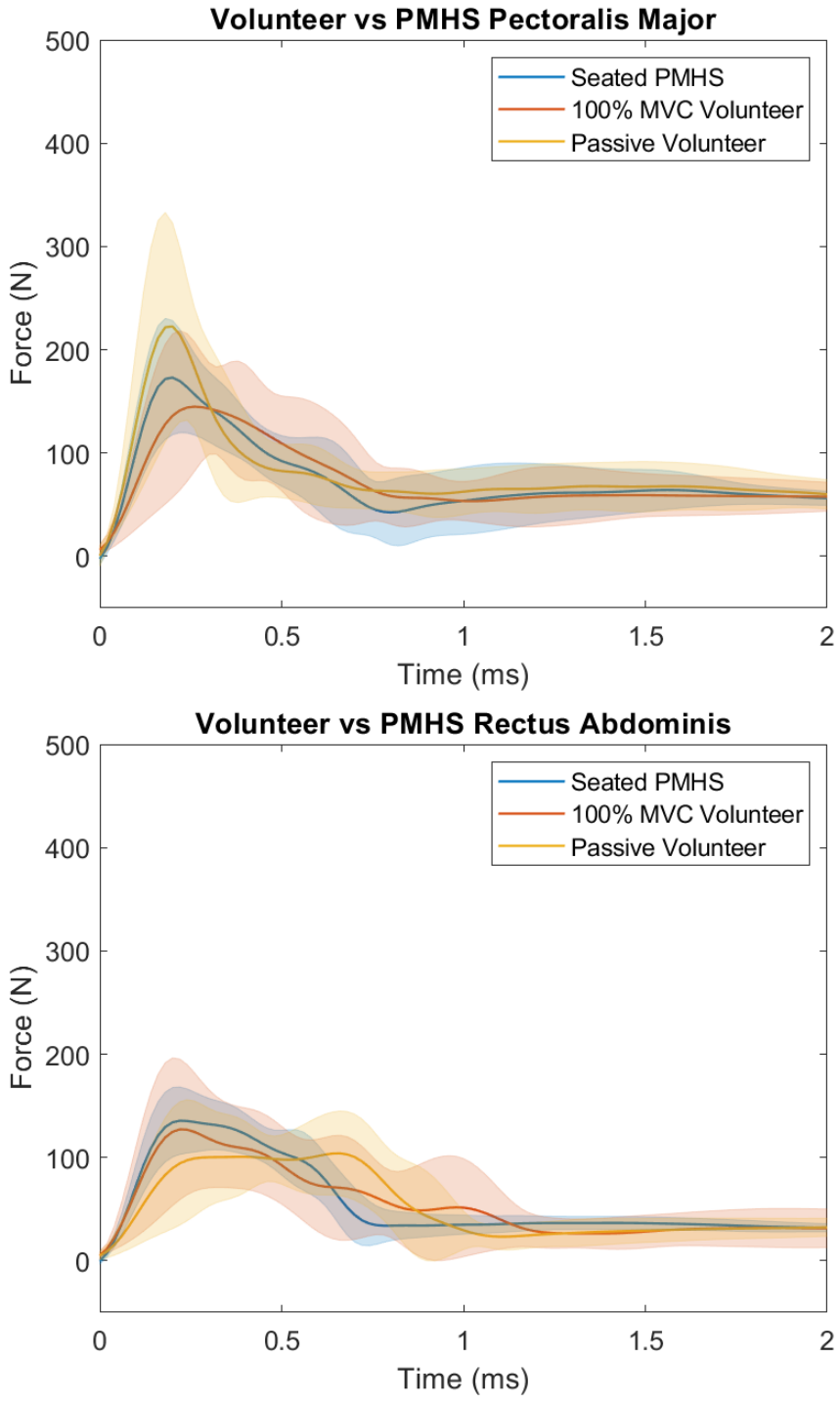

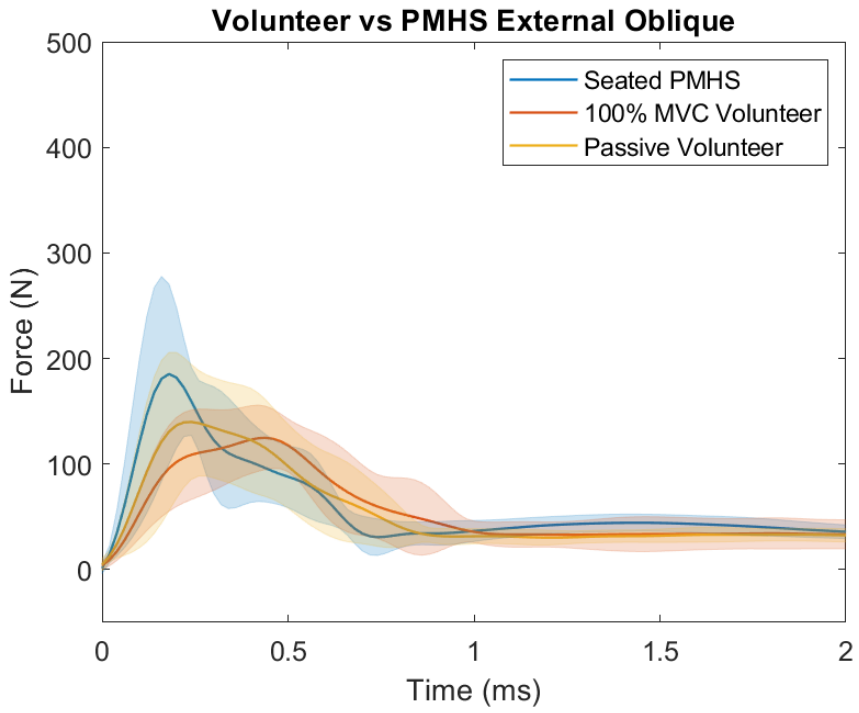
Volunteer vs PMHS External Oblique
Seated PMHS
100% MVC Volunteer
Passive Volunteer
Force (N)
Time (ms)
0
100
200
300
400
500
0
0.5
1
1.5
2

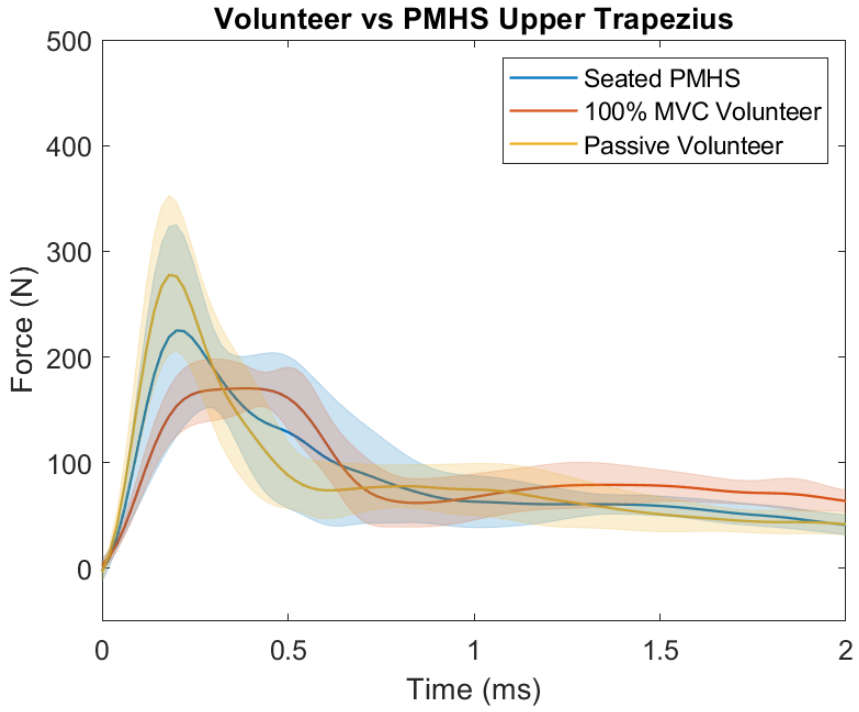
Volunteer vs PMHS Upper Trapezius
Seated PMHS
100% MVC Volunteer
Passive Volunteer
Force (N)
Time (ms)
0
100
200
300
400
500
0
0.5
1
1.5
2

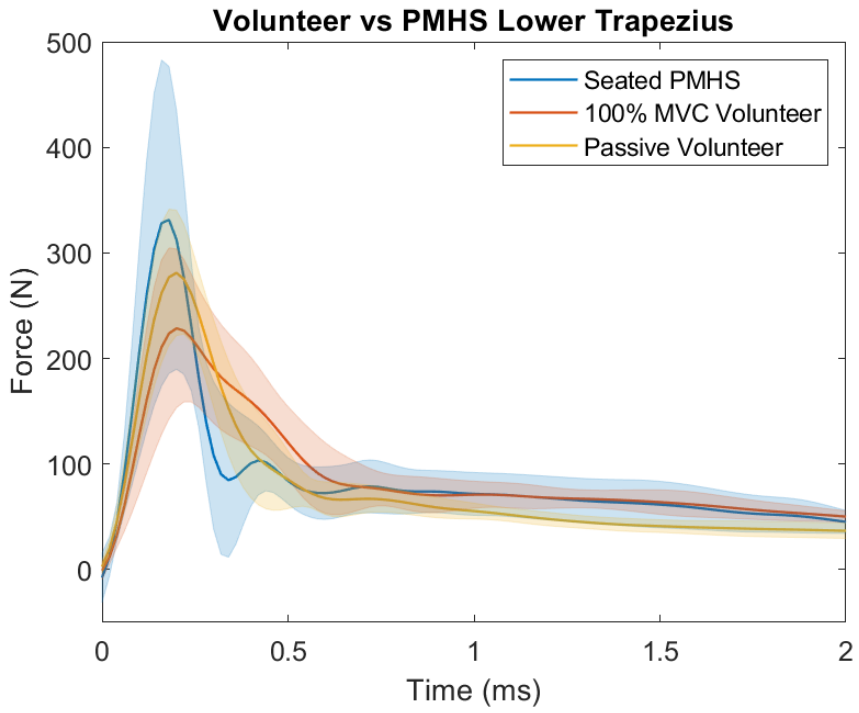
Volunteer vs PMHS Lower Trapezius
Seated PMHS
100% MVC Volunteer
Passive Volunteer
Force (N)
Time (ms)
0
100
200
300
400
500
0
0.5
1
1.5
2

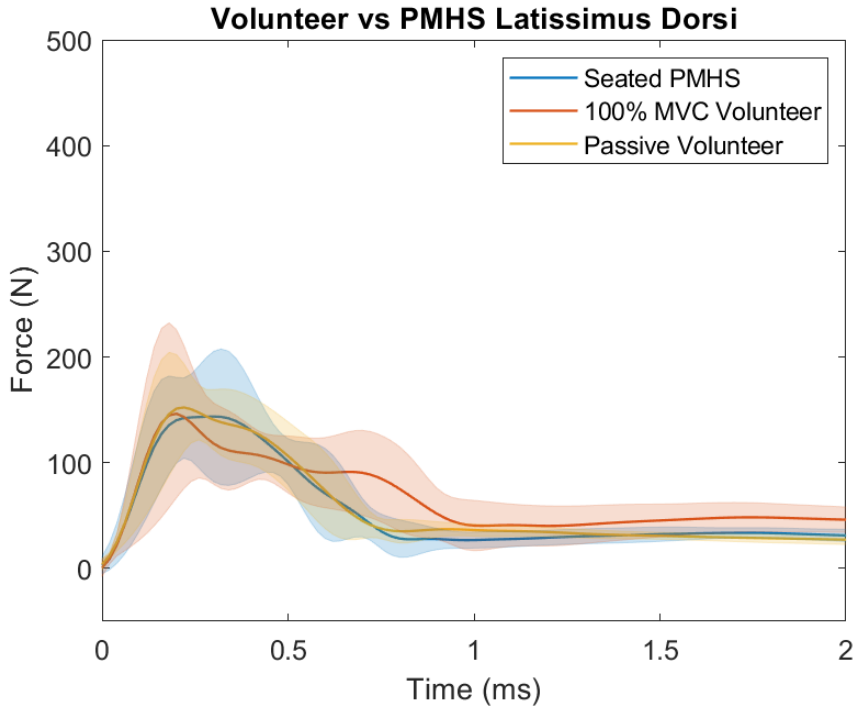
Volunteer vs PMHS Latissimus Dorsi
Seated PMHS
100% MVC Volunteer
Passive Volunteer
Force (N)
Time (ms)
0
100
200
300
400
500
0
0.5
1
1.5
2

Appendix 22: Superficial tissue temperatures during the mechanical testing on drop tower

PMHS	Muscle	Temperature (°F)
PMHS 1	Pectoralis Major	60.3
	Rectus Abdominis	63.8
	External Oblique	60.7
	Upper Trapezius	61.5
	Lower Trapezius	62.6
	Latissimus Dorsi	61.6
	Water Bath	**58.3**
PMHS 2	Pectoralis Major	50.7
	Rectus Abdominis	58.5
	External Oblique	63.1
	Upper Trapezius	61.7
	Lower Trapezius	57.1
	Latissimus Dorsi	62.1
	Water Bath	**59.7**
PMHS 3A	Pectoralis Major	60.9
	Rectus Abdominis	60.4
	External Oblique	61.1
	Upper Trapezius	60.7
	Lower Trapezius	60.6
	Latissimus Dorsi	61.7
	Water Bath	**59.1**
PMHS 3B	Pectoralis Major	60.3
	Rectus Abdominis	59.5
	External Oblique	59.6
	Upper Trapezius	59.5
	Lower Trapezius	61.2
	Latissimus Dorsi	60.3
	Water Bath	**59.9**

Appendix 23: Displacement- and force-time histories for all cadaveric tissue from drop tower mechanical testing.

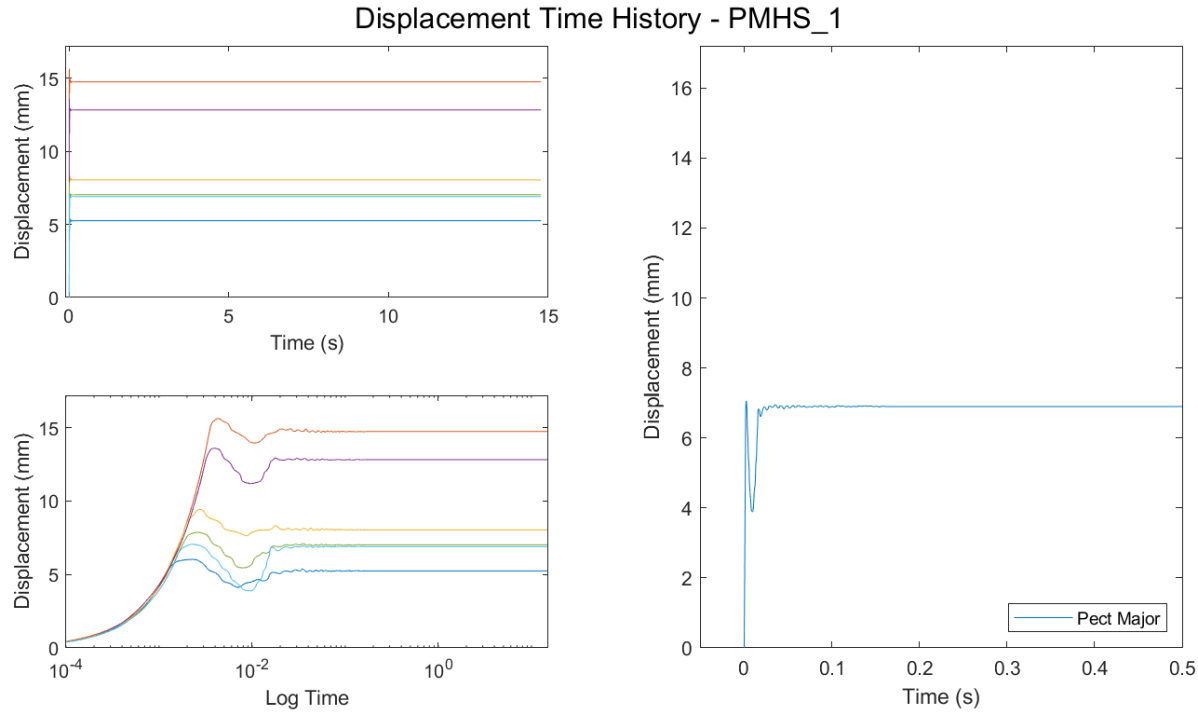

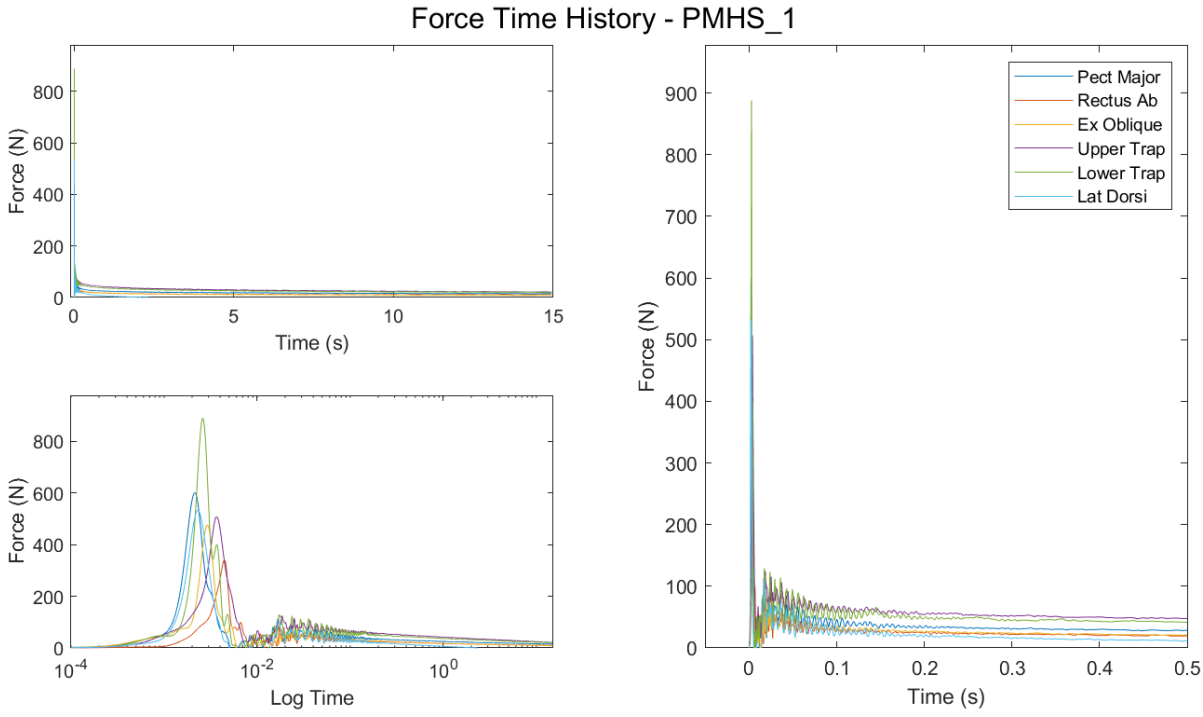

Displacement Time History - PMHS_2

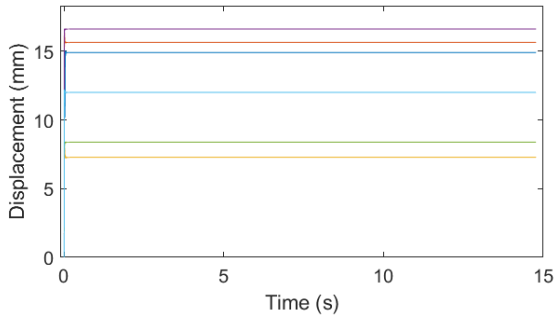

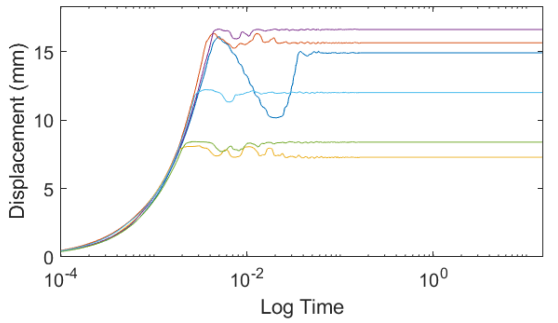

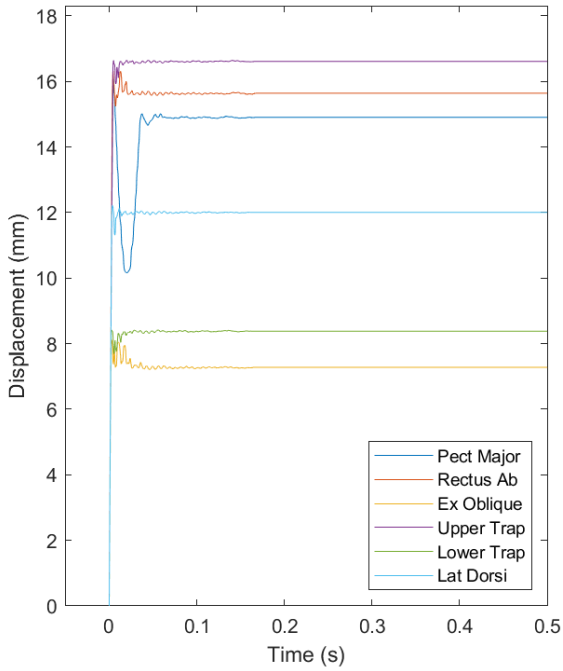

Force Time History - PMHS_2

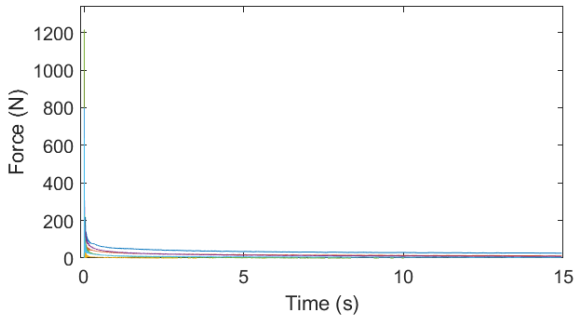

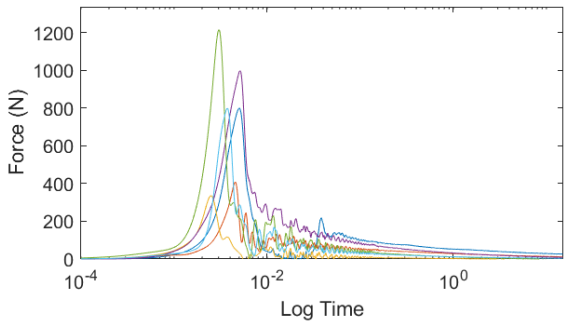

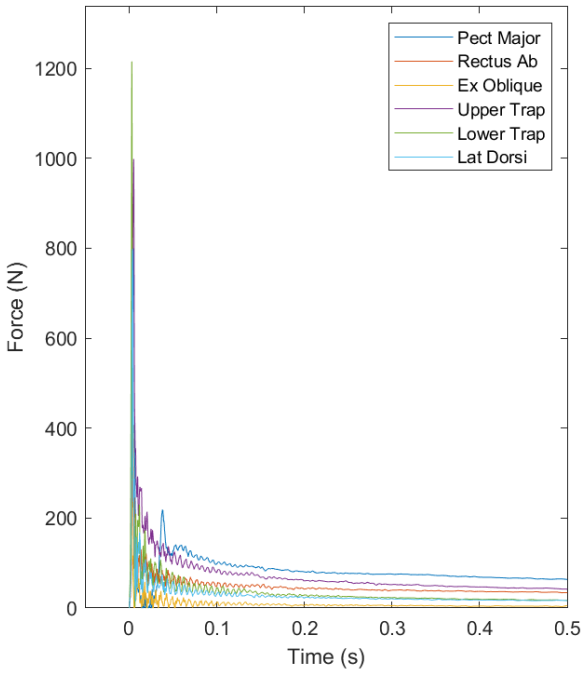

Displacement Time History - PMHS_3a

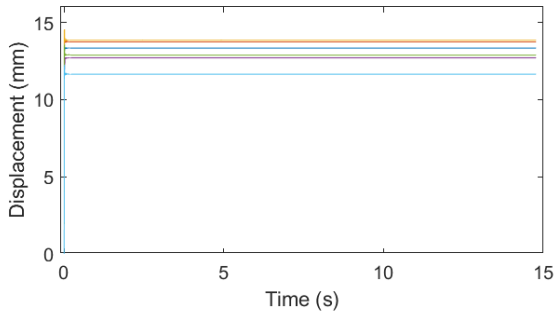

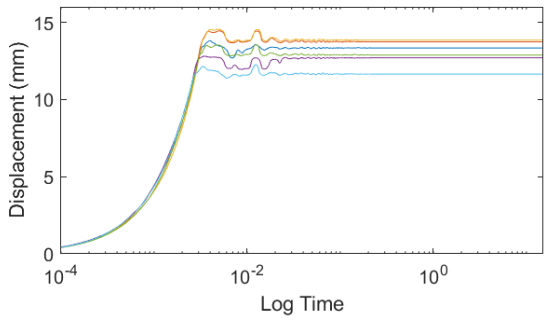

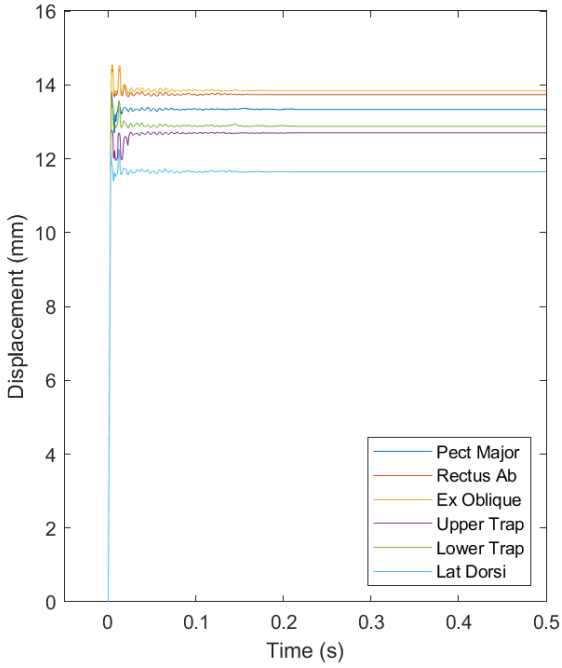

Force Time History - PMHS_3a

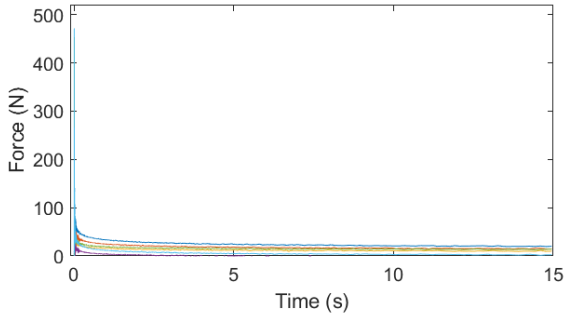

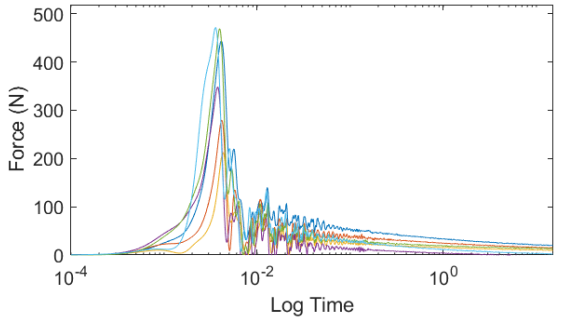

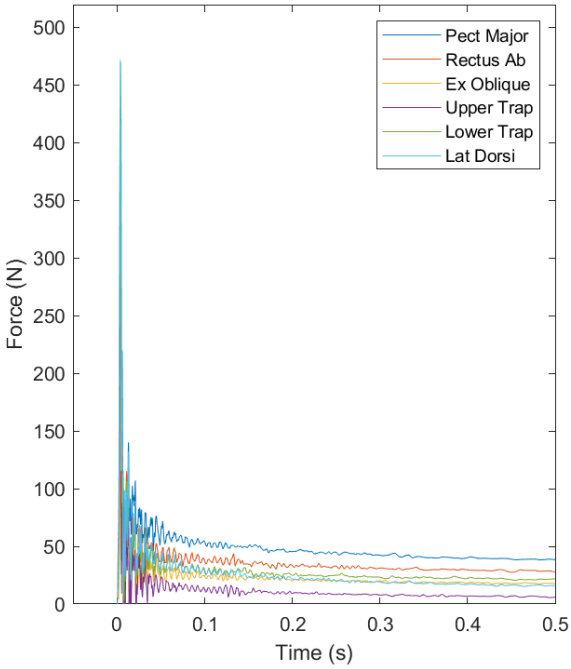

Displacement Time History - PMHS_3b

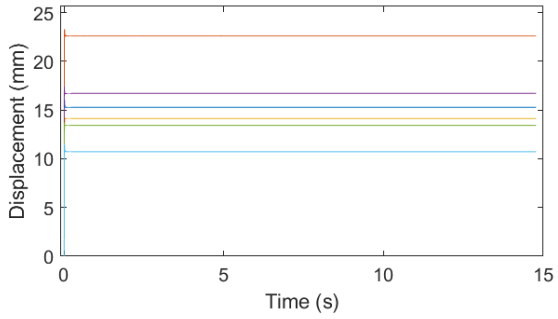

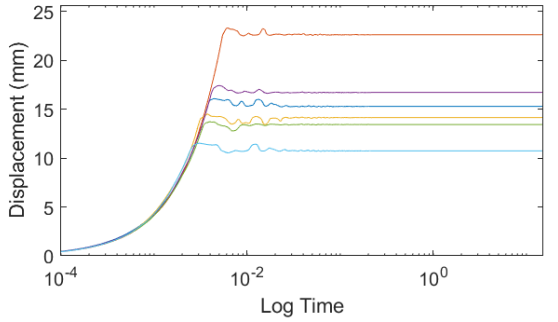

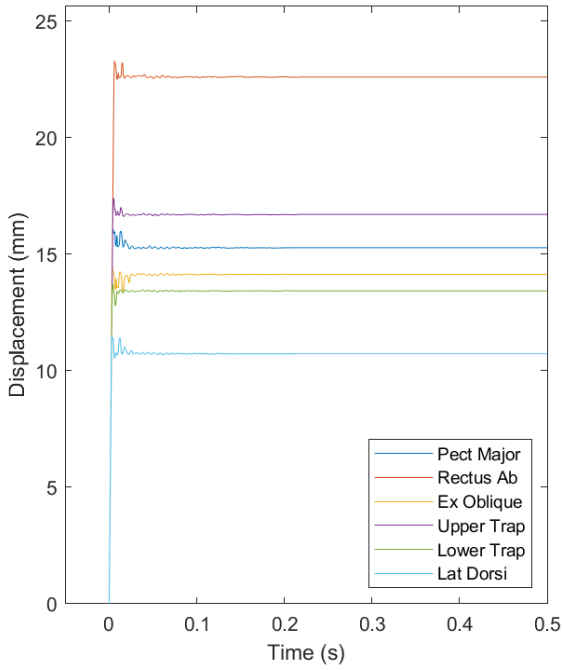

Force Time History - PMHS_3b

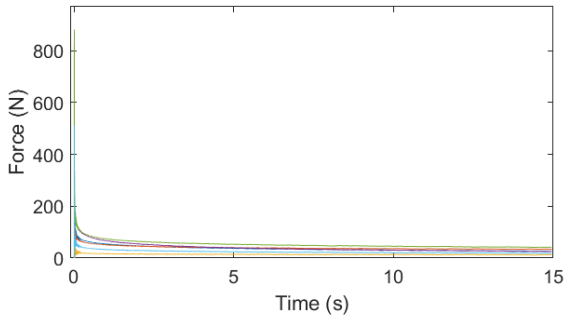

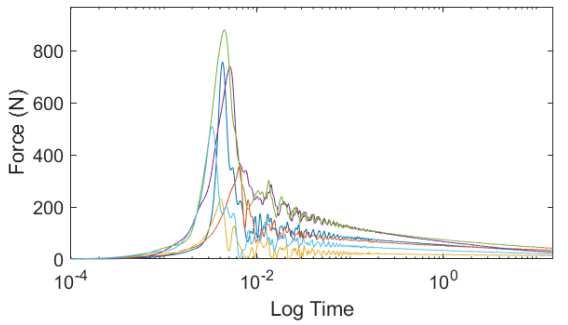

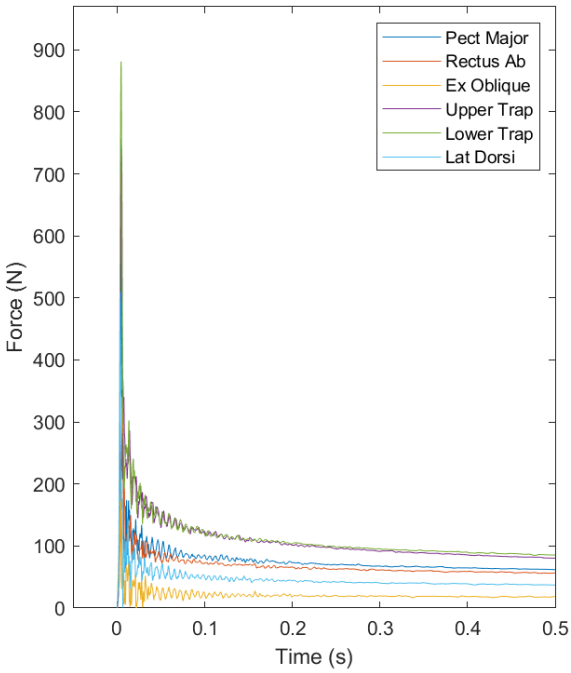

Appendix 24: Compressive strain - force relationship for each muscle.

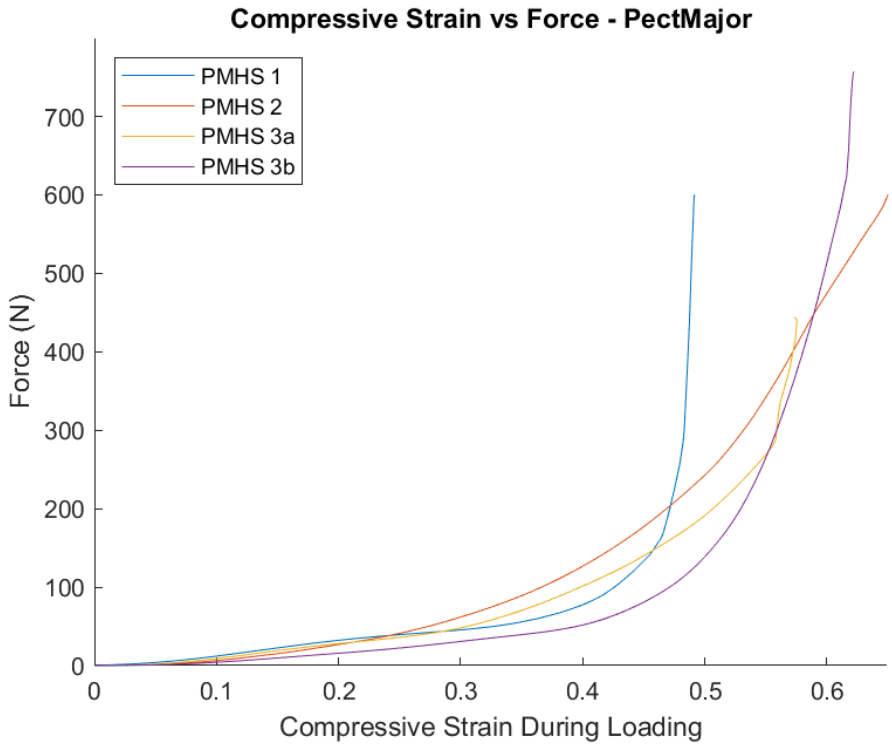

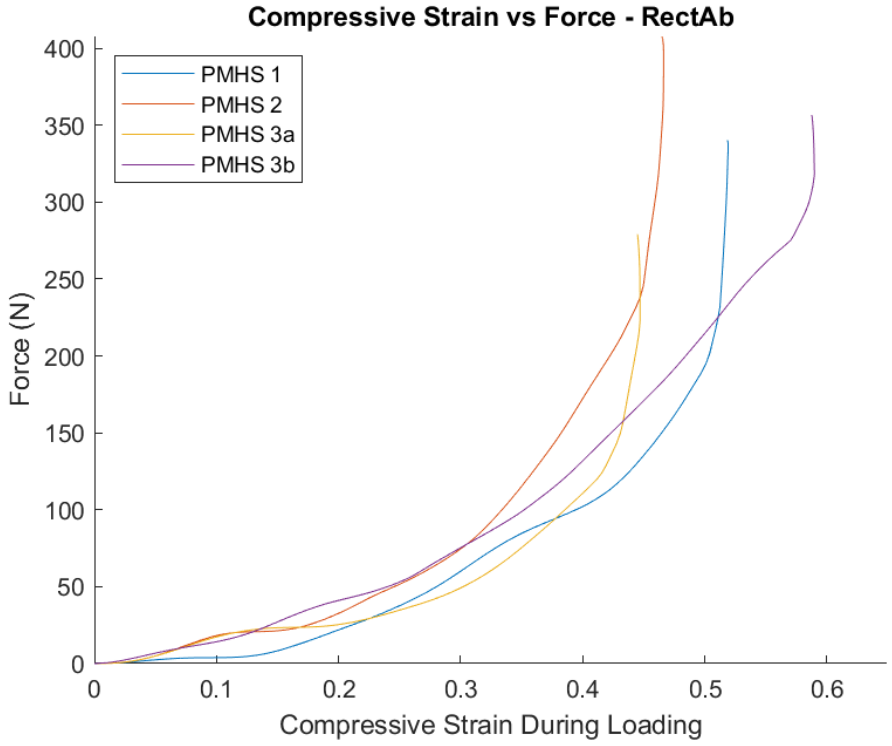

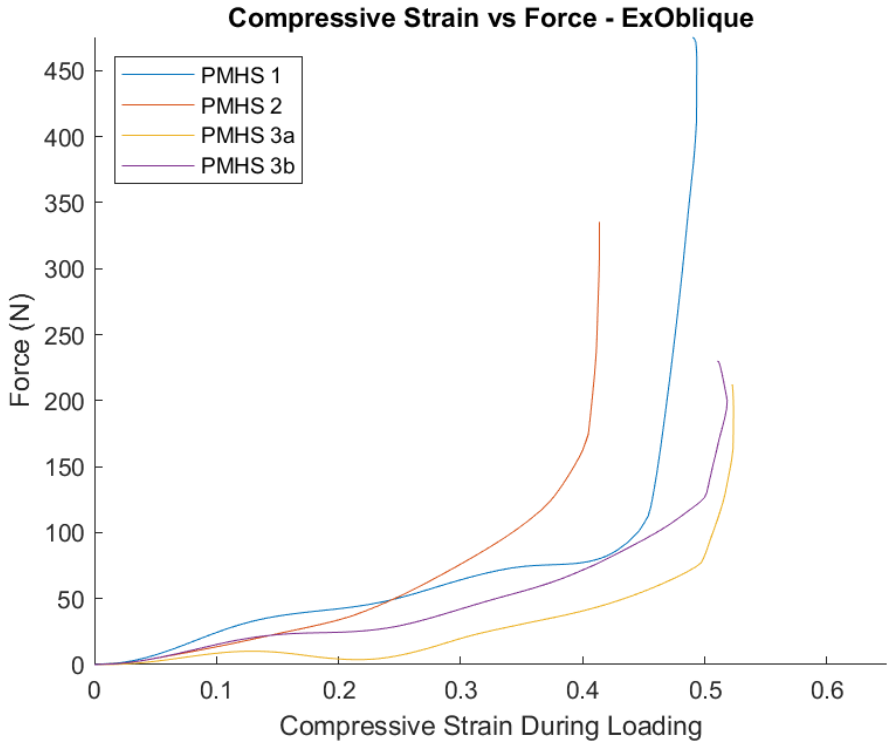
Compressive Strain vs Force - ExOblique
PMHS 1
PMHS 2
PMHS 3a
PMHS 3b
Force (N)
0
50
100
150
200
250
300
350
400
450
0
0.1
0.2
0.3
0.4
0.5
0.6
Compressive Strain During Loading

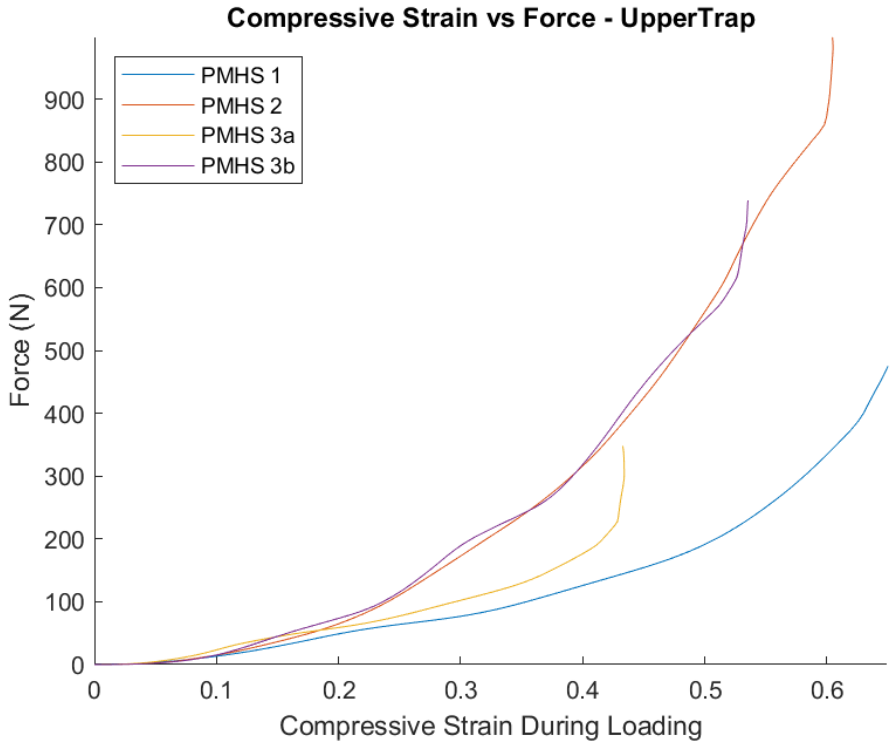
Compressive Strain vs Force - UpperTrap
PMHS 1
PMHS 2
PMHS 3a
PMHS 3b
Force (N)
0
100
200
300
400
500
600
700
800
900
0
0.1
0.2
0.3
0.4
0.5
0.6
Compressive Strain During Loading

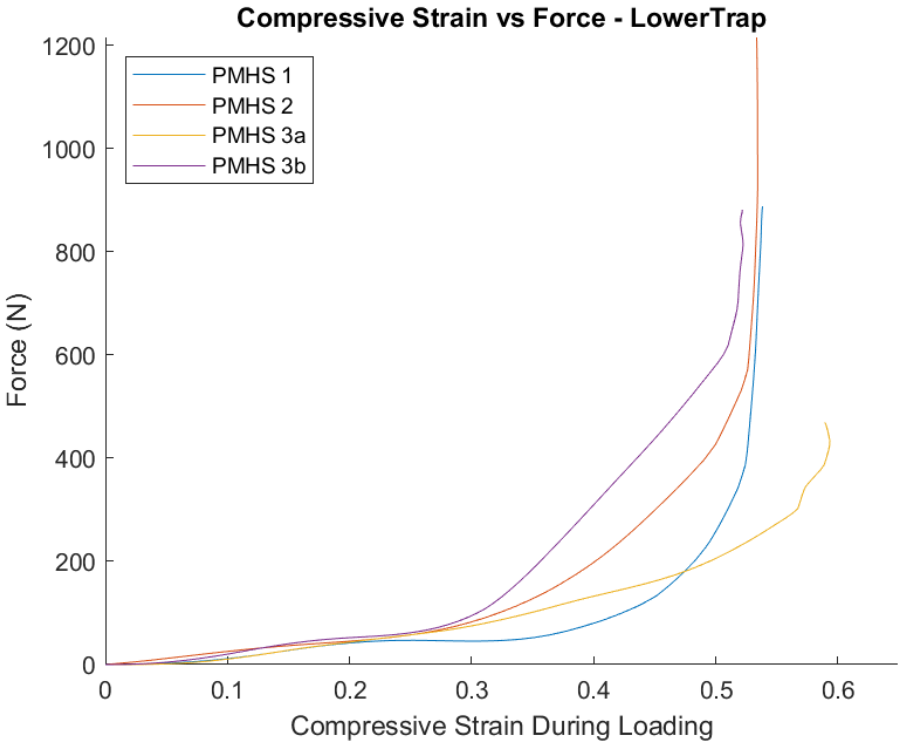
Compressive Strain vs Force - LowerTrap
PMHS 1
PMHS 2
PMHS 3a
PMHS 3b
Force (N)
Compressive Strain During Loading
0
200
400
600
800
1000
1200
0
0.1
0.2
0.3
0.4
0.5
0.6

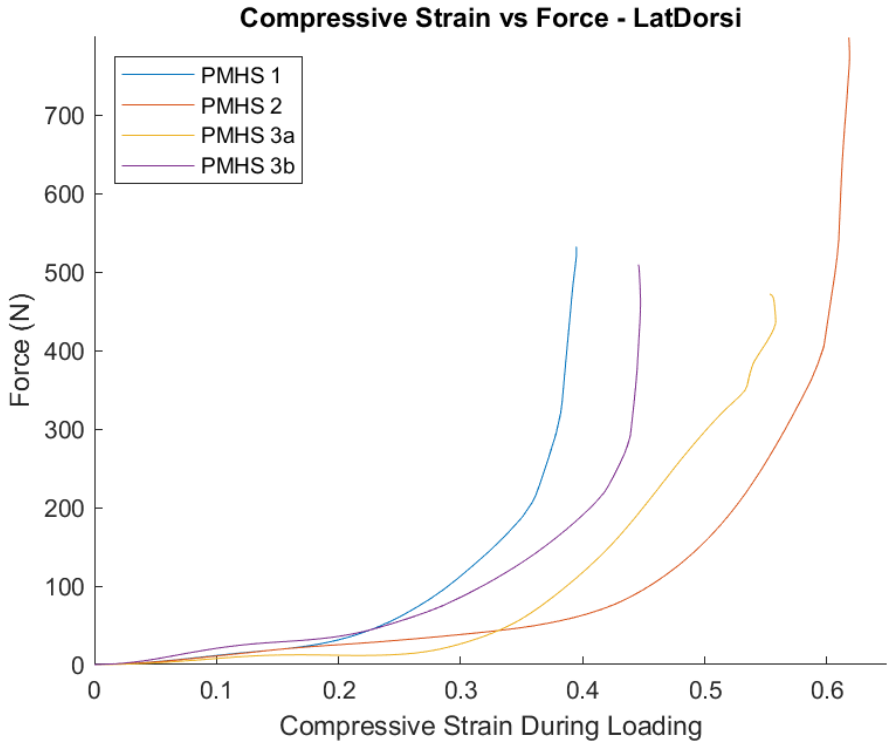
Compressive Strain vs Force - LatDorsi
PMHS 1
PMHS 2
PMHS 3a
PMHS 3b
Force (N)
Compressive Strain During Loading
0
100
200
300
400
500
600
700
0
0.1
0.2
0.3
0.4
0.5
0.6

Appendix 25: The parameters for individual QLV fits per muscle and PMHS.

The average parameters for the QLV models of each PMHS data using stress-strain.

Muscle	Parameters	PMHS 1	PMHS 2	PMHS 3a	PMHS 3b	Mean ± SD
Pectoralis Major	C_1	0.022	0.040	0.070	0.091	**0.056 ± 0.031**
	C_2	0.268	0.270	0.555	0.189	**0.321 ± 0.139**
	C_3	0.690	0.730	0.359	0.711	**0.623 ± 0.176**
	C_{inf}	0.020	0.020	0.016	0.010	**0.017 ± 0.005**
	A (MPa)	0.030	0.034	0.028	0.024	**0.029 ± 0.004**
	B	10.31	9.009	8.463	9.045	**9.207 ± 0.782**
Rectus Abdominis	C_1	0.026	0.029	0.045	0.026	**0.032 ± 0.009**
	C_2	0.749	0.602	0.610	0.625	**0.647 ± 0.069**
	C_3	0.171	0.289	0.290	0.288	**0.260 ± 0.059**
	C_{inf}	0.054	0.08	0.055	0.061	**0.063 ± 0.012**
	A (MPa)	0.047	0.035	0.041	0.052	**0.044 ± 0.007**
	B	7.609	9.720	8.850	6.944	**8.281 ± 1.243**
External Oblique	C_1	0.024	0.055	0.153	0.024	**0.064 ± 0.061**
	C_2	0.673	0.606	0.819	0.800	**0.725 ± 0.102**
	C_3	0.250	0.324	0.029	0.140	**0.186 ± 0.129**
	C_{inf}	0.053	0.015	0.000	0.037	**0.026 ± 0.023**
	A (MPa)	0.055	0.070	0.015	0.059	**0.050 ±0.024**
	B	8.360	8.550	8.600	6.420	**7.983 ± 1.047**
Upper Trapezius	C_1	0.088	0.002	0.050	0.093	**0.058 ± 0.042**
	C_2	0.373	0.434	0.680	0.445	**0.483 ± 0.135**
	C_3	0.528	0.551	0.270	0.442	**0.448 ± 0.127**
	C_{inf}	0.010	0.013	0.000	0.020	**0.011 ± 0.008**
	A (MPa)	0.120	0.244	0.150	0.255	**0.192 ± 0.067**
	B	5.454	6.059	6.630	6.088	**6.058 ± 0.481**
Lower Trapezius	C_1	0.055	0.001	0.030	0.080	**0.042 ± 0.034**
	C_2	0.281	0.876	0.410	0.763	**0.583 ± 0.282**
	C_3	0.650	0.123	0.559	0.140	**0.368 ± 0.276**
	C_{inf}	0.015	0.000	0.001	0.018	**0.009 ± 0.009**
	A (MPa)	0.003	0.023	0.094	0.069	**0.047 ± 0.042**
	B	14.442	10.940	6.480	8.578	**10.110 ± 3.415**

Muscle	Parameters	PMHS 1	PMHS 2	PMHS 3a	PMHS 3b	Mean ± SD
Latissimus Dorsi	C_1	0.010	0.001	0.022	0.023	**0.014 ± 0.010**
	C_2	0.915	0.63	0.442	0.740	**0.682 ± 0.198**
	C_3	0.065	0.368	0.535	0.148	**0.279 ± 0.213**
	C_{inf}	0.010	0.000	0.000	0.089	**0.025 ± 0.043**
	A (MPa)	0.034	0.005	0.020	0.030	**0.022 ± 0.013**
	B	11.694	11.410	9.545	10.650	**10.825 ± 0.960**

The average parameters for each QLV model for each PMHS for force-displacement.**Error! Not a valid link.**

Appendix 26: The average ideal strain input for each of the muscles

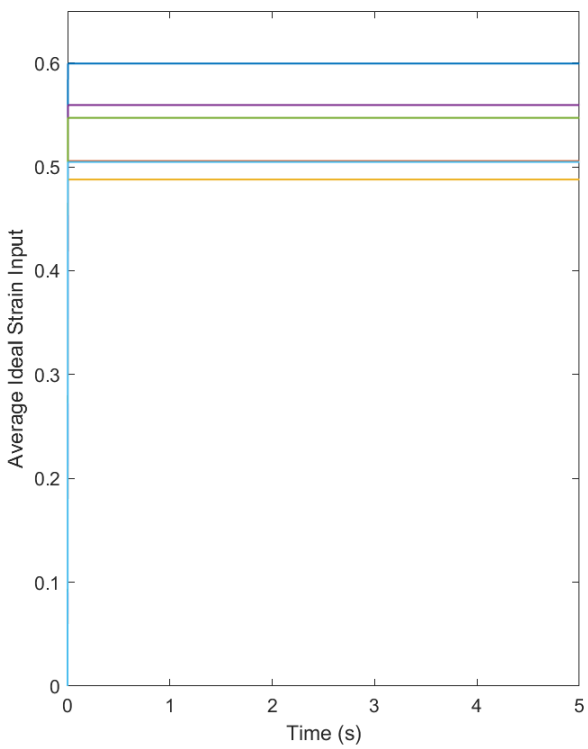

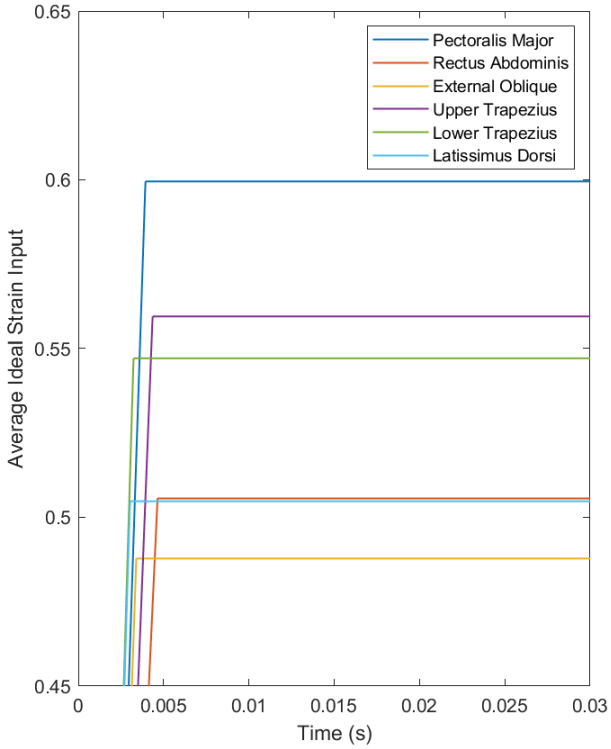

Appendix 27: The average QLV model fits for each muscle

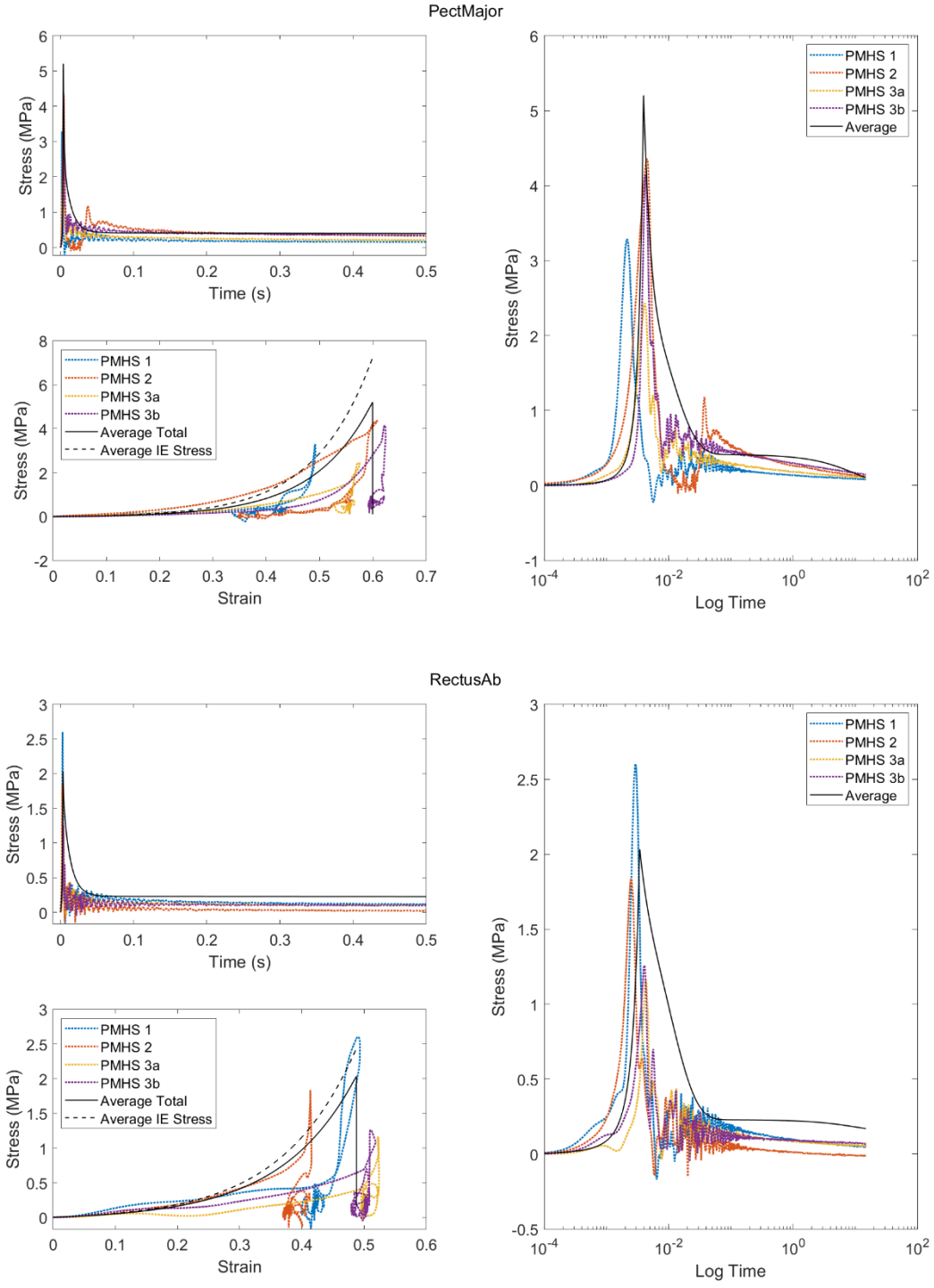

ExOblique

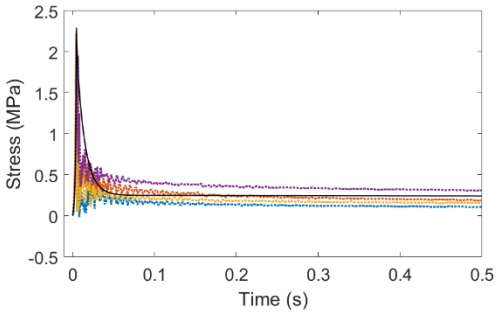

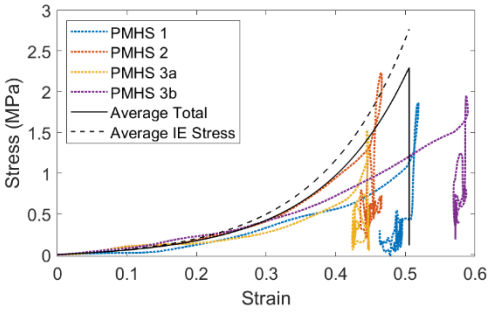

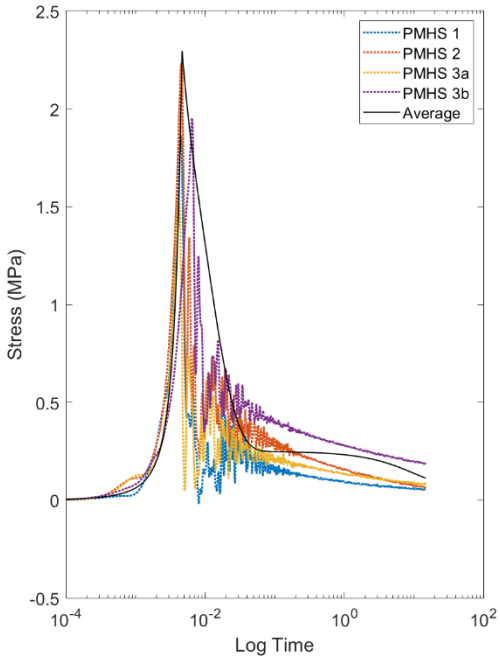

UpperTrap

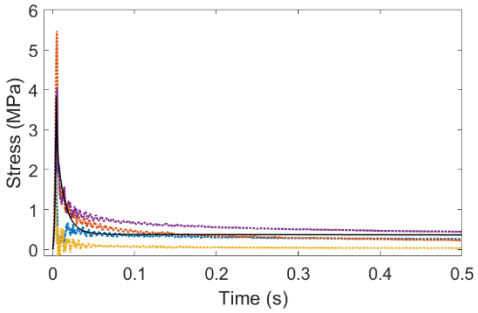

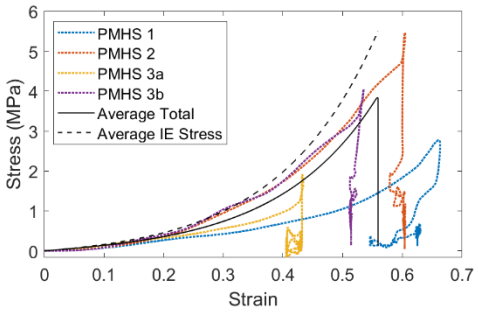

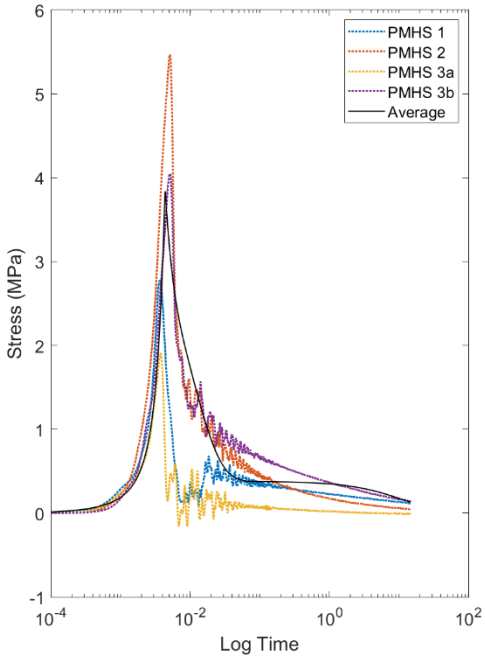

LowerTrap

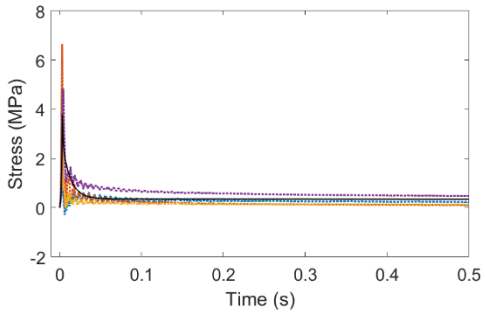

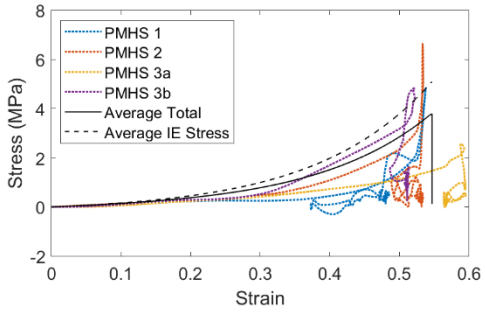

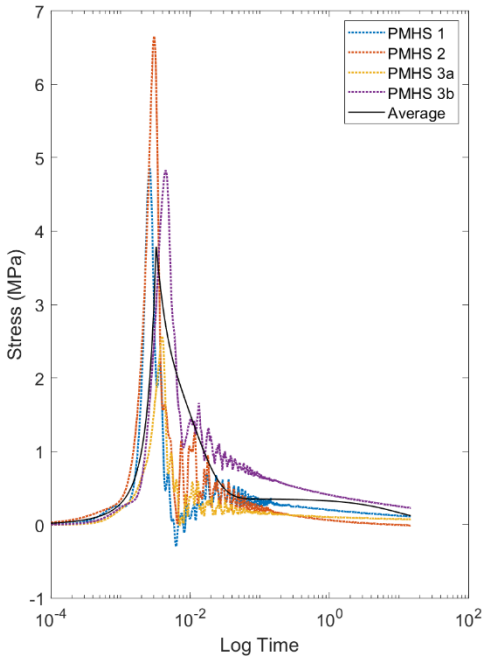

LatDorsi

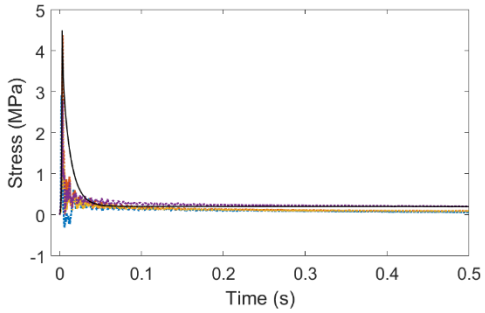

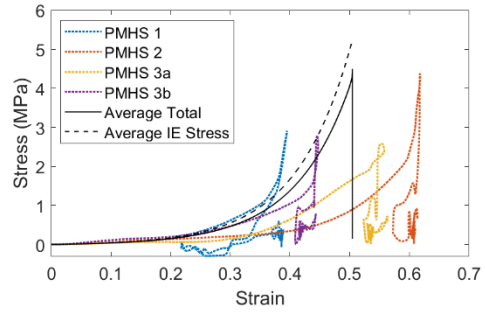

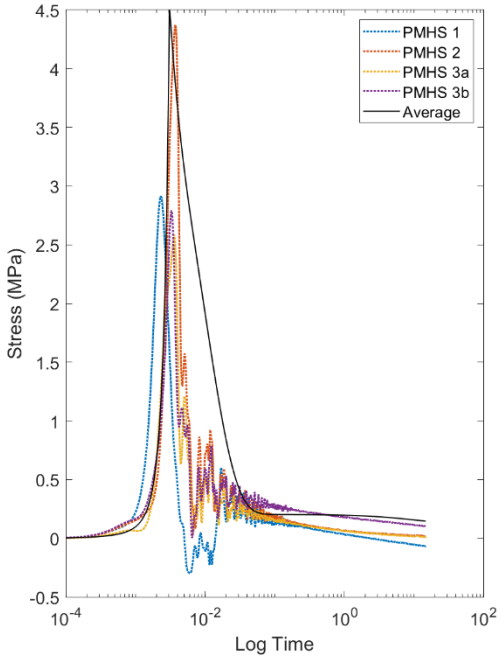

Appendix 28: The ratios and scaled parameters for QLV instantaneous elastic function parameter

Muscle	Parameter	Average (MPa)	Average (N)	Ratio	Scale Factor	Scaled Parameter (MPa)	Scaled Parameter (N)
Pectoralis Major	A	0.029	5.325	Pass Vol/ Seat PMHS	0.163	0.005	0.866
				100% Vol/ Seat PMHS	0.513	0.015	2.733
				50% Vol/ Seat PMHS	0.424	0.012	2.257
				Supine Vol/ Supine PMHS	0.173	0.005	0.920
Rectus Abdominis	A	0.044	7.982	Pass Vol/ Seat PMHS	0.510	0.022	4.068
				100% Vol/ Seat PMHS	2.695	0.119	21.511
				50% Vol/ Seat PMHS	3.019	0.133	24.102
				Supine Vol/ Supine PMHS	0.331	0.015	2.645
External Oblique	A	0.05	9.087	Pass Vol/ Seat PMHS	0.866	0.043	7.874
				100% Vol/ Seat PMHS	2.542	0.127	23.102
				50% Vol/ Seat PMHS	2.015	0.101	18.310
				Supine Vol/ Supine PMHS	0.612	0.031	5.558
Upper Trapezius	A	0.192	35.130	Pass Vol/ Seat PMHS	1.149	0.221	40.374

Muscle	Parameter	Average (MPa)	Average (N)	Ratio	Scale Factor	Scaled Parameter (MPa)	Scaled Parameter (N)
				100% Vol/ Seat PMHS	3.575	0.686	125.594
				50% Vol/ Seat PMHS	3.676	0.706	129.128
Lower Trapezius	A	0.073	13.270	Pass Vol/ Seat PMHS	0.484	0.035	6.417
				100% Vol/ Seat PMHS	1.269	0.093	16.844
				50% Vol/ Seat PMHS	1.214	0.089	16.103
Latissimus Dorsi	A	0.022	4.073	Pass Vol/ Seat PMHS	0.195	0.004	0.795
				100% Vol/ Seat PMHS	1.742	0.038	7.095
				50% Vol/ Seat PMHS	1.345	0.030	5.478

Appendix 29: The scaled QLV models for the volunteers at each muscle

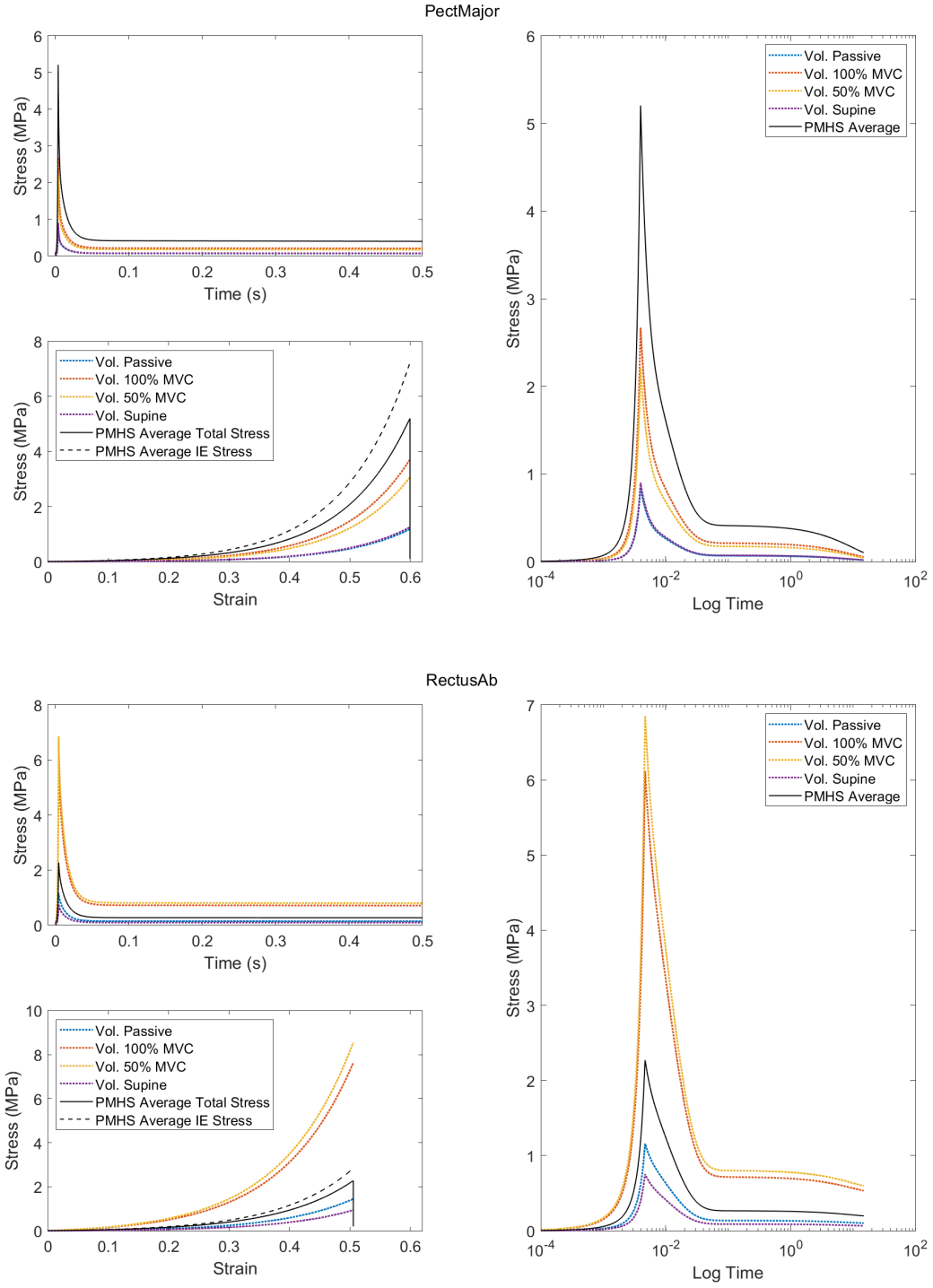

ExOblique

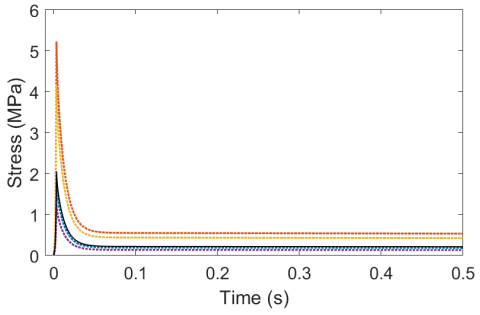

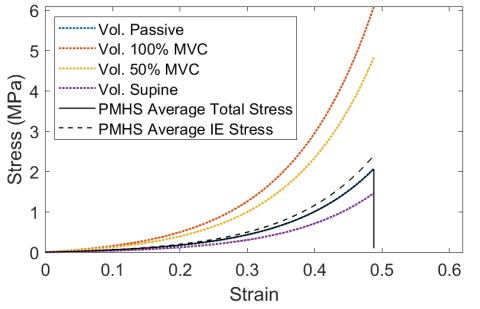

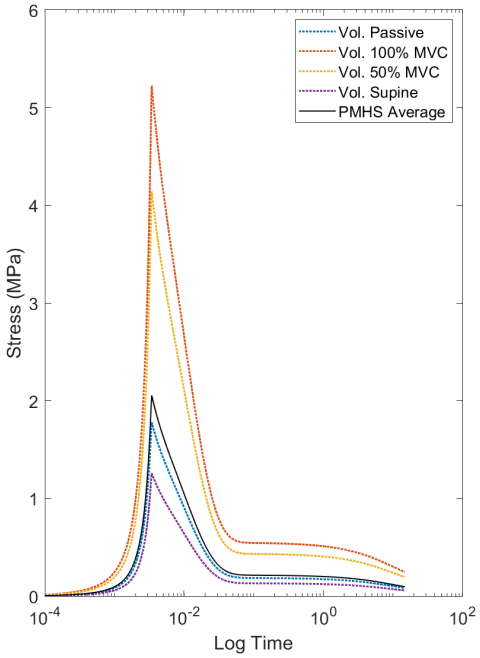

UpperTrap

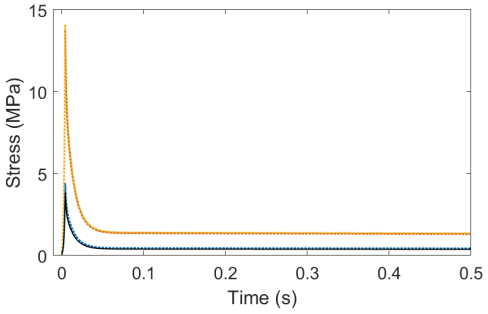

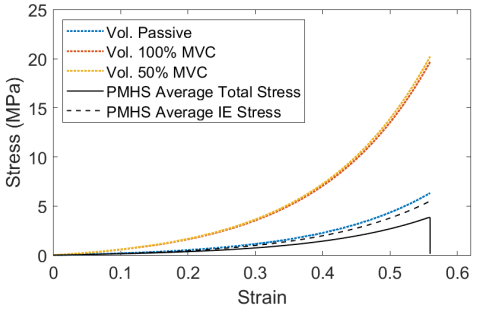

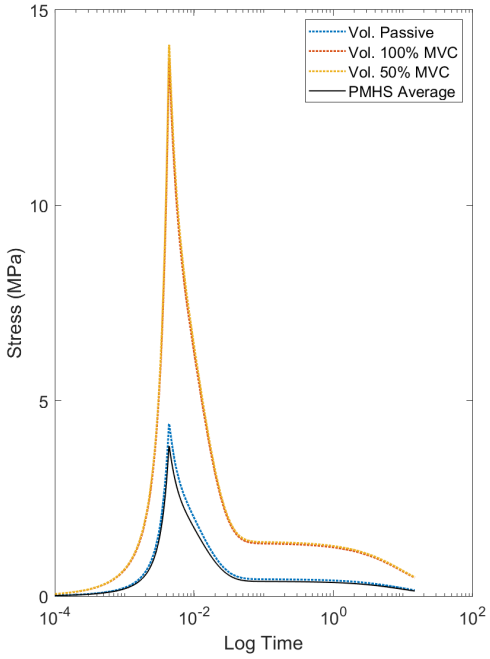

LowerTrap

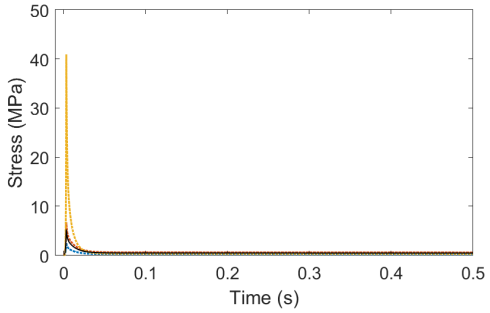

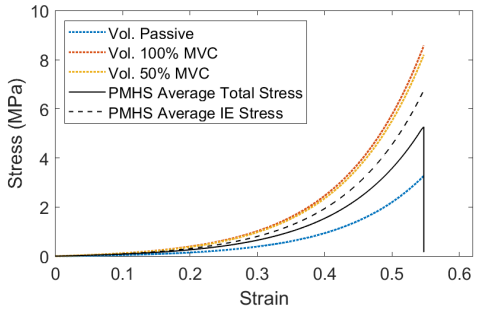

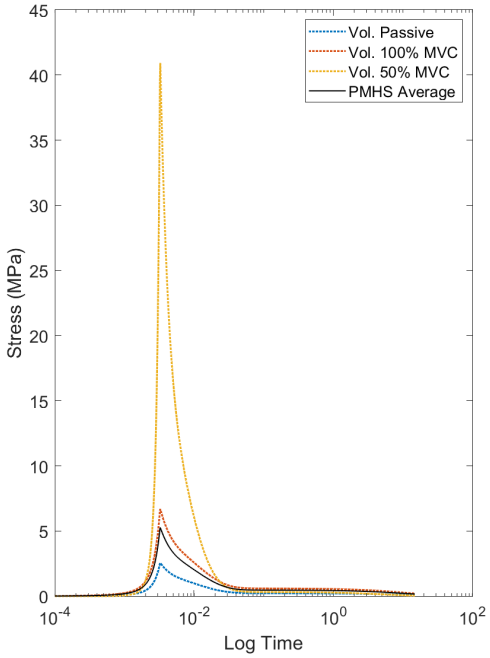

LatDorsi

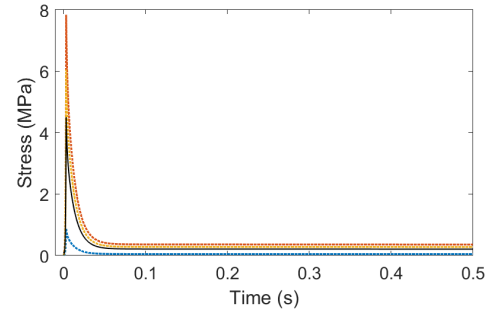

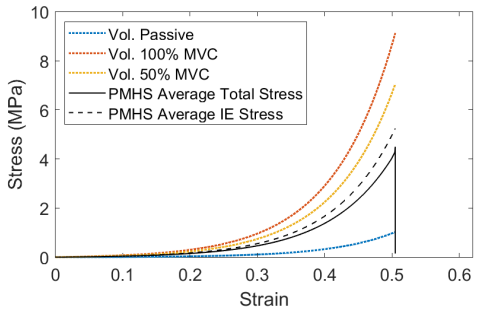

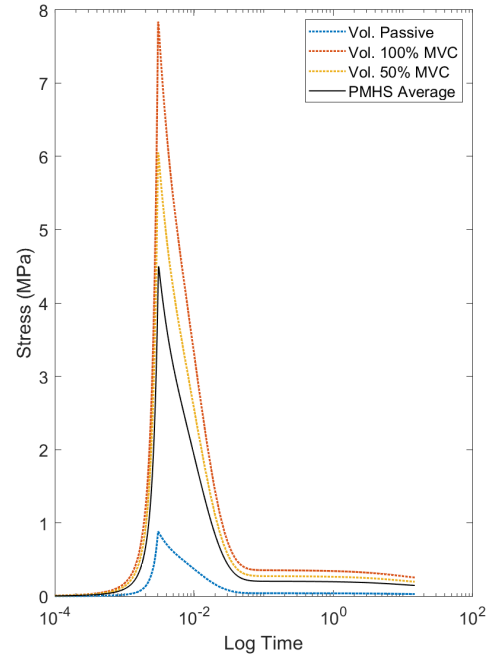

Appendix 30: Validation curves for external oblique using scaled QLV models